Single Ion Implantation

Thomas Schenkel

Lawrence Berkeley National Laboratory

T_Schenkel@LBL.gov

Dopant fluctuation effects and single atom electronics

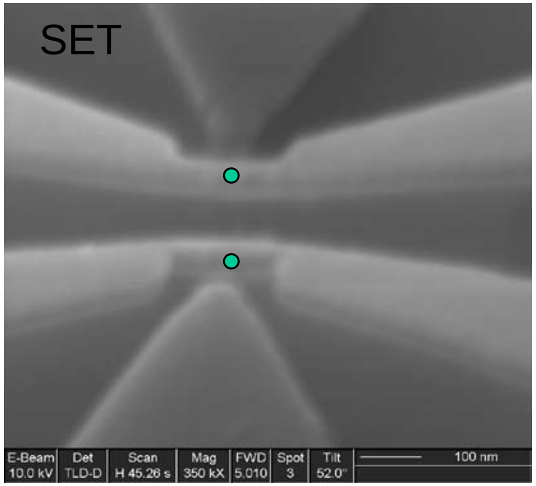

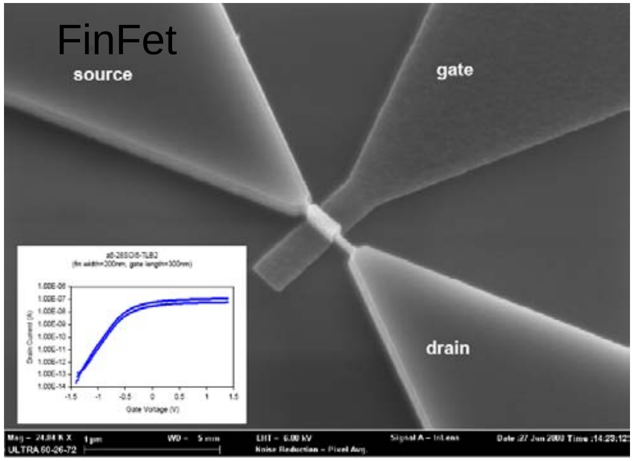

- S. J. Park, et al., J. Vac. Sci. Technol. 22, 3115 (2004)
- C. C. Lo, et al., Semc. Sci. Tech. 24, 10522 (2009)

“Atoms are large” and affect transport in scaled devices, characteristic length scale in silicon devices: Bohr radius

$$2\times a_0 = 2\times \varepsilon_{Si}\frac{m_0}{m_{eff}}\ 0.53\overset{o}{A} \approx 3-4\ nm$$

$$(\varepsilon_{Si} = 11.8,\ m_{eff} \approx 0.2\ m_0)$$

- routine lithographic access to 10-20 nm scale
- transport properties sensitive to presence of single dopant atoms
- understanding single dopant effects can benefit CMOS scaling

•post-CMOS opportunities ?

→ can we control, couple and readout states of single atom qubits coherently ?

→ test of quantum computing architectures

Desiderata for single ion implantation

1. flexibility in selection of ion species and implant energy
    - collimation of a broad beam vs. FIB
2. ability to image the region of interest without accidental implantation and damage
    - 5 nm imaging resolution is modest with scanning probes, but quite challenging in a FIB
3. ion placement resolution <5 nm (less or same as straggling)
    - beam spot size vs. collimator diameter
4. reliable single ion detection
5. retain array structures during annealing (minimize diffusion)
    - dopant specific diffusion mechanisms

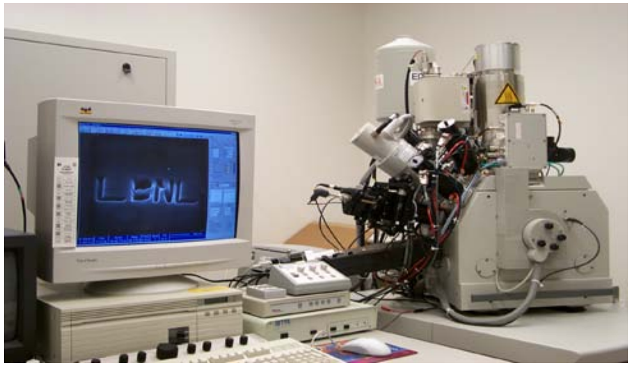

Commercial FIB system

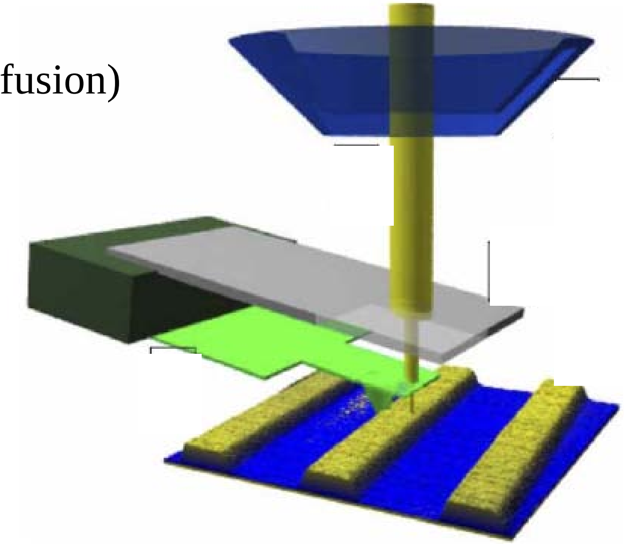

Schematic of ion beam integrated with scanning probe

Deterministic Doping – Single Ion Implantation

1. **Exact numbers of dopants**

2. **In precise locations in a device**

3. **All electrically active**

4. **And no other sources of variability are introduced during processing**

Detection of low energy single ion impacts

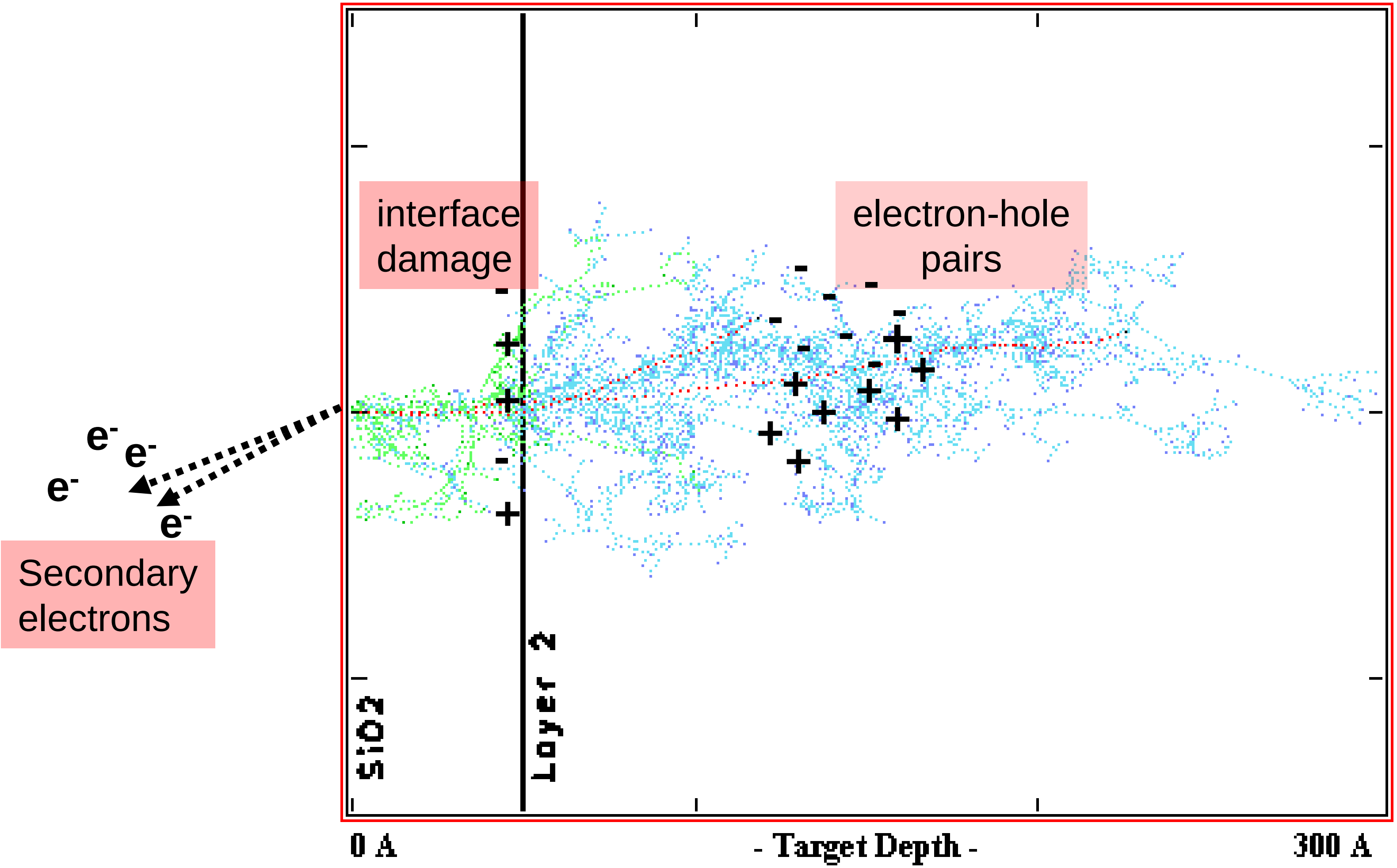

interface damage

electron-hole pairs

e^- e^- e^- e^-

Secondary electrons

SRIM screen shot

Single Ion Detection in Readout Transistors through ion impact induced current changes

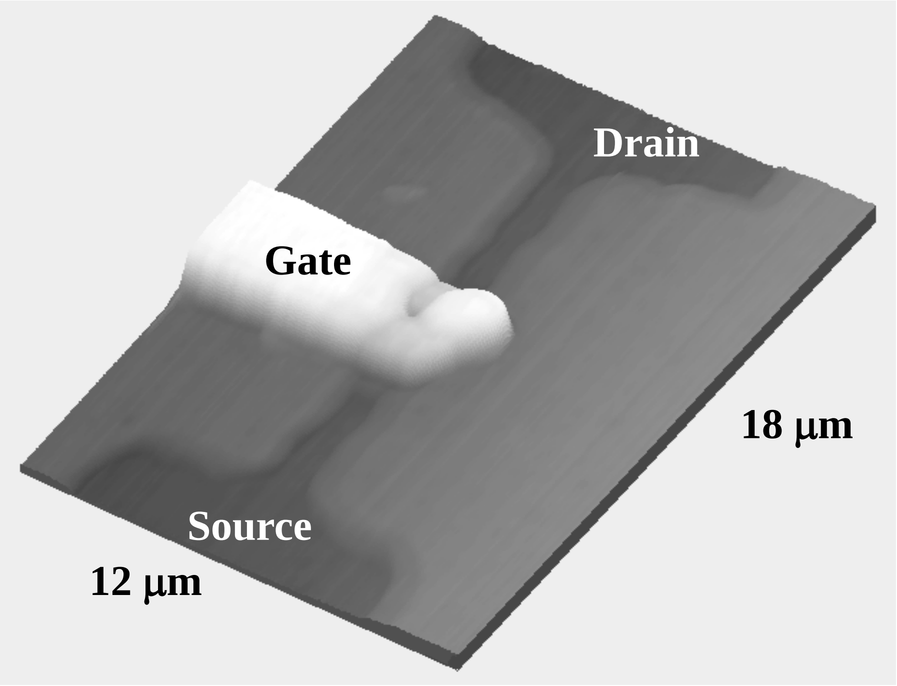

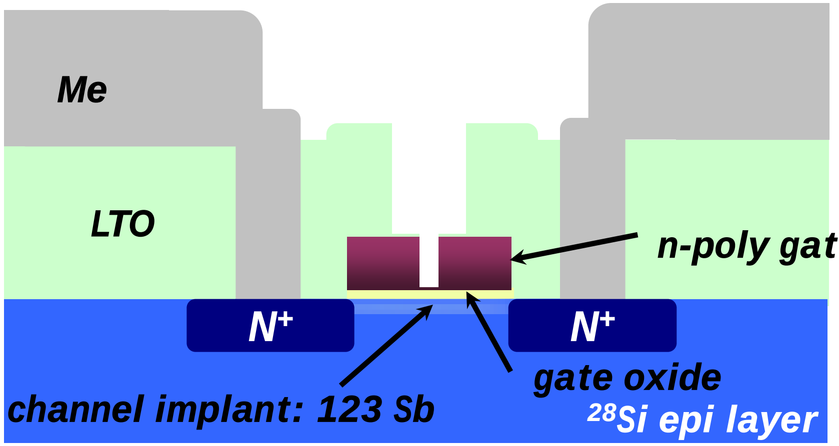

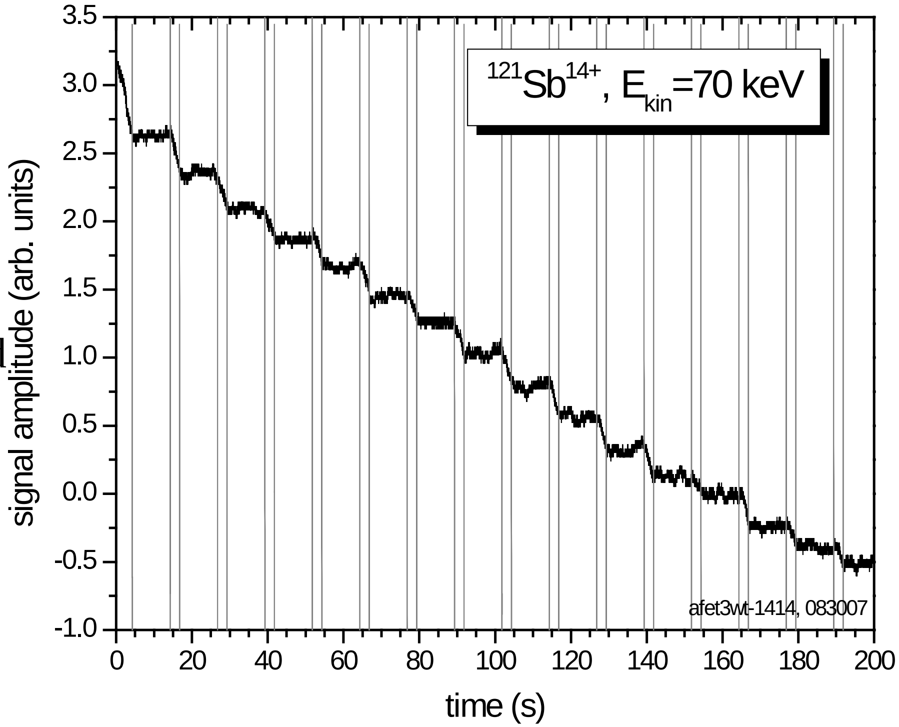

- single ions deposit charges in the gate oxide, fixed charges lead to effective gate field increases, increasing channel currents (I_{sd} in plot on right is inverted)
- detection of current transients from single ion impacts (dI~ few 10^{-4} dI/I, in 2x2 μm aFets at room temperature)

Single ion impact detection at room temperature in sub-100 nm scale FinFets

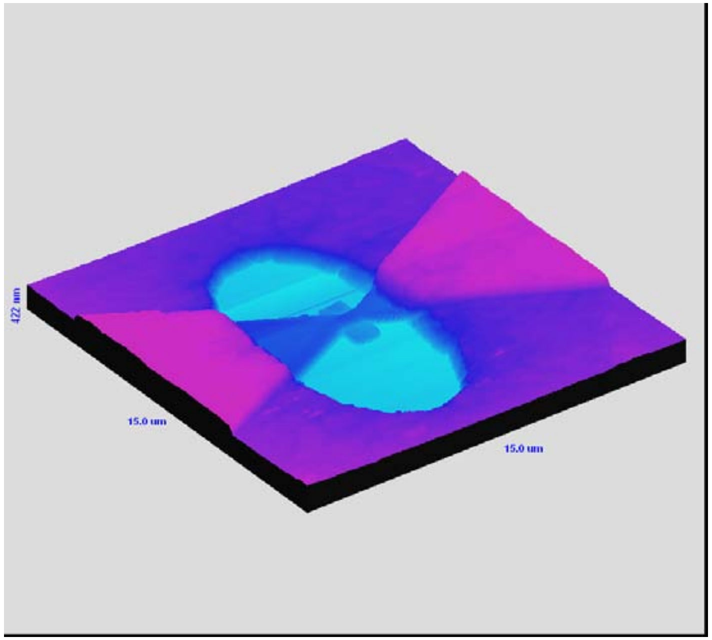

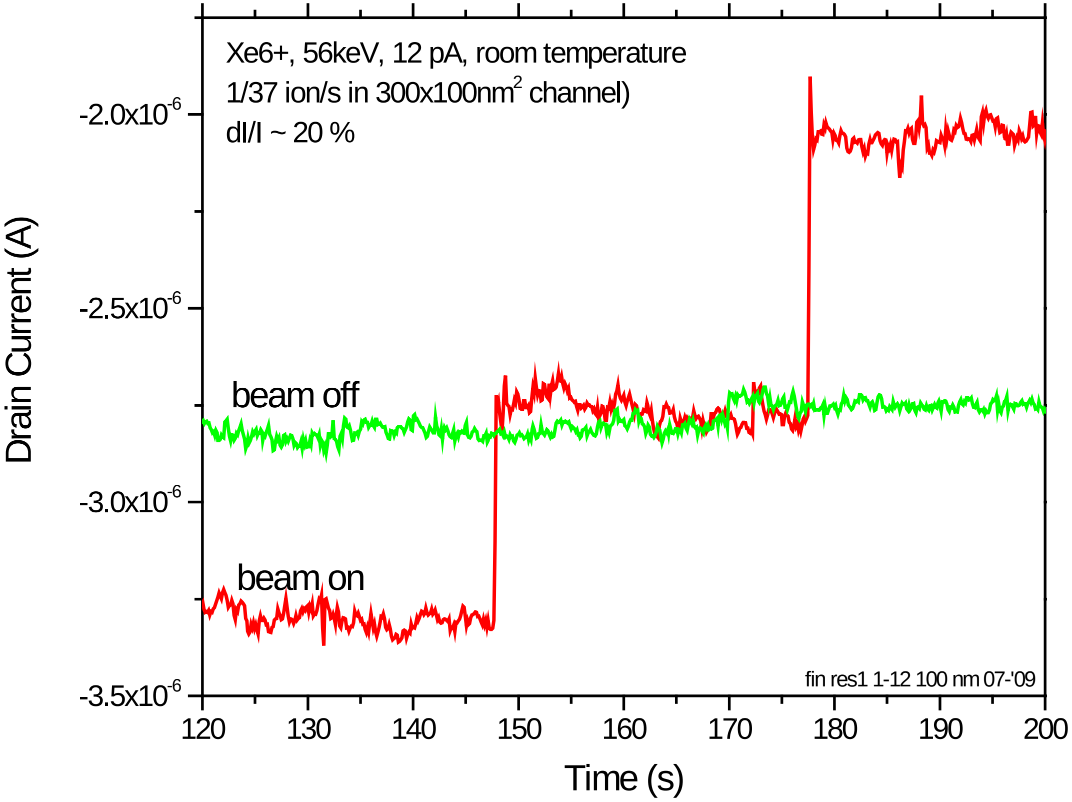

Left: in situ scanning probe image of FinFet structure
Right: Single ion impact signals from a FinFet at room temperature

Deterministic Doping – Single Ion Implantation

1. Exact numbers of dopants
2. **In precise locations in a device**
3. All electrically active
4. And no other sources of variability are introduced during processing

Single Ion Placement with Scanning Probe Alignment

- Non-destructive imaging and nm-apertures for nm-accuracy

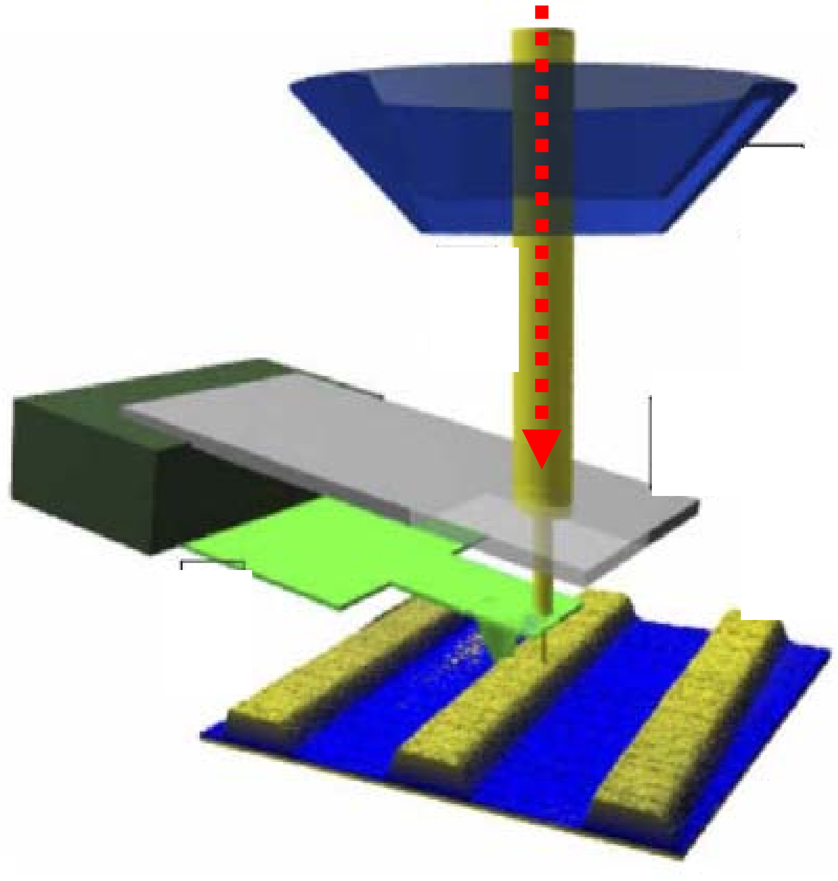

A. Persaud, et al.,
Nano Letters 5, 1087 (2005)

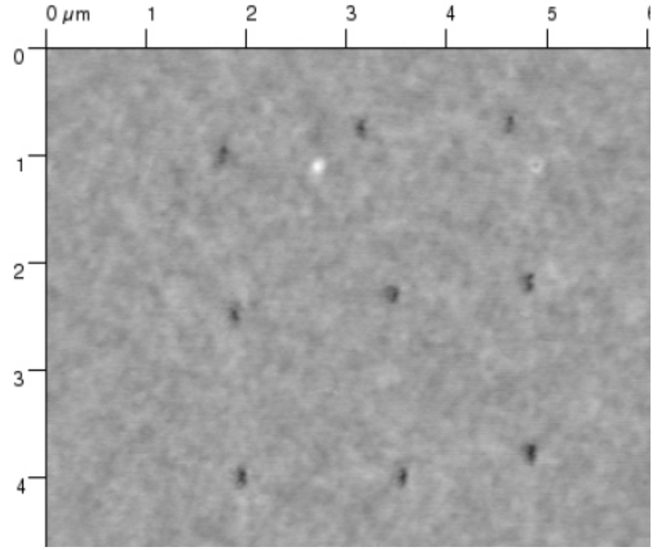

array of 90 nm dots in PMMA from ion implantation with scanning probe alignment

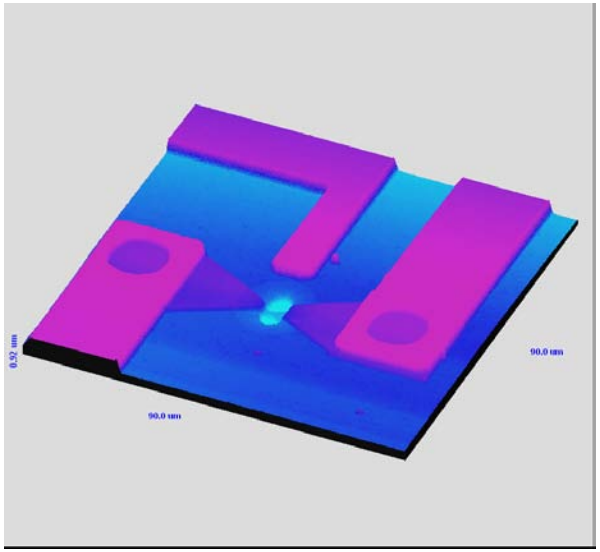

in situ scanning probe image of a FinFet

Ion Implantation with Scanning Probe Alignment

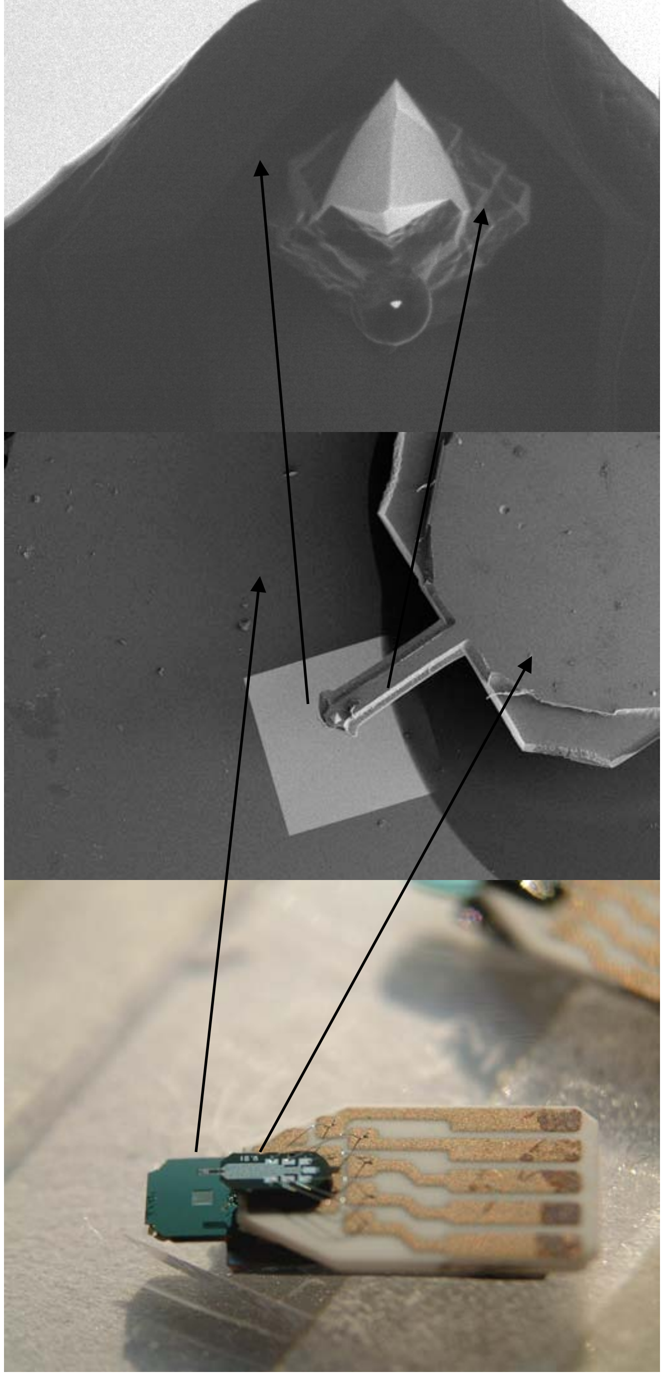

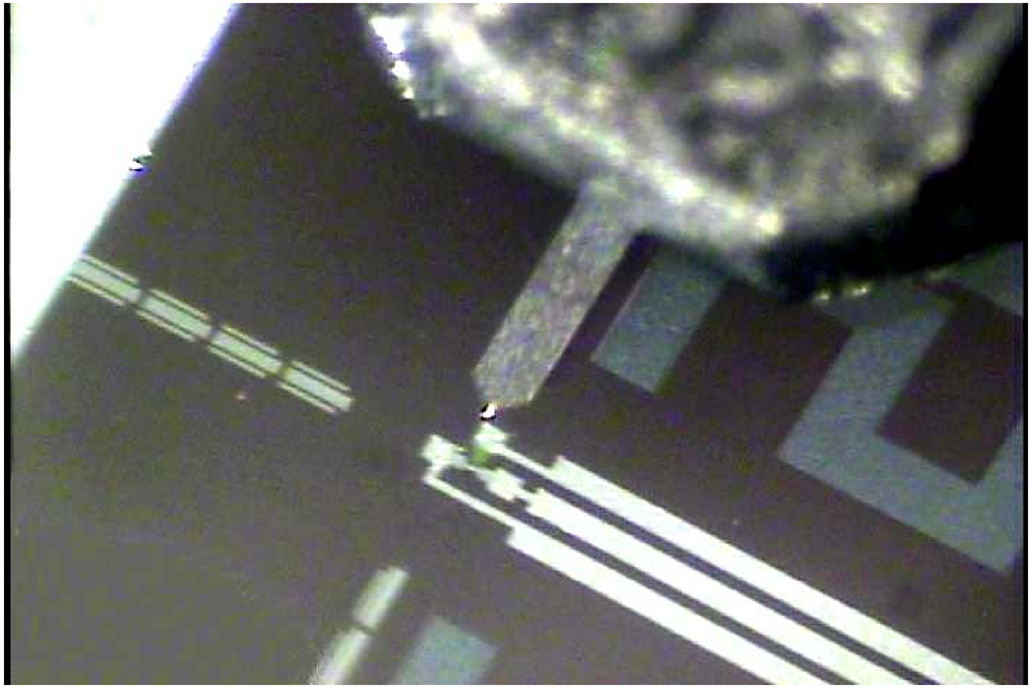

- Single Ion Implantation with Scanning Probe setup connected to high vacuum beam line
- scan range of target stage is 0.1 x 0.1 mm^2
- probe tip can be moved across 1 mm field
- piezo-cantilevers co. I. Rangelow, University Ilmenau
- holes down to 2 – 5 nm diameters by FIB and TEM processing
- integration of many cantilevers in parallel under development

Deterministic Doping – Single Ion Implantation

1. **Exact numbers of dopants**
2. **In precise locations in a device**
3. **All electrically active**
4. **And no other sources of variability are introduced during processing**

Dopant diffusion – intrinsic vs. TED, OED, ORD

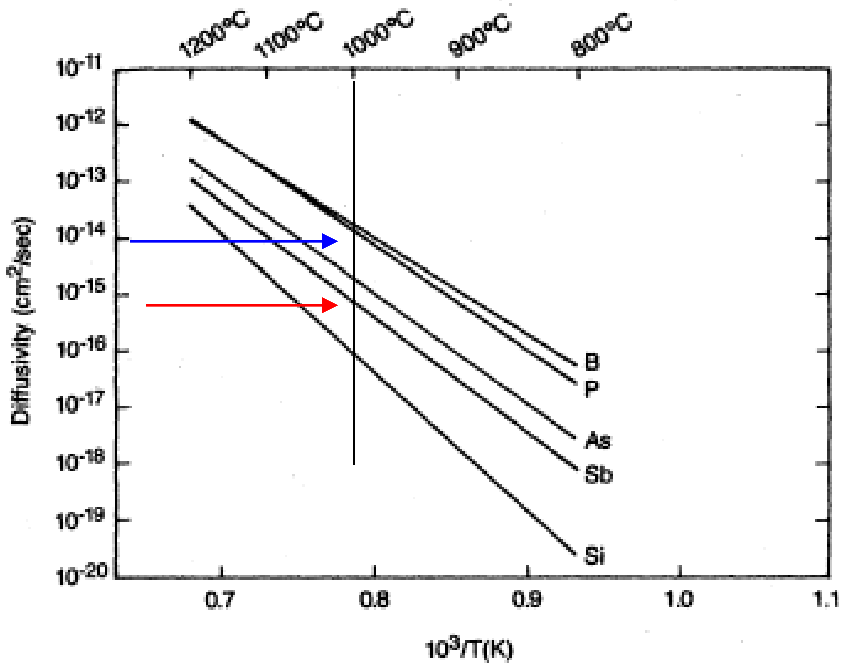

FIG. 10. Experimental values of self- and dopant diffusivity under intrinsic doping conditions. An analytic expression for self-diffusion is given in Eqs. (9.7) and (9.8). Expressions describing dopant diffusivities under intrinsic and extrinsic conditions are summarized in Appendix B.

- dopants diffuse through coupling to defects

- **P**: interstitials → OED
- **Sb**: vacancies → ORD
- **As**: vacancy – interstitial mix

Fahey, Griffin, Plummer,
Rev. Mod. Phys. 1989

Carrier profiles of Phosphorus implants in ^{28}Si – ORD vs. OED

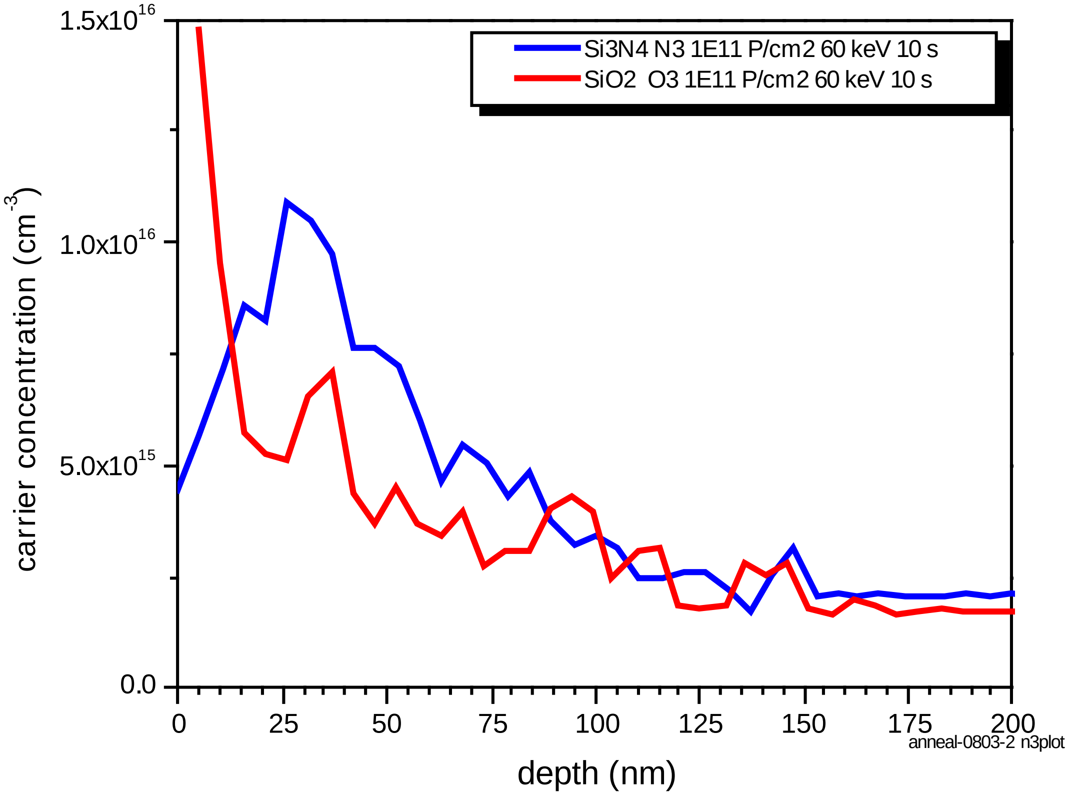

- Spreading Resistance Analysis of carrier concentration shows 80% activation of a P implant (60 keV, 1E11 cm^{-2}) after RTA at 1000 ºC for 10 s
- Si_3N_4 gate dielectric film retards defect mediated diffusion, SiO_2 enhances it
- S.-J. Park et al., Microelectronic Engineering 73–74 (2004) 695–700

SIMS of low dose Phosphorus implants in 28-Si

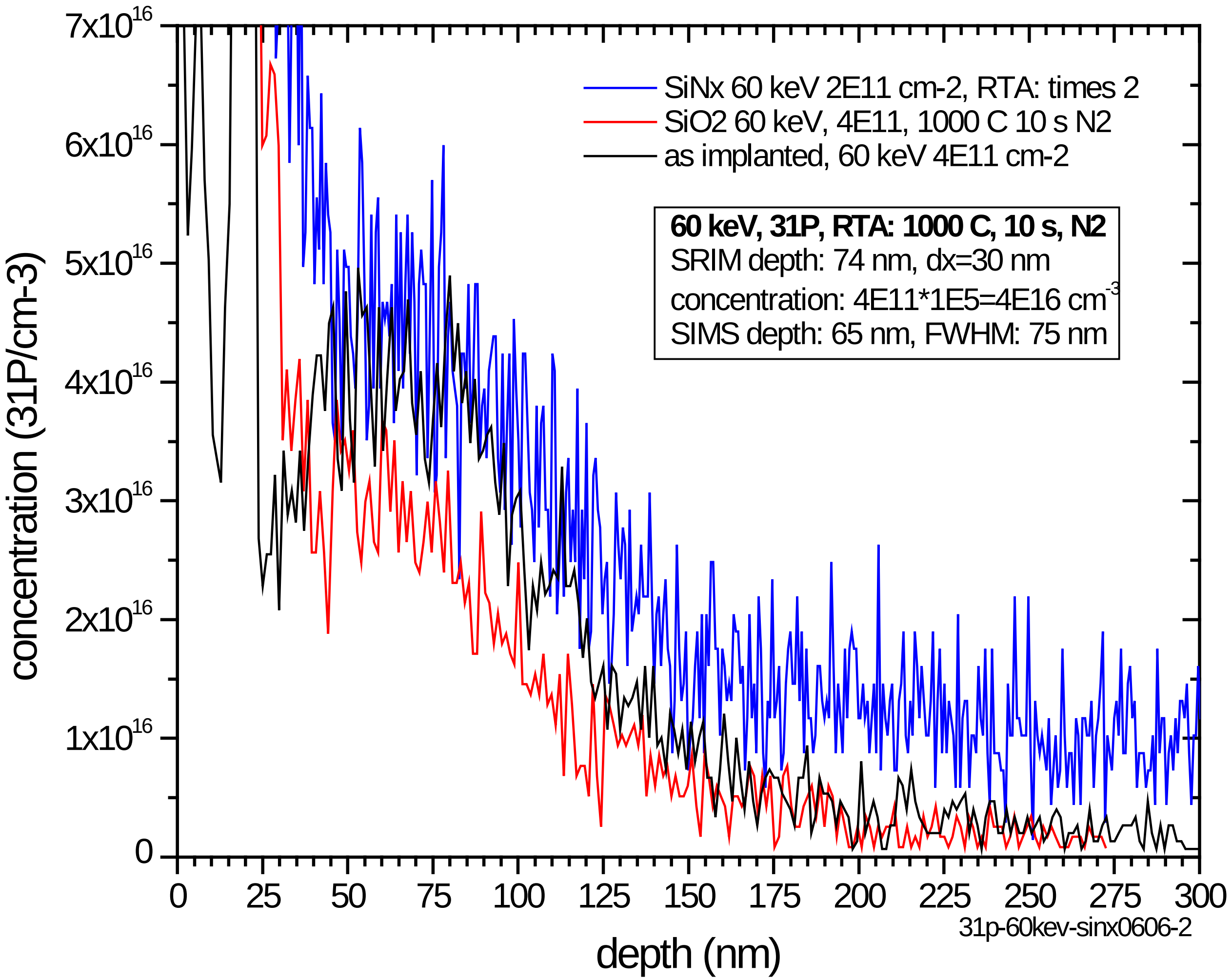

60 keV, 31P, RTA: 1000 C, 10 s, N2
SRIM depth: 74 nm, dx=30 nm
concentration: 4E11*1E5=4E16 cm^{-3}
SIMS depth: 65 nm, FWHM: 75 nm

- metrology challenging in low dose regime (<1E12 cm^-2) important for single atom devices
- SIMS of low dose 31P has to avoid mass interference at 31 u from 30SiH
- use of 28Si avoids this problem
- Nucl. Instr. Meth. B 267, 2563 (2009)

tracking dopant profiles during thermal processing, Sb shows minimal diffusion / segregation among shallow donors in silicon

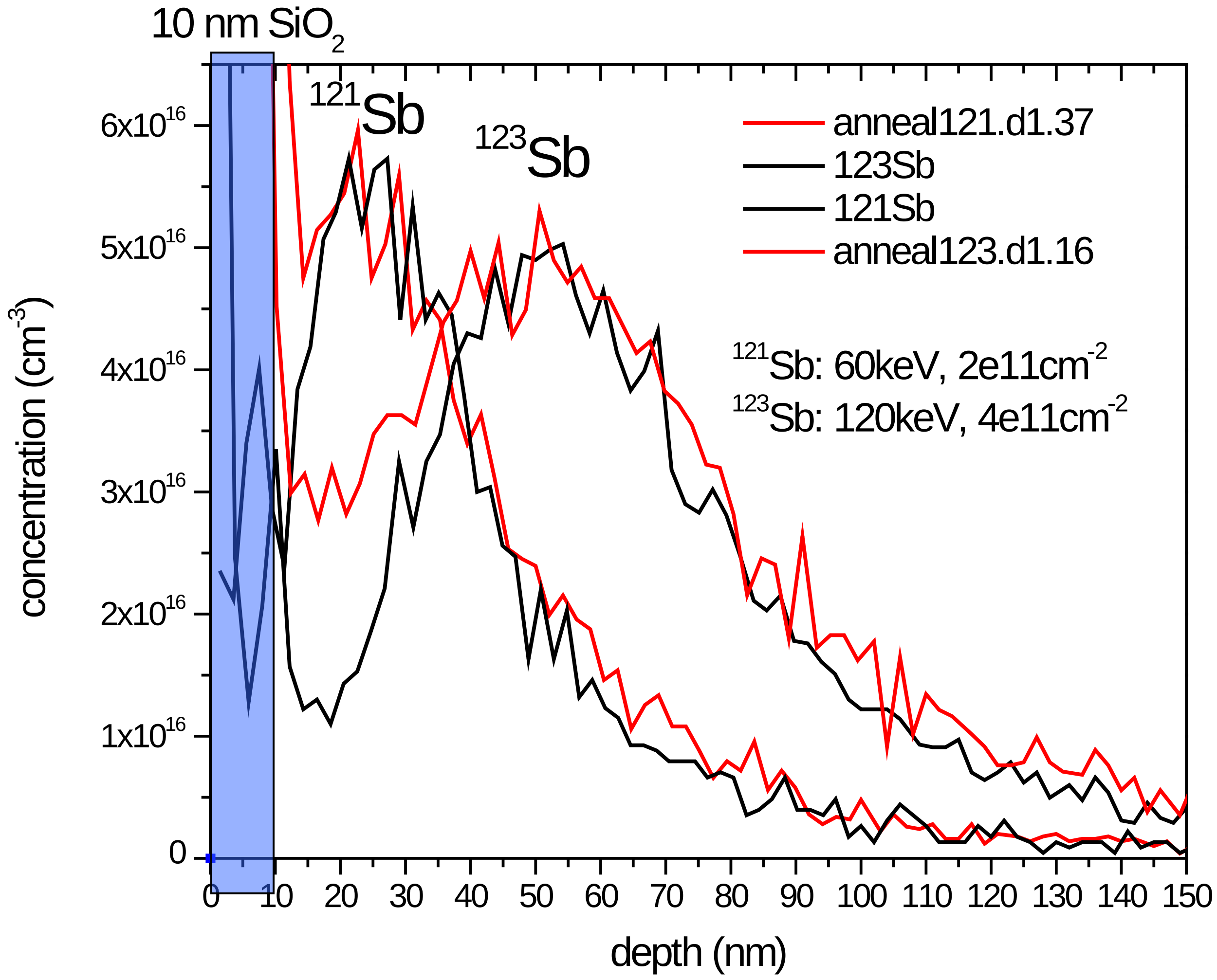

- SIMS depth profile of 121-Sb atoms as implanted and after annealing at 850º C for 10 s

SIMS of P, As and Sb from a test structure on a spin readout Fet chip

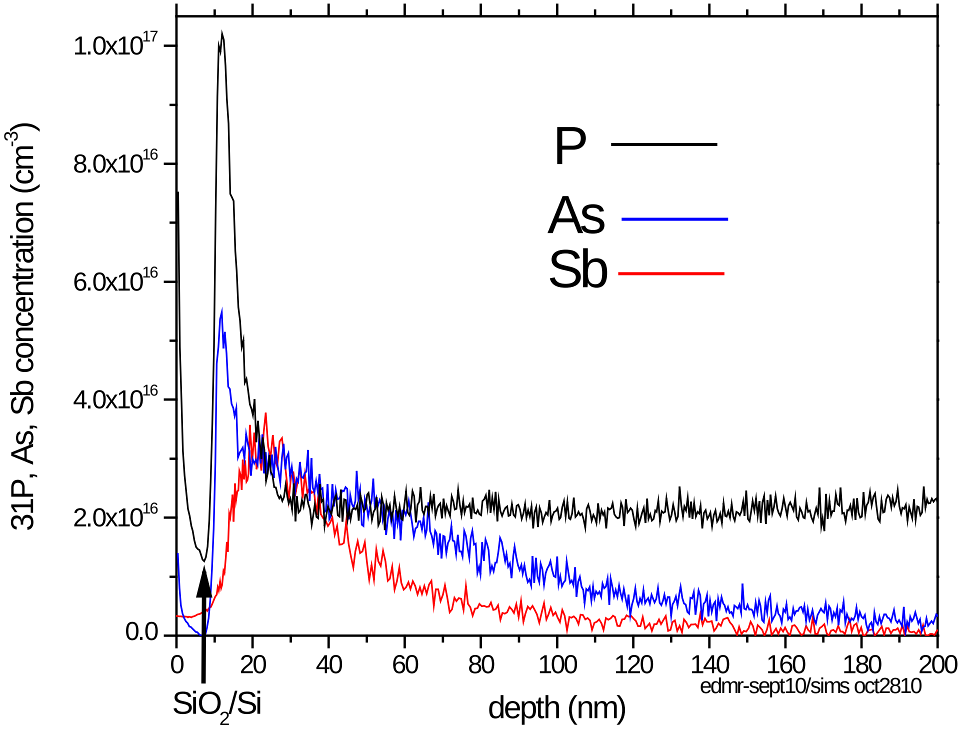

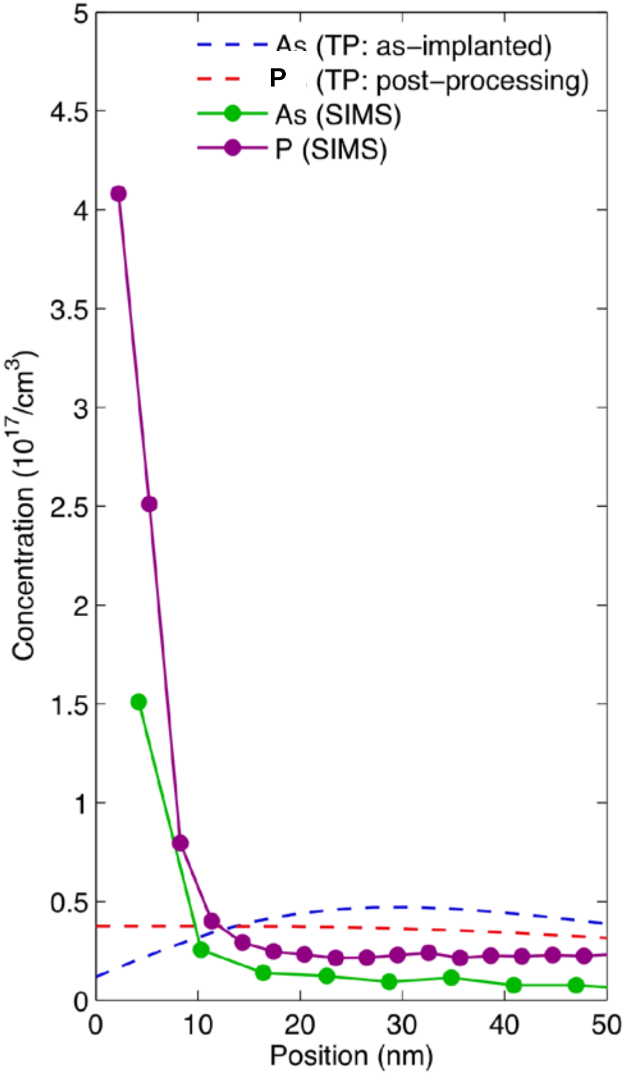

- As and Sb channel implants
- P present as 2E16 cm^-3 background doping in the 28Si epi layer
- a 20 nm gate oxide was growth after channel implants plus additional anneal at 1000 C for 20 min. to increase mobility
- segregation of P and As is not captured in process simulations

Probing donor spins with Electrically-Detected Magnet Resonance (EDMR)

- Accumulation-mode Field Effect Transistors (aFETs)
  - Neutral donors in channel, gate-tunable conduction electron (2DEG) density (polarization)
  - Strength of EDMR (vs. tunneling): spectroscopic signature of donor species and optimization for scaling from large ensembles to single donor
  - Access to small spin numbers and probing of spin quality

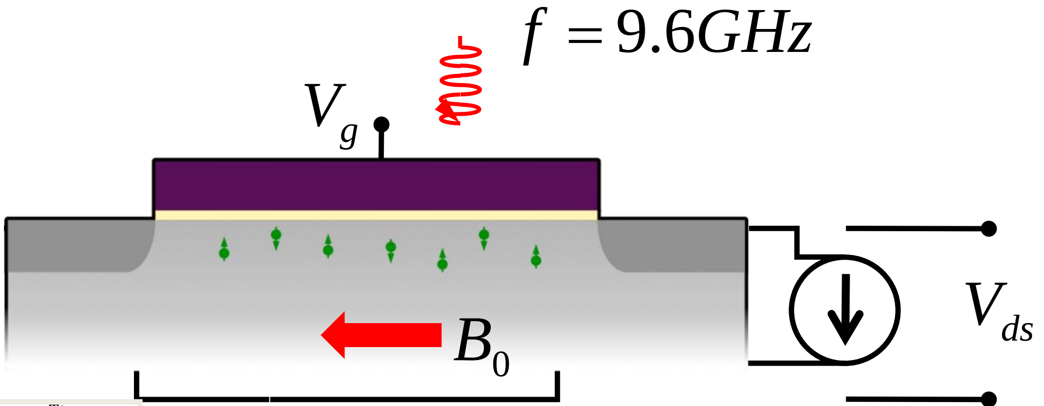

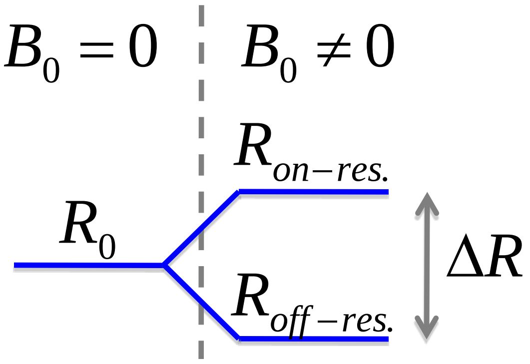

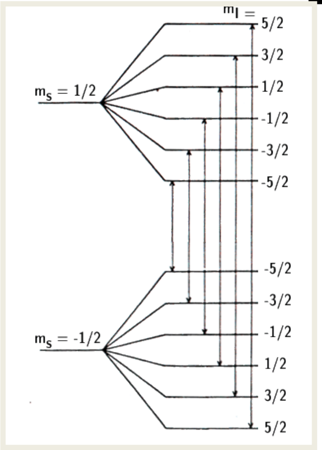

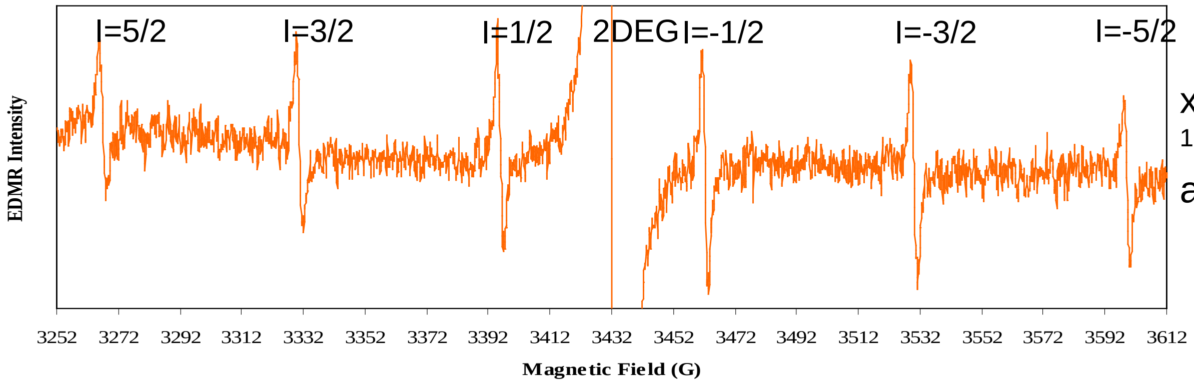

x-band EDMR with ^{121}Sb implanted aFets at 5 K

- C. C. Lo, et al., Appl. Phys. Lett. (2007)

Deterministic Doping – Single Ion Implantation

1. **Exact numbers of dopants**
2. **In precise locations in a device**
3. **All electrically active**
4. **And no other sources of variability are introduced during processing**

damage recovery after FIB processing and single ion implant runs

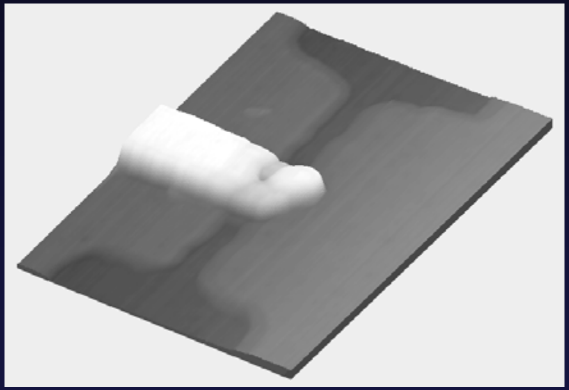

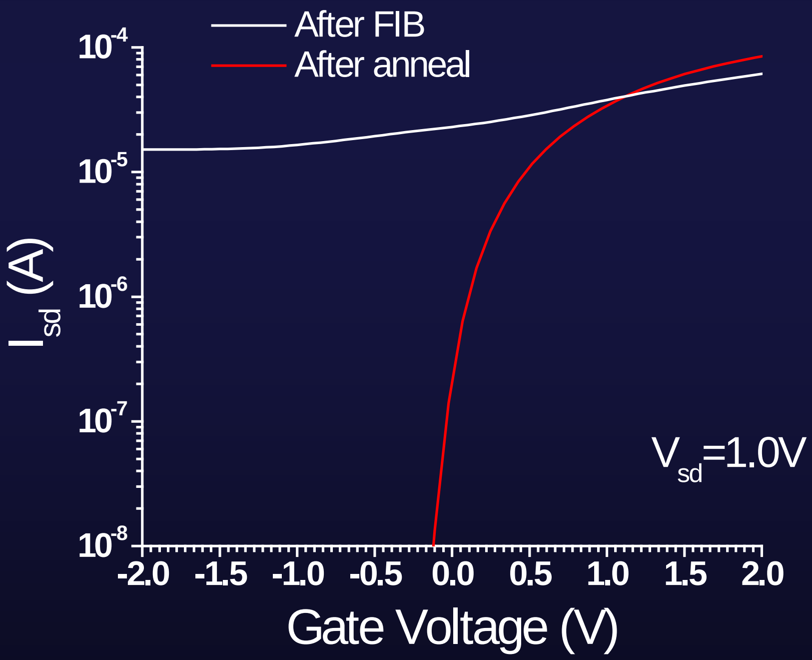

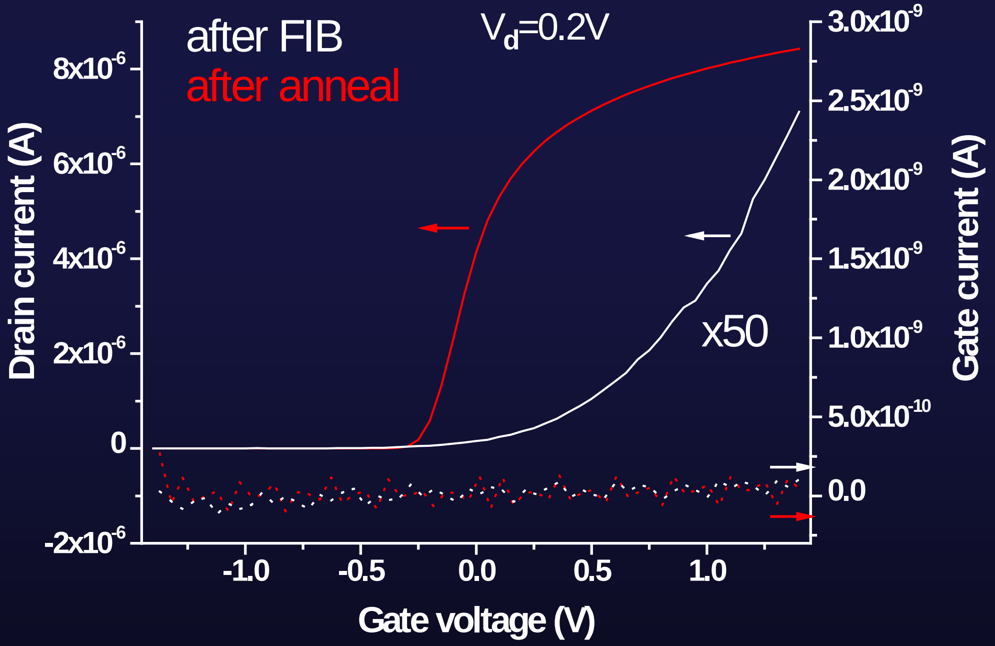

- need to keep track of all other sources of variation and/or need to have single dopant sensitivity in device characterization

Low temperature transport studies

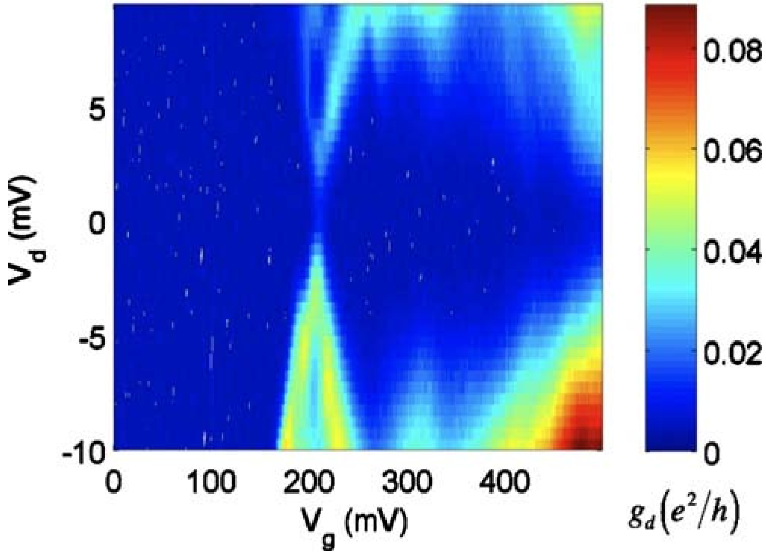

- we know that you want solutions for room temperature devices
- we know that you know that we like to do basic research
- the merit of low temperature magneto-transport research:
  - → Enhance understanding of single dopant transport effects
    - → impact on scaled CMOS processing
  - → Exploration of disruptive, post-CMOS device concepts
    - → quantum computing with electron and nuclear spins
    - → quantum – classic hybrids
    - → classical spin logic

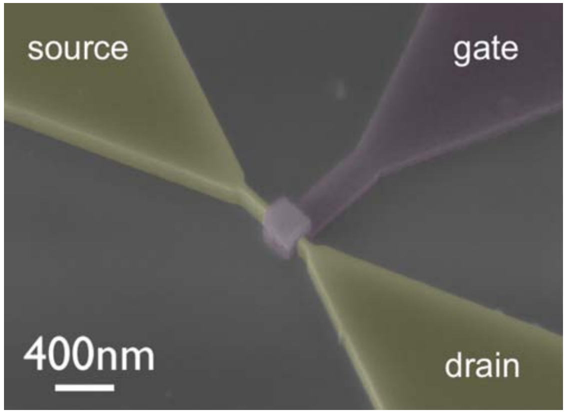

Transport measurements (4.2K)

- Two devices show strong resonance peaks *after* turn-on:

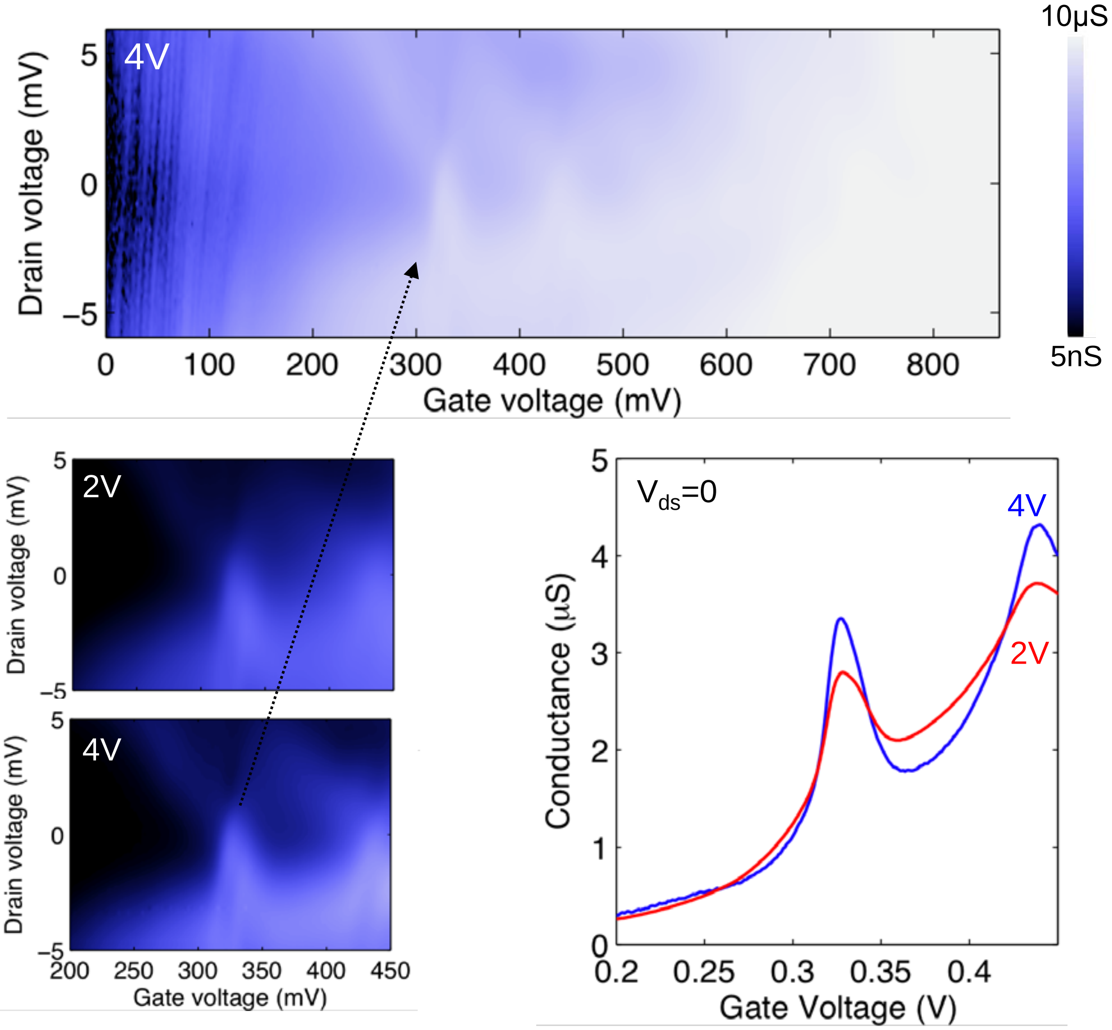

$$l_l = 76\text{nm}, w_l = 50\text{nm}$$

FinFets with spin injection side gates, EDMR studies in progress …

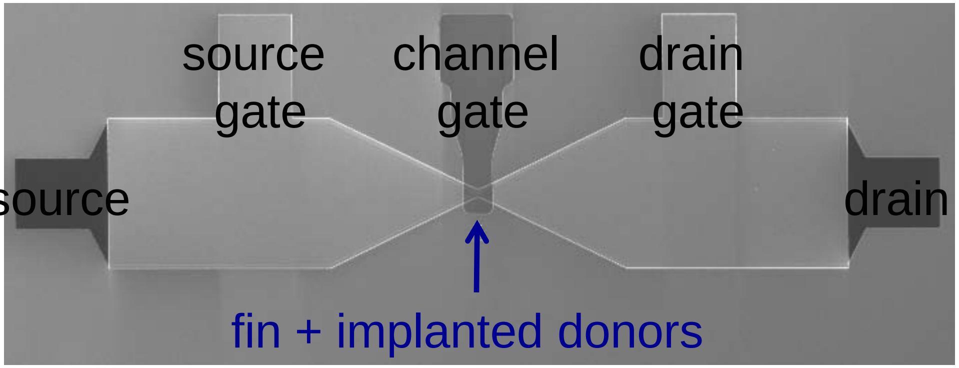

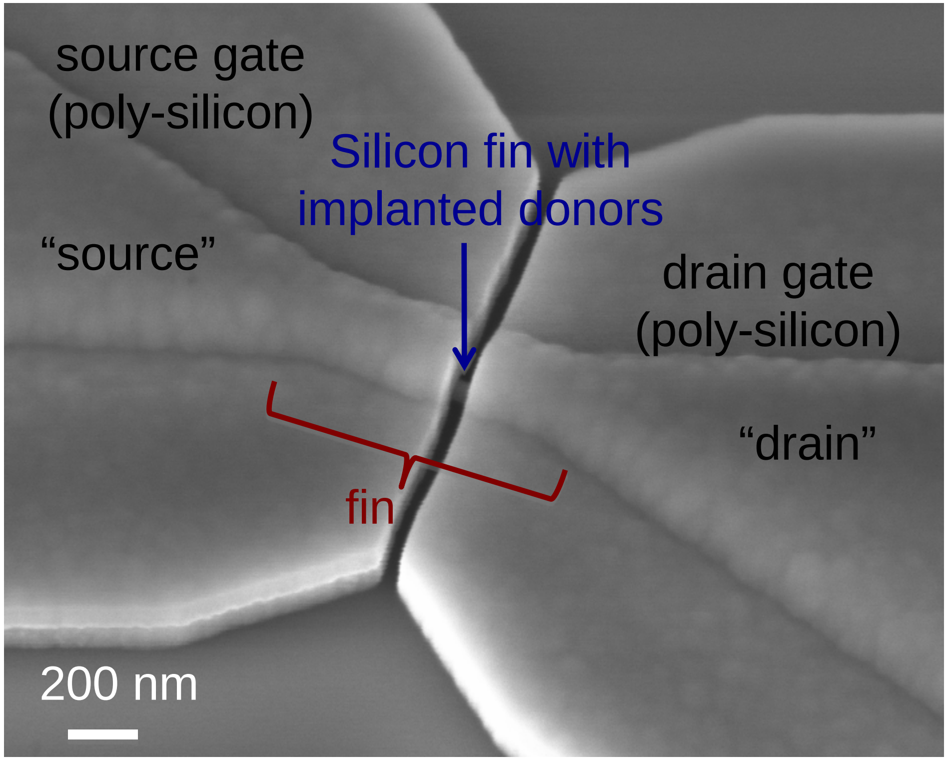

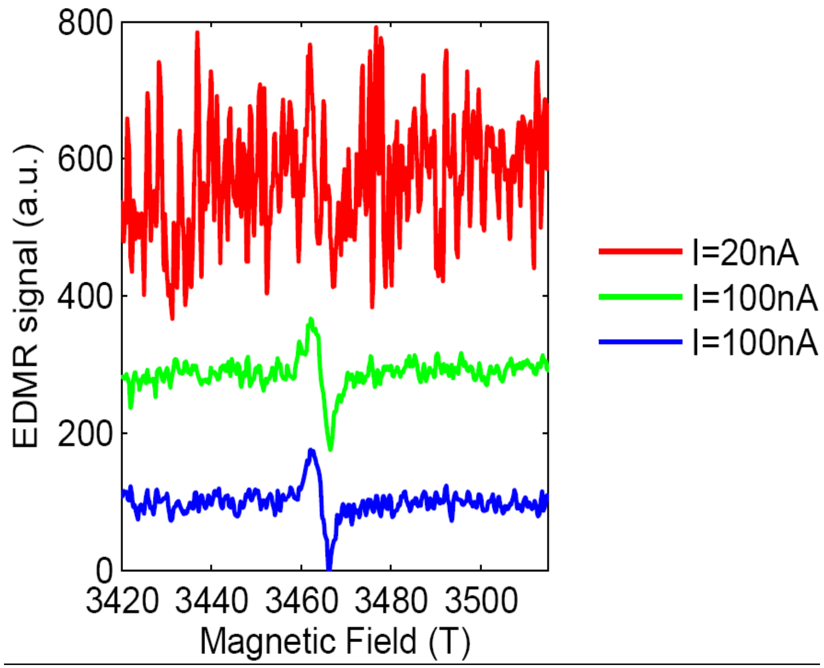

- x-band EDMR data from FinFETs, 2DEG signal only (incl. some contribution form sides gates)
- side gates enable future implementation of spin injection contacts without inducing large inhomogeneous broadening
- side gates eliminate random donor in-diffusion from n+ doped contact regions into the channel, enabling ultra-short channels
- single donors in scaled FinFet channels approximate tunable quantum dots

Outlook: Deterministic Doping – Single Ion Implantation

1. **Implant exact number of dopants into devices - detect every ion**
   - Key issue: detection efficiency, speed, counting overhead
   - Single ion detection by
     - Detection of secondary electrons (or photons), or detection of electron – hole pairs
     - Detection of changes in transistor channel currents
     - Imaging of surface topography changes
2. **Control the precise location of dopants**
   - Key issue: placement precision, position retention during thermal processing, implant induced damage and associated performance variations
   - Sources of positioning errors
     - Implantation spot size - Mask opening or focused beam spot size
     - Range straggling - Lower for heavier ions and lower implant energies
     - Diffusion and segregation during annealing, specific for dopant species
3. **Ensure every dopant is electrically active and**
4. **Control all other sources of variability during processing**
   - implant induced damage, mobility changes, …
   - (low temperature) magneto-transport and spin resonance techniques can aid understanding of single dopant transport effects and be useful for process engineering

→ **Opportunities to explore Post-CMOS device concepts**

Acknowledgments

- **Graduate students**
    - Christoph Weis
    - Cheuk Chi Lo
- **Special thanks to**
    - Staff of the UC Berkeley Microlab
    - Staff of the LBNL-NCEM
    - Staff of The Molecular Foundry
- **Contact:** T_Schenkel@LBL.gov

- **Team members**
    - Jeff Bokor, UC Berkeley & Molecular Foundry
    - Steven Lyon, Princeton University
    - Alexei Tyryshkin, Princeton University
    - Birgitta Whaley, UC Berkeley
- **Collaborators**
    - Ivan Chakarov, Silvaco, Santa Clara, CA
    - Ivo Rangelow, Technical University Ilmenau

This work is supported by LPS-NSA and DOE

- Backup slides

Outlook

- **potential application opportunities - (What is the potential impact on ITRS?)**
  - deterministically doped Fets in mass production ? Probably not.
  - alternatives to channel dopants: e. g. fully depleted planar SOI
    - with many remaining challenges e. g. diffusion of dopants form S/D contacts
  - value of R&D in deterministic doping and single atom device research
    - understanding transport (including at low T) in scaled devices enables us to understand, track and reduce sources of performance variability
    - potentially disruptive device concepts emerge in the limit of single atom dominated devices
      - both for post-CMOS classical, quantum and classical-quantum hybrid logic and memory concepts
- **Challenges and potential solutions for the next 10 – 15 years**
  - demonstration of viable post-CMOS strategies
    - new state variables
    - single atom device concepts
    - multi-qubit quantum logic demonstrations with single atom qubits

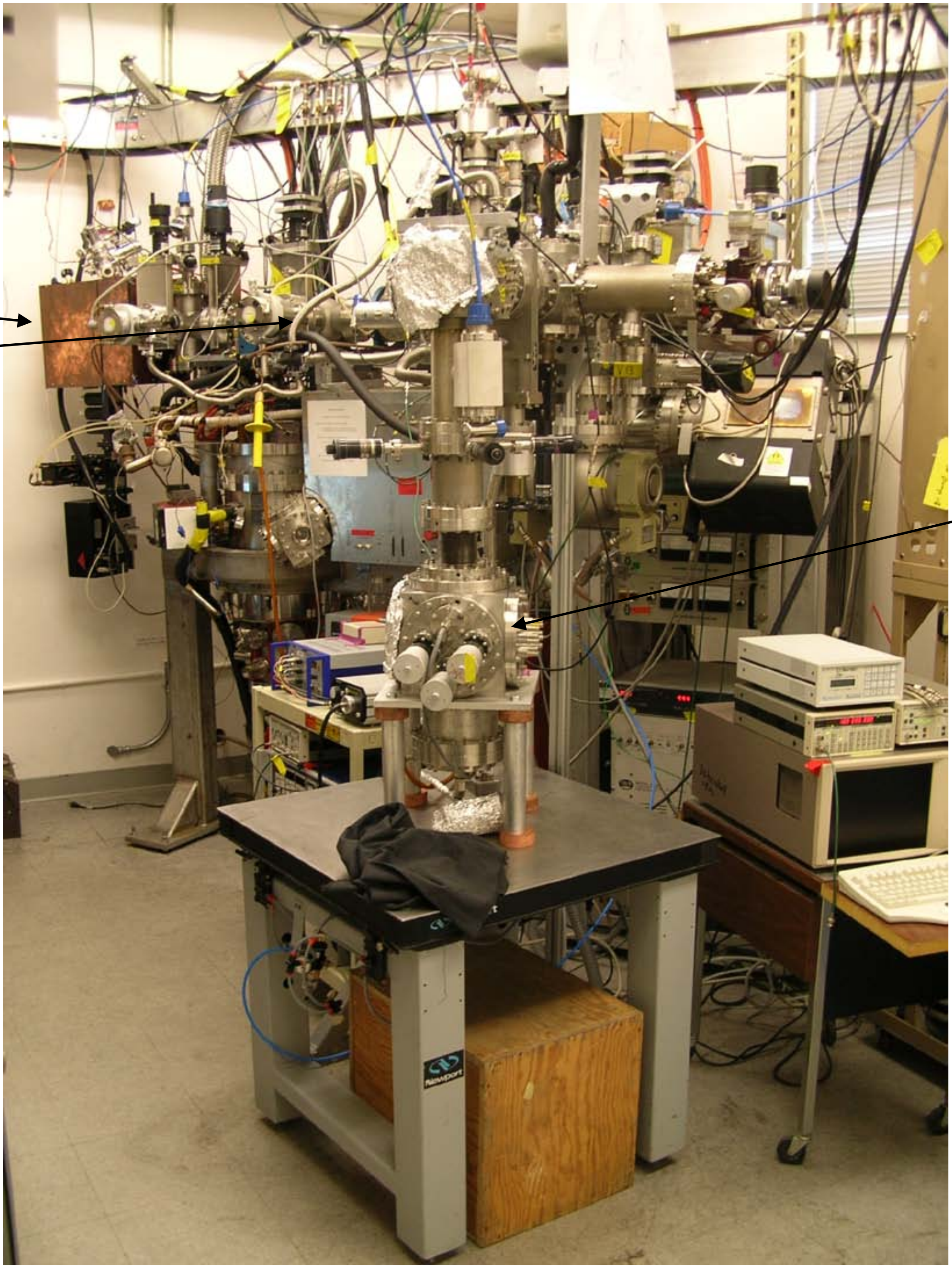

Ion sources
and beam line

Single ion implant
chamber with AFM

- C. C. Lo, A. Persaud, S. Dhuey, D. Olynick, F. Borondics, M. C. Martin, Hans. A. Bechtel, J. Bokor, and T. Schenkel, “Device fabrication and transport measurements of FinFets built with 28-SOI wafers towards donor qubits in silicon”, Semicond. Sci. Technol. 24, 105022 (2009)
- T. Schenkel, C. C. Lo, C. D. Weis, A. Schuh, A. Persaud, and J. Bokor, “Critical issues in the formation of quantum computer test structures by ion implantation”, Nucl. Instr. Meth. B 267, 2563 (2009)
- C. D. Weis, A. Schuh, A. Batra, A. Persaud, I. W. Rangelow, J. Bokor, C. C. Lo, S. Cabrini, D. Olynick, S. Duhey, and T. Schenkel, “Mapping of ion beam induced current changes in FinFETs”, Nucl. Instr. Meth. B 267, 1222 (2009)
- C. D. Weis, A. Schuh, A. Batra, A. Persaud, I. W. Rangelow, J. Bokor, C. C. Lo, S. Cabrini, E. Sideras-Haddad, G. D. Fuchs, R. Hanson, D. D. Awschalom, and T. Schenkel, “Single-atom doping for quantum device development in diamond and silicon”, J. Vac. Sci. Techn. B 26, 2596 (2008)

Outlook: Towards -*coherent*- single atom devices

- single atom device development requires a method for reliable single atom doping

- desired are high spatial resolution and flexibility in dopant species, as well as 100% single dopant detection

- ion implantation with scanning probe alignment, combined with single ion impact sensing through monitoring of 2DEG upsets is a universal tool for single atom placement

- this enables systematic studies of dopant fluctuation effects and tests of quantum computer architectures (qubit readout, control & coupling) in e. g. silicon and diamond

EAG℠

Bi depth profiling after PAI and SPER – nice single atom placement control due to minimal straggling

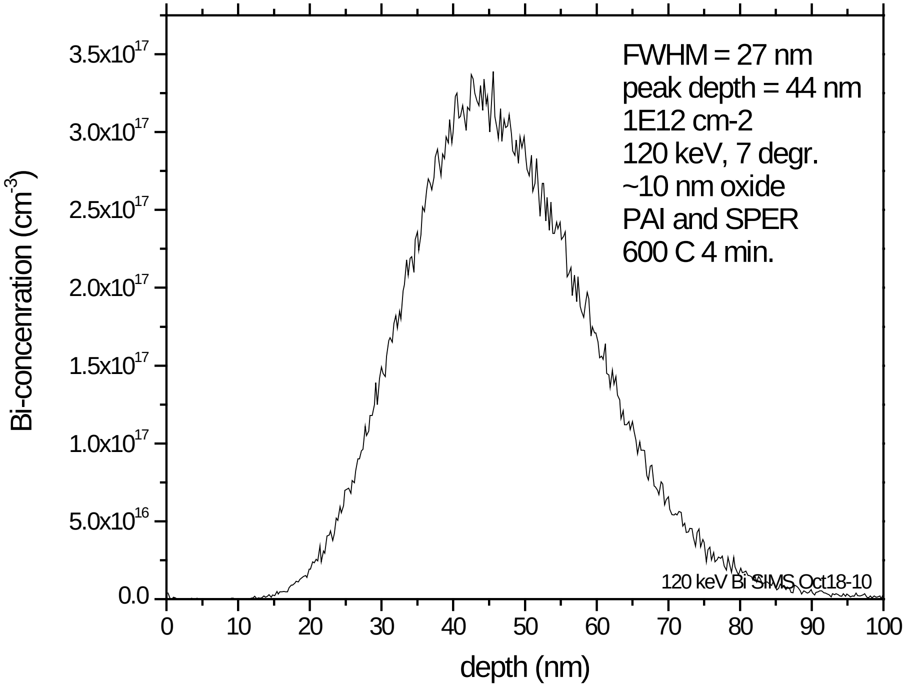

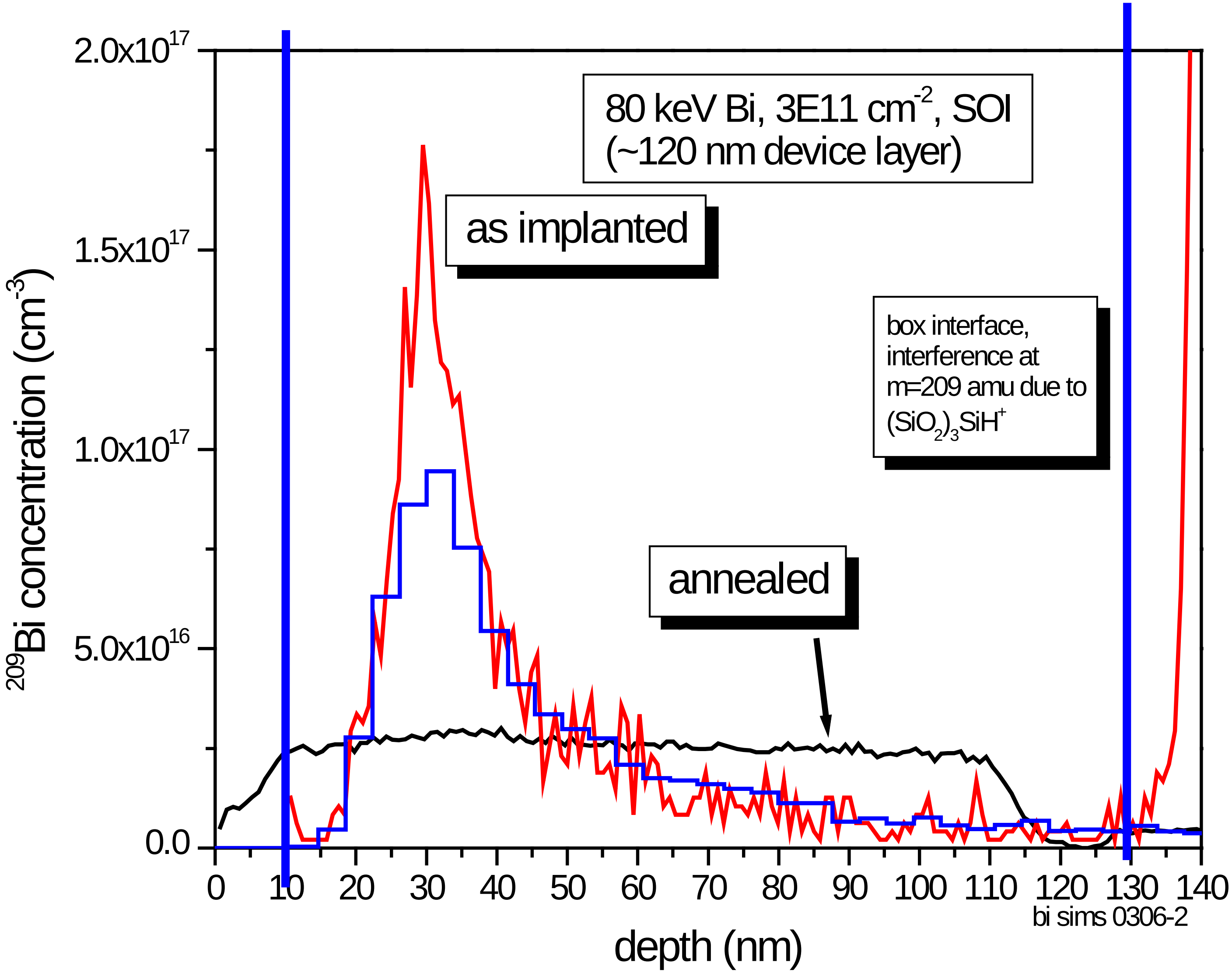

RTA: 1000 C, 10 s, N2

Box seems to be worse in driving Bi segregation !

Spatially resolved, *in situ* monitoring of (single) ion implantation

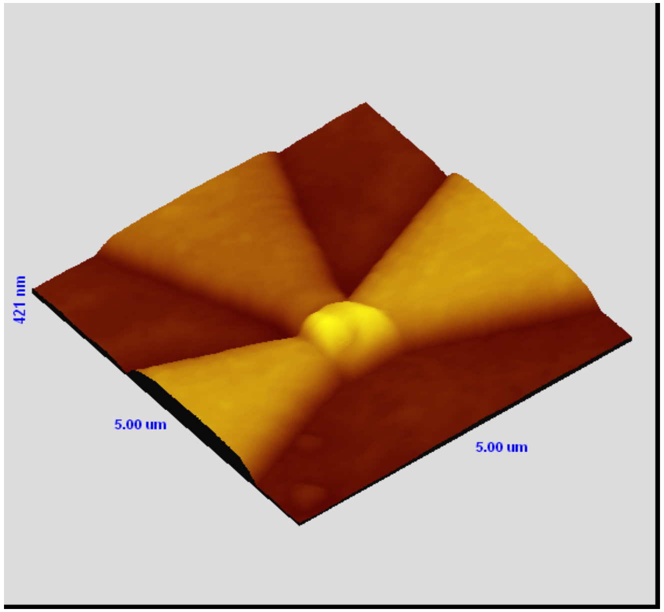

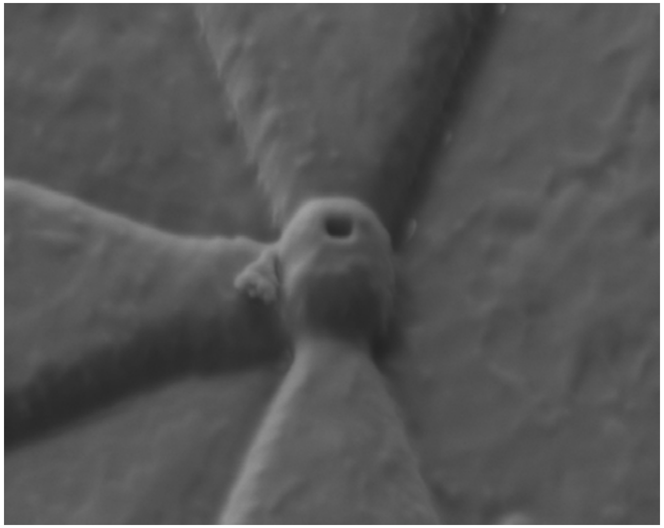

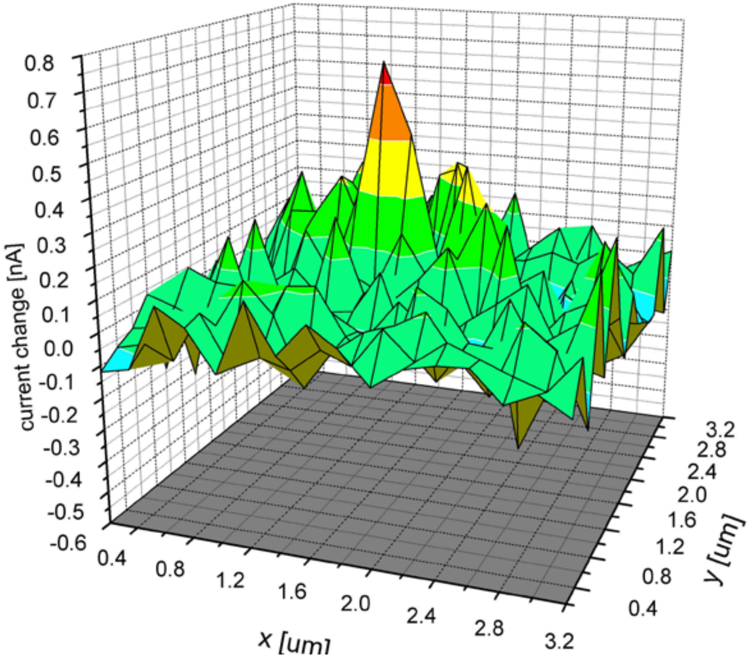
(08_07_3:28pm) 3x3um^2, 16x16 dots, 100nm hole, 30s beam on, Ar2+

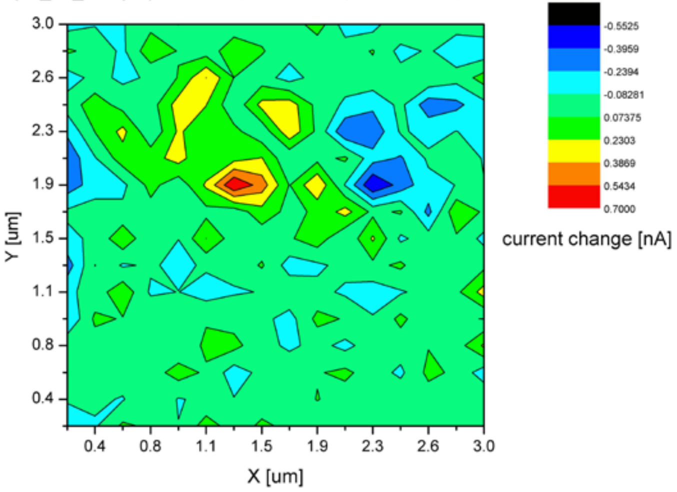
(08_07_3:28pm) 3x3um^2, 16x16 dots, 100nm hole, 30s beam on, Ar2+

SIMS depth profile of antimony from a test structure on a spin readout Fet chip

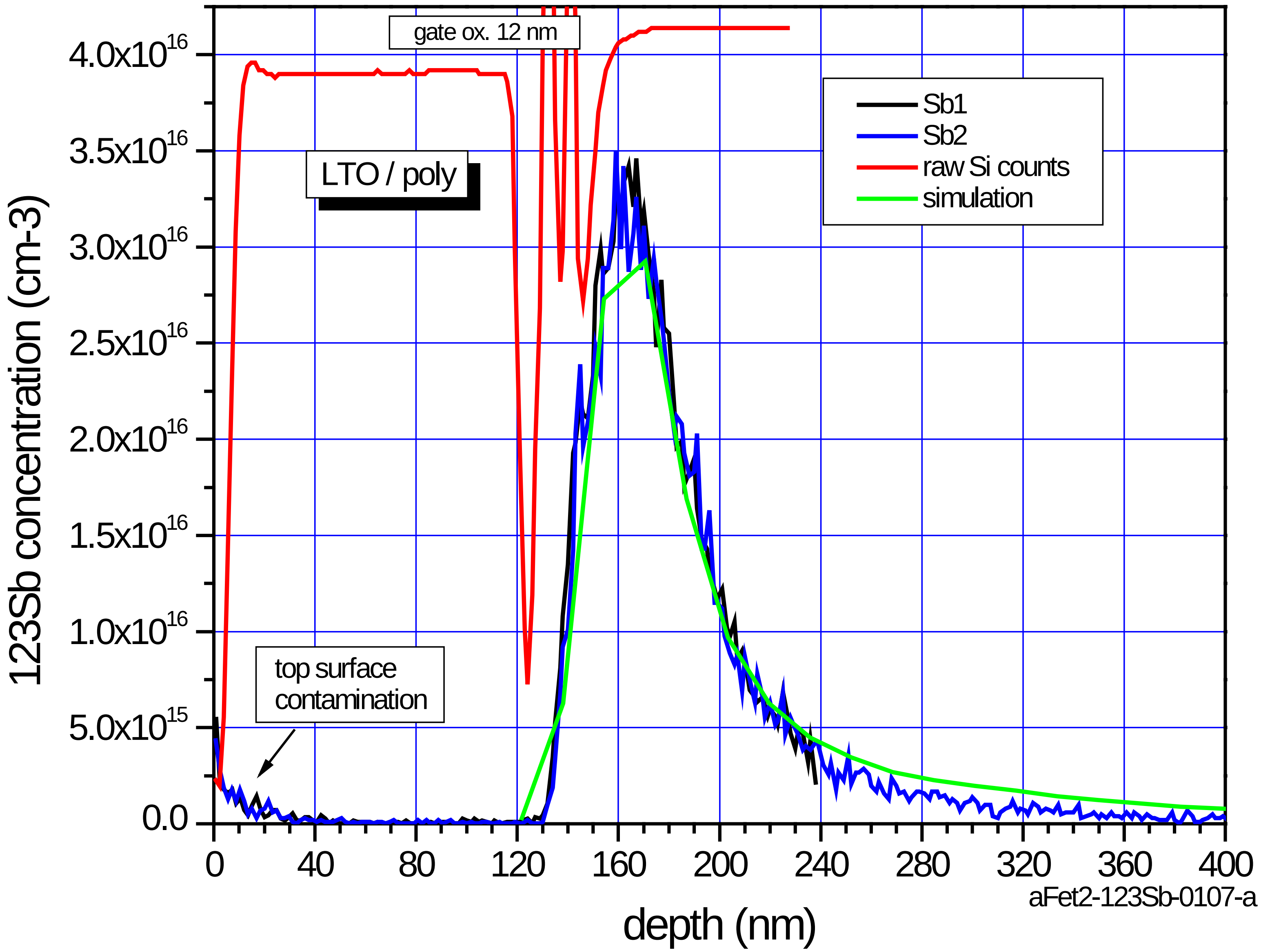

-minimal diffusion of Sb under full thermal budget in FET processing

Controlled Nanoscale Doping of Semiconductors by *Molecular Monolayers*

Ali Javey

Electrical Engineering and Computer Sciences
Berkeley Sensor and Actuator Center (BSAC)

University of California at Berkeley

The need for a new nanoscale doping process

- **Conventional Ion Implantation**
  - Accurate dose control
  - Induced crystal lattice damage
  - Clustering of group III elements and desorption of group V elements
  - Difficult to achieve ultrashallow junctions and uniform doping in nonplanar devices

- **Conventional Surface Doping (e.g. SOD)**
  - Does not induce lattice damage
  - Hard to control dopant dose
  - Often leaves residues/contaminants on the surface
  - Poor uniformity

- **Monolayer Doping (Berkeley Approach):**
  - Utilization of self-limiting monolayers
  - Compatible with planar and non-planar structures
  - High dopant dose uniformity and control

Monolayer Doping of Semiconductors

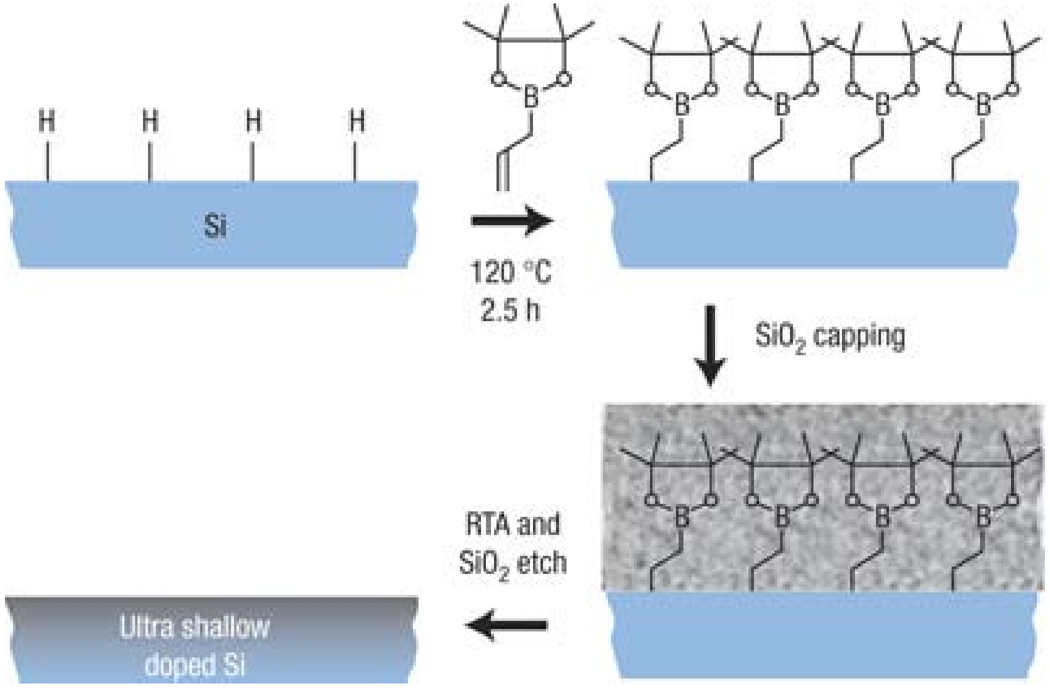

Strategy:

1. **Dopant monolayer formation on Si**
2. **Capping with SiO_2 cap**
3. **RTA to diffuse the B atoms**

Unique Features

- ☐ **Lack of damage to the lattice**
- ☐ **Ultrashallow Junction Formation**
- ☐ **Precise control over the dose at nanoscale**
- ☐ **Self-limiting process**

Chemistry is important!

Johnny Ho, et al, Nature Materials, 2008.
Johnny Ho, et al, Nano Letters, 2009.
Johnny Ho, et al, APL, 2009.

Surface Analysis by XPS

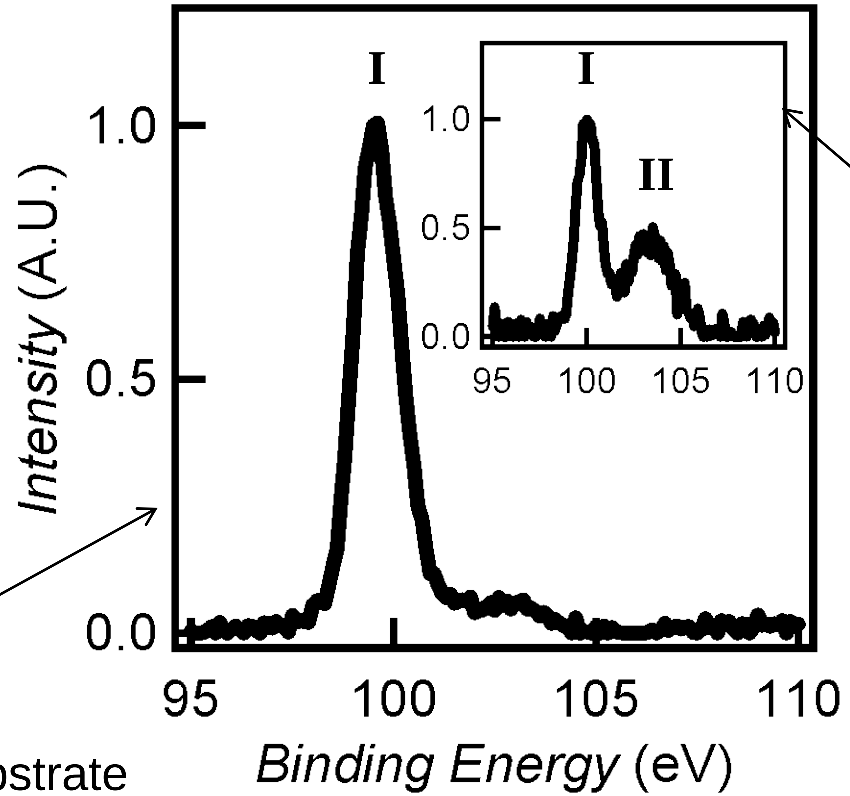

XPS for a “neat” Si substrate

XPS for a surface functionalized Si substrate

I: corresponds to the reduced Si state
II: corresponds to the oxidized Si state

The functionalized surfaces are highly stable and resistive to oxidation.

Sub-5 nm Junctions by Monolayer Doping and *Spike Annealing*

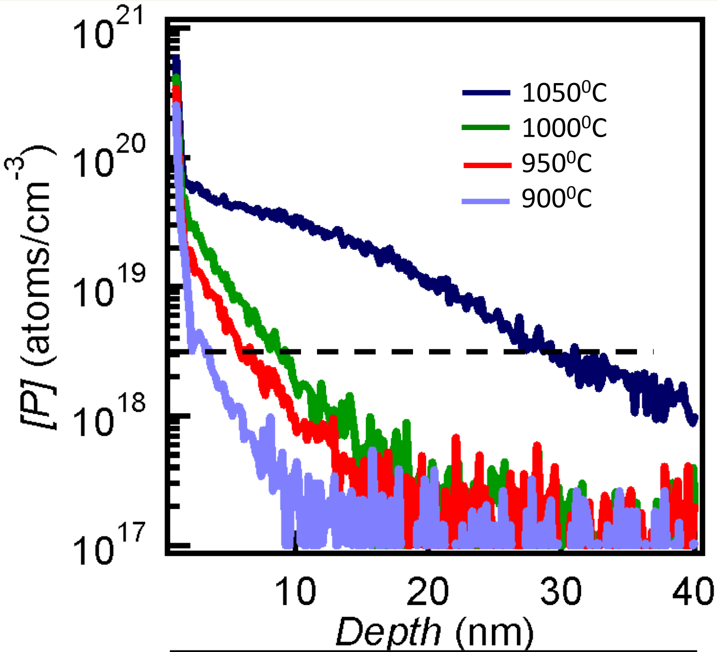

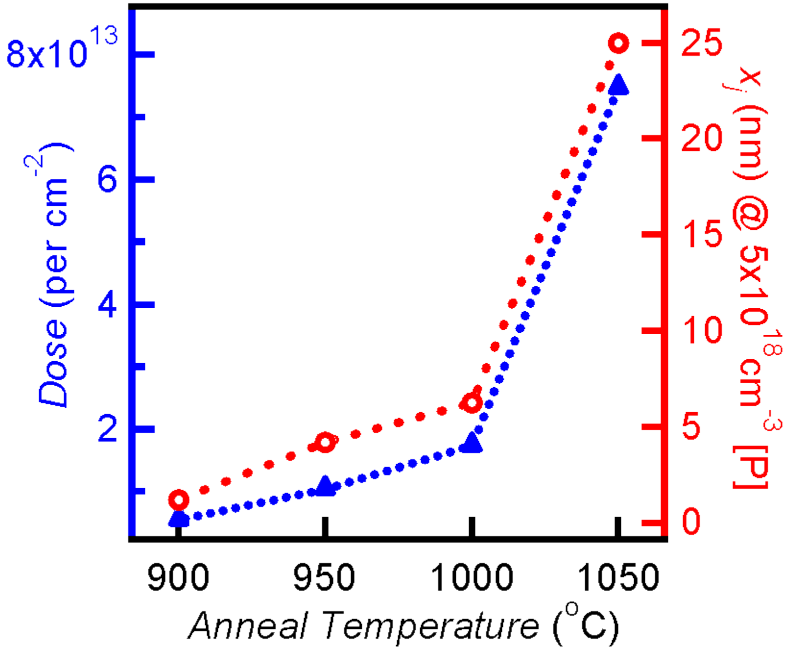

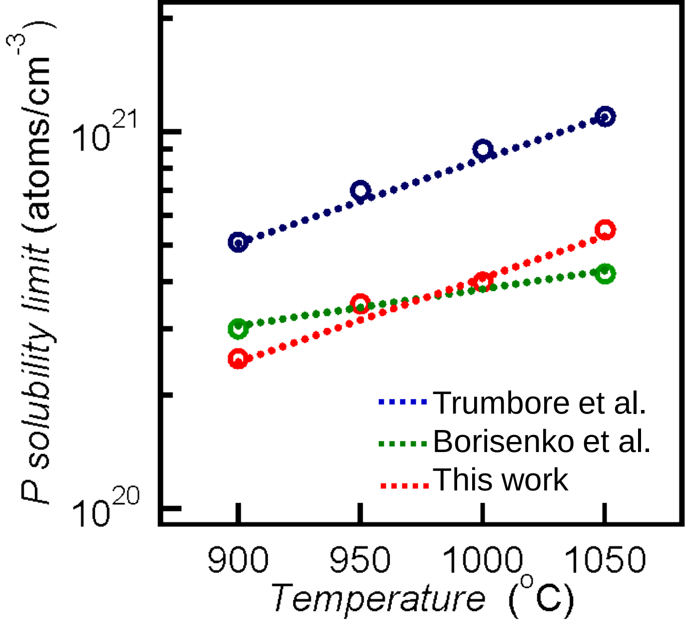

❖ Sub-5 nm junctions can be attained by conventional Spike Anneal (RTA)

❖ The ability to attain ultrashallow junctions with spike anneal is due to the lack of transient enhanced diffusion, often encountered in ion implantation.

J. C. Ho, et al., Nano Letters, 2009.

Electrical Characterization of USJs

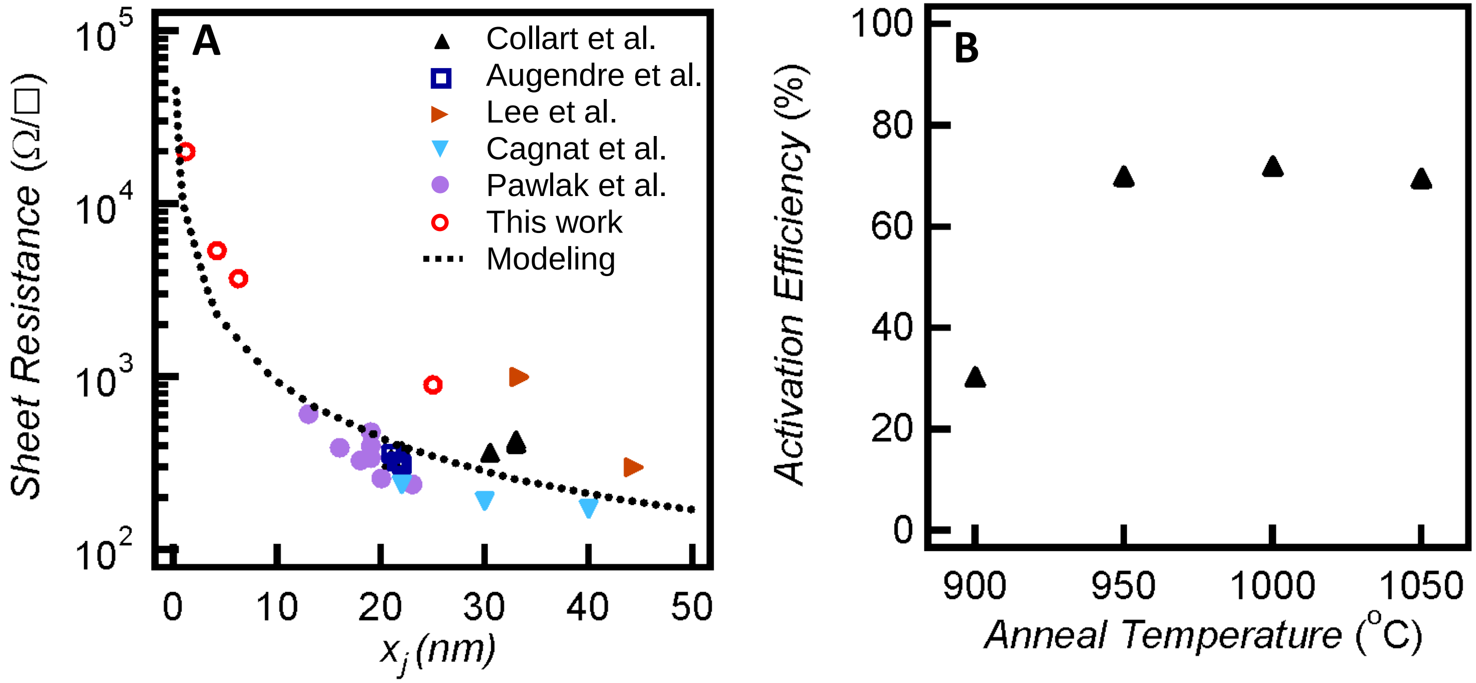

- From SIMS and Sheet resistance measurements, it is evident that majority of the dopants are electrically active – expected for a surface diffusion process such as the monolayer doping.

Dopant Dose Control

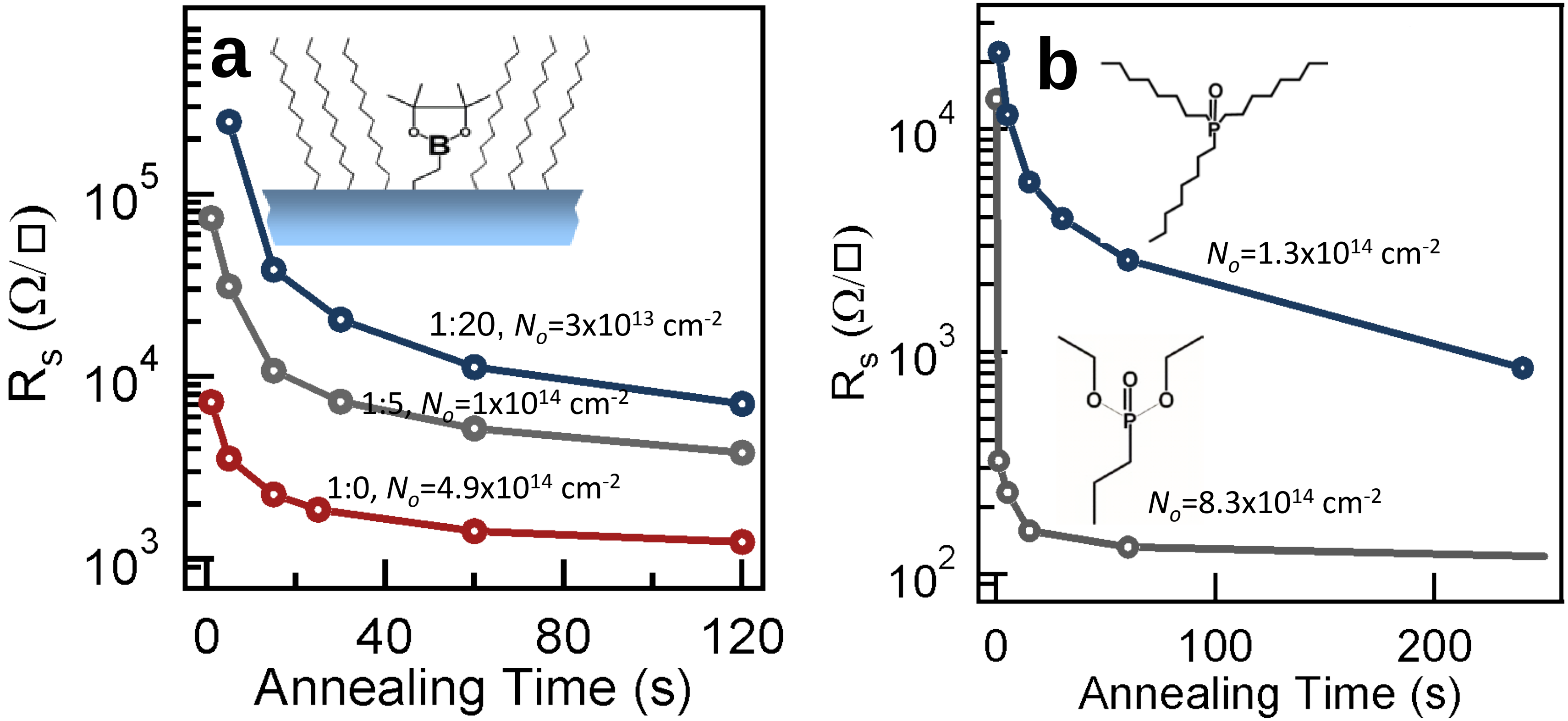

<u>The areal dose can be modulated by</u>:

a) Mix monolayer formation consisting of blank and active precursor components.

b) Structural design of the molecular precursors, with larger molecular footprints resulting in smaller dose.

Non-Contact Sheet Resistance Measurements

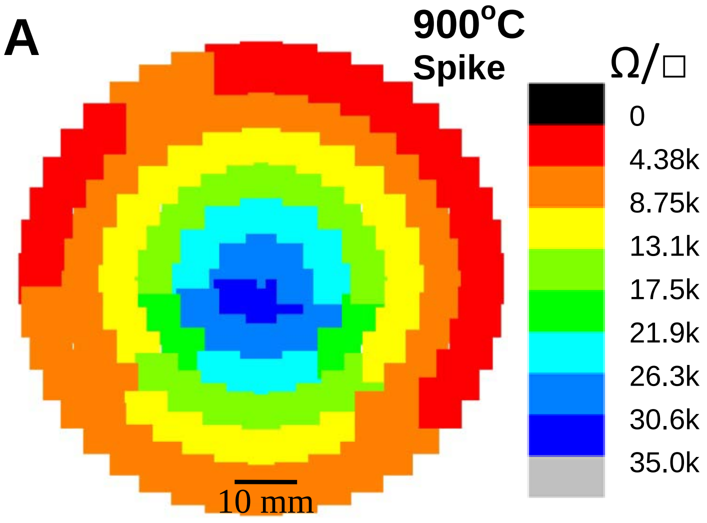

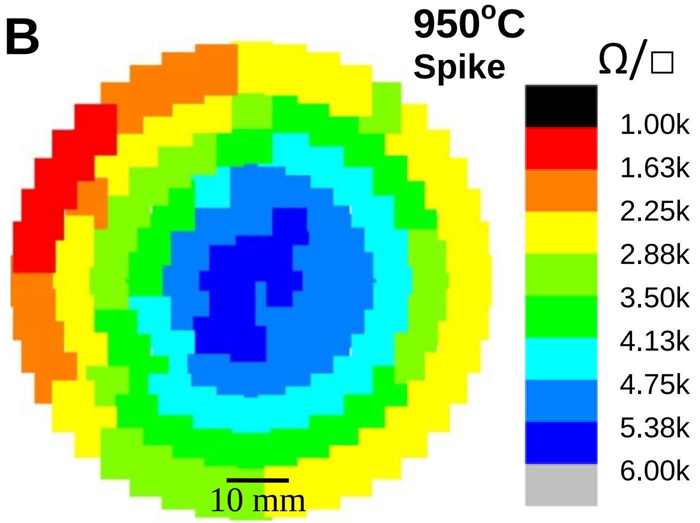

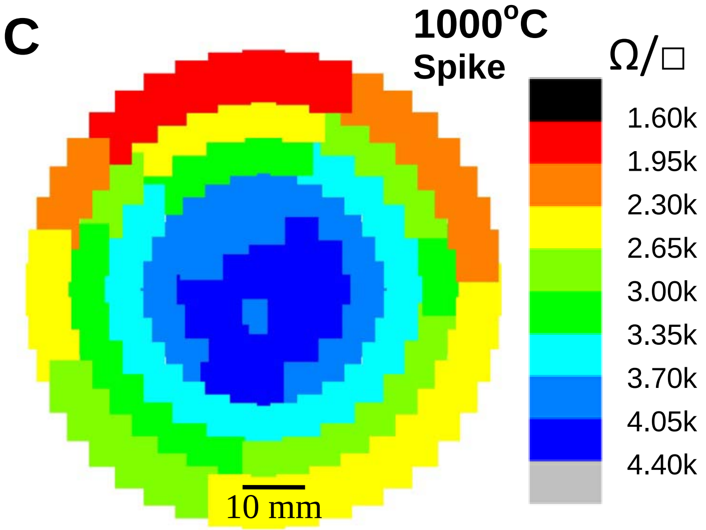

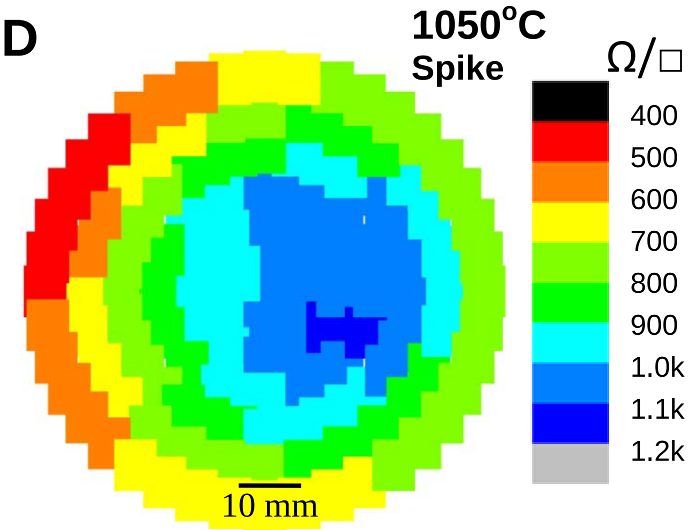

The uniformity is limited by the temperature uniformity of spike anneal tool used in the experiments.

Precursor Monolayer Uniformity

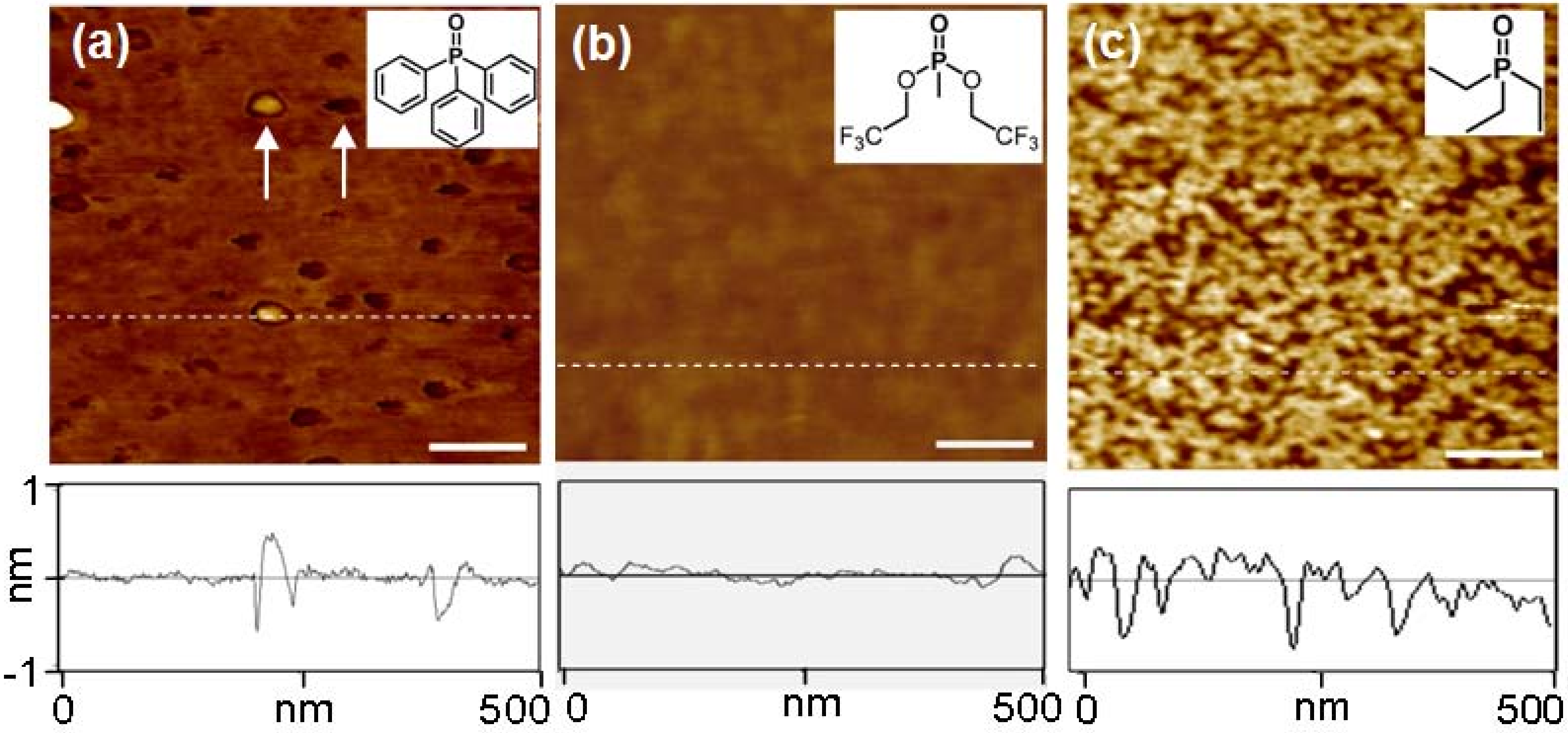

Monolayer with high packing density and low defects

No monolayer

Monolayer with high defect density

To achieve uniform doping, a highly uniform monolayer is desired. The monolayer quality is governed by the molecular precursor design.

R. Yerushalmi, et al., Angew. Chem. Int. Ed., 47, 4440-4442, 2008

Monolayer Doping for Metal Contact Engineering

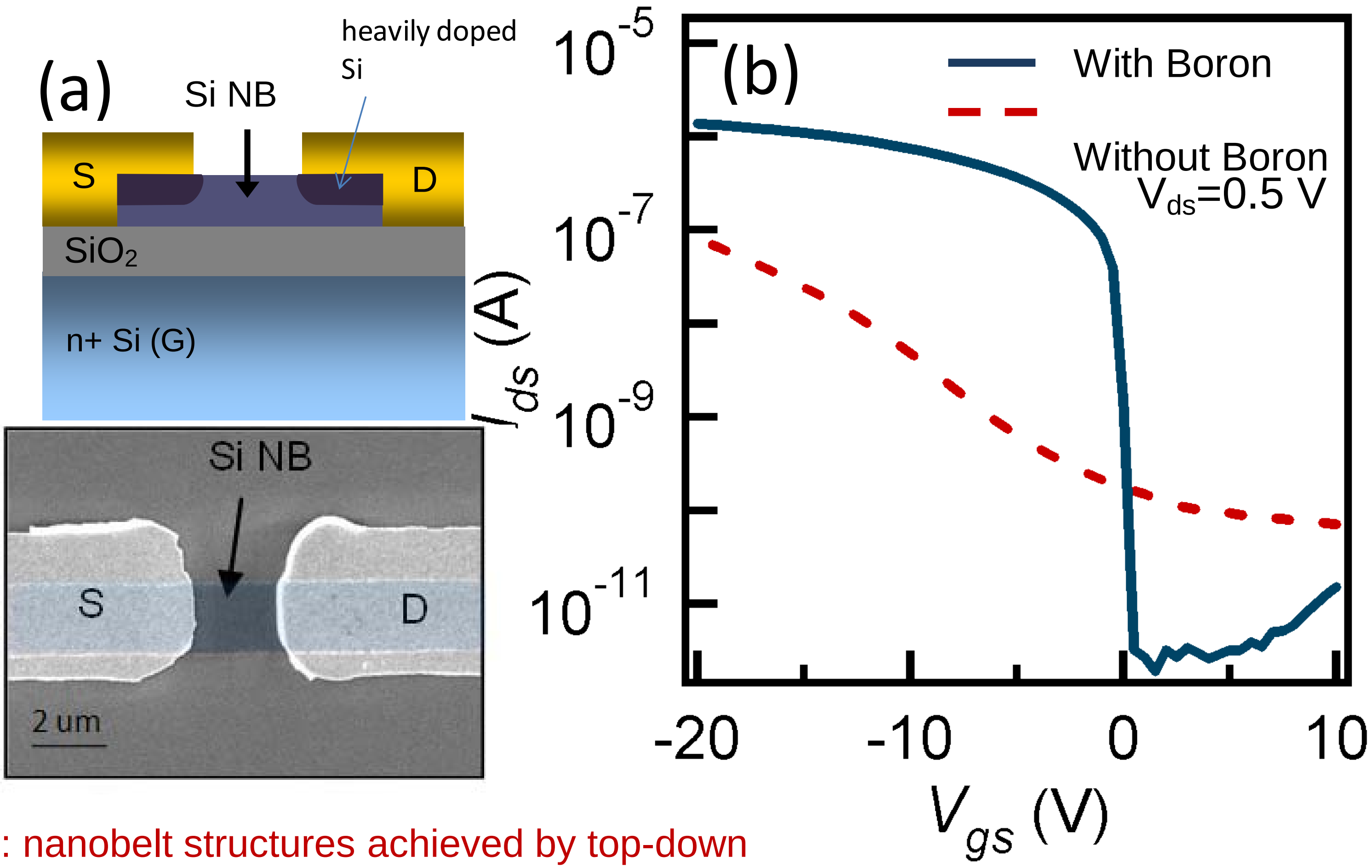

Si NB: nanobelt structures achieved by top-down patterning of SOI (top Si thickness ~20 nm)

- The monolayer is applied underneath the metal contacts to form self-aligned heavily doped regions under the metals.

Post-growth Doping of Nanowires

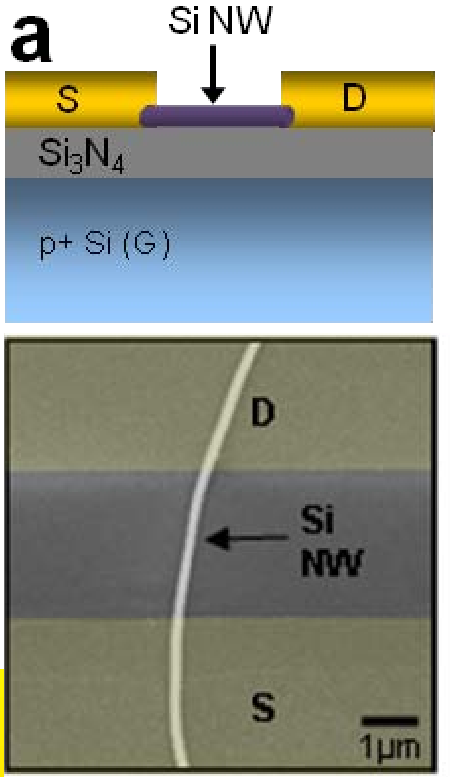

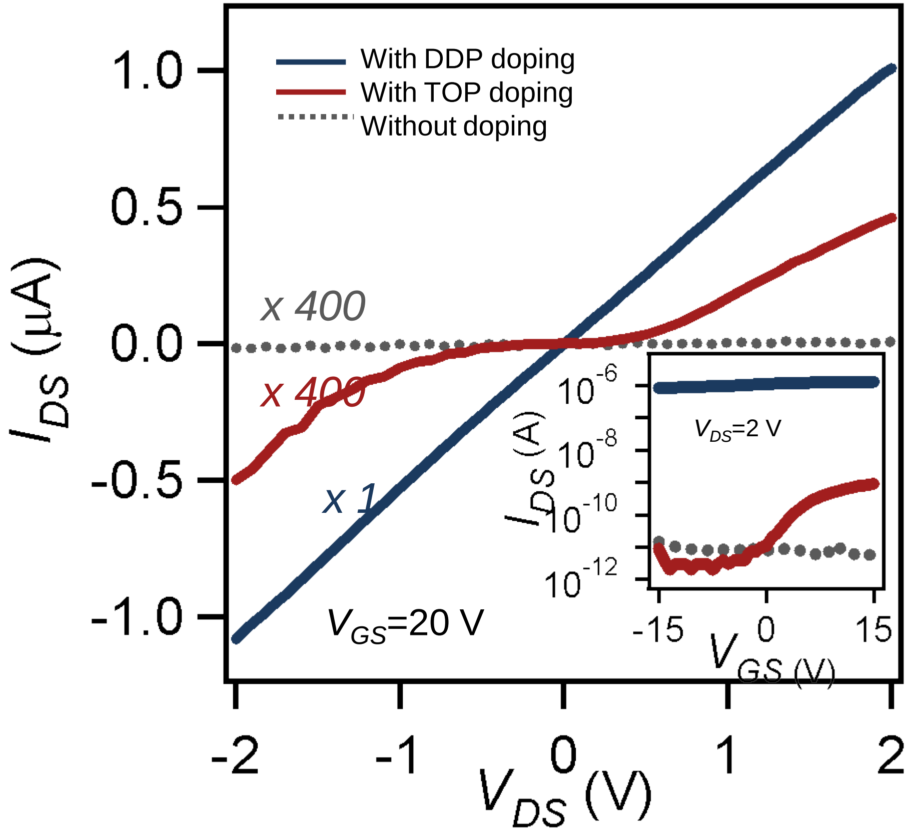

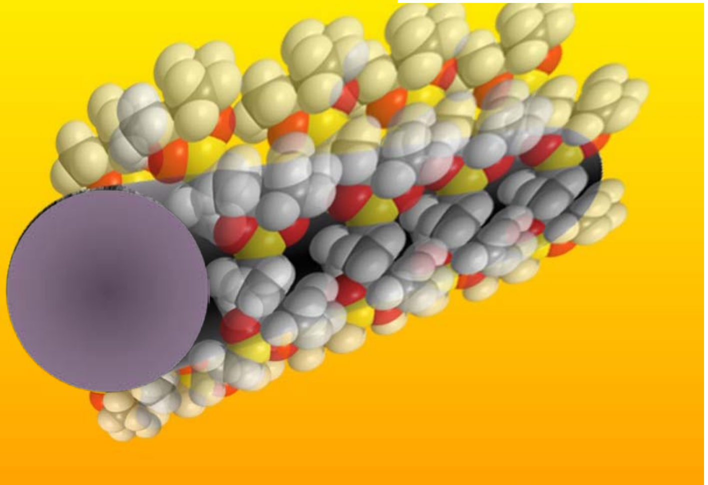

- Nanowires are uniformly n-doped by phosphorous.

- Smaller DDP results in heavy doping while the larger TOP results in light doping.

Doping of Ultrathin III-V on Insulators (XOI)

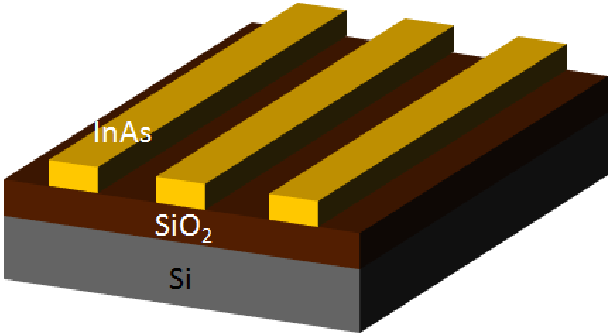

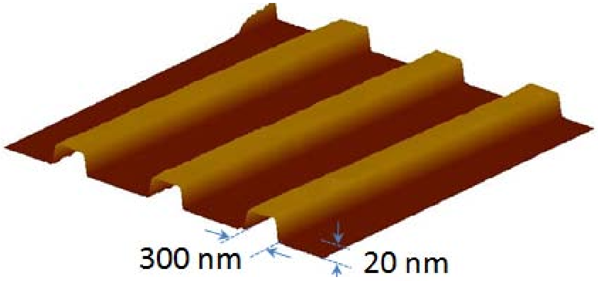

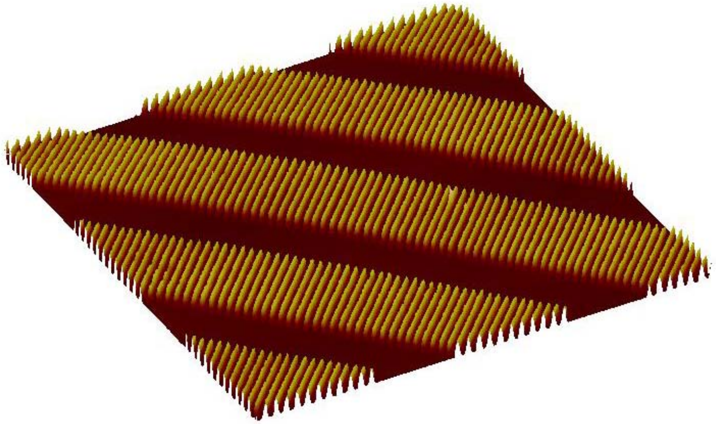

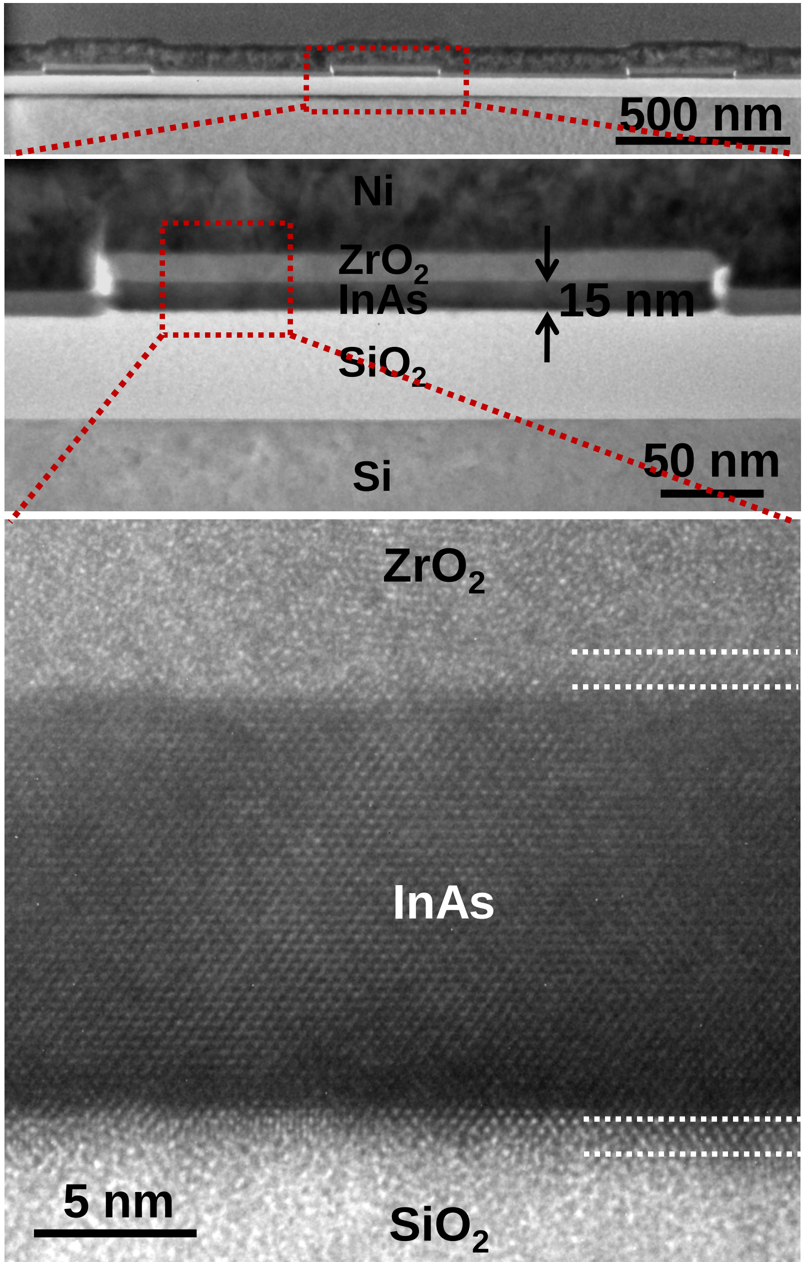

- InAs patterned thin film on a Si/SiO_2 substrate

Hyunhyub Ko, Kuniharu Takei, et al, Nature, 2010.

Nanoscale Doping of III-V Semiconductors– *n-doping*

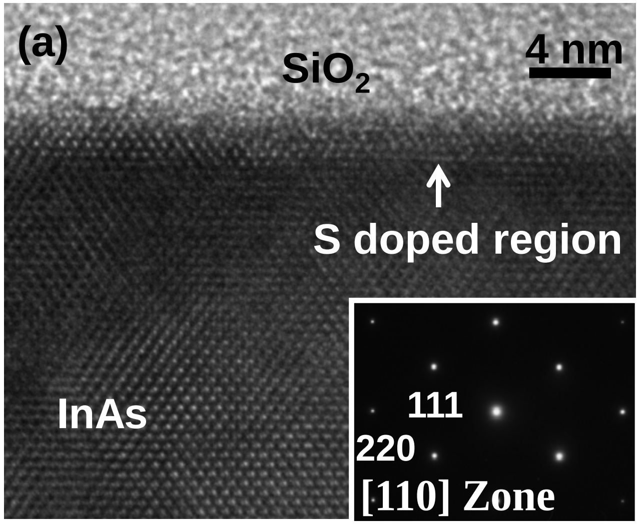

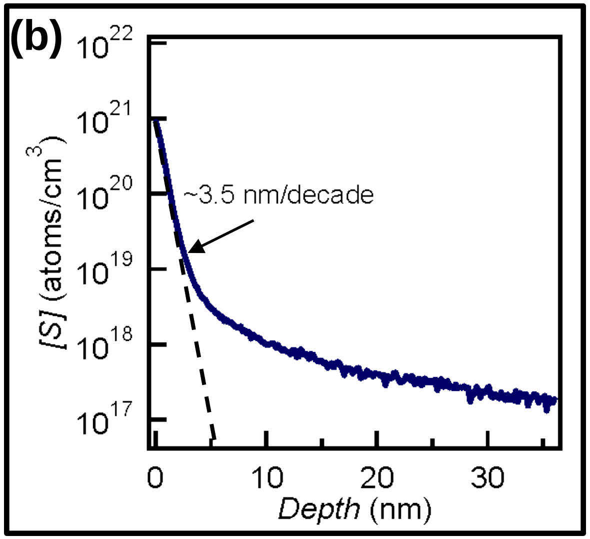

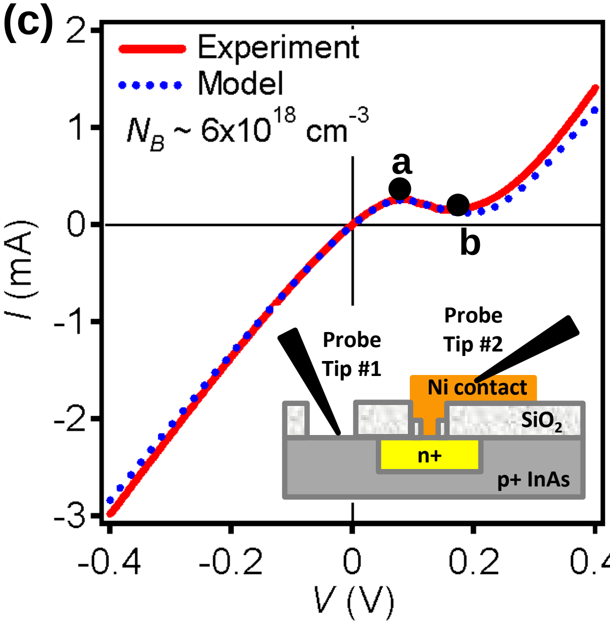

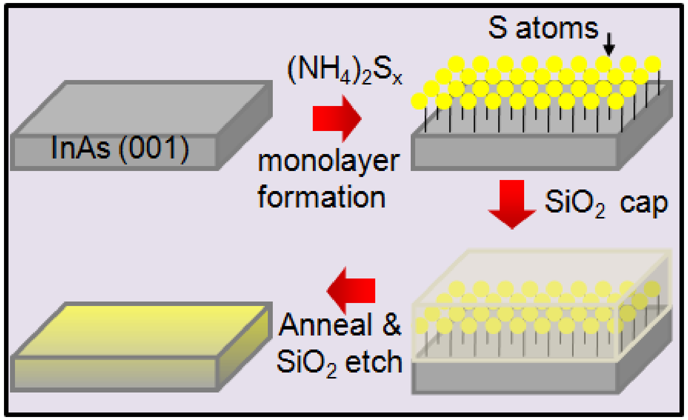

- ❑ **Anneal at 450^{0}C for 300s**
- ❑ **Abrupt dopant profile (~3.5 nm/decade)**
- ❑ **Lack of defects in the junctions**
- ❑ **Diodes with rectifying or negative differential resistance (NDR) behavior**
- ❑ **NDR confirms heavy S doping and a sharp junction interface**

Johnny Ho, Alexandra Ford, et al. APL, 2009.
Johnny Ho, et al, Nature Materials, 2008

Example of Lattice Damage Induced By Ion Implantation

InAs NWs after Zn ion implantation (35 keV) and subsequent annealing at 375 ºC for 30 min

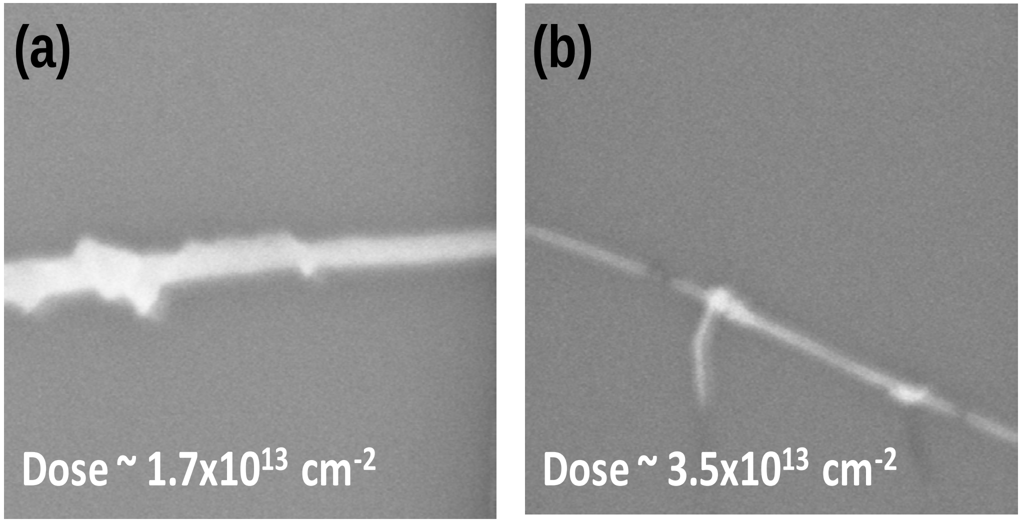

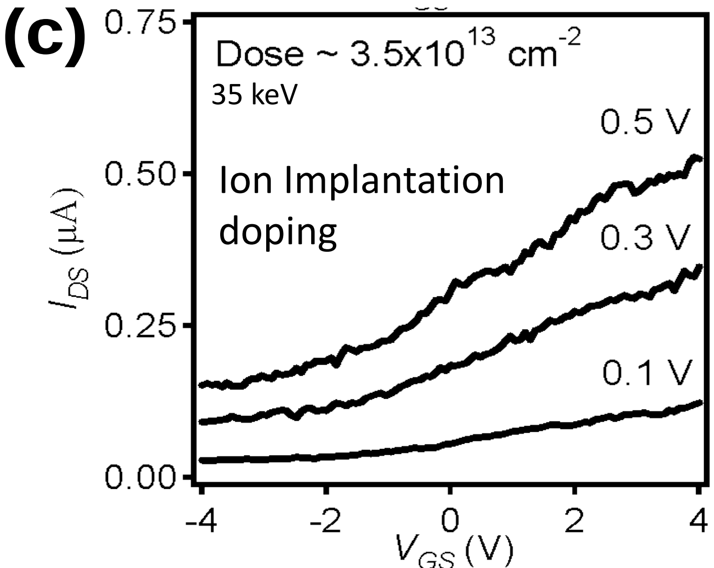

NWs remain n-type with poor electrical properties after Zn implantation

The results show the difficulty of using ion implantation for III-V nanowires

Nanoscale Doping of III-V Semiconductors– *p-doping*

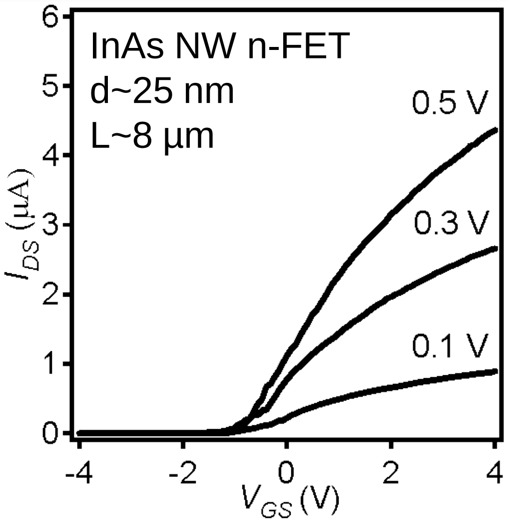

Blank Zn surface doping of NW

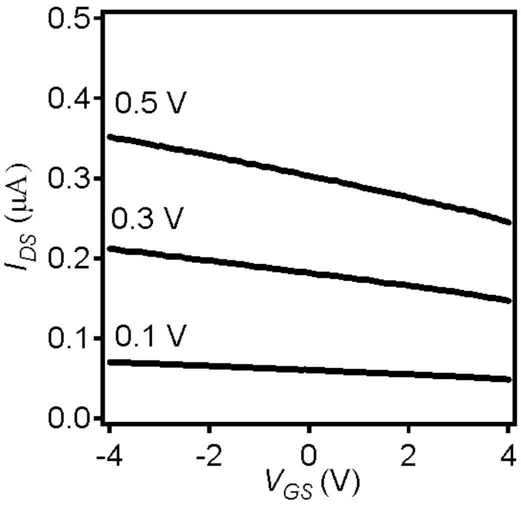

Degenerate p-doping of InAs nanostructures with electrically active [Zn] ~ $1x10^{19}$ cm^{-3} can be readily achieved by the surface doping scheme, enabling the exploration of a wide range of devices.

A. Ford, A. Javey, et al, submitted, 2009.

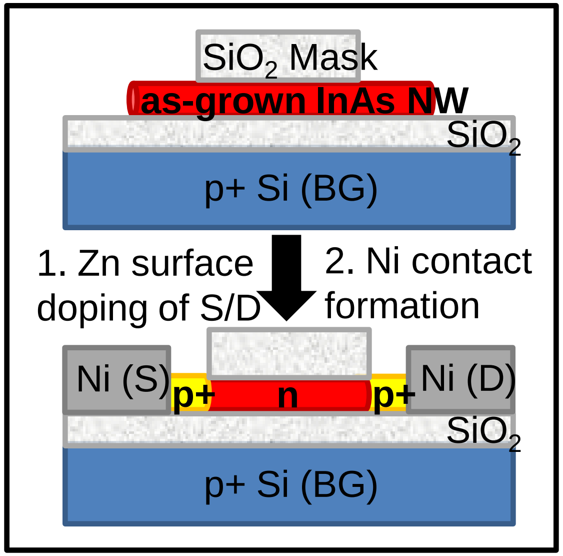

1. Zn surface doping of S/D

2. Ni contact formation

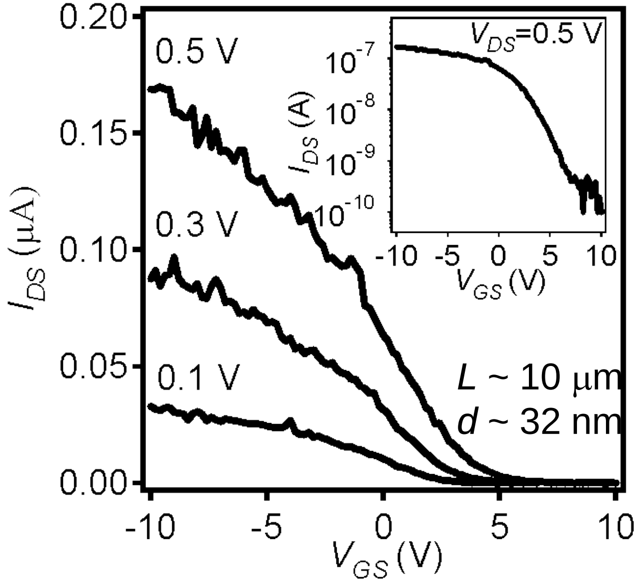

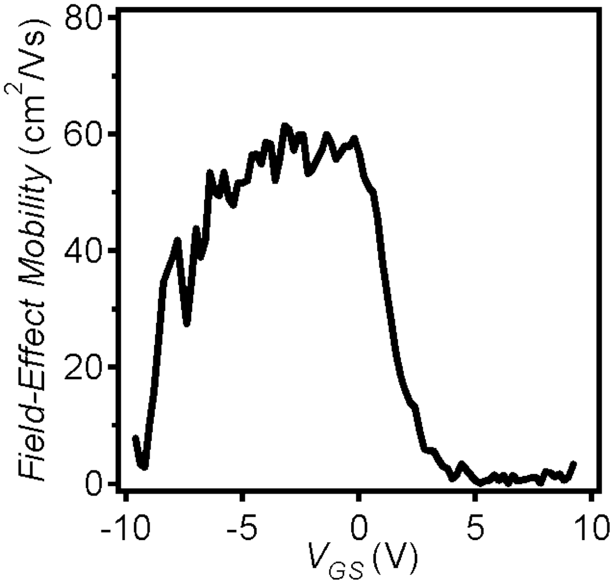

First InAs p-MOSFET: achieved by the surface doping scheme, demonstrating the ability to degenerately dope III-V through an equilibrium process without inducing defects – essential for exploring III-V TFETs

Conclusions

- Monolayer doping approach presents a versatile route toward controlled nanoscale doping of semiconductors
  - Sub-5 nm junctions may be readily enabled by conventional annealing methods due to the lack of lattice damage during the dopant incorporation
  - Dopant dose and profile can be accurately controlled by the structure design of the molecular precursors as well as the annealing conditions
  - The process is highly applicable to both planar and non-planar structures, and can be utilized for novel metal contact engineering of nanoscale devices
  - The process may be generic for all semiconductors by using the appropriate surface chemistry

Acknowledgements

Current/past members

Dr. Zhiyong Fan
Dr. Hyunhyub Ko
Dr. Yu-Lun Chueh
Dr. Paul Leu
Dr. Roie Yerushalmi
Dr. Kuniharu Takei
Dr. Morten Madsen
Dr. Jaehyun Moon
Dr. Cary Pint
Dr. Min Hyung Lee

Johnny Ho
Alexandra Ford
Zachery Jacobson
Toshitake Takahashi
Onur Ergen
Rehan Kapadia
Zhenxing Zhang
Steven Chuang
Daniel Ruebusch
Xiaobo Zhang
Haleh Razavi
JaeWon Do
Aimee Moriwaki
Ali Rathore
Maxwell Zhang
Hui Fang


Javey Group, October 2009

- ☐ *$$$*: BSAC, MARCO/MSD, DARPA, Intel, SEMATECH, NSF, DOE/LBNL, ARO, SRC, Sloan Foundation, MDV
- ☐ *Collaborators:* Krishna Sanjay, Ming Wu, Ron Fearing, Jing Guo, Jeff Bokor, Eugene Haller, Joel Ager, Prashant Majhi, Sayeef Salahuddin, Bernhard Boser

Towards Atomically Precise Silicon Devices in all 3D

Professor Michelle Y. Simmons

Director, Centre of Excellence for
Quantum Computation and Communication Technology

University of New South Wales

Sydney, Australia

Michelle.Simmons@unsw.edu.au

THE UNIVERSITY OF NEW SOUTH WALES
THE UNIVERSITY OF MELBOURNE
ANU THE AUSTRALIAN NATIONAL UNIVERSITY
Griffith UNIVERSITY
The University of Sydney Australia
THE UNIVERSITY OF QUEENSLAND AUSTRALIA
Australian Government Department of Defence Defence Science and Technology Organisation

Leadership in Silicon Quantum Computation

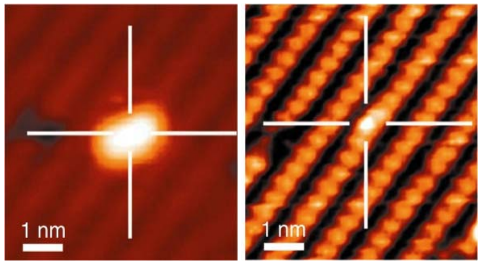

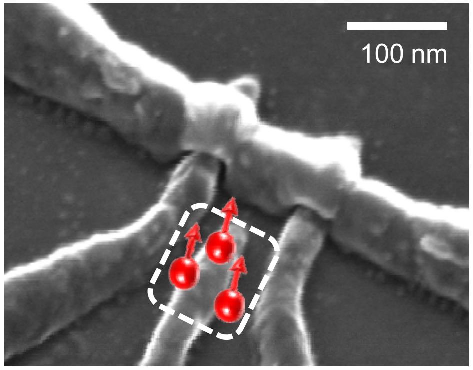

1. World Leading Single P Atom Fabrication and Devices
   Simmons, *Phys. Rev. Lett.* (2003);
   Jamieson, Dzurak, *Appl. Phys. Lett.* (2005);
   Rogge, Hollenberg, *Nature Physics (2008)*
2. Developed Single Electron Transistor Technology for Read-Out
   Dzurak, Jamieson, Hollenberg, *Nano Letters* (2007); *Nano Letters* (2007); Simmons, *Nano Letters* (2009)
3. World's Smallest Precision Transistor
   Simmons, *Nature Nanotechnology (2010)*
4. Probed Electron Spin of Single P Atom
   Jamieson, Dzurak, *Nano Letters (2010)*
5. First Demonstration of Single Shot Spin Readout in Silicon
   Morello, Dzurak, Jamieson, Hollenberg, *Nature (2010).*

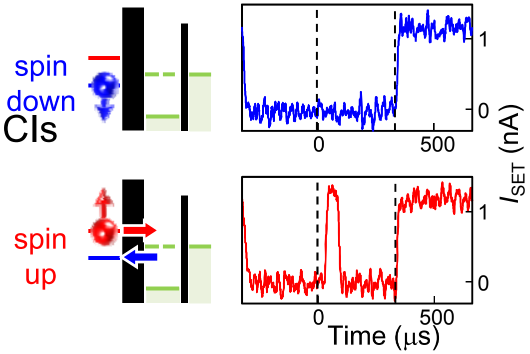

Competitive edge in Silicon Quantum Computation:

- 12% of publications world-wide in silicon quantum computing are from the CIs
- World-leading dual track single atom fabrication capability
- Scalable architecture – compatible materials with the silicon industry
- Demonstrated extremely long relaxation times ~ 6 seconds
- US funding NSA/ARO support – $1 M p.a.
- Collaborative Research and Development Agreement (CRADA) with Sandia National Laboratories

Leadership in Optical Quantum Computation

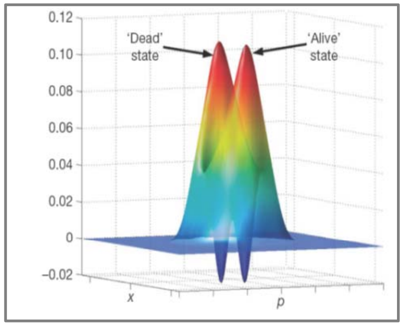

1. World's First Fully Characterised Two-qubit Entangling Gate
   US Patent 7173272; Pryde, White, Ralph, *Nature* 426, 264 (2003); *Phys. Rev. Lett.* 93, 080502 (2004)
2. Proposed Coherent State Quantum Computation
   Ralph, *Phys. Rev. A* 68, 030503 (2003)
3. Demonstrated World's First Three-qubit Gate (Tofolli)
   Pryde, Ralph, White, *Nature Physics* 5, 134 (2009)
4. World's Highest Precision Measurement with Photon Qubits
   Pryde and Wiseman, *Nature* 450, 393 (2007)
5. First Demonstration of Quantum Chemistry on a Quantum Computer
   White, *Nature Chemistry* 2, 106 (2010)

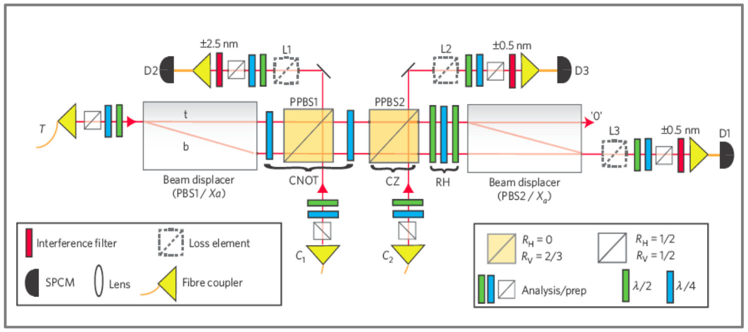

Competitive edge in Optical Quantum Computation:

- 5 of the top 20 publications world-wide in optical quantum computing are from the CIs
- High precision operation: e.g. low gate errors and noise
- Scalable architectures: e.g. linear optics and cluster states
- Exploit strong Australian quantum optics capability
- Expansion of CRADA with Sandia to include quantum photonics for scale-up

Leadership in Quantum Communication

1. First demonstration of complete bright source quantum key distribution
   Ralph, *Phys. Rev. A* (2000); Symul, Lam, Ralph, *Phys. Rev. Lett.* (2004); *Phys. Rev. Lett.* (2005)
2. Fastest random number generators
   Symul, Lam, Ralph, with *Nature Photonics* (2010)
3. Pioneering quantum teleportation theory and experiment
   Symul, Lam, Ralph, *Phys. Rev. Lett.* (1998); *Phys. Rev. Lett.* (2003)
4. First demonstration of quantum state sharing
   Symul, Lam, Ralph, *Phys. Rev. Lett.* (2004)
5. First heralded noiseless linear amplifiers
   Pryde, Ralph, *Nature Photonics* 4, 316 (2010)
6. World's best technology for quantum memory
   Sellars, *Nature* 465, 1052 (2010)

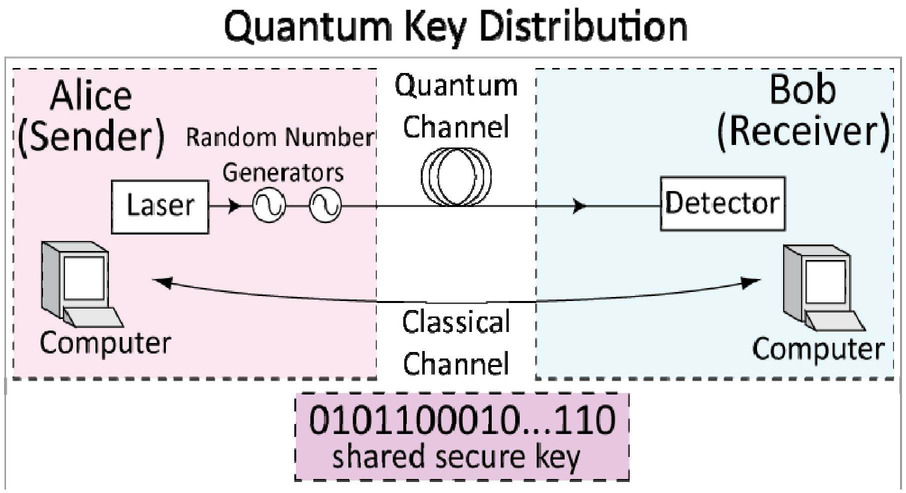

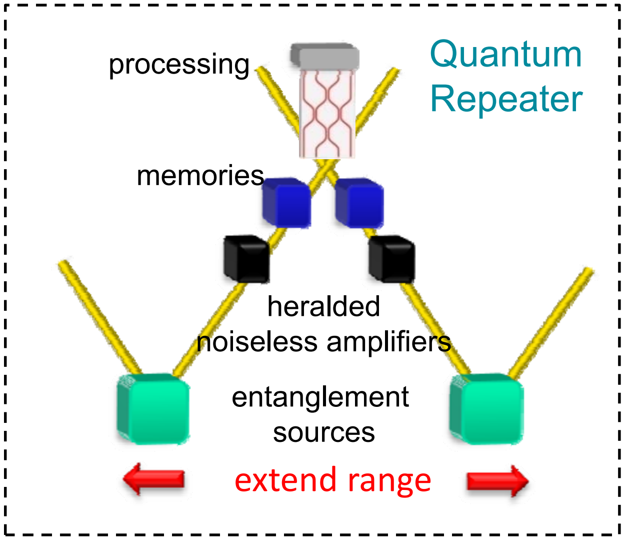

Competitive edge in Quantum Communication:

- Developed high bit rate broadband cryptography system
- World's leading optical quantum memory
- Access to unique commercial dark fibre network (ANU/DSTO/Government)
- Specialised expertise in the critical components need to build a quantum repeater: sources (ANU, GU, Toshiba), detectors (UQ, Toshiba, ADFA), amplifiers (GU) and memory (ANU)

Centre of Excellence: International Collaborators

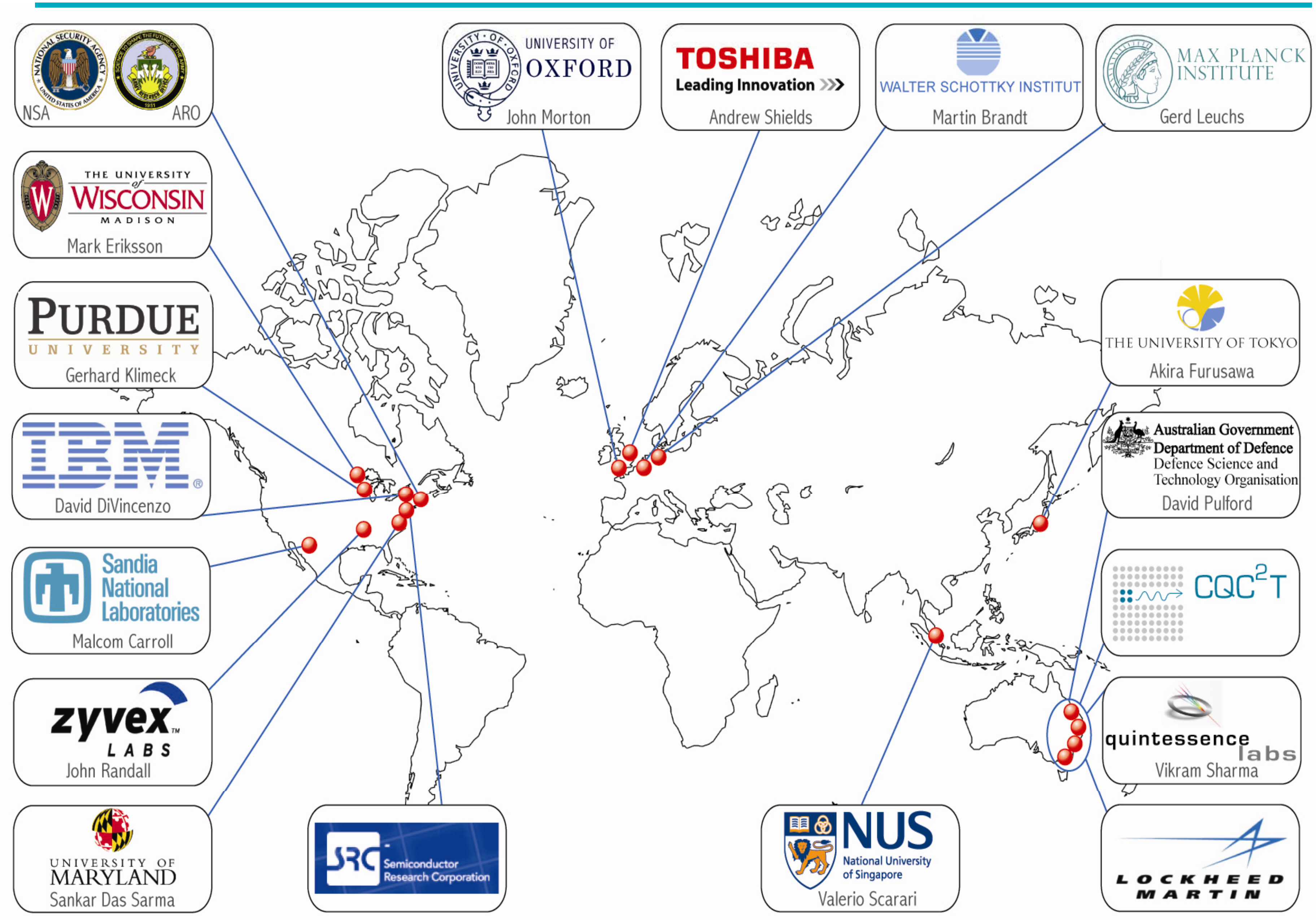

NSA ARO

UNIVERSITY OF OXFORD
John Morton

TOSHIBA
Leading Innovation
Andrew Shields

WALTER SCHOTTKY INSTITUT
Martin Brandt

MAX PLANCK INSTITUTE
Gerd Leuchs

THE UNIVERSITY of WISCONSIN MADISON
Mark Eriksson

PURDUE UNIVERSITY
Gerhard Klimeck

IBM
David DiVincenzo

Sandia National Laboratories
Malcom Carroll

zyvex LABS
John Randall

UNIVERSITY OF MARYLAND
Sankar Das Sarma

SRC Semiconductor Research Corporation

NUS National University of Singapore
Valerio Scarari

THE UNIVERSITY OF TOKYO
Akira Furusawa

Australian Government
Department of Defence
Defence Science and Technology Organisation
David Pulford

CQC^{2}T

quintessence labs
Vikram Sharma

LOCKHEED MARTIN

Outline

- Atomic-scale fabrication strategy
  - Motivation and goals
  - Atomistic understanding of fabrication process

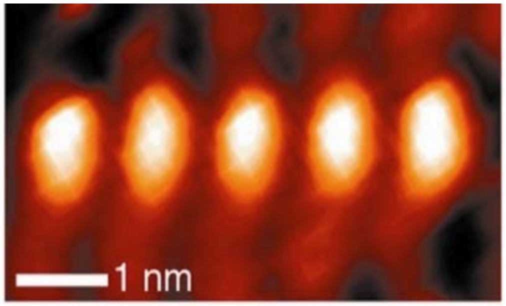

- Electrical transport in precision STM-patterned devices
  - Narrowest conducting wires
  - Tunnel gap devices
  - Development of gating technology

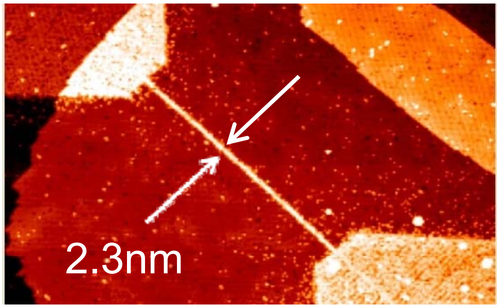

- Si band-structure in nano to atomic scale devices
  - World's smallest atomic precision transistor
  - Quantum dots down to the single donor level
  - Towards spin read-out and double donors

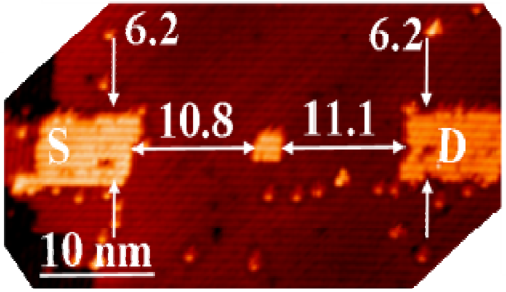

Geometric/Equivalent Scaling: 3D atomic-precision transistors

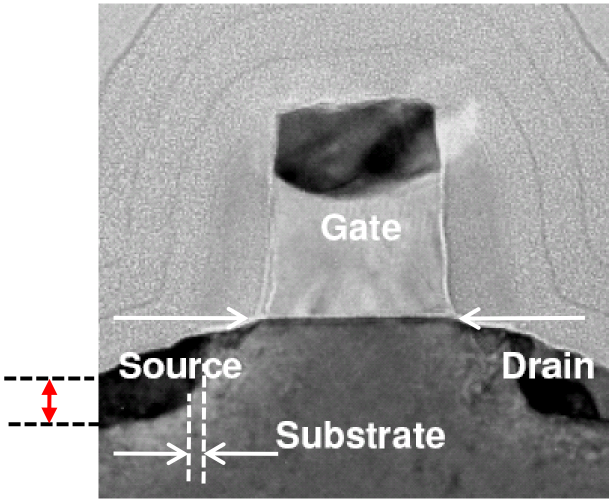

45 nm node

22 nm node requirements and beyond:

- source-drain junction depths ~ 10nm
- junction abruptness ~1.4nm/decade
- gate length ~14nm
- junction resistance ~500Ω/□

LITHOGRAPHICALLY PLACING P ATOMS

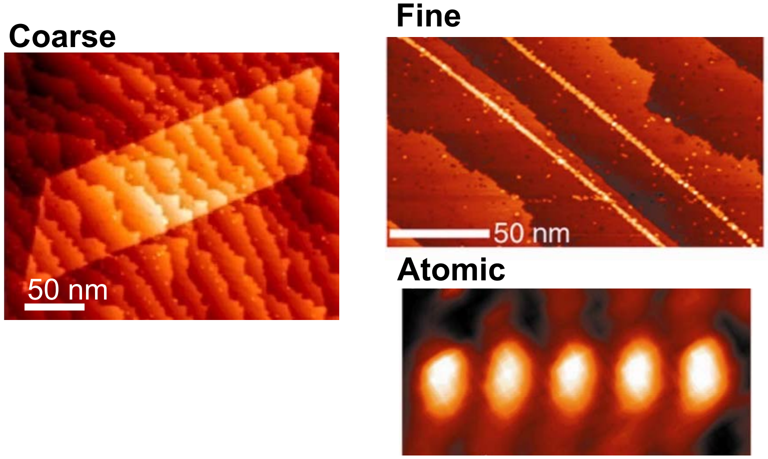

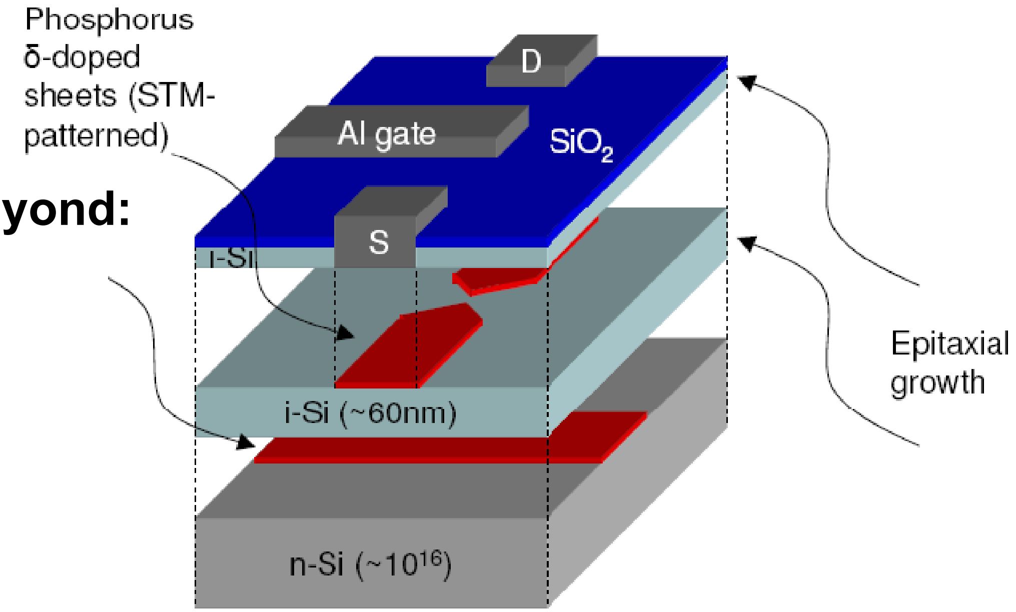

3D ATOMISTIC CONTROL: STM-PATTERNED TRANSISTOR

Development of single P atom qubits

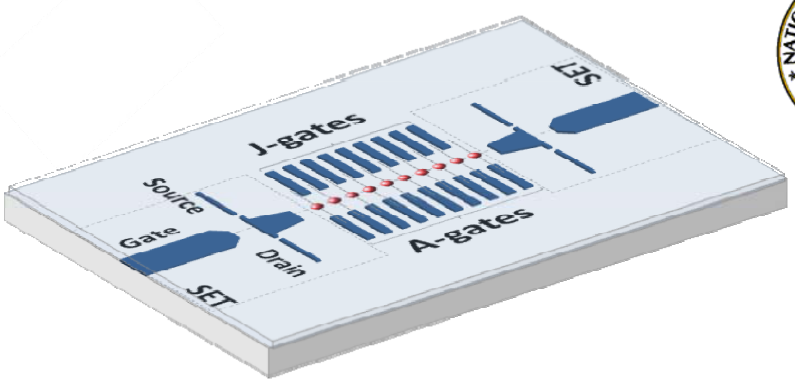

Electron spins of ^{31}P donor atoms in ^{28}Si

Advantages:

- relaxation T_1 long
- compatible with existing multi-billion dollar silicon microelectronics industry and scaleable

Disadvantages:

- require the ability to dope Si with atomic precision aligned to nanometer sized surface gates

LITHOGRAPHICALLY PLACING P ATOMS

Coarse

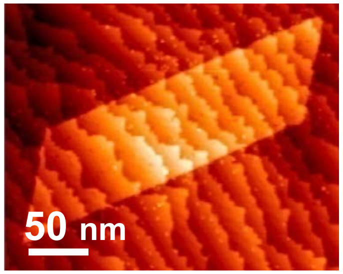

Fine

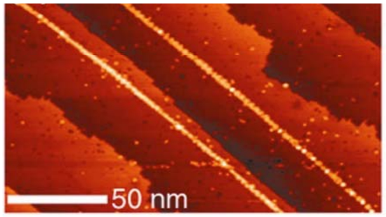

Atomic

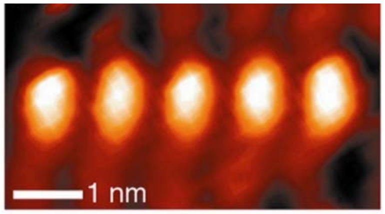

Atomic Fabrication Strategy in Silicon

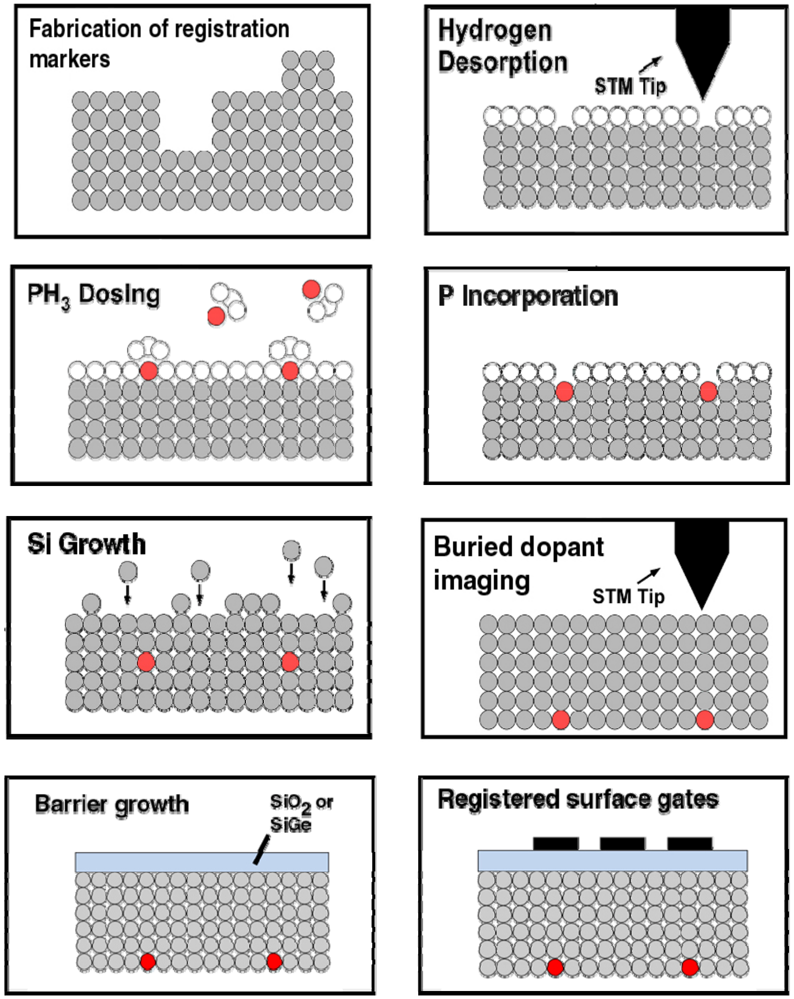

Custom-designed scanning tunneling microscopy (STM) and molecular beam epitaxy (MBE) system

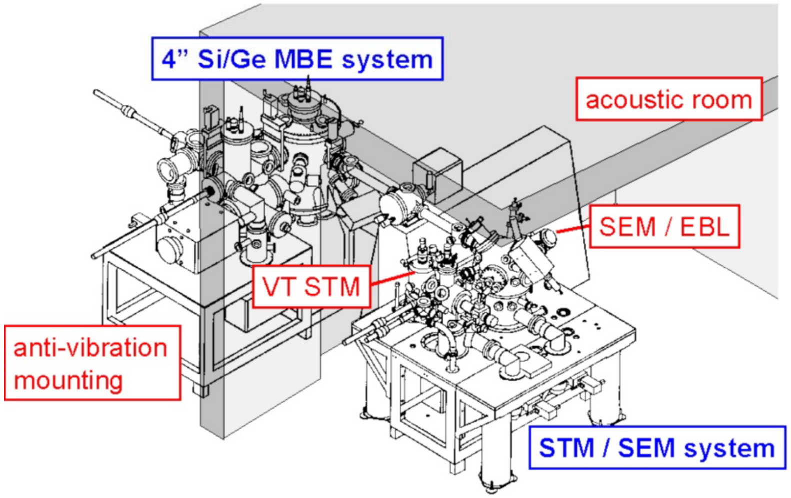

M.Y. Simmons *et al.*, J. Molecular Simulation **31** (6-7), 505-514 (2005)
M.Y. Simmons *et al.*, Int. J. Nanotechnology **5** (2-3), 352 (2008)

Atomistic understanding of gaseous PH_3 dopant source

UNDERSTANDING P INCORPORATION CHEMISTRY

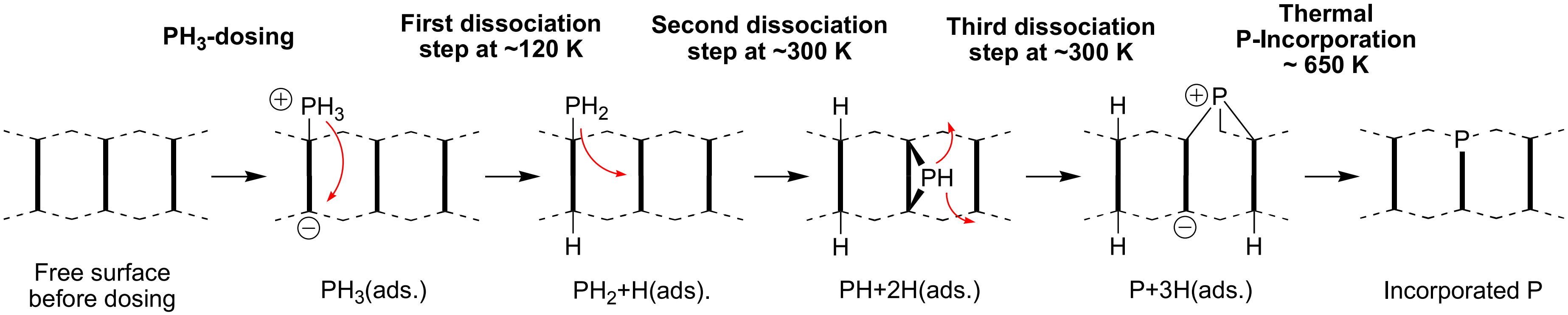

PH_3-dosing

First dissociation step at ~120 K

Second dissociation step at ~300 K

Third dissociation step at ~300 K

Thermal P-Incorporation ~ 650 K

Free surface before dosing

PH_3(ads.)

PH_2+H(ads).

PH+2H(ads.)

P+3H(ads.)

Incorporated P

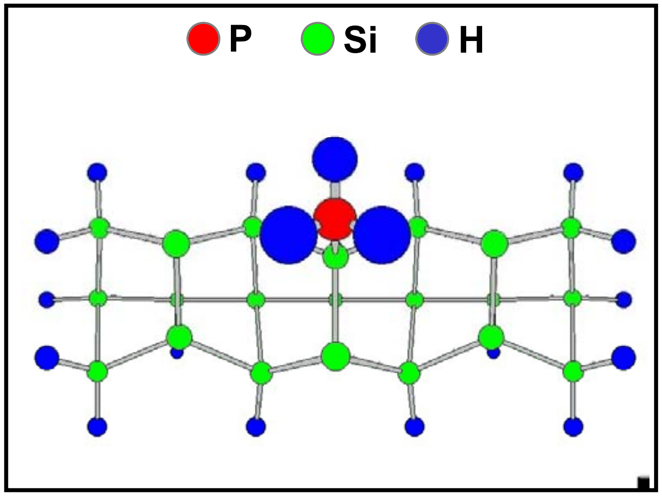

Kinetic Monte Carlo Algorithm: computes time evolution of atomic structures of PH_x on Si(100)

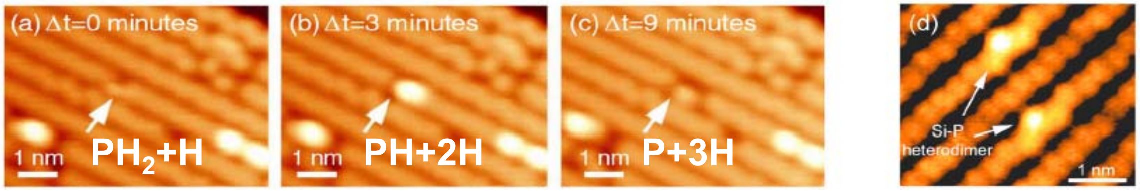

one dimer wide

two dimer wide

three dimer wide

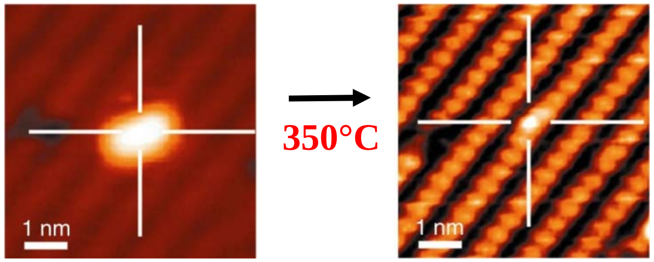

S.R. Schofield, Phys. Rev. Lett. **91** 136104 (2003).
H. F. Wilson *et al.*, Phys. Rev. Lett. **93**, 226102 (2004);
O. Warschkow, *et al.*, Phys. Rev. B **72**, 125328 (2005);
M. Radny *et al.*, Phys. Rev. B **74**, 113311 (2006)

Extremely high density of dopants in the layer

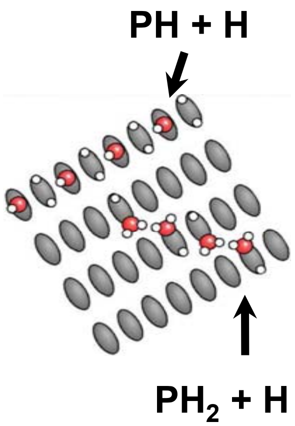

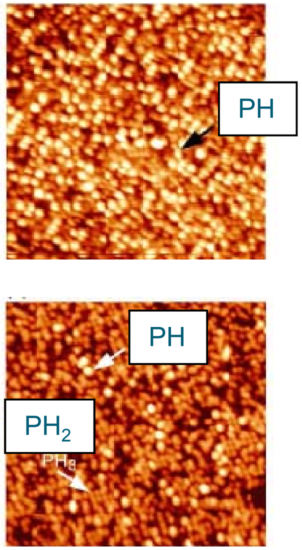

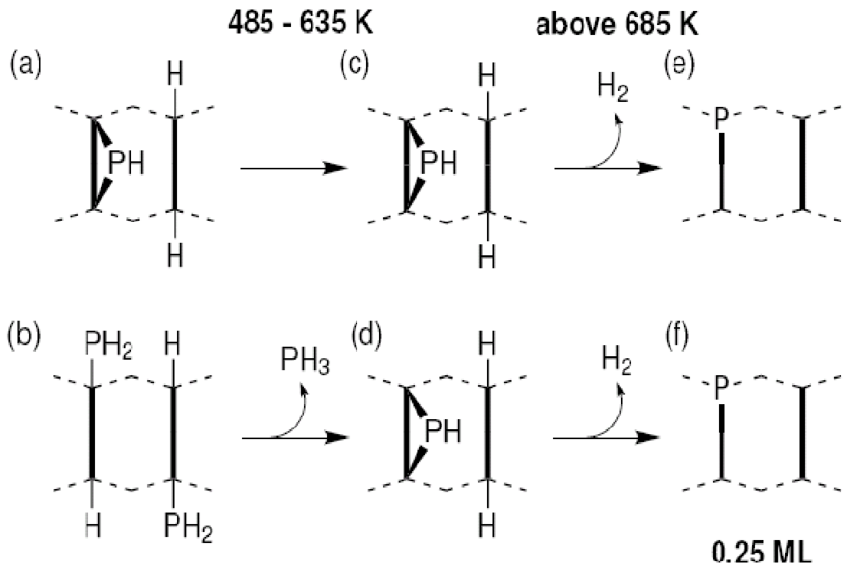

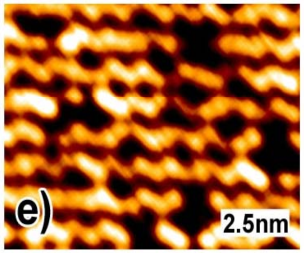

S.R. Schofield et al., J. Phys. Chem B ***110***, *3173 (2006).*
H. Wilson et al., *Phys. Rev. B* ***74,*** *195310 (2006).*

CONTROLLABLE 0.25ML P COVERAGE

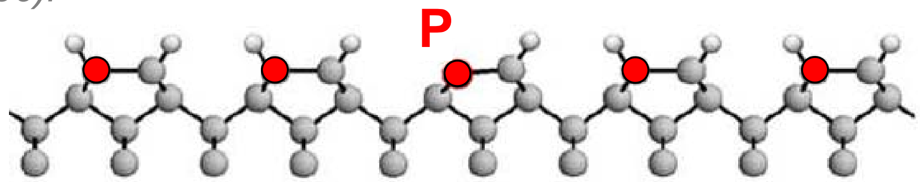

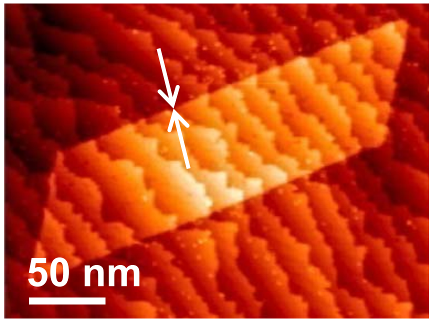

- One in every 4 silicon atoms is a P atom.
- Average separation of P atoms is less than 1nm
- The Bohr radius of P in Si ~2.5nm

With STM lithography the dopant concentration changes by 6 orders of magnitude over 1nm which corresponds to 0.17nm/decade

Extremely high density of dopants in the layer

bulk Si:
6 degenerate valleys

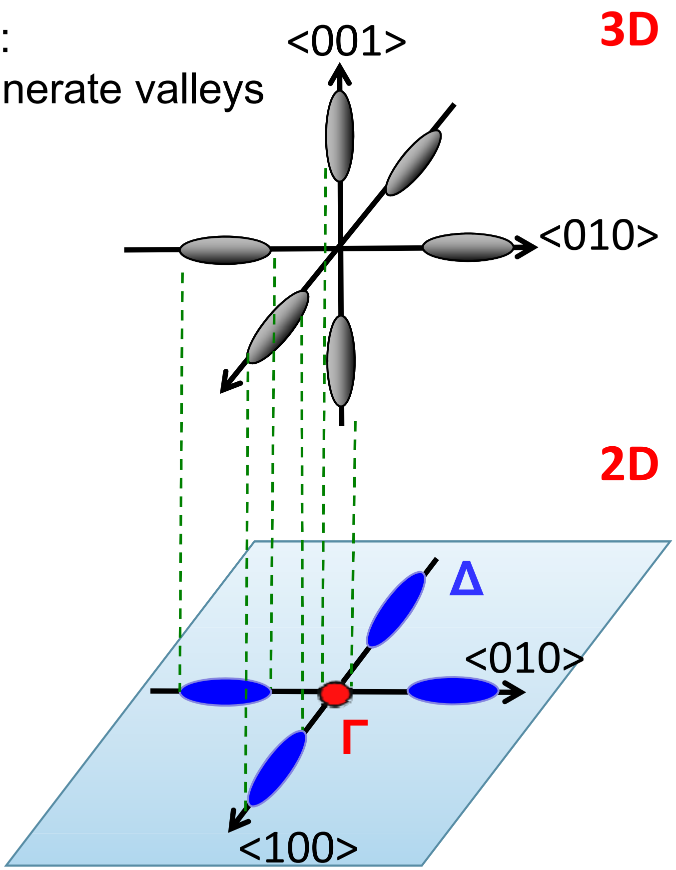

strain, confinement:
2 + 4-fold degeneracy

DFT calculations of band structure

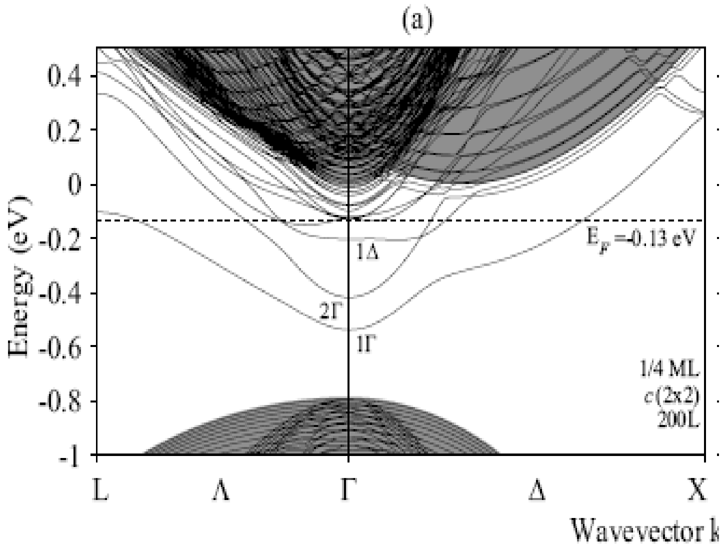

⇒ impurity band created below the conduction band

⇒ band gap narrowing of Si

⇒ doping density is so high both
2 Gamma bands and
4 fold degenerate Delta bands occupied

D. Carter, *et al. Phys. Rev. B* **79**, 033204 (2009)

Lithographically confining the dopants using STM

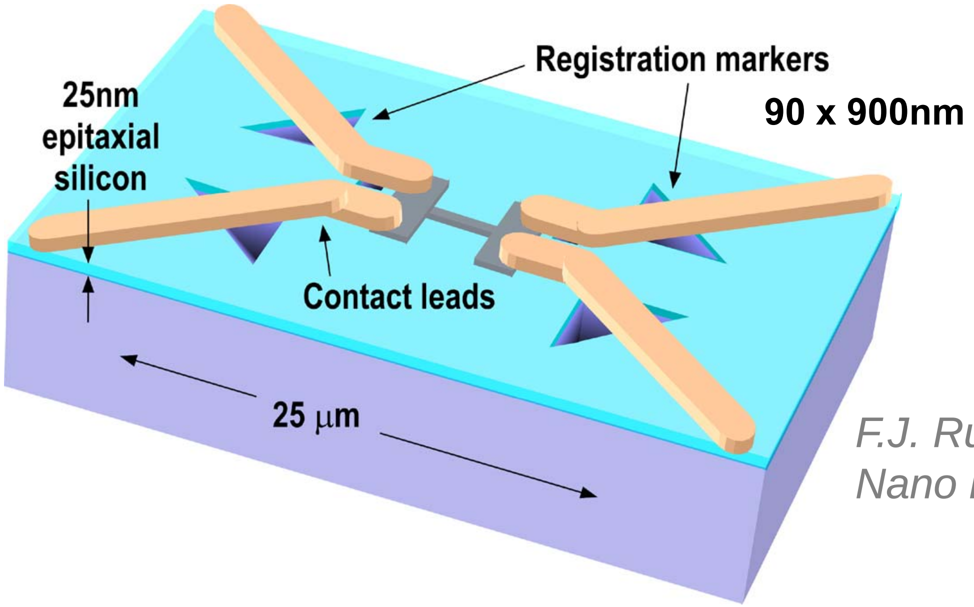

Fabrication of Al ohmic contacts aligned to buried phosphorus doped nanostructure

F.J. Ruess, L. Oberbeck, M.Y. Simmons et al., Nano Letters ***4*** *1969 (2004) .*

OHMIC CONDUCTION THROUGH WIRES

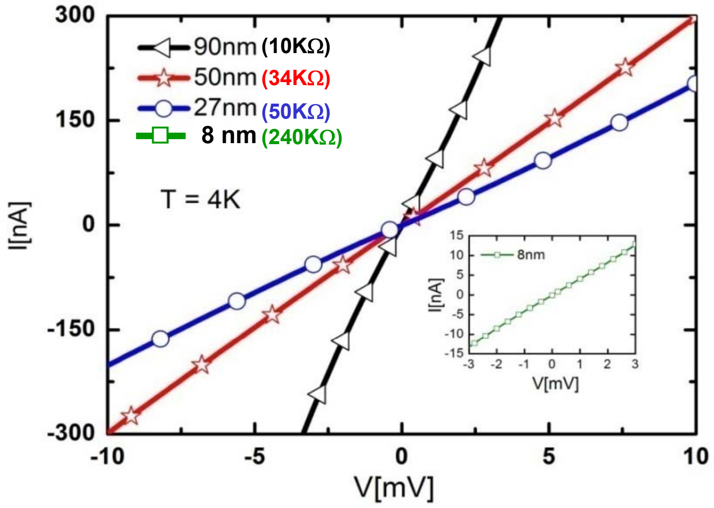

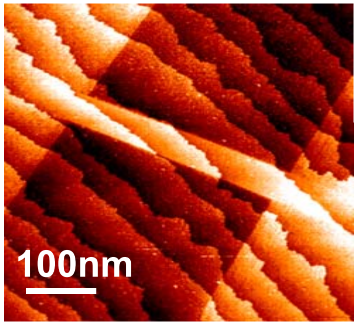

50 nm × 320nm wire

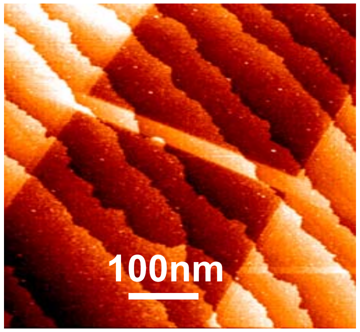

27 nm × 320nm wire

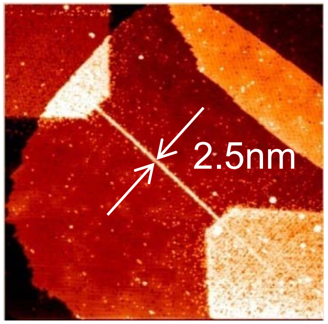

2.5 nm × 50nm wire

F.J. Ruess et al. Applied Physics Letters **92**, 0521011 (2008)
F.J. Ruess, Small 3, 563 (2007)

Gating STM-patterned tunnel gaps

TOP GATE ON NATIVE OXIDE

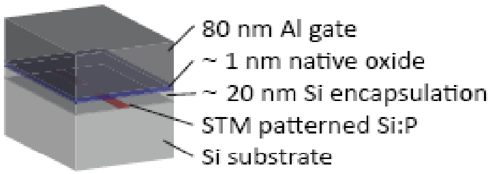

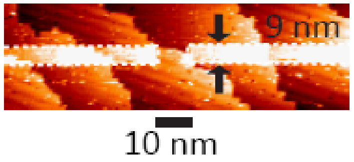

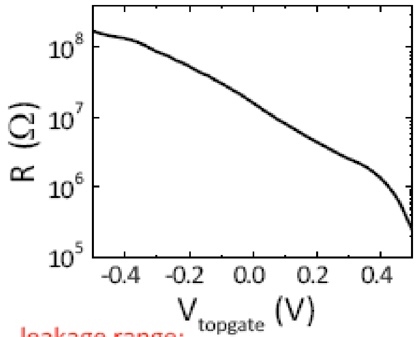

leakage range:
-500 mV to +500 mV

TOP GATE ON UHV OXIDE

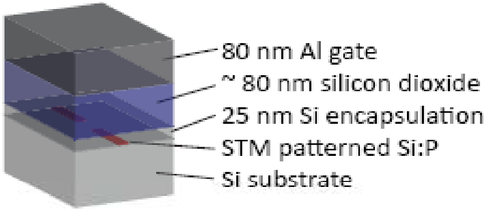

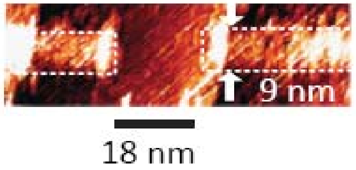

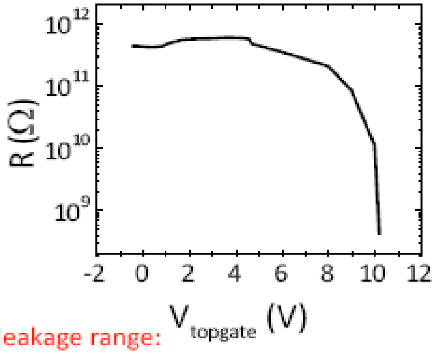

leakage range:
-10 V to +10 V

IN-PLANE GATE

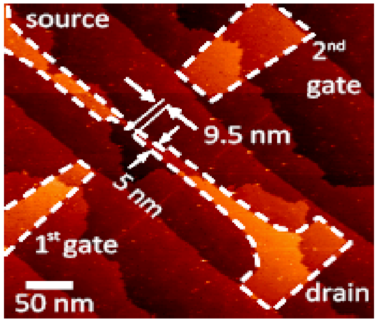

Gap-gate separation: 67 nm and 69 nm

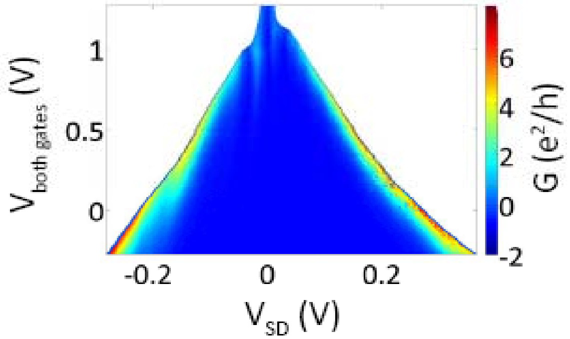

leakage range:
-1700mV to +1700 mV

	Resistance change	Leakage range
Native oxide (D75)	10^5 Ω - 10^8 Ω (1000 %)	-500 mV to 500 mV
UHV oxide (D7)	10^8 Ω - 10^{11} Ω (1000 %)	-10 V to 10 V
In-plane gate (D90)	6 MΩ - 66 GΩ (3000 %)	-1700 mV to 1700 mV

In-plane gates afford a large gating range with better stability

Quantum dot architectures towards single donor devices

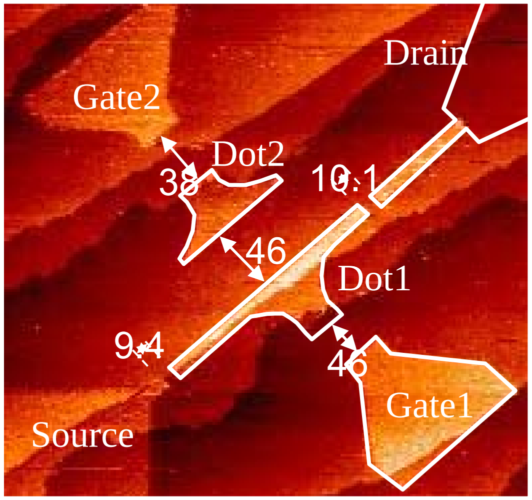

All epitaxial in–plane gated 5 terminal Si:P dot

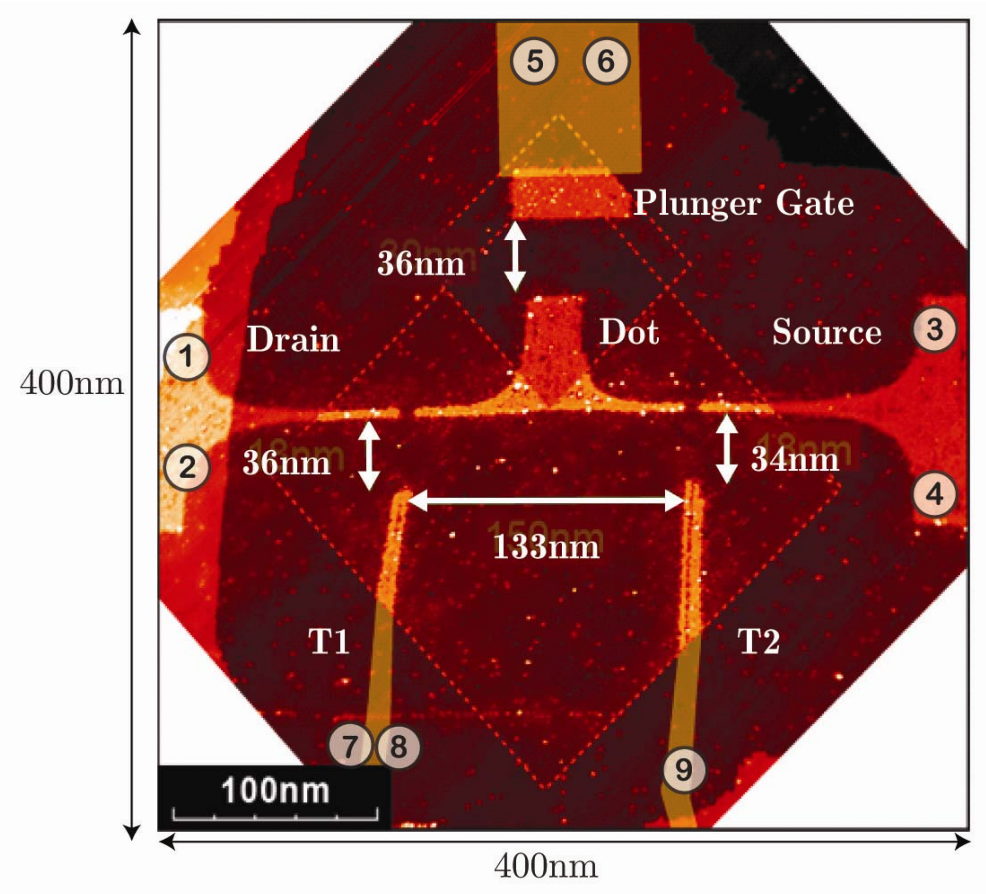

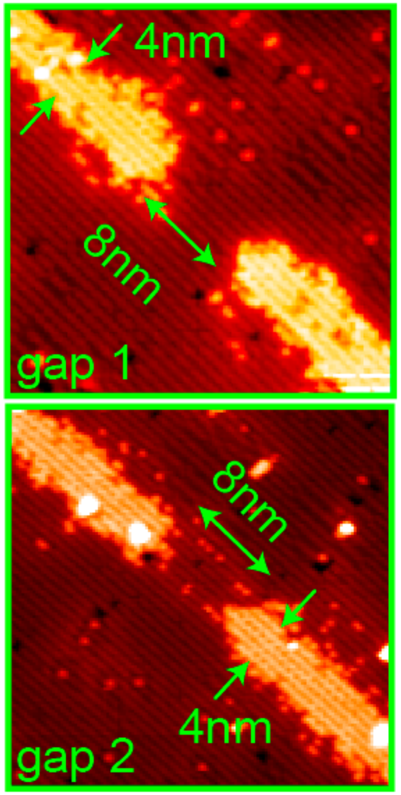

- use knowledge from previous experiments => 8nm tunneling gaps
- in-plane plunger and barrier gates
- optimize capacitive coupling with gate geometry and shape of dot
- area of dot ≈ 2000 nm^2 → 4000 electrons

4000 donor Si:P quantum dot

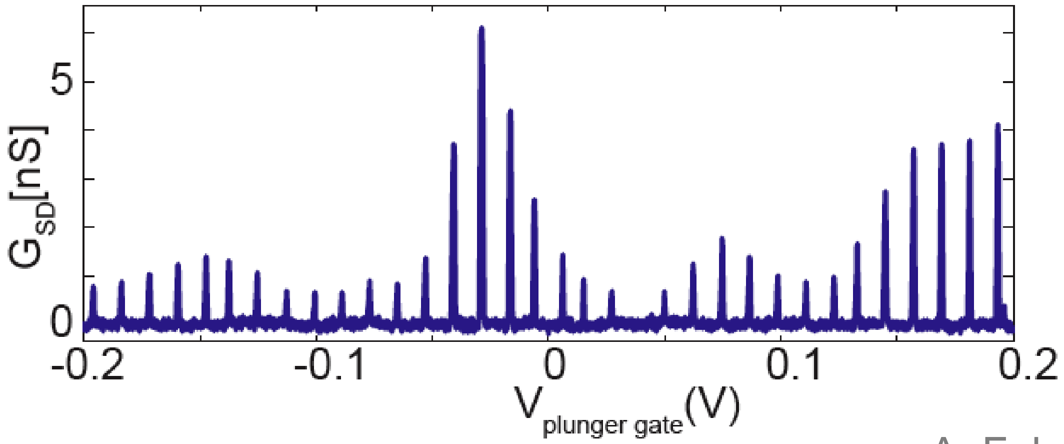

Size of dot = 2000nm^2
Estimated # of electrons
on the dot ~ 4000
Sum Capacitance of dot = 46aF
Charging energy = 3.3meV

Changing in-plane gate:
depletes ~ 50 electrons

A. Fuhrer *et al.*, Nano Letters 9, 707 (2009).

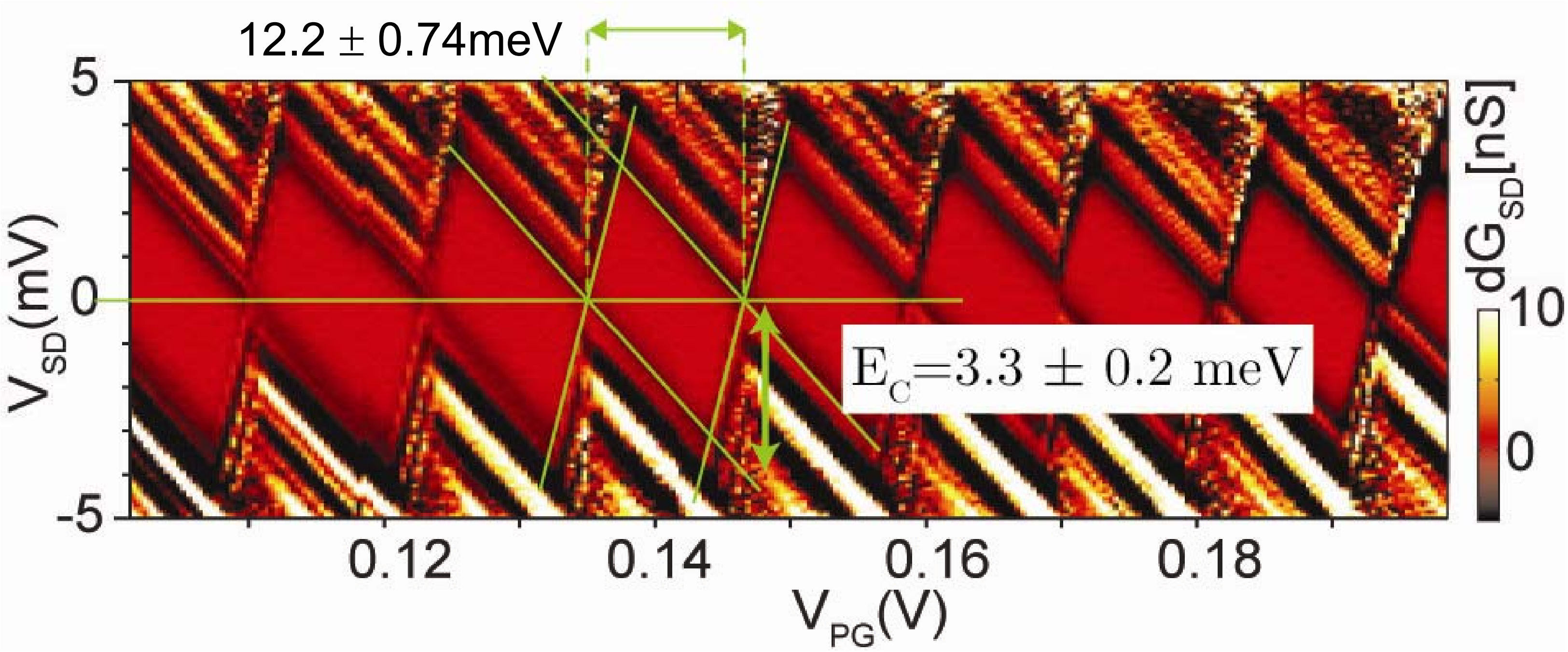

Comparison of top gated and in-plane gates

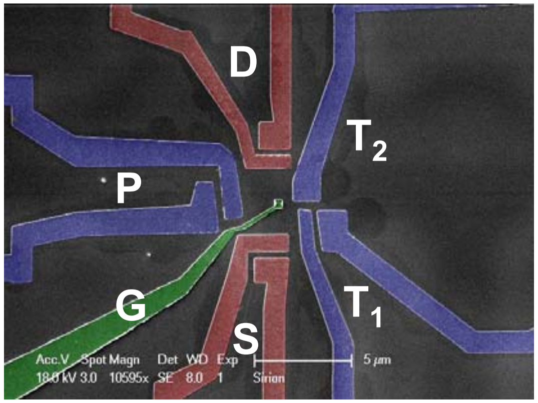

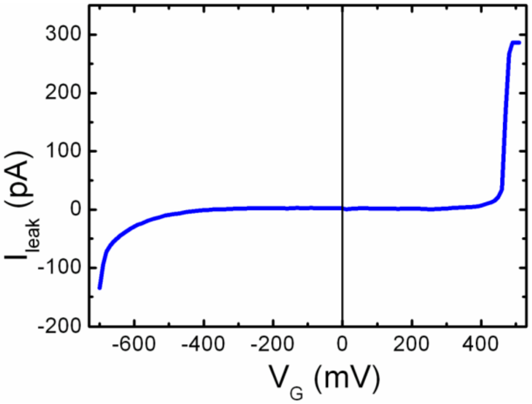

- top gate on native SiO_2 barrier has a gate range of ±400 mV

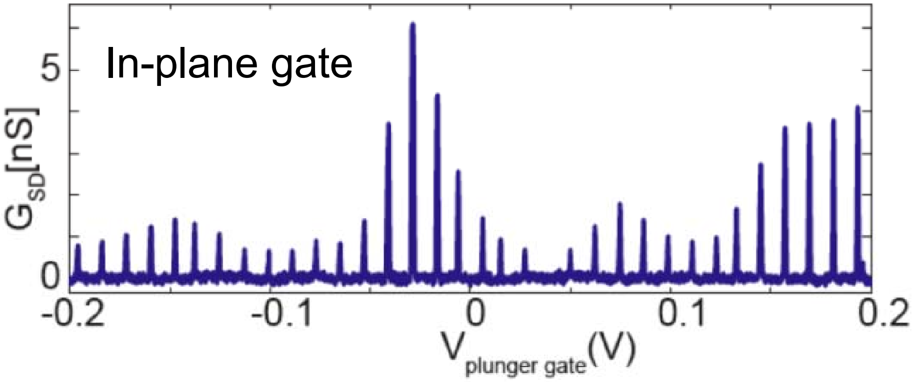

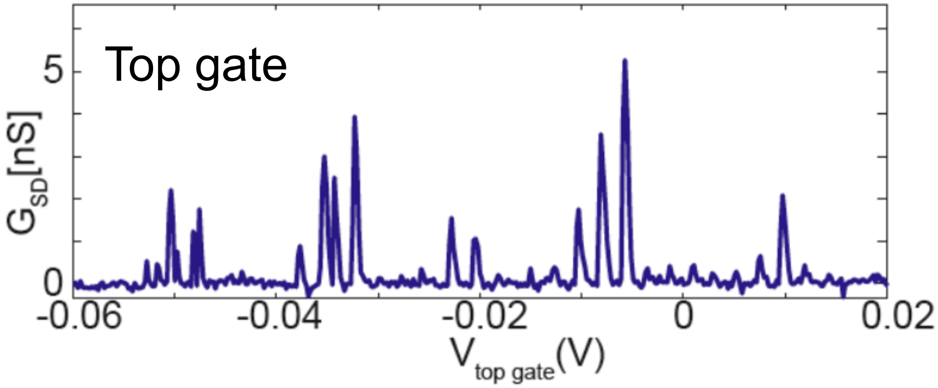

- Coulomb blockade oscillations: $\Delta V_G = e / C_G = 2.2$ mV => can tune electron number by ~ 350
- more noise: top gate affects the stability of the device
- **Epitaxial in-plane gates allow stability comparable or better than that of quantum dots in other material systems**

Worlds smallest atomically precise transistor

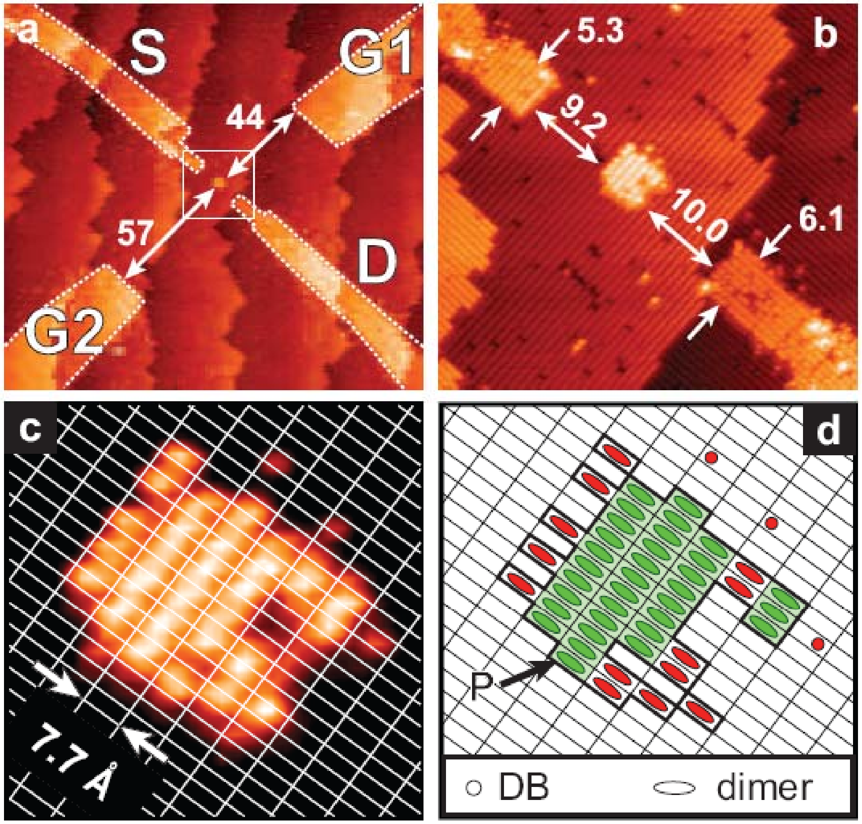

Nature Nanotechnology 5, 502 (2010)

We can estimate the number of donors incorporated from the size of the lithographic patch created by STM. Typically require 3 adjacent dimers to incorporate 1P atom.

Statistical incorporation study for similar dot sizes ➔ **6±3 donors** most likely

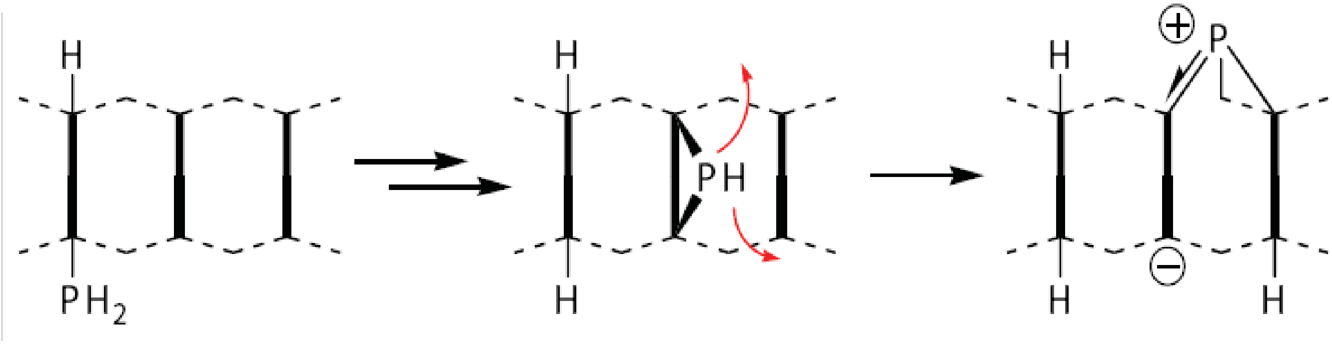

Extremely dense excited state energy spectrum

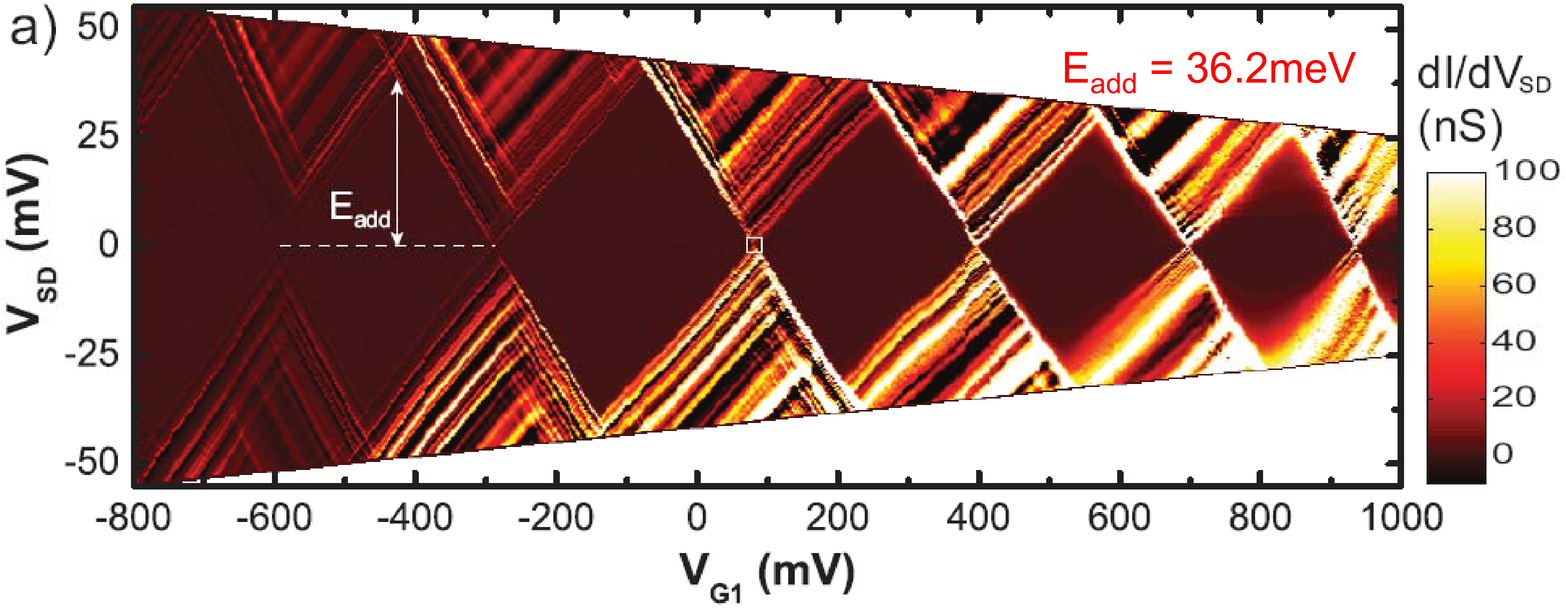

- Surprisingly high density of lines of increased conductance
- Rise in addition energy as electron occupation is lowered
  → indicative of a few-electron dot
- Gate voltage dependence of tunnel barriers:
  → Increase in device conductance
  → change in coupling asymmetry

Importance of features at the atomic-scale

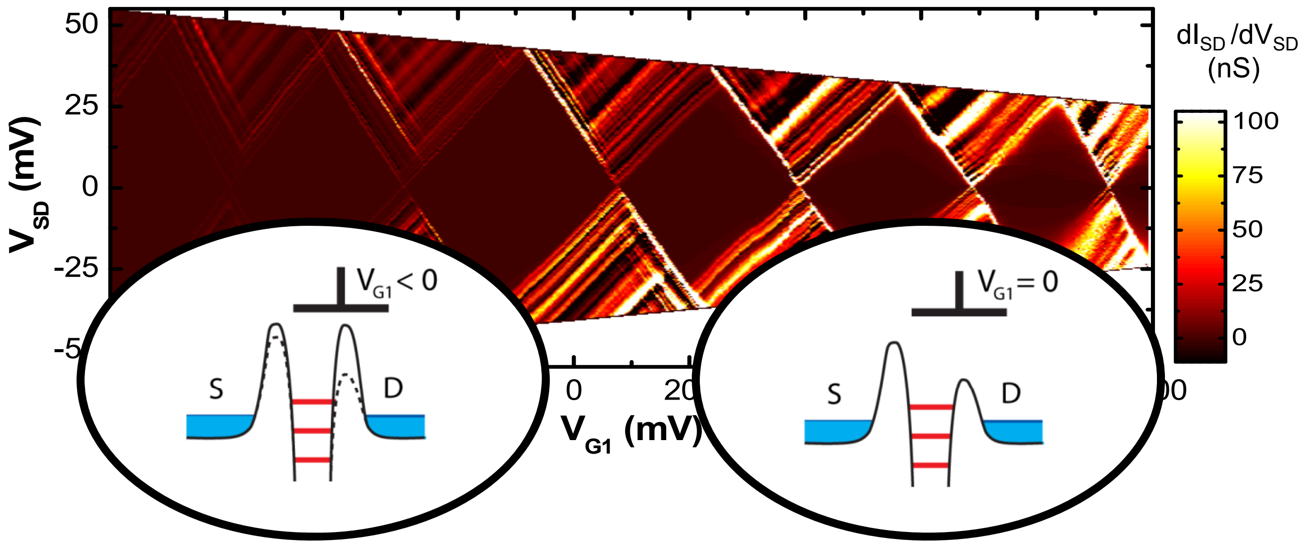

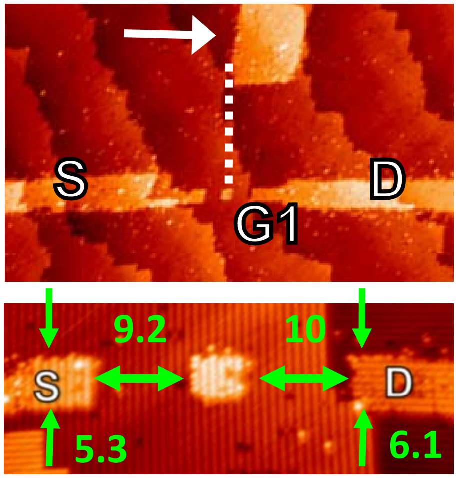

Tunnel coupling:

- $V_{G1} > 0$: predominantly lines with positive slope

  → stronger *tunnel coupling* to D
  (higher gap aspect ratio: 0.61 > 0.58)

- Gate G1 shifted towards D: coupling asymmetry changes with gate voltage

Nature Nanotechnology 5, 502 (2010)

Surprisingly dense excitation spectrum

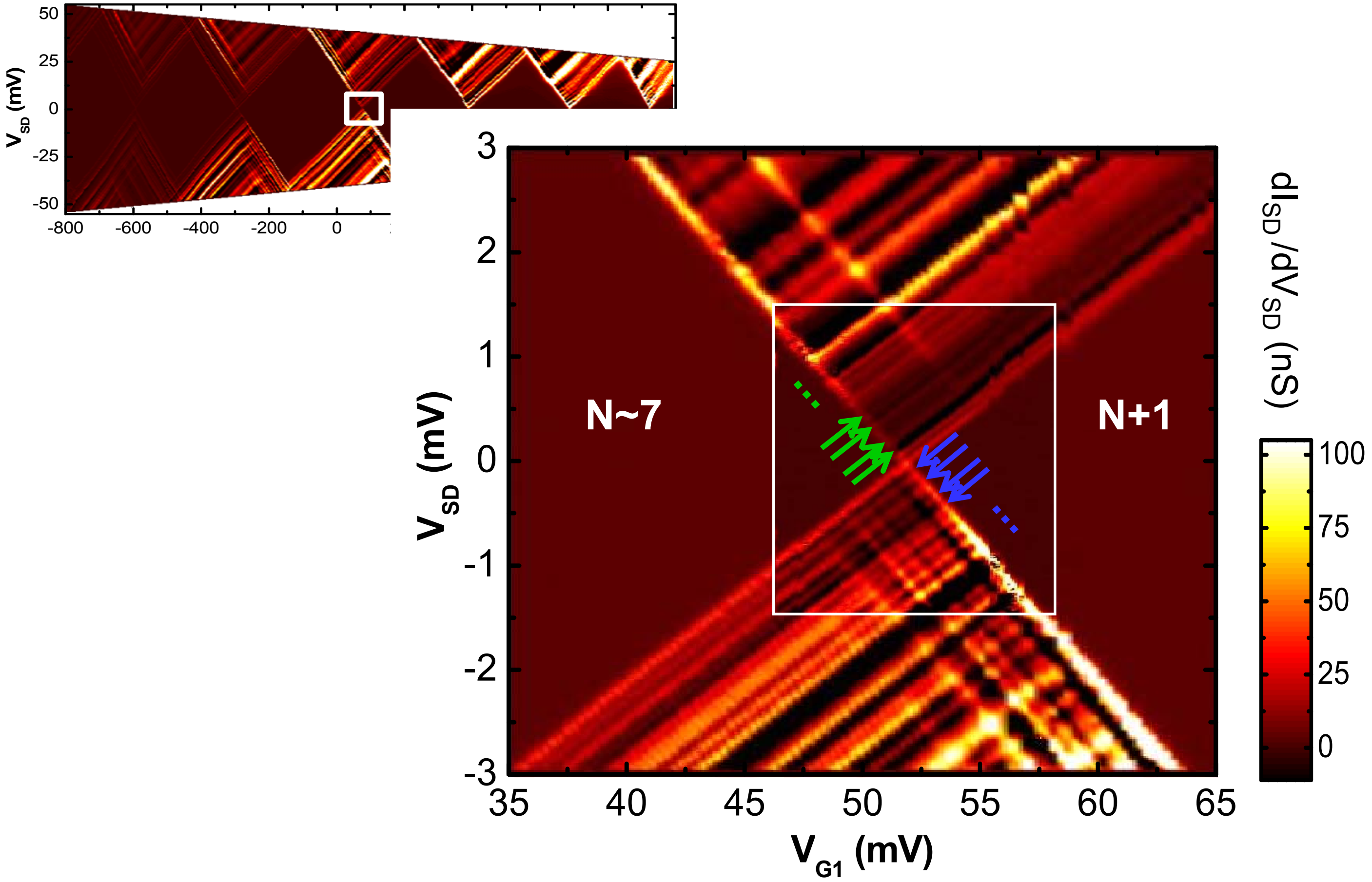

Energy spectrum

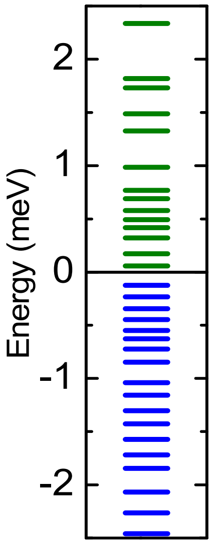

(only lines w. pos. Slope)

- Close-up reveals even higher density of resonant features

- Average level spacing **ΔE = 100μeV**

➔ What is the origin of these features?

Density of states at the Fermi energy

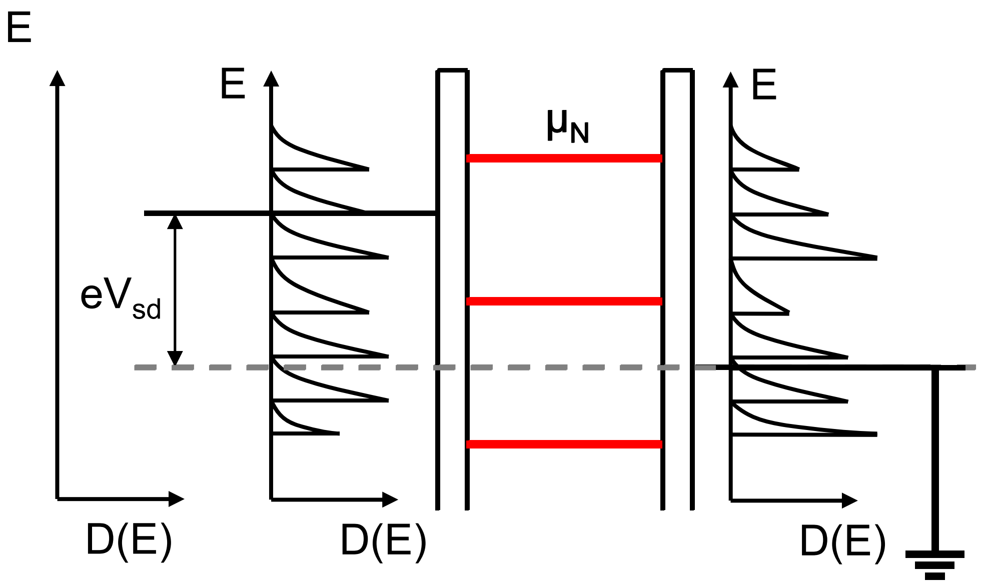

Mean energy spacing from lateral confinement of the dot:

$$\Delta E = \frac{\pi\hbar^2}{g m^* A} \quad \sim 12\ \mathrm{meV}$$

$m^*_{ave} = 0.28\ m_e$

$g = g_{spin}$ x $g_{valley} = 12$

Sub band separation from lateral confinement of the leads:

$$\Delta E_n = \frac{\hbar\omega_0}{g} = \frac{\hbar}{g}\sqrt{\frac{8V}{m^* l^2}} \approx 7\mathrm{meV}$$

Valley splitting in silicon

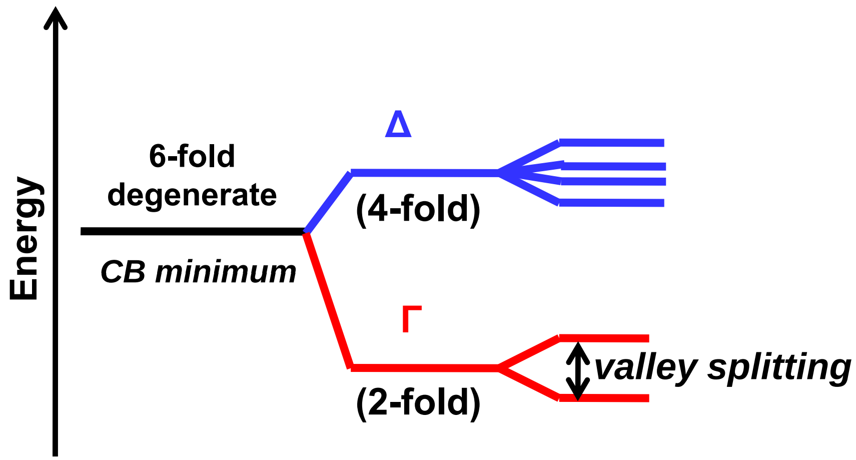

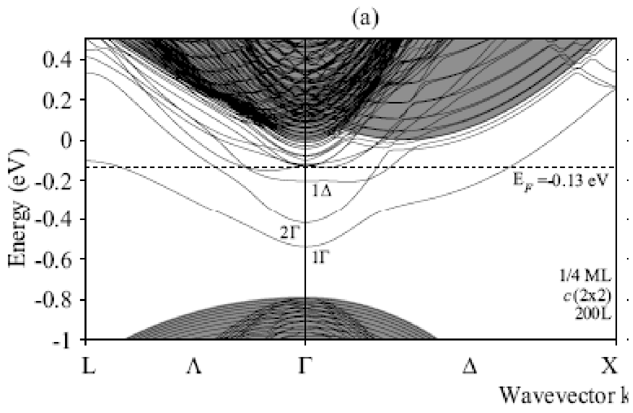

D.J. Carter, Phys. Rev. B 79, 033204 (2009).

bulk Si:
6 degenerate valleys

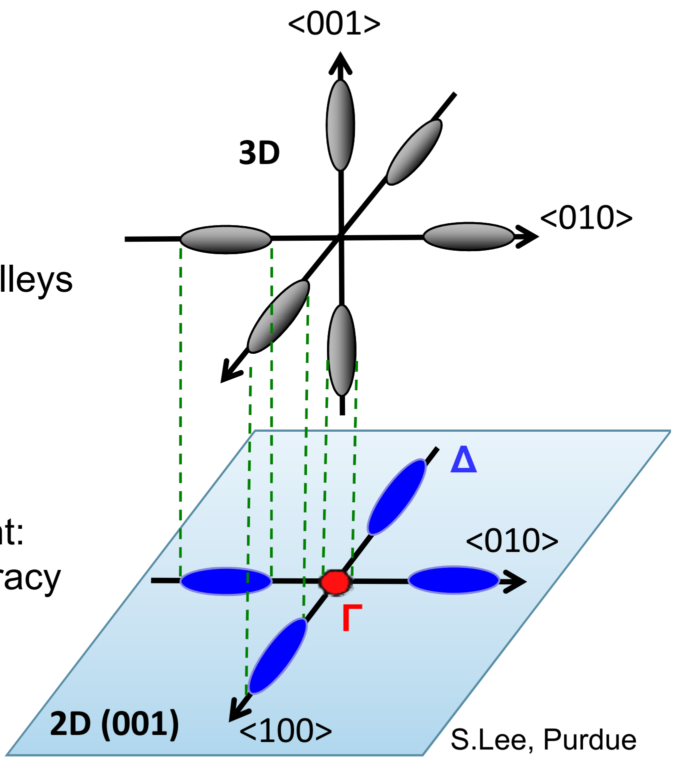

S.Lee, Purdue

strain, confinement:
2 + 4-fold degeneracy

steep confinement, interfaces:

splitting of remaining degeneracy due to difference in fast oscillating part of the wavefunctions

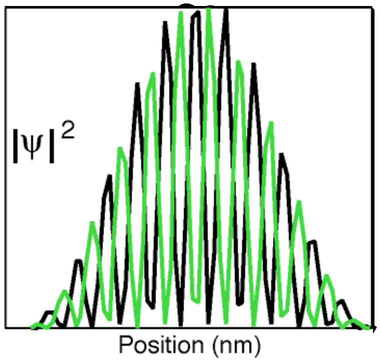

Collaboration with Mark Friesen and Mark Eriksson, Wisconsin-Madison

Calculating the spectrum of the 7 donor dot

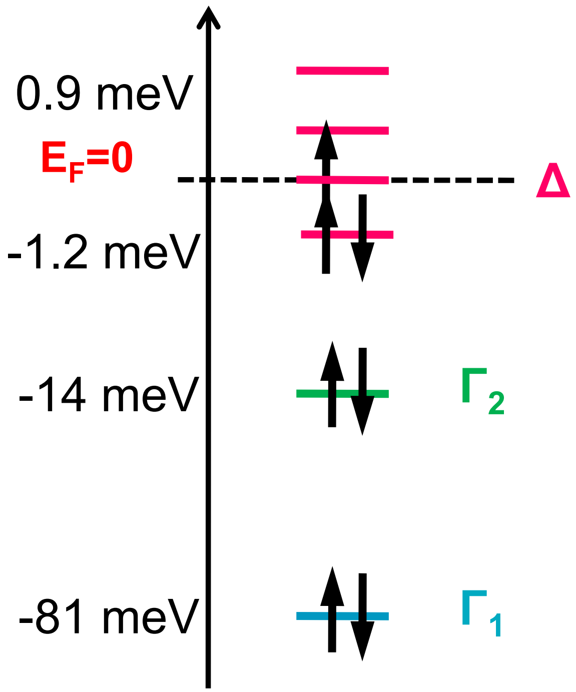

For 3 electrons in Δ shell: there are 56 possible configurations with 8 different energies

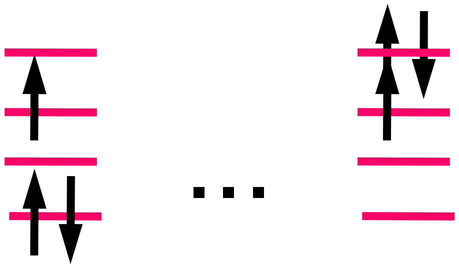

1st excited state (2-fold)

highest excited state (4-fold)

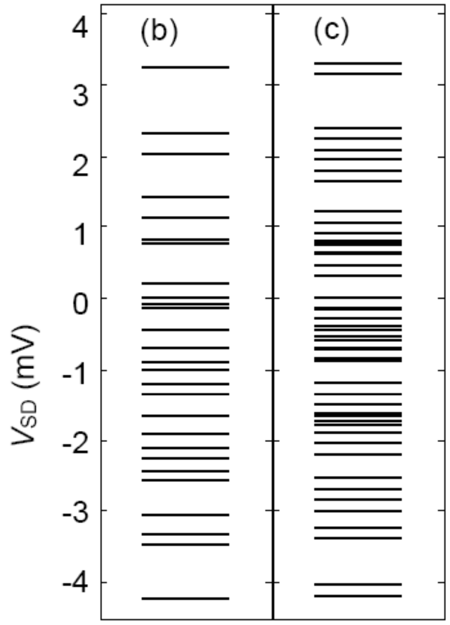

Average energy level spacing ΔE≈100μeV

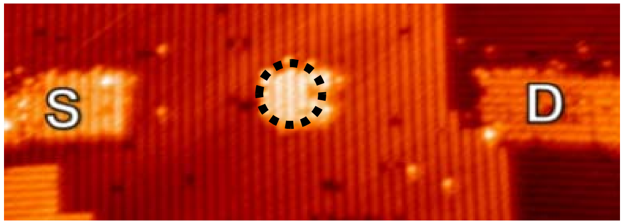

Splitting depends on dot anisotropy

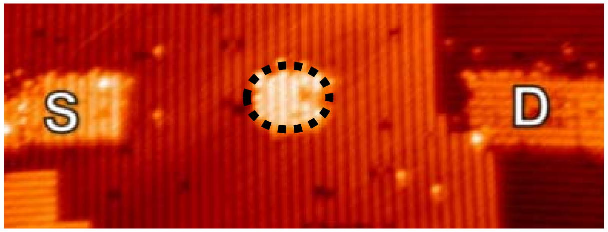

→RESONANCES ARE CONSISTENT WITH VALLEY SPLITTING ON THE DOT

Towards the single donor limit

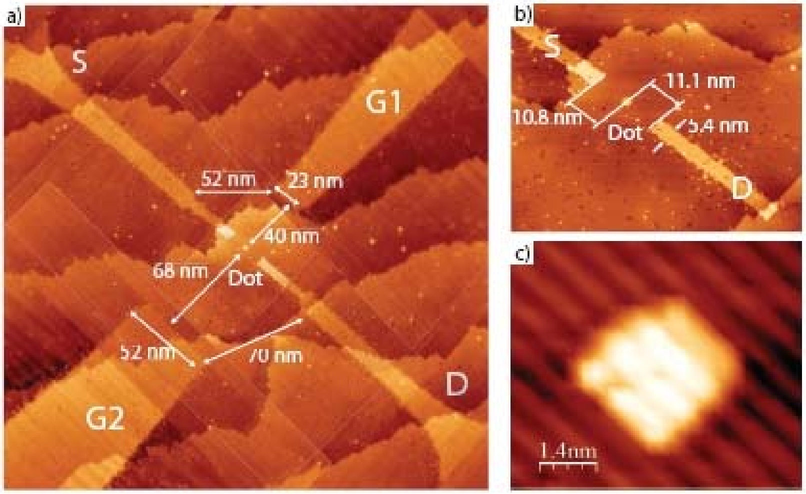

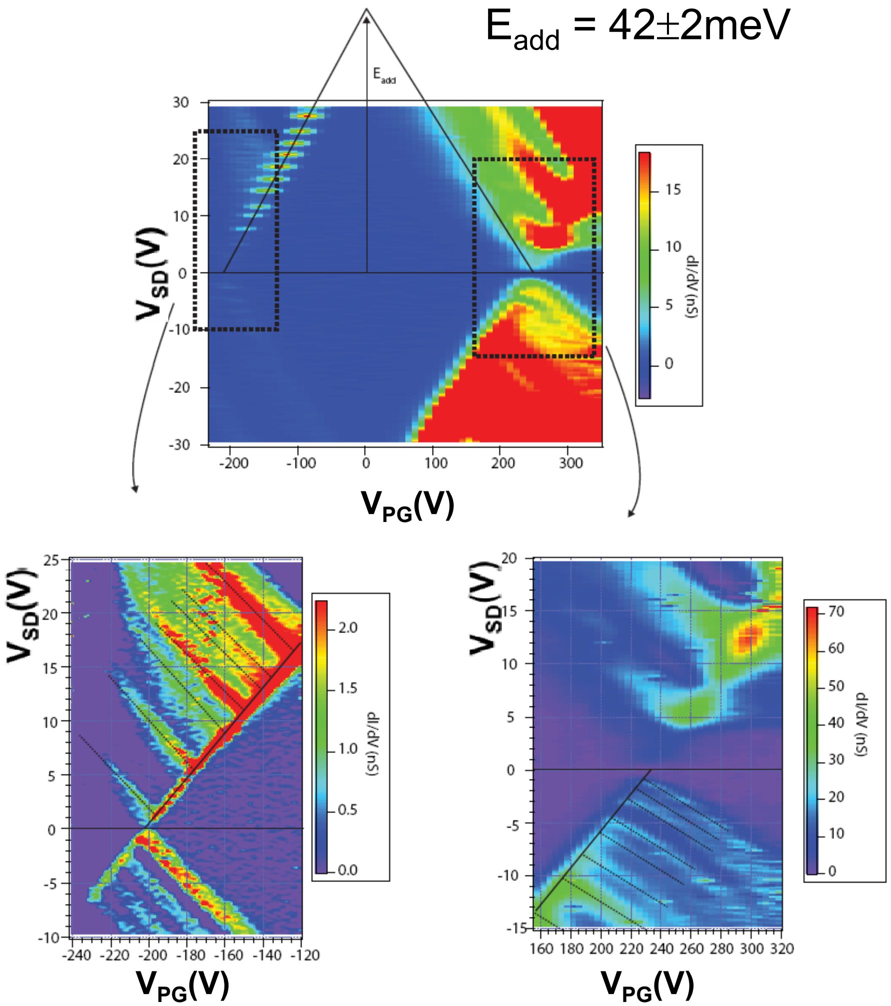
E_{add} = 42±2meV

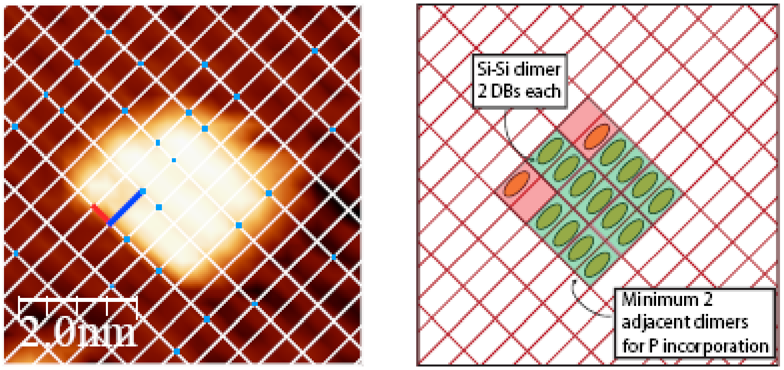

STM lithography reveals that a statistically 1-4 donors can be incorporated

Excited states in a single/few donor device

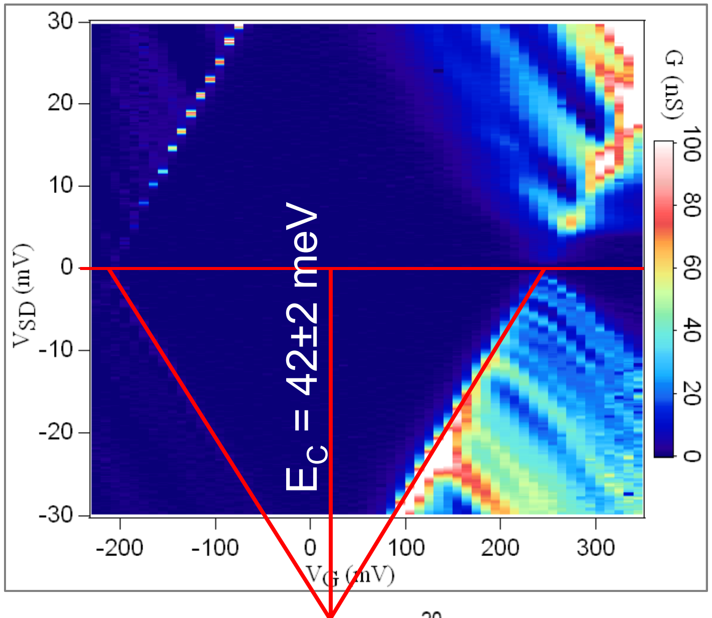

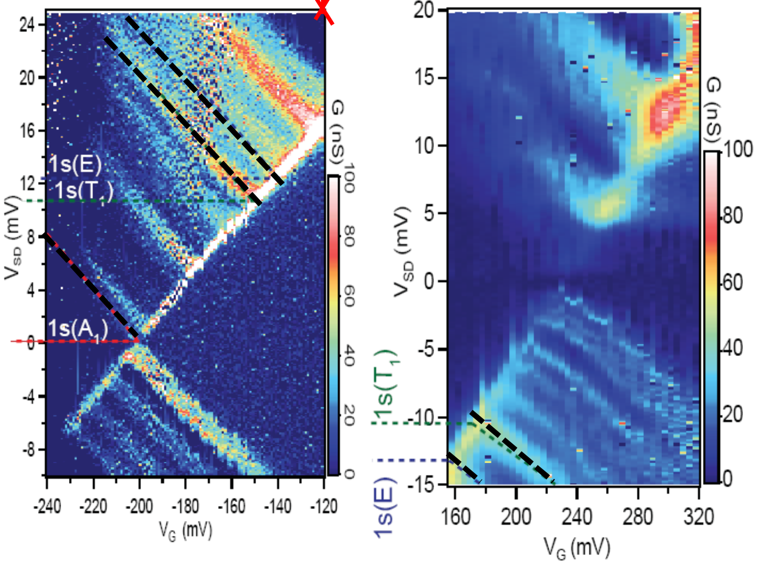

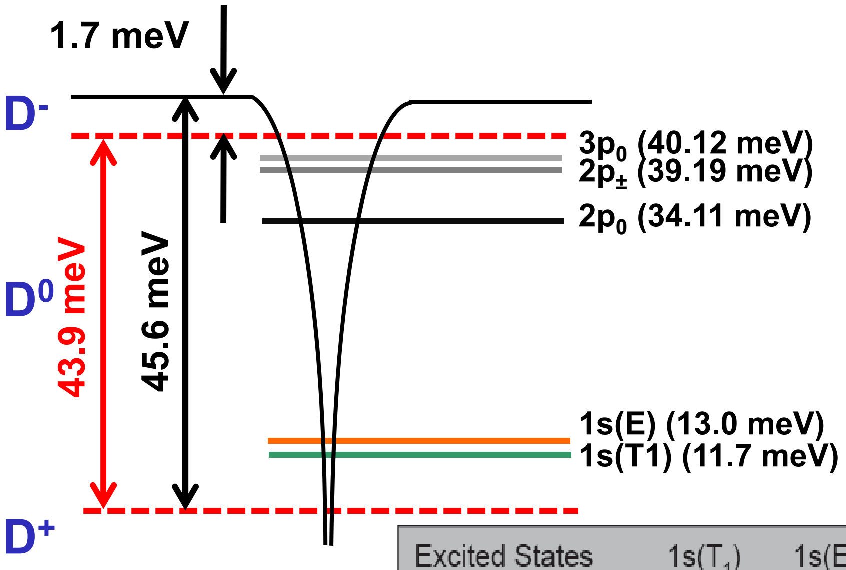

Excited States	1s(T_1)	1s(E)
Bulk Si:P (mV)	11.70	13.01
(+)ve V_G (mV)	10.4±2.8	13.8±1.4
(-)ve V_G (mV)	10.8±1.3	13.9±1.4

- Addition energy ~42±2meV is consistent with the D^0 state of a P donor
- Excited state spectra are consistent with a bulk donor in Si
- Additional lines likely due to van Hove singularities in the leads

Spin read-out of a dot with multiple P donors

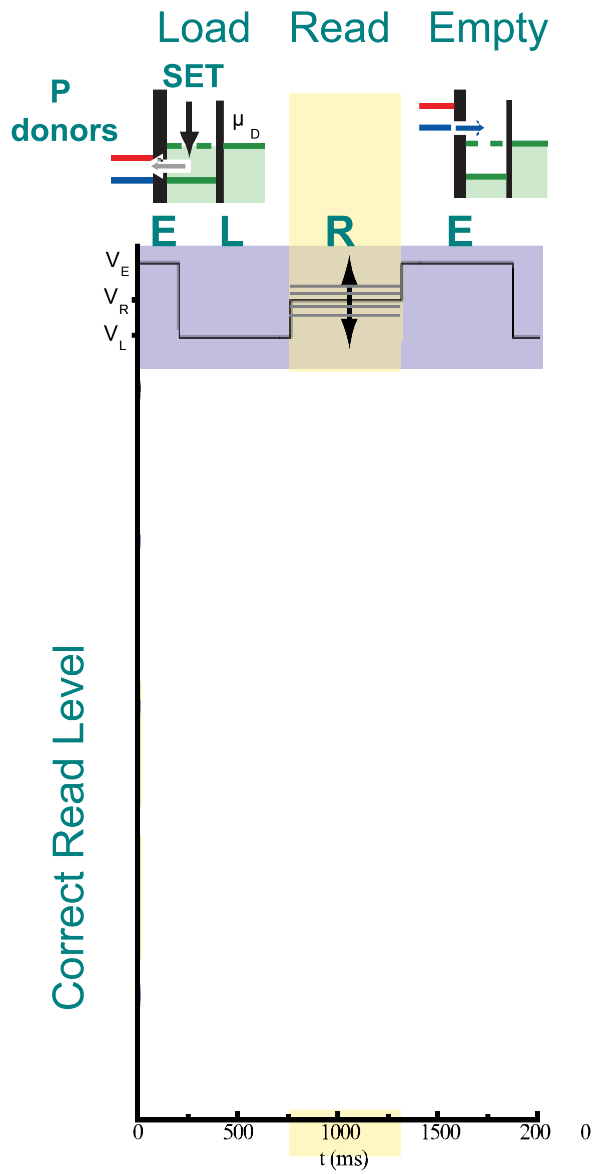

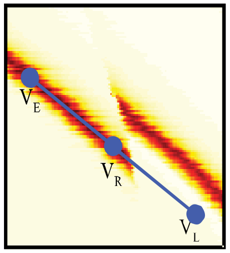

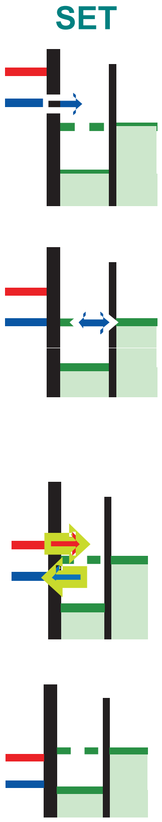

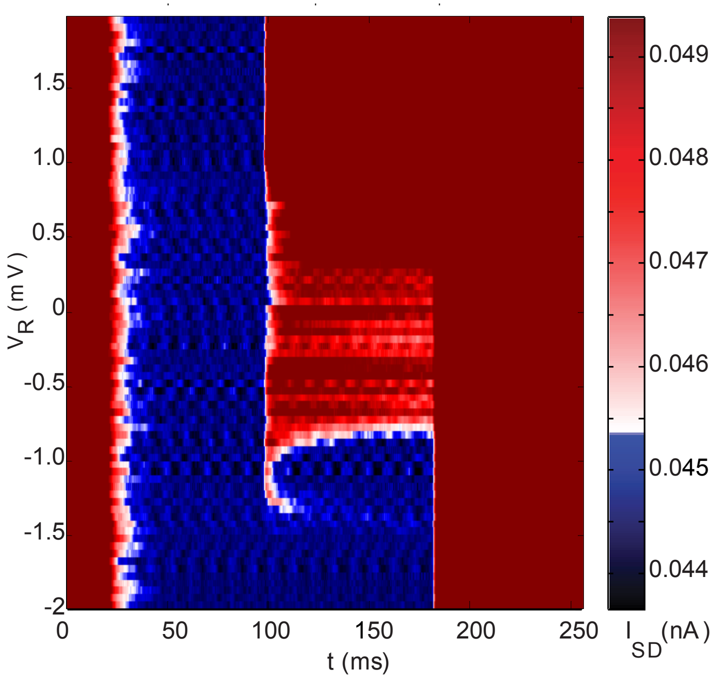

- We can apply suitable gate pulses to in-plane gates
- We get 100% contrast for charge read-out and therefore spin read-out for a single electron
- We can engineer the correct tunnel rates (~100ms)
- We obtain spin read-out for this multi-donor device
- T_1 ~ 1.3s @1.5Tesla.

An engineered double dot device each with < 4 donors

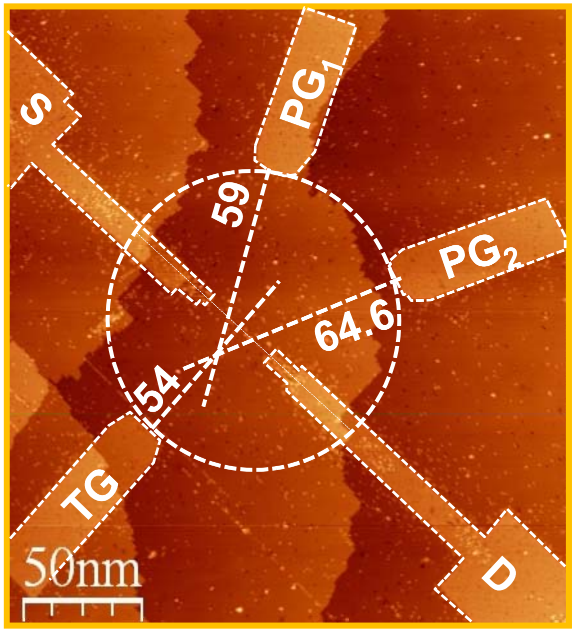

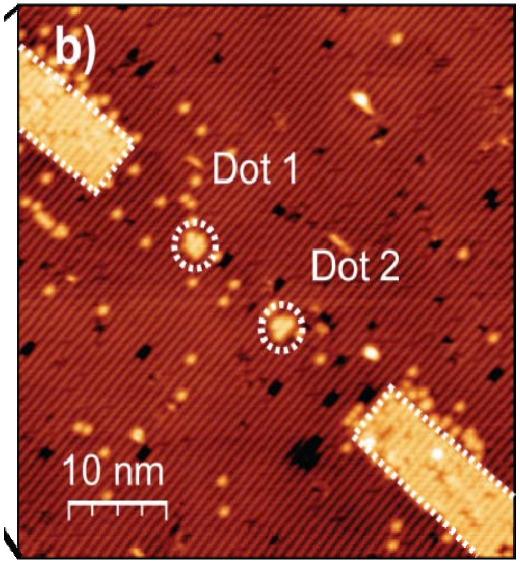

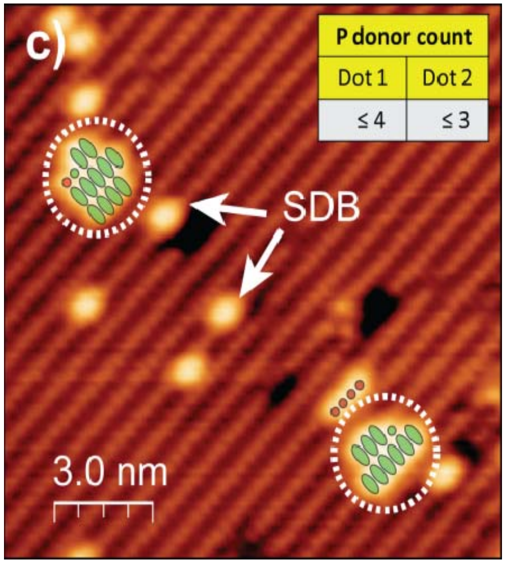

P donor count	
Dot 1	Dot 2
≤ 4	≤ 3

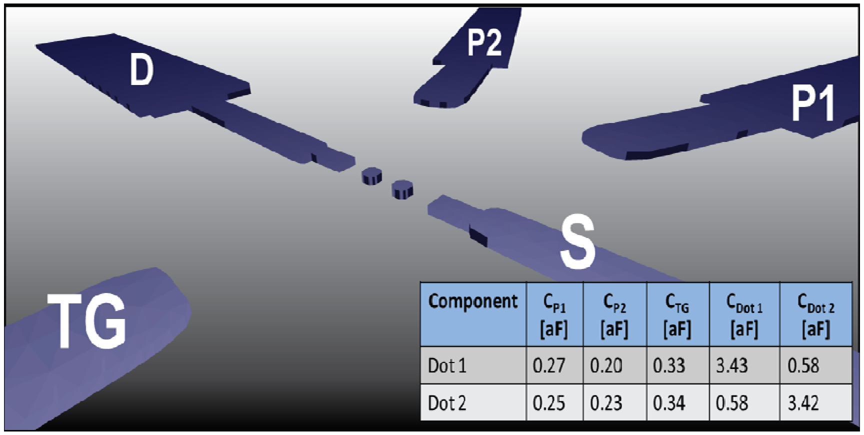

Component	C_{P1} [aF]	C_{P2} [aF]	C_{TG} [aF]	$C_{Dot\,1}$ [aF]	$C_{Dot\,2}$ [aF]
Dot 1	0.27	0.20	0.33	3.43	0.58
Dot 2	0.25	0.23	0.34	0.58	3.42

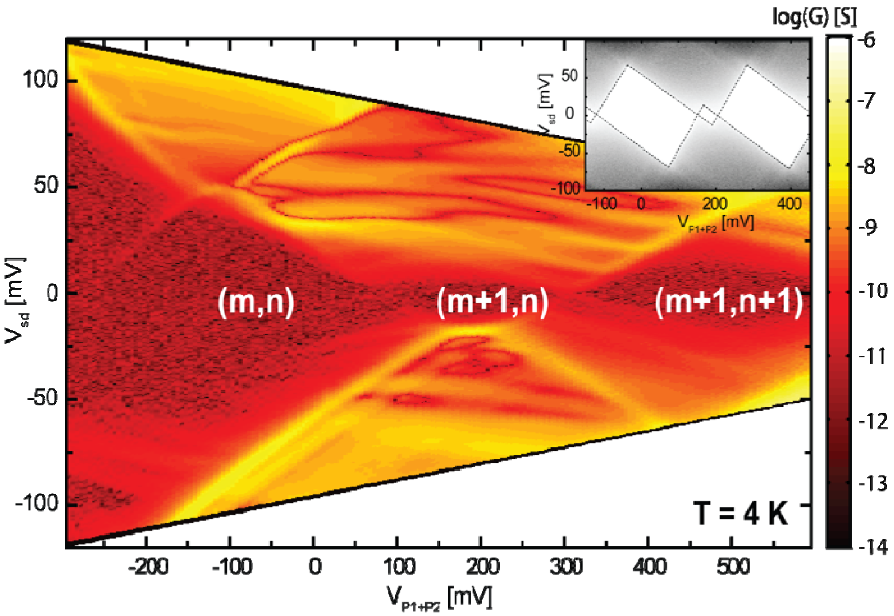

Pushing the limits of device modelling

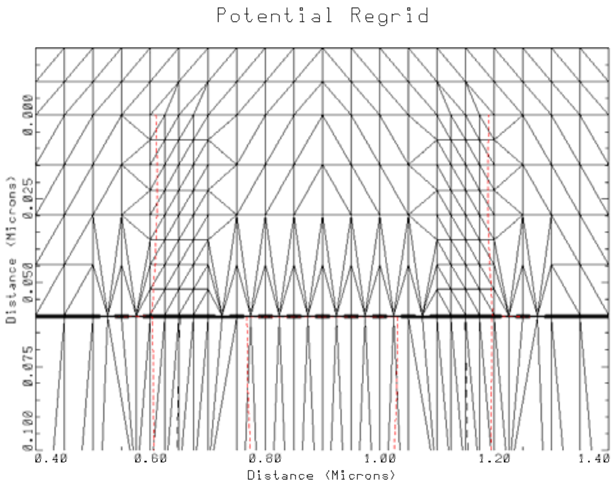

MEDICI SIMULATIONS:
to determine threshold voltage, DIBL etc
Chang, Haensch (IBM)

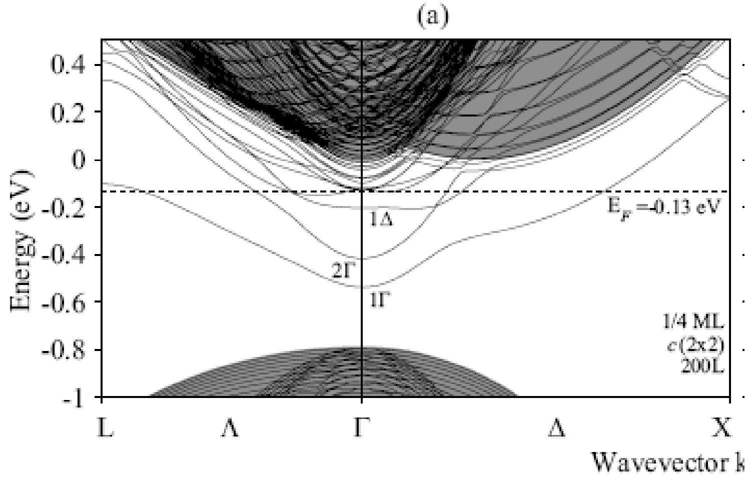

DENSITY FUNCTIONAL THEORY:
to determine band structure
Hollenberg (Melbourne) Warshkow (Sydney)

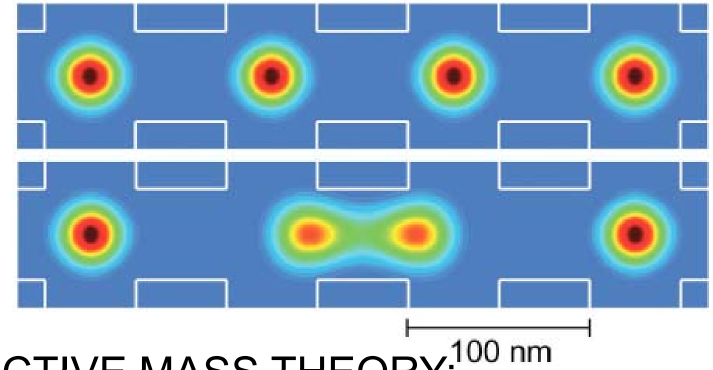

EFFECTIVE MASS THEORY:
to determine barrier heights and shapes
Friesen, Eriksson (Madison- Wisconsin)

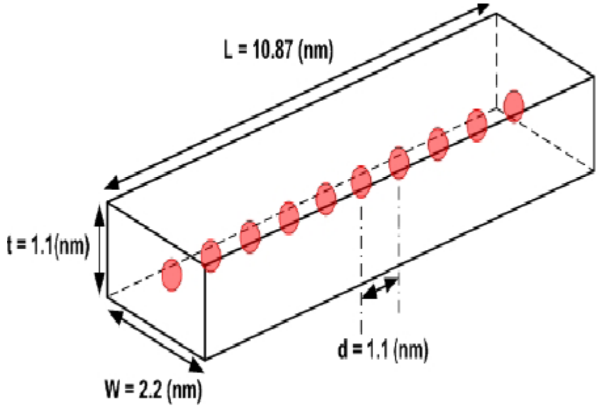

NEMO:
tight binding to determine transport
Klimeck (Purdue)

Summary

Investigated the role of valley splitting in silicon quantum dots

- Demonstrated atomic placement of single atoms in silicon
- Demonstrated operation of narrowest conducting wires in silicon
- Demonstrated superior stability and precision of in-plane gates
- Demonstrated electron transport through many to few electron silicon quantum dots
- Demonstrated the Worlds smallest precision transistor
- Highlighted the importance of valley splitting in nanoscale devices
- Demonstrated transport at the few to single donor level

Currently measuring spin dependent transport in silicon devices where donors are placed with atomic precision doping

The Research Team: Atom Builders


Custom designed scanning tunneling microscope


Combined scanning electron and scanning tunneling microscope

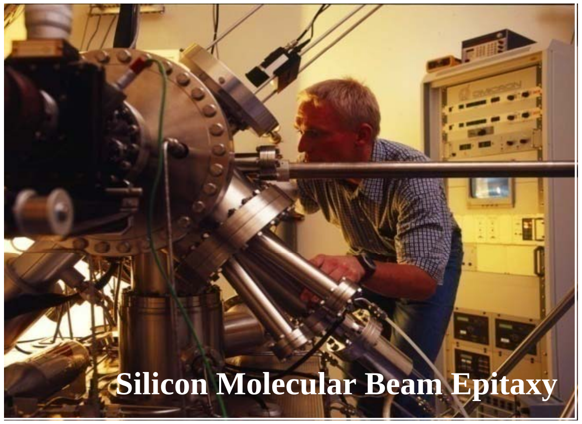
Silicon Molecular Beam Epitaxy

PhD:
S.R. Schofield, J.L. O’Brien,
T. Hallam, F. Ruess, J. Goh
W. Pok, F. Ratto, D. Thompson,
M. Fuschle, H .Campbell,
S.McKibben, C. Polley,
B. Weber, H. Buech, W. Klesse

Postdocs:
L. Oberbeck, N.J. Curson
T. G.C. Reusch, M.J. Butcher
G. Scappucci, F.J. Ruess,
X.J. Zhou, **W.R. Clarke,** A. Fuhrer,
W. Lee, S. Mahapatra, J. Miwa,
X. Kun

STM theory:
H. Wilson, **O. Warschkow,**
N. Marks, D. McKenzie,
M. Radny, P. Smith

Collaborators:

M. Friesen, M. Eriksson,
G. Klimeck, L.C.L. Hollenberg,
H.Ryu, S.Lee, M. Brandt, H.
Huebl, F. Koehne

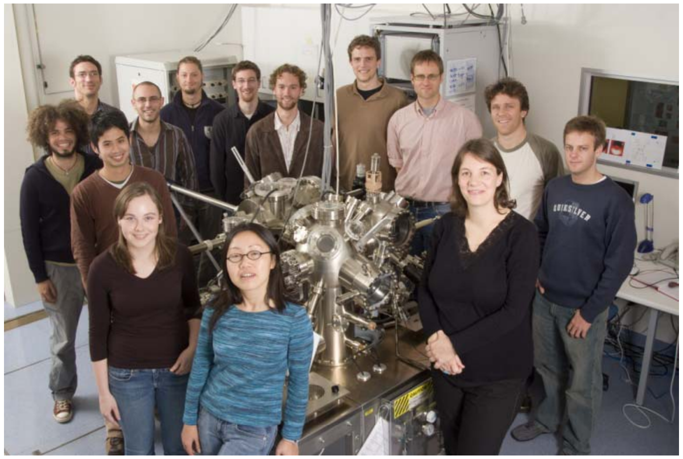

With thanks to:

Australian Government
Australian Research Council

invent

SRC Semiconductor Research Corporation

National Security Agency
United States of America

Science to Shape the Future of the Army
Army Research Office
1951

Doapnt Activation in Si and Ge by Low Temperature Microwave Anneal

Yao-Jen Lee

National Nano Device Laboratories, Taiwan

Outline

- **Introduction**
- **Topics**
  - **A low-temperature microwave anneal process for Boron-doped ultra-thin Si$_{0.2}$ Ge$_{0.8}$ epi-layer (*IEEE Electron Device Lett., vol. 30, no. 2, pp. 123–125,*Feb. 2009.)**
  - **P^{31} activation in single crystalline germanium by low temperature microwave annealing (Accepted by IEEE EDL)**
  - **SiN layer for larger strain stress after low temperature dopant activation process**
  - **65 nm poly-Si TFTs fabrication (IEDM 2009)**
  - **TiN gate poly-Si TFTs fabirication (*IEEE Electron Device Lett., vol. 31, no. 5, pp. 437–439,*May. 2010.)**
- **Conclusions**

Roadmap from ITRS

Year of Production	2009	2010	2011	2012	2013
MPU/ASIC M1 Pitch (nm)	54	45	38	32	27
L_g: Physical L_{gate} for high performance logic (nm)	29	27	24	22	20
E.O.T (Equivalent Oxide Thickness, nm)	1	0.95	0.88	0.75	0.65
Junction depth (nm)	13	12	10.5	9.5	8.7

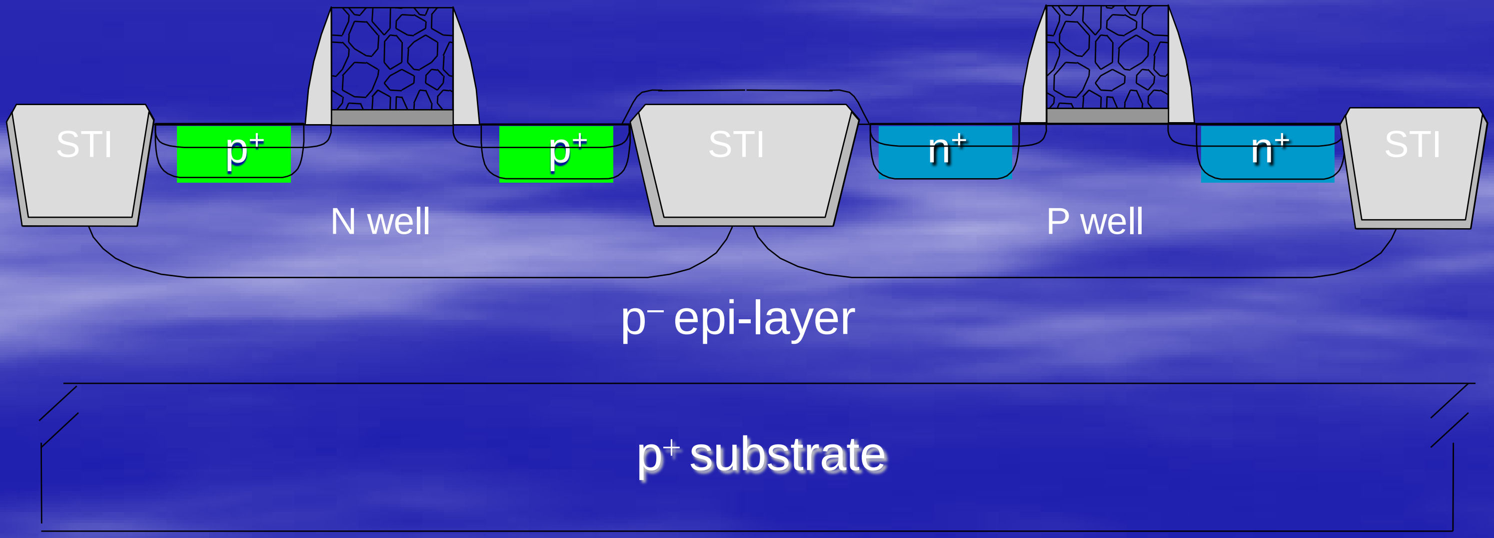

Doapnt Activation Methods

- Conventional furnace
- RTA
- Spike RTA
- Laser anneal
- Flash anneal
- Solid Phase Epi (SPE): low temperature
- Microwave anneal: Low or high temperature

High Temperature Microwave Anneal

- [1] K. Thompson, Yogesh B. Gianchandani, John Booske, *IEEE*, and Reid F. Cooper, "Direct Si-Si Bonding by Electromagnetic Induction Heating," *J. Micro Electro Mechanical Systems*, Vol. 11, No. 4, 2002, pp. 285-292.
- [2] K. Thompson, J. H. Booske, Y. B. Gianchandani, and R. F. Cooper, "Electromagnetic Annealing for the 100 nm Technology Node," *IEEE Electron Device Lett.*, 23, 2002, pp. 127 - 129.
- [3] K. Thompson, John H. Booske, Reid F. Cooper, and Yogesh B. Gianchandani, "Electromagnetic Fast-Firing for Ultra-Shallow Junction Formation," *IEEE Trans Semiconductor Manufacturing*, Vol. 16, No. 3, 2003, pp. 460-468.

High Temperature Microwave Anneal

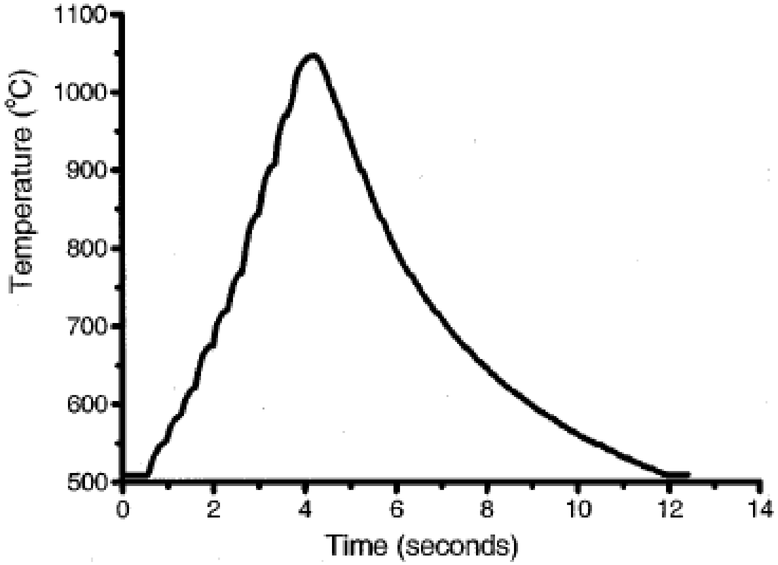

Fig. 1. Temperature transient for a 75 mm silicon wafer heated in the microwave system in the TM111 mode at 1000 W.

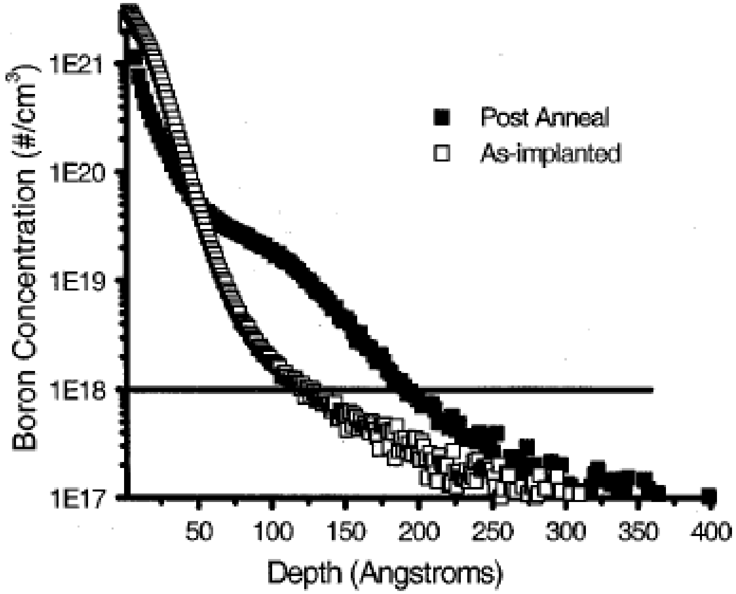

Fig. 5. Profile of boron concentration before and after anneal for BF$_2$ implant at 1100 eV and $5 * 10^{15}/\text{cm}^3$ dose. Very little diffusion ~ 6.5 nm occurs for a resulting sheet resistance of 950 Ω/sq.

[2] K. Thompson, J. H. Booske, Y. B. Gianchandani, and R. F. Cooper, "Electromagnetic Annealing for the 100 nm Technology Node," *IEEE Electron Device Lett.*, 23, 2002, pp. 127 - 129.

Mobility Enhancement in Ge Film

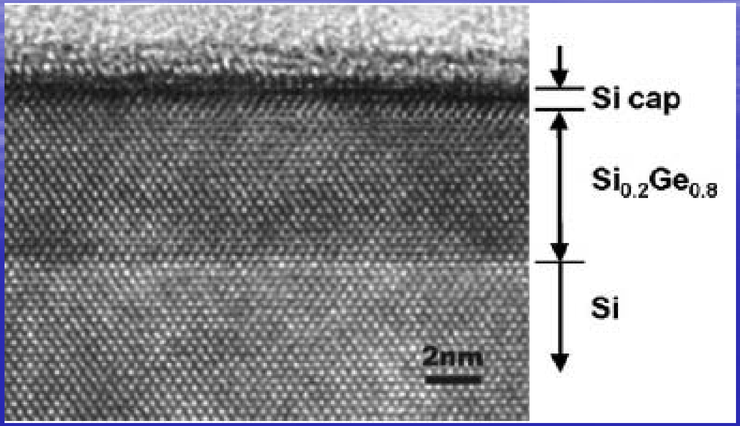

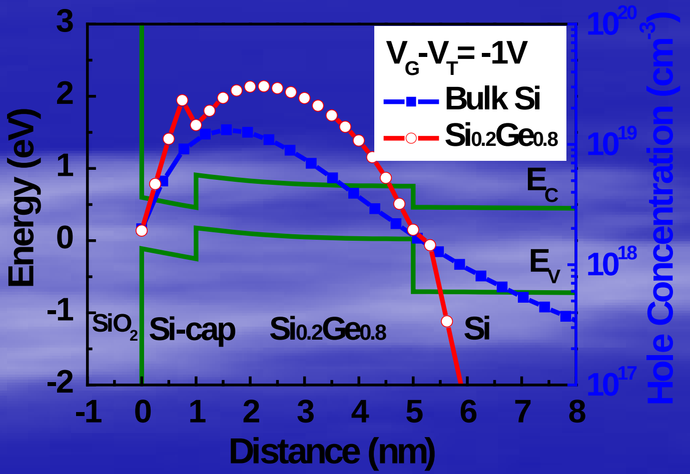

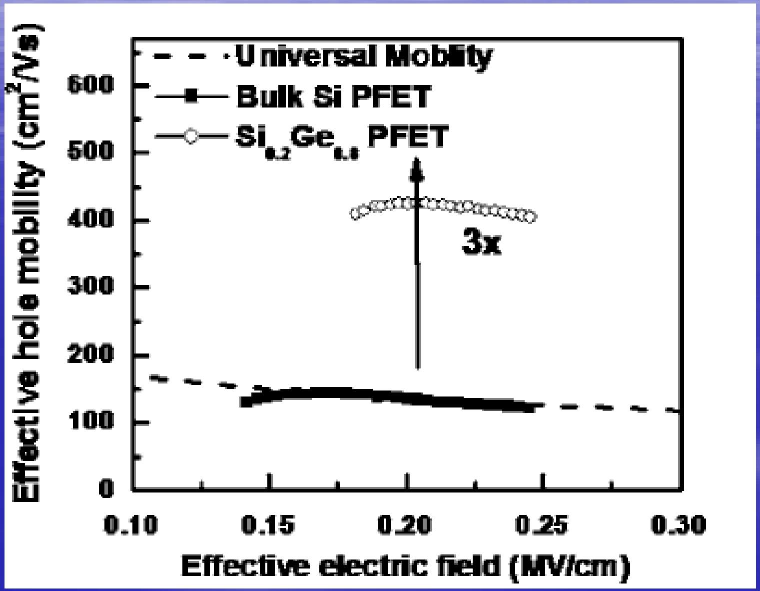

- Higher hole concentration in Si/$Si_{0.2}Ge_{0.8}$/Si quantum well due to the Ge/Si hetero-junction confinement.
- ~3x hole mobility enhancement for the $Si_{0.2}Ge_{0.8}$ quantum well SB

C-Y Peng, et al., 2007

Outline

- Introduction
- Topics
  - A low-temperature microwave anneal process for Boron-doped ultra-thin $Si_{0.2}$ $Ge_{0.8}$ epi-layer (*IEEE Electron Device Lett., vol. 30, no. 2, pp. 123–125,*Feb. 2009.)
  - P^{31} Activation in Single Crystalline Germanium by Low Temperature Microwave Annealing (Accepted by IEEE EDL)
  - SiN layer for larger strain stress after low temperature dopant activation
  - 65 nm poly-Si TFTs fabrication (IEDM 2009)
  - TiN gate poly-Si TFTs fabirication (*IEEE Electron Device Lett., vol. 31, no. 5, pp. 437–439,*May. 2010.)
- Conclusions

Process Flow

- N-type Si (100) Substrate
- 28 nm Si buffer layer deposited by UHVCVD
- 3 nm $Si_{0.2}Ge_{0.8}$ layer grown on the Si buffer layer by UHVCVD
- 3~4 nm Si capping layer grown in situ on the top of the epi-Ge layer
- 2 cm^2 sections implanted by BF_2 at 15 KeV to a dose of 5e15 cm^{-2}

Process Flow (*cont.*)

- Anneal Methods
  - Conventional RTP Anneal
  - Low temperature microwave anneal

Experimental Results (*cont.*)

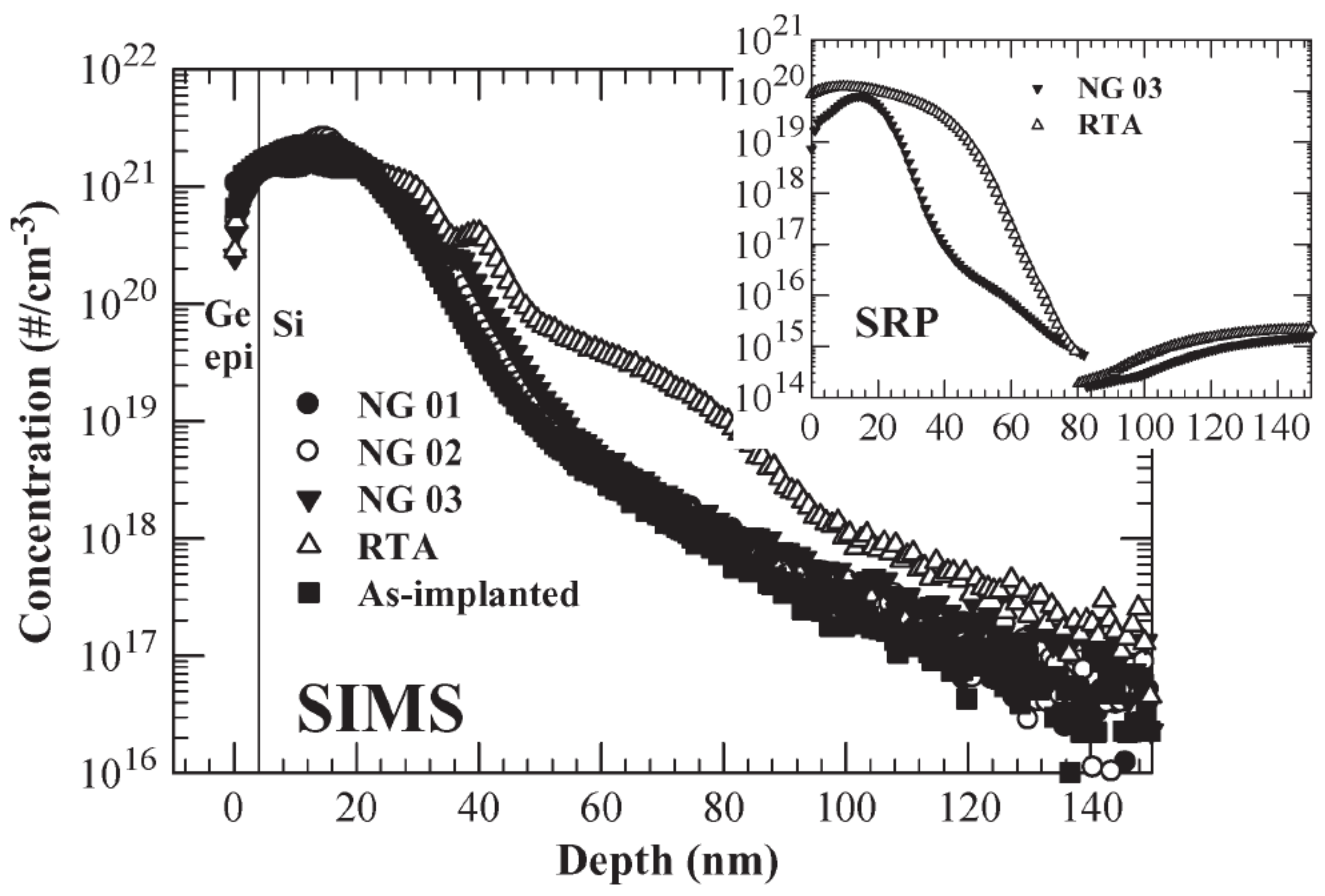

The boron distribution after the RTA of 900 °C for 30 s depicts a deeper boron distribution. The insert figure is the carrier concentration, which indicates the profile of dopant activation concentration, measured by SRP.

Experimental Results (*cont.*)

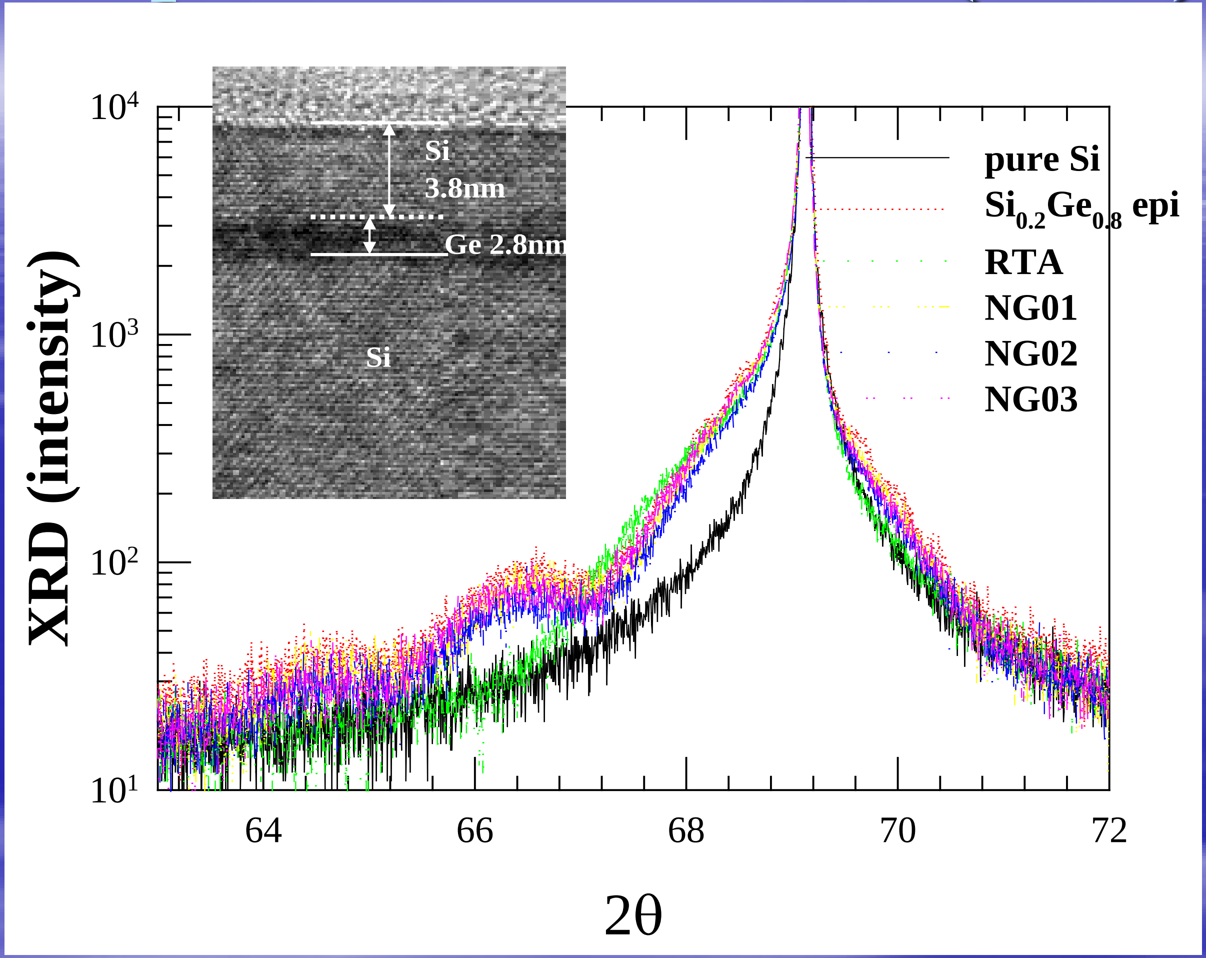

High-resolution double-crystal symmetrical ω/2θ scans of $Si_{0.2}Ge_{0.8}$ epi-layer and Si substrate. The inset figure is a TEM image, and the structure consists of $Si/Si_{0.2}Ge_{0.8}/Si$ layers, with the thicknesses of Ge and Si capping layers as 3.8 and 2.8 nm, respectively.

Outline

- **Introduction**
- **Topics**
  - **A low-temperature microwave anneal process for Boron-doped ultra-thin Si$_{0.2}$ Ge$_{0.8}$ epi-layer (*IEEE Electron Device Lett., vol. 30, no. 2, pp. 123–125,*Feb. 2009.)**
  - **P^{31} Activation in Single Crystalline Germanium by Low Temperature Microwave Annealing (Accepted by IEEE EDL)**
  - **SiN layer for larger Strain Stress after low temperature dopant activation**
  - **65 nm poly-Si TFTs fabrication (IEDM 2009)**
  - **TiN gate poly-Si TFTs fabirication (*IEEE Electron Device Lett., vol. 31, no. 5, pp. 437–439,*May. 2010.)**
- **Conclusions**

Process Flow

- P-type Si (100) Substrate
- 10 nm Si buffer layer by UHVCVD
- 200 nm pure Ge film grown on the Si buffer layer by UHVCVD, and then implanted by P^{31} at 25 KeV to a dose of 5e15 cm^{-2}
- Anneal methods:
  - Conventional RTA
  - Low temperature microwave anneal
- Rs, SIMS, TEM, and SRP

Temperature Profiles and Chamber Setting

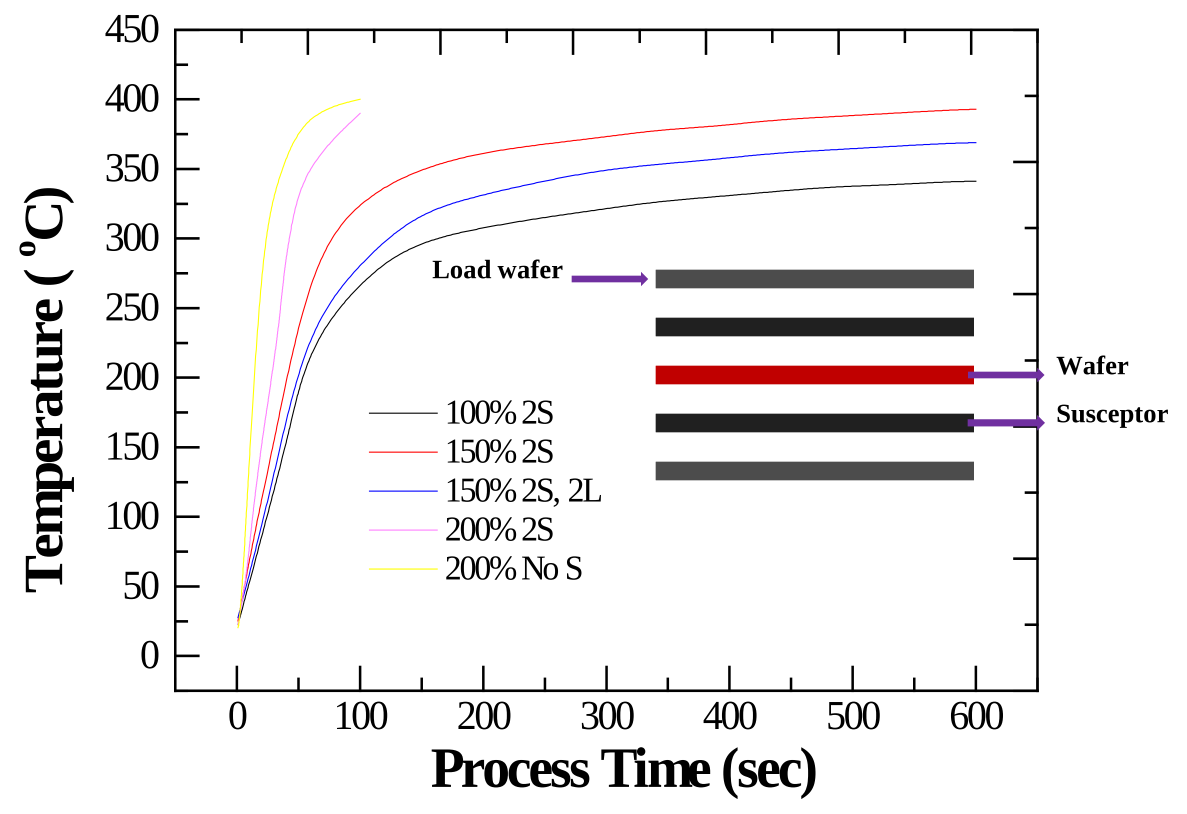

- Temperature versus process time during microwave annealing in different setting conditions, S is represented susceptor and L is represented load wafer.

Conditions and Rs of Microwave Anneal and RTA

	RTA	i	ii	iii	iv	v	vi
Power	**N**	**100%**	**150%**	**150%**	**150%**	**200%**	**200%**
Susceptor (pc.)	**N**	**2**	**2**	**2**	**2**	**N**	**2**
Load wafer (pc.)	**N**	**N**	**N**	**N**	**2**	**N**	**N**
Process time (sec.)	**60**	**600**	**600**	**300 two cycles**	**600**	**100**	**100**
R_s (Ω/□)	**120**	**316.3**	**162.3**	**215.4**	**276.3**	**133.2**	**200.1**
T_{max}(°C)	**550**	**341.3**	**392.8**	**373**	**368.9**	**400**	**390**

P^{31} SIMS Profiles

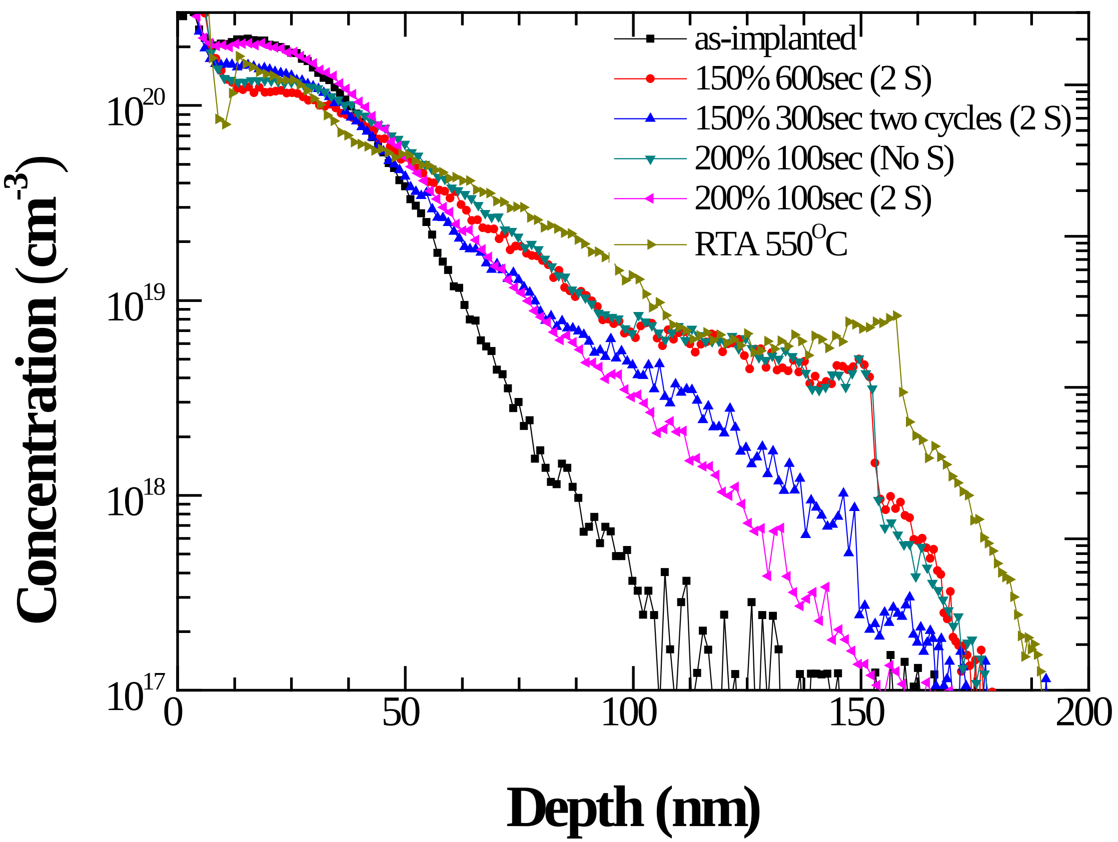

- Diffusion profiles of implanted P before and after microwave annealing in different conditions and RTA at 550°C for 60s.

SRP and TEM

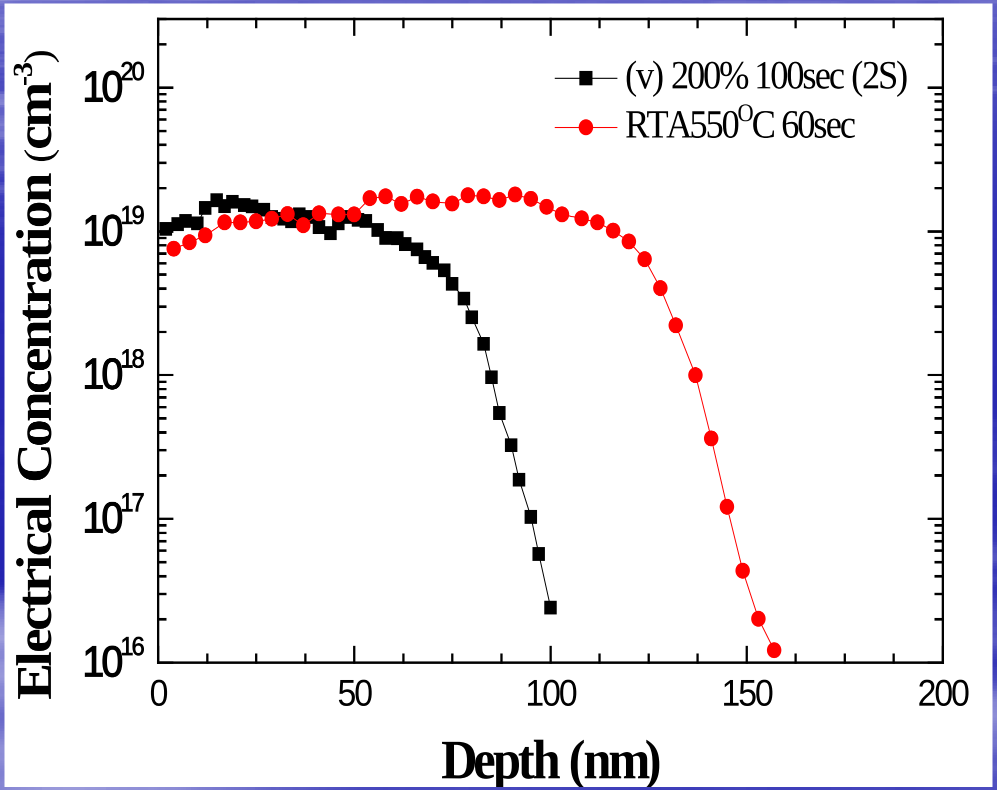

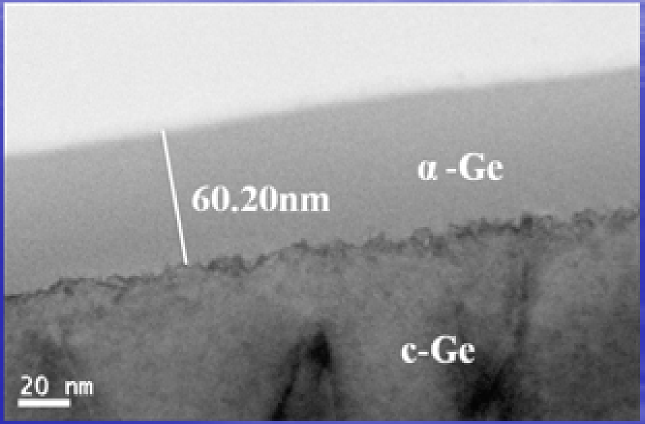

(a)

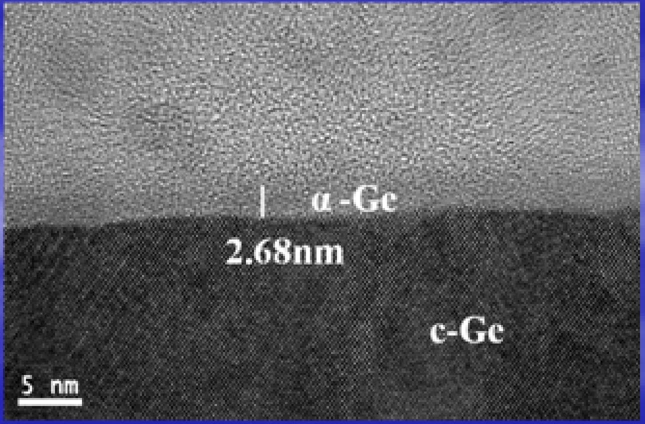

(c)

- SRP depth profiles of P in Ge from microwave anneal and RTA.

Outline

- Introduction
- Topics
  - A low-temperature microwave anneal process for Boron-doped ultra-thin $Si_{0.2}$ $Ge_{0.8}$ epi-layer (*IEEE Electron Device Lett., vol. 30, no. 2, pp. 123–125,*Feb. 2009.)
  - P^{31} Activation in Single Crystalline Germanium by Low Temperature Microwave Annealing (Accepted by IEEE EDL)
  - **SiN layer for larger strain stress after low temperature dopant activation**
  - 65 nm poly-Si TFTs fabrication (IEDM 2009)
  - TiN gate poly-Si TFTs fabirication (*IEEE Electron Device Lett., vol. 31, no. 5, pp. 437–439,*May. 2010.)
- Conclusions

Process Flow

- P-type Si (100) Substrate
- Implanted by P^{31} at 15 KeV to a dose of 5e15 cm^{-2}
- 20nm~200nm SiN deposition by PECVD
- Anneal methods:
  - RTA
  - Microwave anneal
- Rs, SIMS, and Stress measurement

P^{31} SIMS Profile by Low Temperature Microwave and RTA

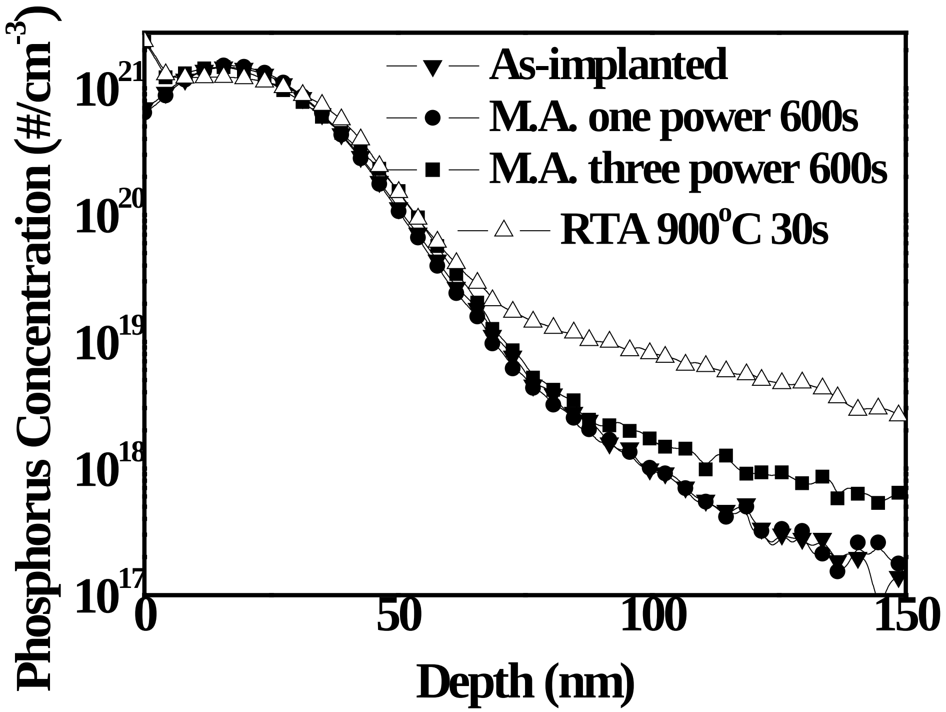

- The phosphorus distribution after the 900°C for 30 s is deeper.

Comparisons of Strain Enhancement by Microwave Anneal and RTA

Splits	Temperature	Initial SiNx (Gpa)	After anneal (Gpa)	Rs (Ω/sq.)
M.A. 3P. 600s	493°C	0.287	1.68	94.53
M.A. 3P. 100s	420°C	0.321	0.944	102.6
M.A. 3P. 100s by 6 cycles	420°C	0.321	1.51	94.47
RTA 900°C 30s	900°C	0.32	1.57	56.78

Strain Magnitude Enhancement by Low Temperature Anneal

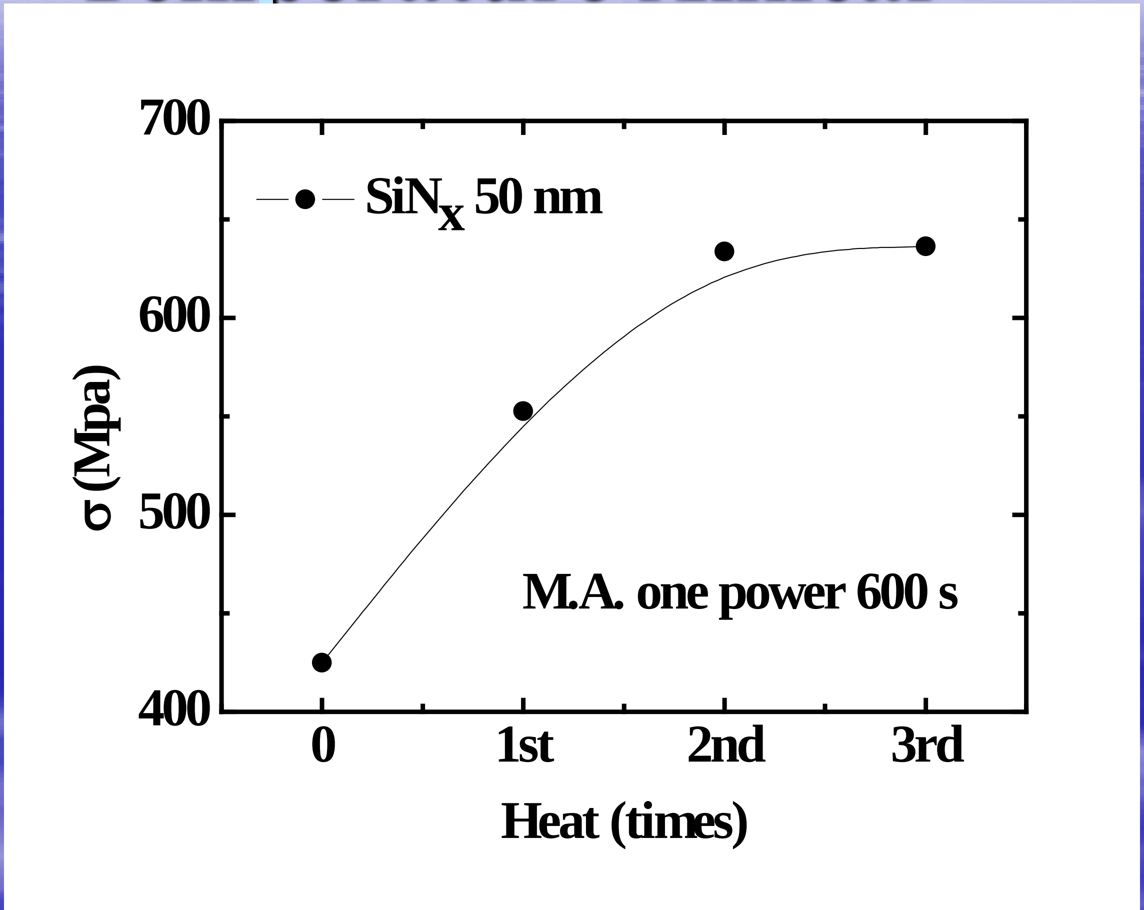

- 50nm SiN$_x$ thickness, microwave power is 600~700W. The strain magnitude becomes saturated.

Stress Shift Multiplied by Thickness (Δσt) versus Nitride Thickness

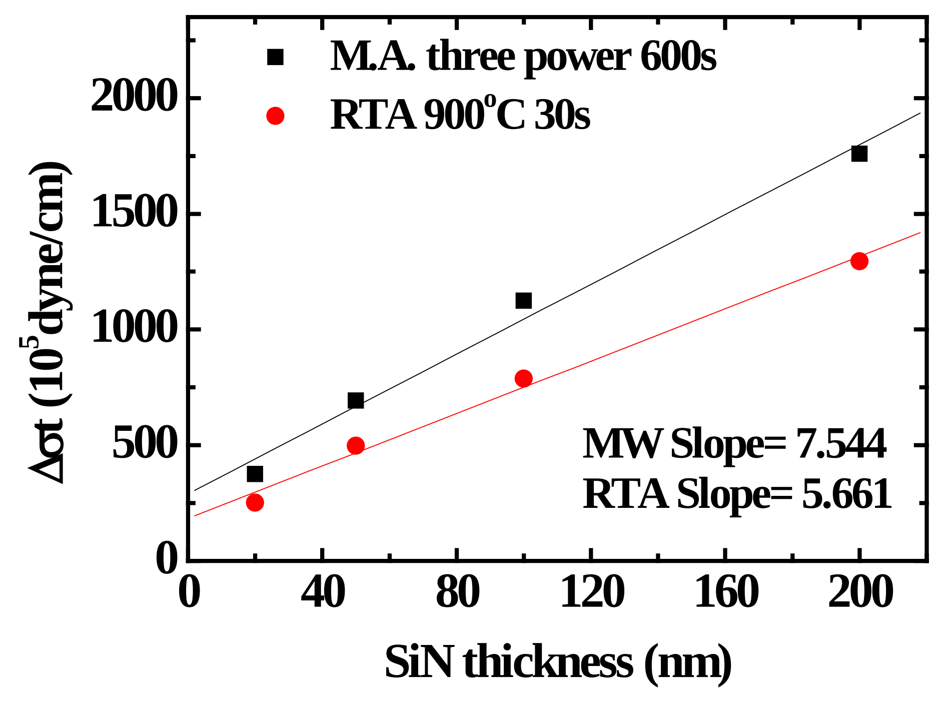

- Comparisons of the stress profiles of different post annealing methods.

Outline

- **Introduction**
- **Topics**
  - **A low-temperature microwave anneal process for Boron-doped ultra-thin $Si_{0.2}$ $Ge_{0.8}$ epi-layer (** ***IEEE Electron Device Lett., vol. 30, no. 2, pp. 123–125,*** **Feb. 2009.)**
  - **P^{31} Activation in Single Crystalline Germanium by Low Temperature Microwave Annealing (Accepted by IEEE EDL)**
  - **SiN layer for larger Strain Stress after low temperature dopant activation**
  - **65 nm poly-Si TFTs fabrication (IEDM 2009)**
  - **TiN gate poly-Si TFTs fabirication (** ***IEEE Electron Device Lett., vol. 31, no. 5, pp. 437–439,*** **May. 2010.)**
- **Conclusions**

TEM Cross Section Image

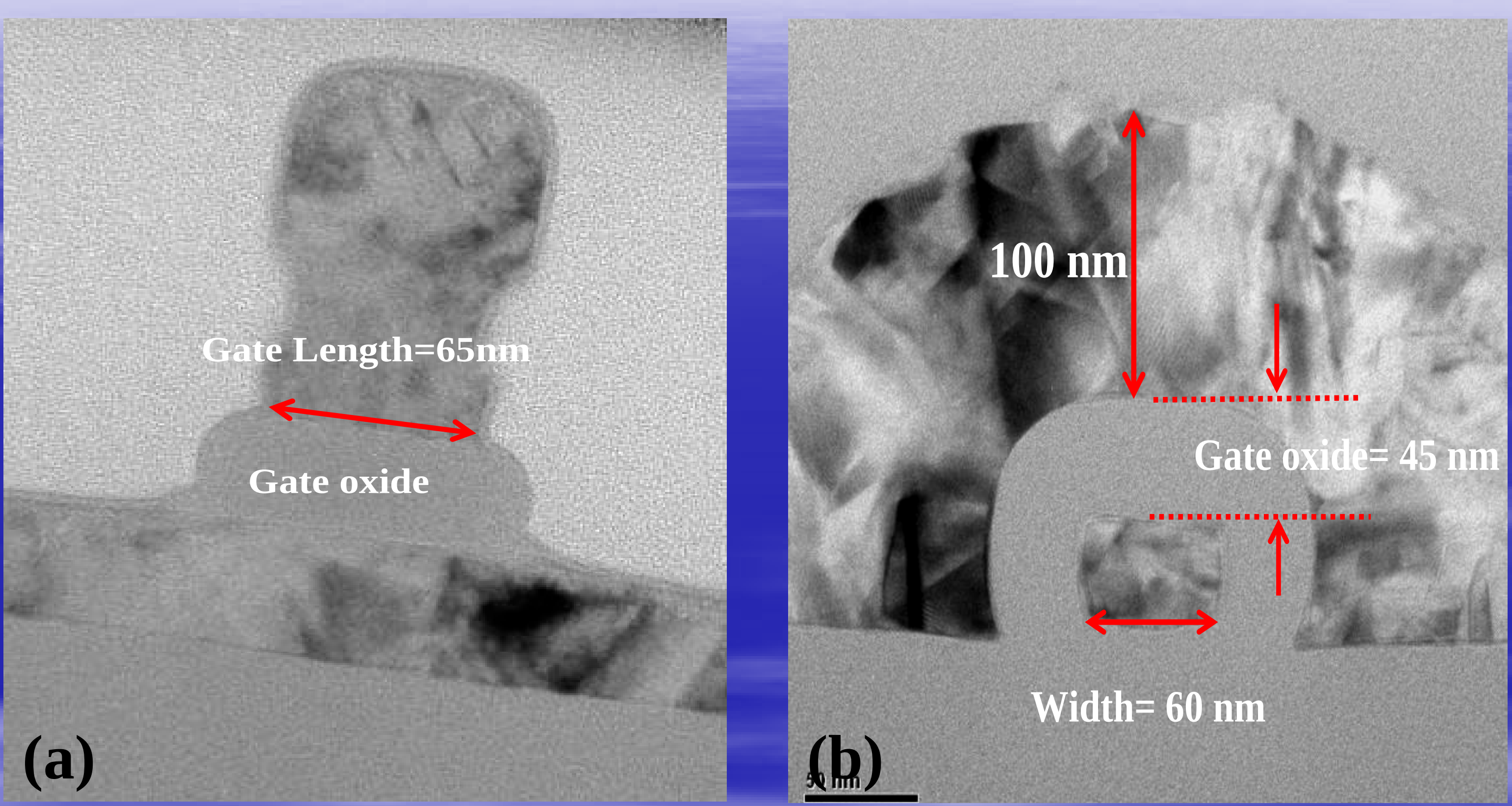

- **TFTs gate structure with (a) a 65nm gate length and (b) a 60nm gate width, where the gate oxide thickness is 45 nm and the channel thickness is 45 nm.**

I_D-V_G of p-MOS TFTs Annealed at 900°C for 15 seconds

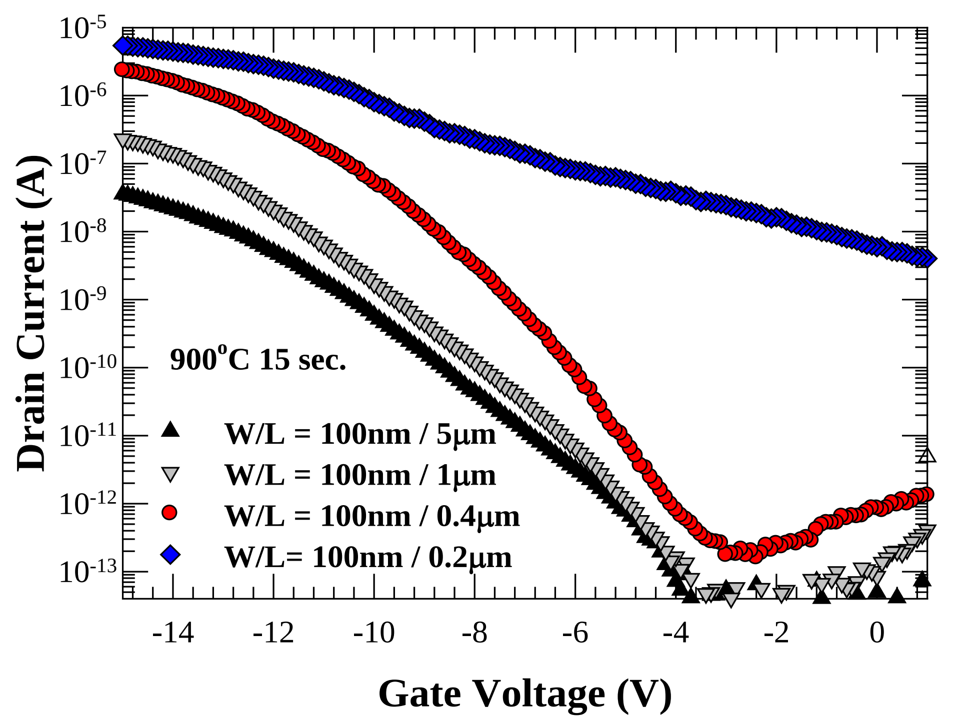

- I_D-V_G of p-MOS TFTs with different gate length (W = 100 nm) annealed by 900°C for 15 seconds.
- As the gate length is less than 0.4-μm, punch-through effects would dominant the electrical characteristics.

I_D-V_G of p-MOS TFTs Annealed at 600°C for 12 hours

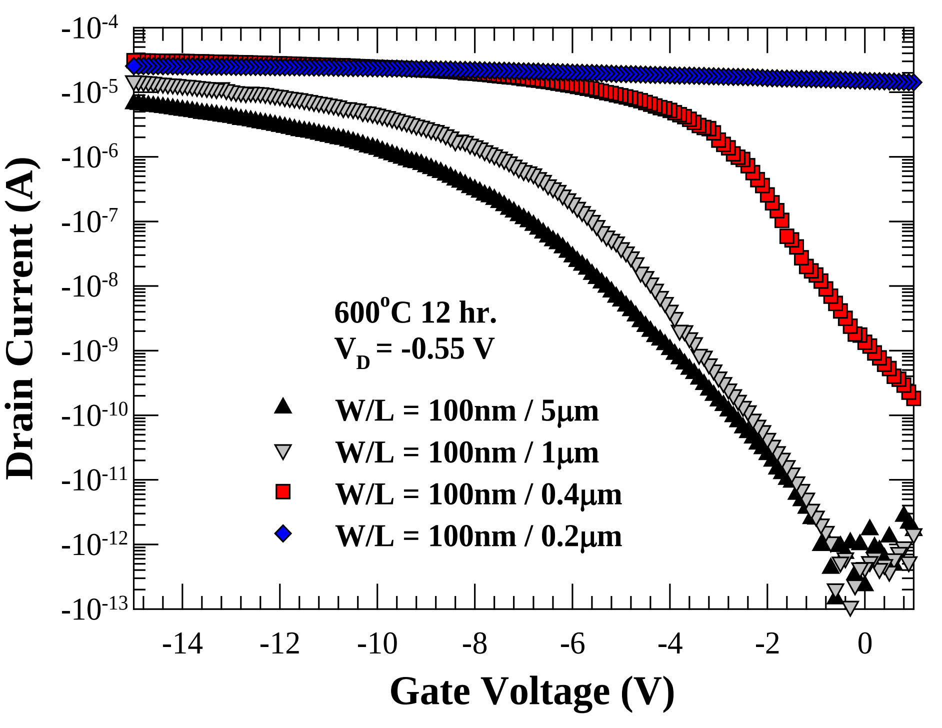

- I_D-V_G of p-MOS TFTs with different gate length (W = 100 nm) annealed at 600°C for 12 hours.
- As the gate length is less than 1µm, punch-through effects would dominant the electrical characteristics.
- The Ion/Ioff ratios are about 10^0 as L = 0.2 µm

I_D-V_G of p-MOS TFTs Annealed by Microwave (I)

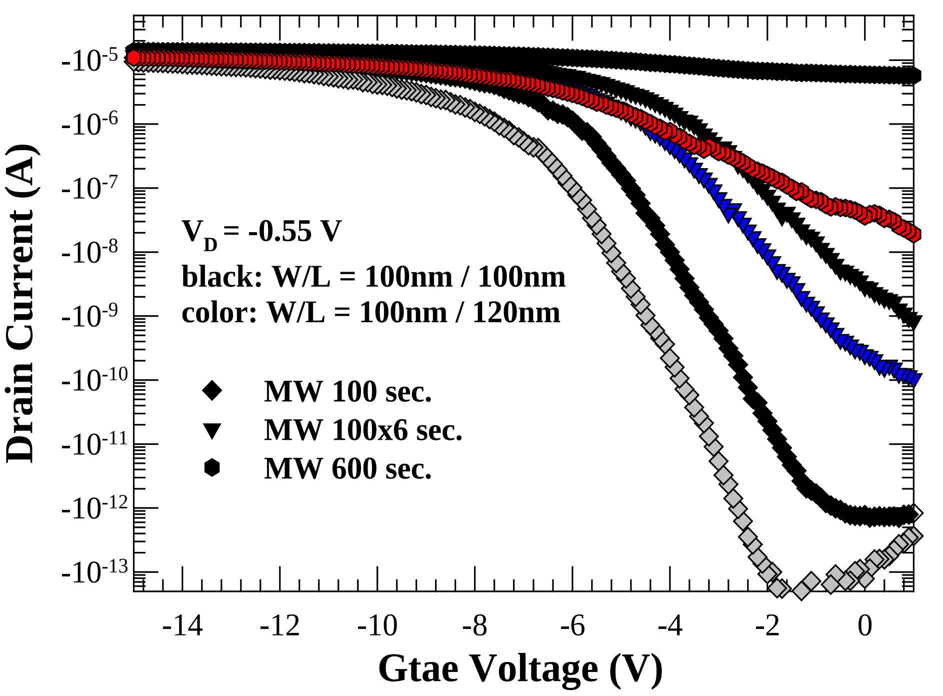

- The Ion/Ioff ratios are about 10^8 for p-MOS TFTs annealed by microwave for 100 seconds with W/L = 100nm/ 120nm, 10^7 for that with W/L = 100nm / 100nm
- Longer time period and higher process temperature would enhance the short channel effect immunity

I_D-V_G of p-MOS TFTs Annealed by Microwave (Ⅱ)

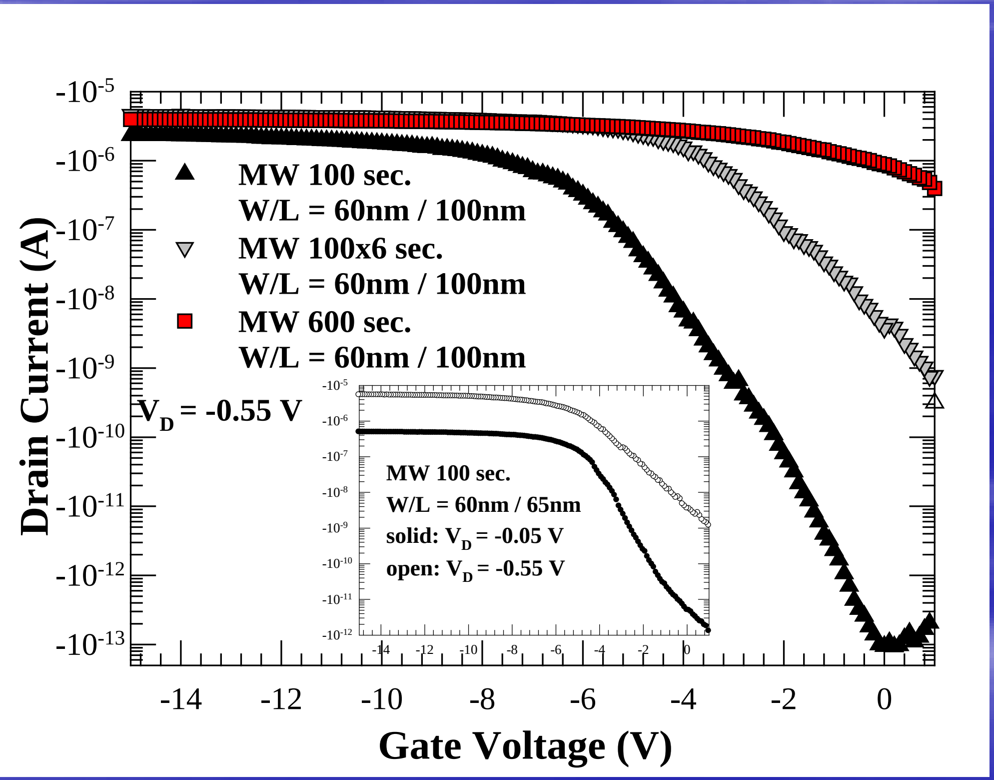

- The Ion/Ioff ratios are about 10^7 for that with W/L = 60nm / 100nm.
- The inset shows the I_D-V_G of p-MOS TFTs with W/L = 60nm / 65nm
- Punch-through effects could be suppressed due to the low temperature anneal process and the fin-like structure.

I_D-V_G of n-MOS TFTs Annealed by Microwave

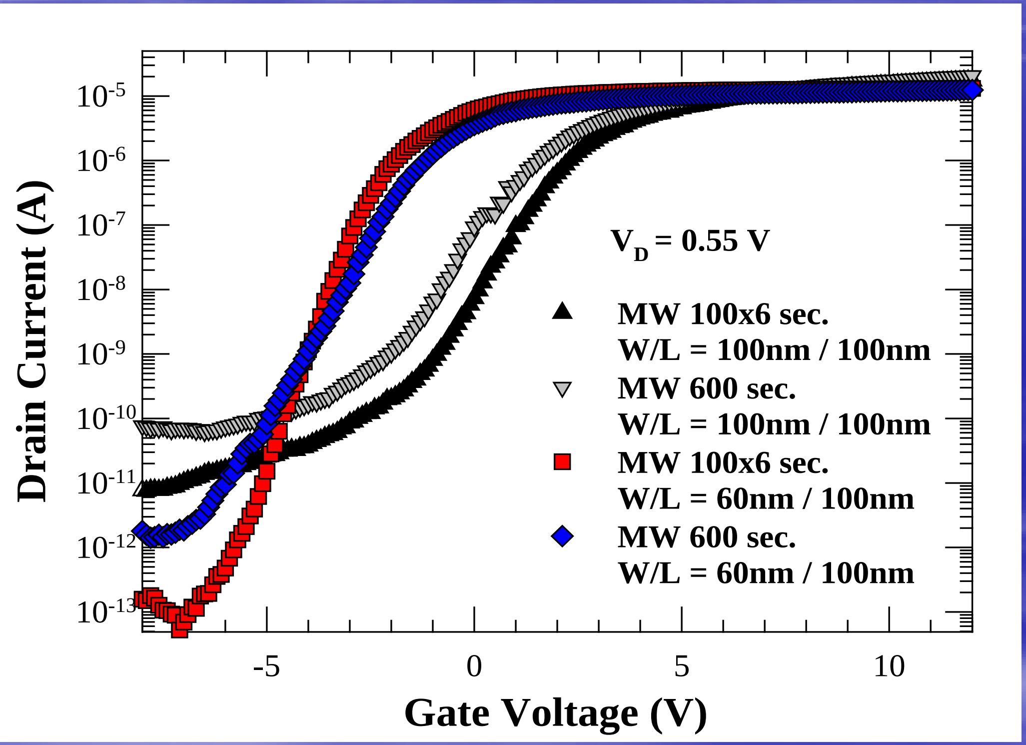

- The Ion/Ioff ratio is about 10^8 for the n-MOS TFT with W/L = 60nm / 100nm.

Transconductance normalized by Width

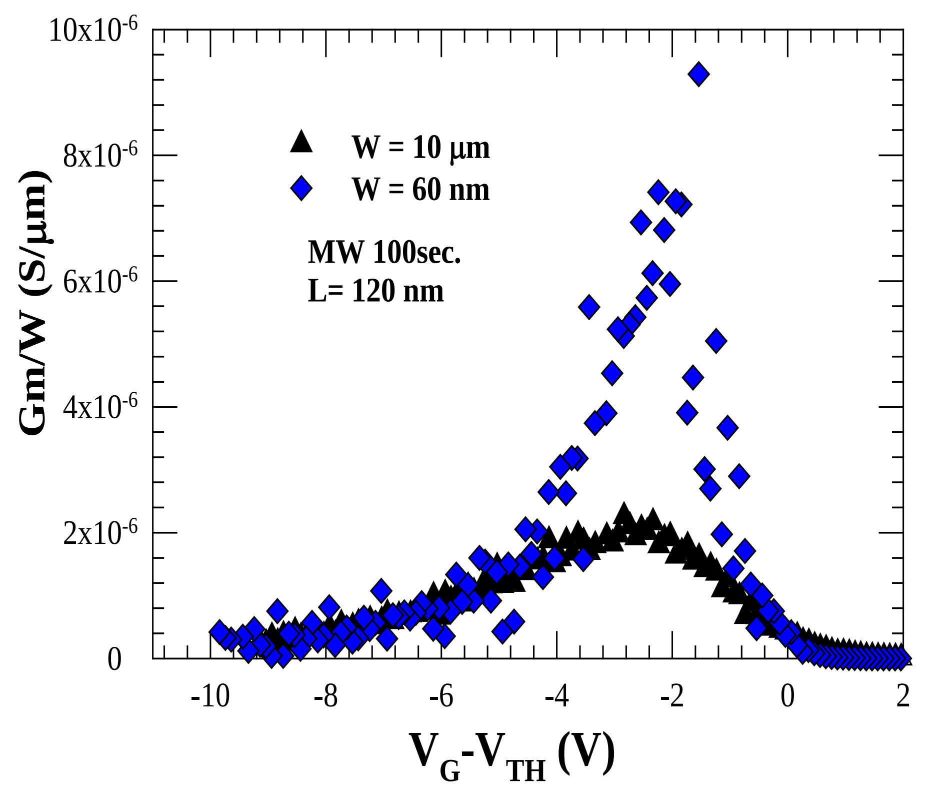

- The maximum channel Gm would increase for 250 % as channel width decreasing from 10 µm to 60 nm.
- Scaling of channel width leading to increase of channel mobility is due to:
  - Larger electric field
  - Lower grain boundaries
  - Lower trap concentration

Sheet Resistance as a Function of Source/Drain Width

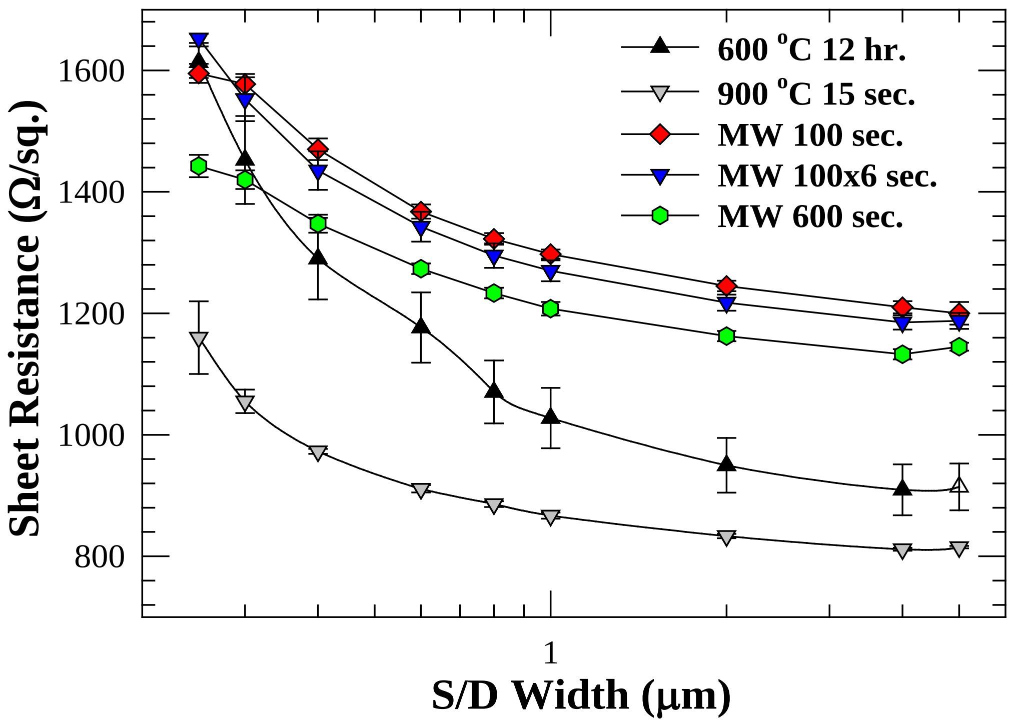

- The average magnitudes of sheet resistance annealed by RTA at 900°C for 15 s and furnace at 600°C for 12 hours are lower than those by microwave anneal

SIMS Profile of the Boron Concentration

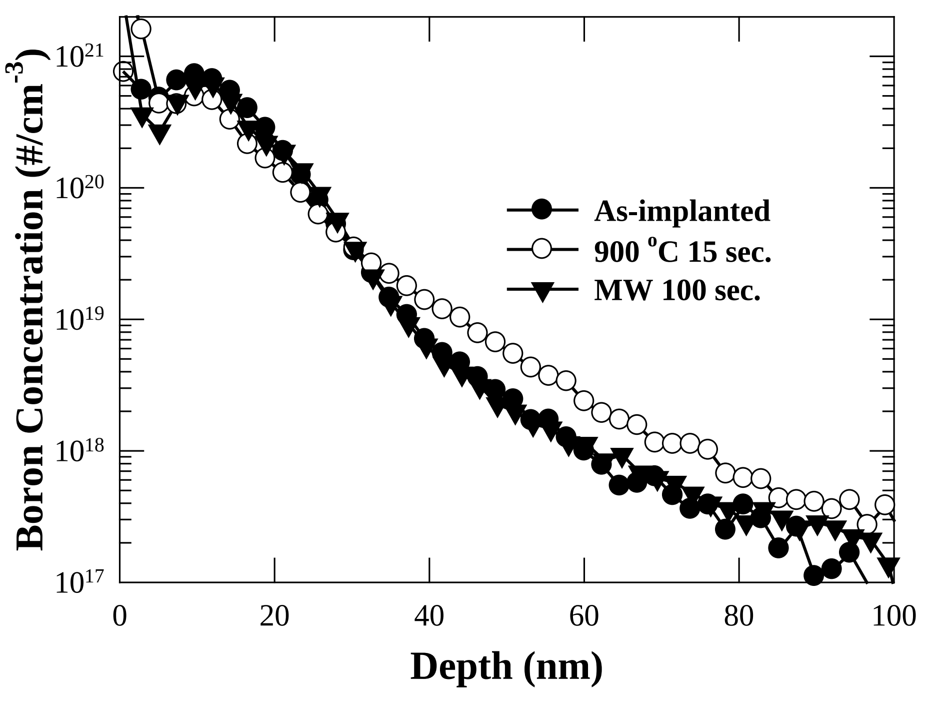

- The boron distribution after the 900°C for 15 seconds shows a deeper boron distribution.
- The splits by low temperature microwave annealing show identical boron distribution, which indicates that the thermal budget provided by the microwave treatment is too low to change the boron profile.

Outline

- **Introduction**
- **Topics**
  - **A low-temperature microwave anneal process for Boron-doped ultra-thin $Si_{0.2}$ $Ge_{0.8}$ epi-layer (*IEEE Electron Device Lett., vol. 30, no. 2, pp. 123–125,*Feb. 2009.)**
  - **P^{31} Activation in Single Crystalline Germanium by Low Temperature Microwave Annealing (Accepted by IEEE EDL)**
  - **SiN layer for larger Strain Stress after low temperature dopant activation**
  - **65 nm poly-Si TFTs fabrication (IEDM 2009)**
  - **TiN gate poly-Si TFTs fabirication (*IEEE Electron Device Lett., vol. 31, no. 5, pp. 437–439,*May. 2010.)**
- **Conclusions**

Anneal time vs. Temperature Profile

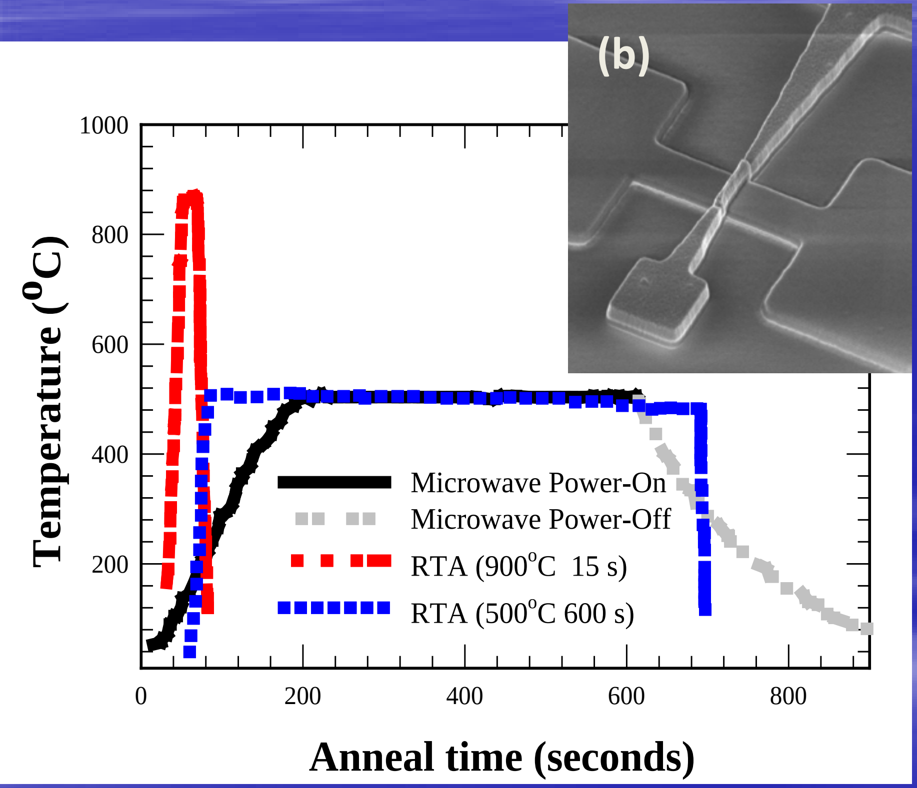

- The microwave (MW) anneal time is defined as the duration for which the microwave power is turned on.

I_D-V_G of TiN p-MOS TFTs

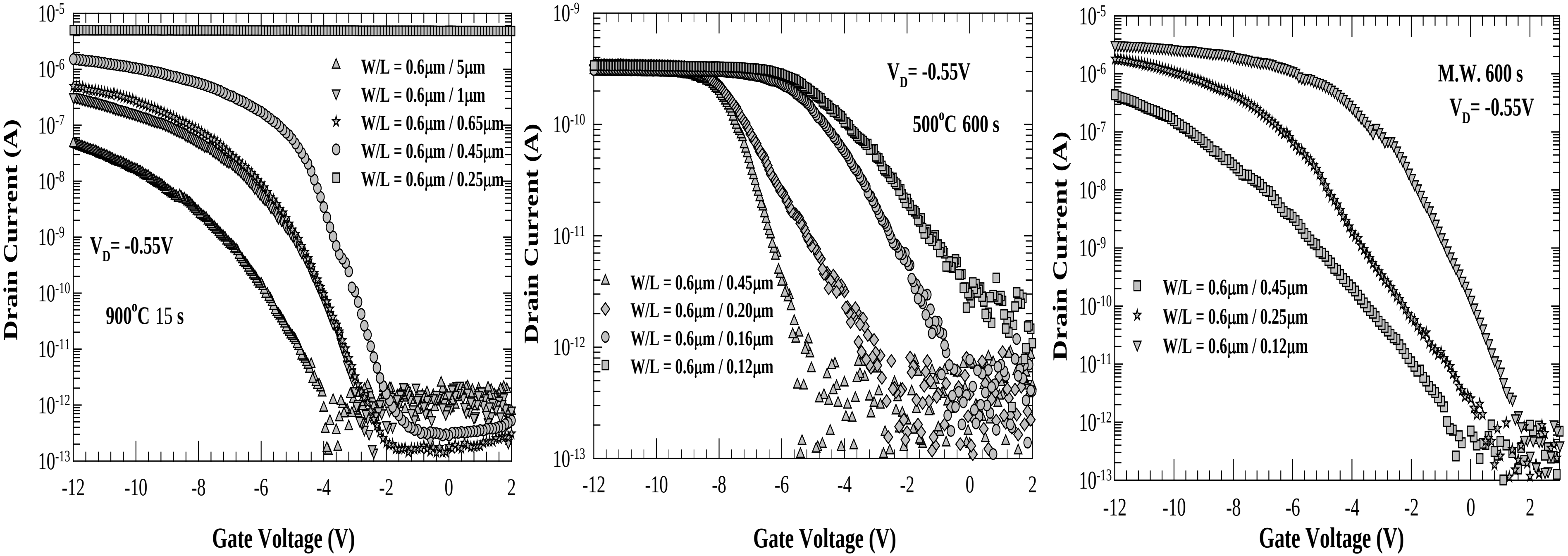

- I_D-V_G of TiN p-MOS TFTs annealed by RTA and microwave annealing. (a) RTA at 900°C for 15 s, (b) furnace at 500°C for 500 s, and (c) microwave annealing for 600 seconds

Anneal time vs. Temperature Profile

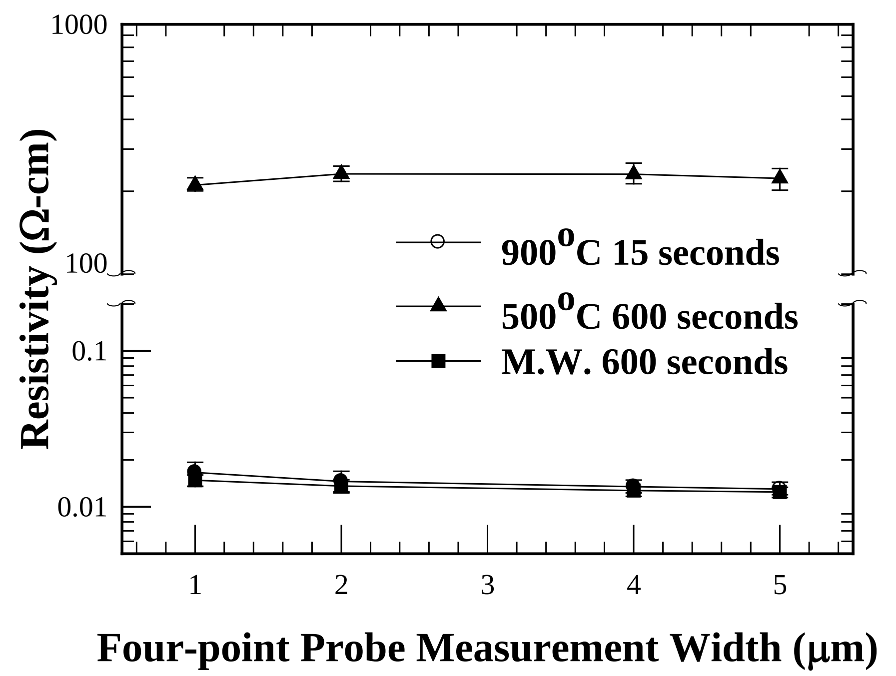

Conclusions

- In our study, different dopant activation conditions are compared with various annealing techniques.
- We have successfully activated the boron, As and P^{31} by low temperature microwave anneal.
- We have also successfully activated the P^{31} inside the pure Ge film and the diffusion could be suppressed.
- Nano-scaled TFTs are also demonstrated by low temperature microwave anneal.

2010.11.12 ITRS 2nd Deterministic Doping Workshop
UC Berkeley

Dopant Distributions in MOSFET Structures by Atom Probe Tomography

Kyoto Univ. K. Inoue

IMR Tohoku Univ. H. Takamizawa, T. Toyama, Y. Shimizu, Y. Nagai, M. Hasegawa

MIRAI-Selete F. Yano, T. Tsunomura, A. Nishida, T. Mogami

Outline

- Dopant visualization techniques with atomic scale resolution
- What is Atom Probe Tomography (APT) ?

  Local Electrode Atom Probe (LEAP)
- How to prepare needle specimen for APT
- Example of dopant distributions by APT (our work)
- Current Problem of APT
- Research groups for dopant distributions by APT in the world

Background

Ideal

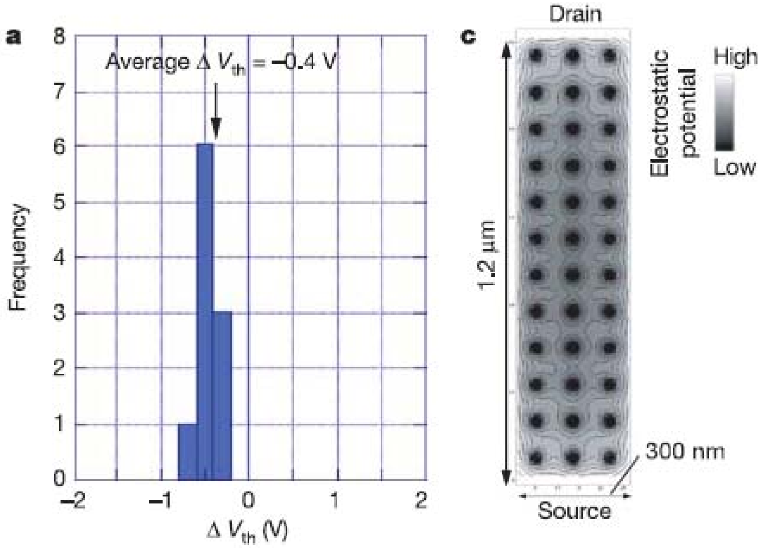

Random

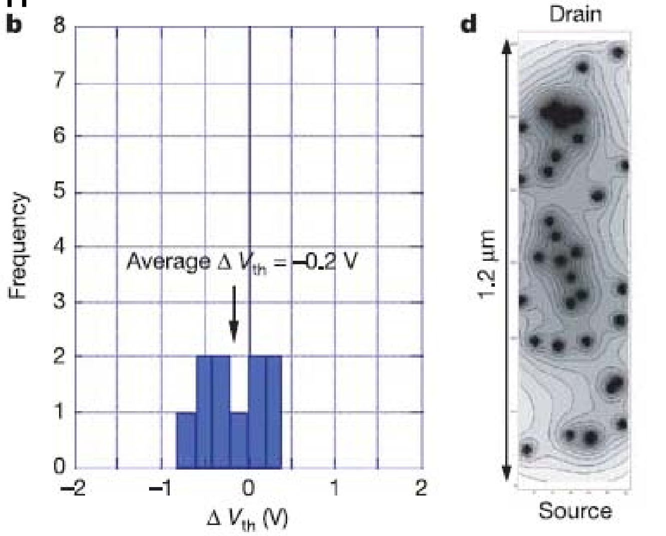

Shinada et al., NATURE Vol 437 (2005) 1128.

Information on number and position of Individual dopant atom

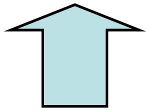

Visualization technique

Dopant distribution Visualization (2D)

Scanning Spreading Resistance Microscopy (SSRM)

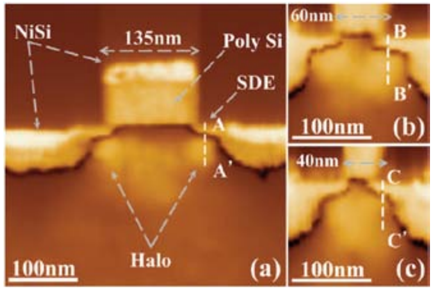

Zhang et al., Appl. Phys. Lett. 90 (2007) 192103

Electron Holography

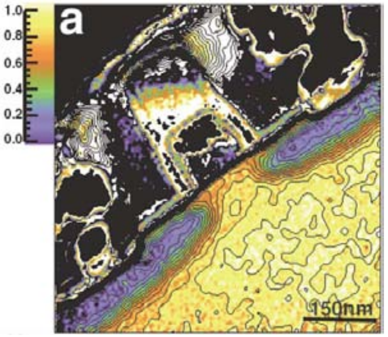

M. A. Gribelyul et al., Phys. Rev. Lett., 89 (2002) 025502

Scanning transmission electron microscope-energy-dispersive X-ray (STEM-EDX)

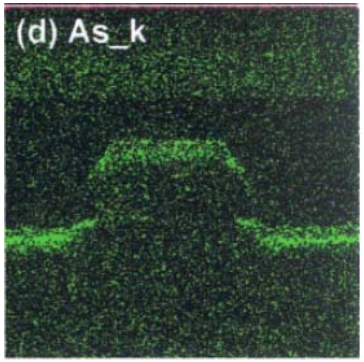

R. Tsuneta et al., J. Electron Microsc 51(2002)167

Scanning Tunneling Microscopy (STM)

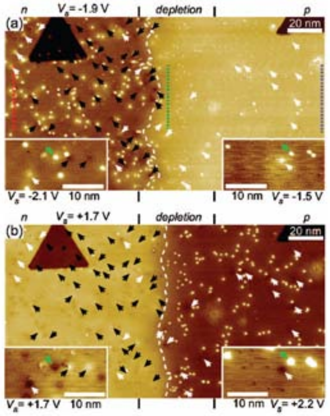

Depth range < 1nm

M. Nishizawa et al., Appl. Phys. Lett. 90 (2007) 122118

Kelvin Probe Force Microscopy

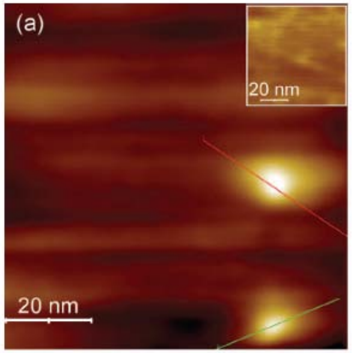

Depth range < 20nm

M. Ligowski et al., Appl. Phys. Lett. 93 (2008) 142101

Spherical aberration corrected STEM

As atoms (Z contrast)

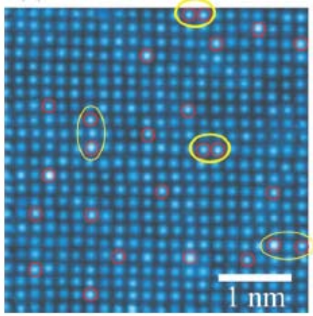

Y. Oshima et al., Phys. Rev. B81 (2010) 035317

Atom Probe Tomography (APT)

3D elemental mapping of materials

Spatial resolution： X,Y:0.5nm, Z:0.2nm

Detection efficiency （all elements）: -50%

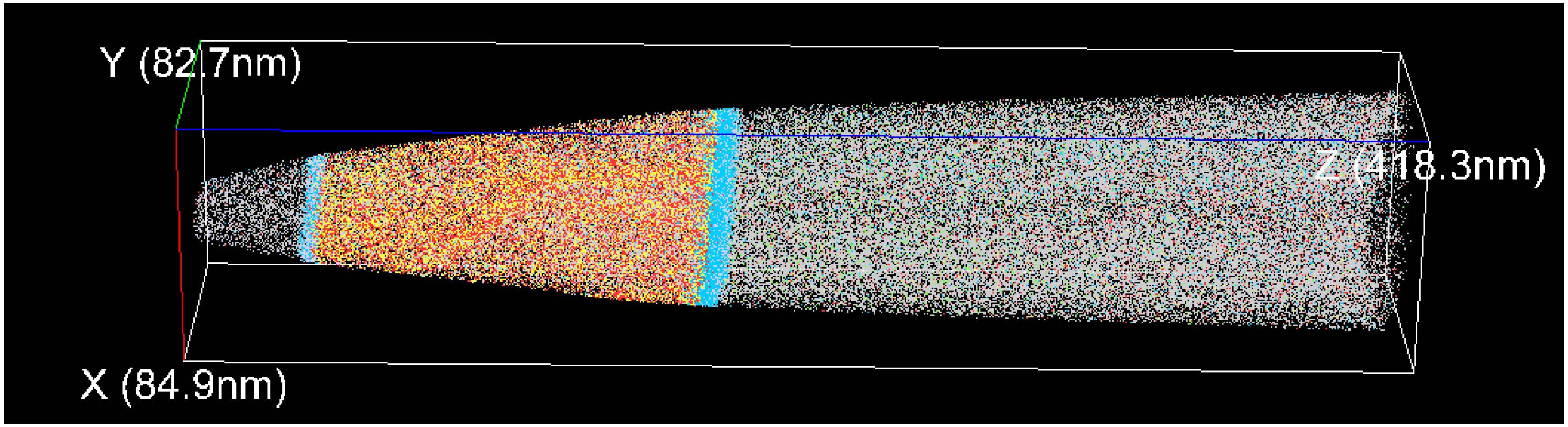

Range:	Si	P	O	B	As
Color:	⬜	🟥	🟦	🟩	🟨
Enable:	☑	☑	☑	☑	☑
Points:	☑	☑	☑	☑	☑

Each dot ⇔ Each atom

Atom probe tomography

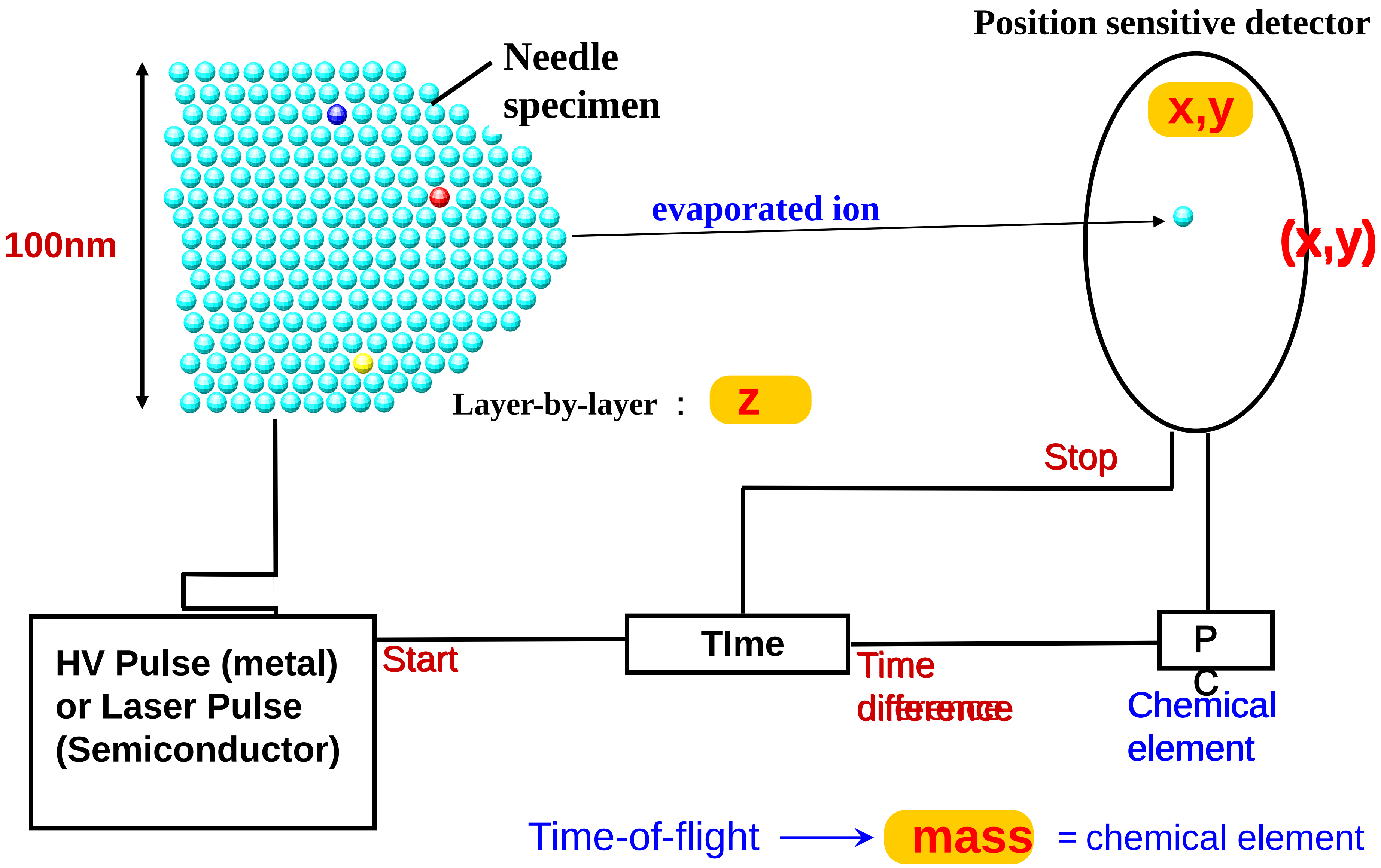

Position sensitive detector

Needle specimen

100nm

evaporated ion

x,y

(x,y)

Layer-by-layer : z

Stop

HV Pulse (metal)
or Laser Pulse
(Semiconductor)

Start

TIme

Time difference

P
C

Chemical element

Time-of-flight → mass = chemical element

Local Electrode Atom Probe: LEAP

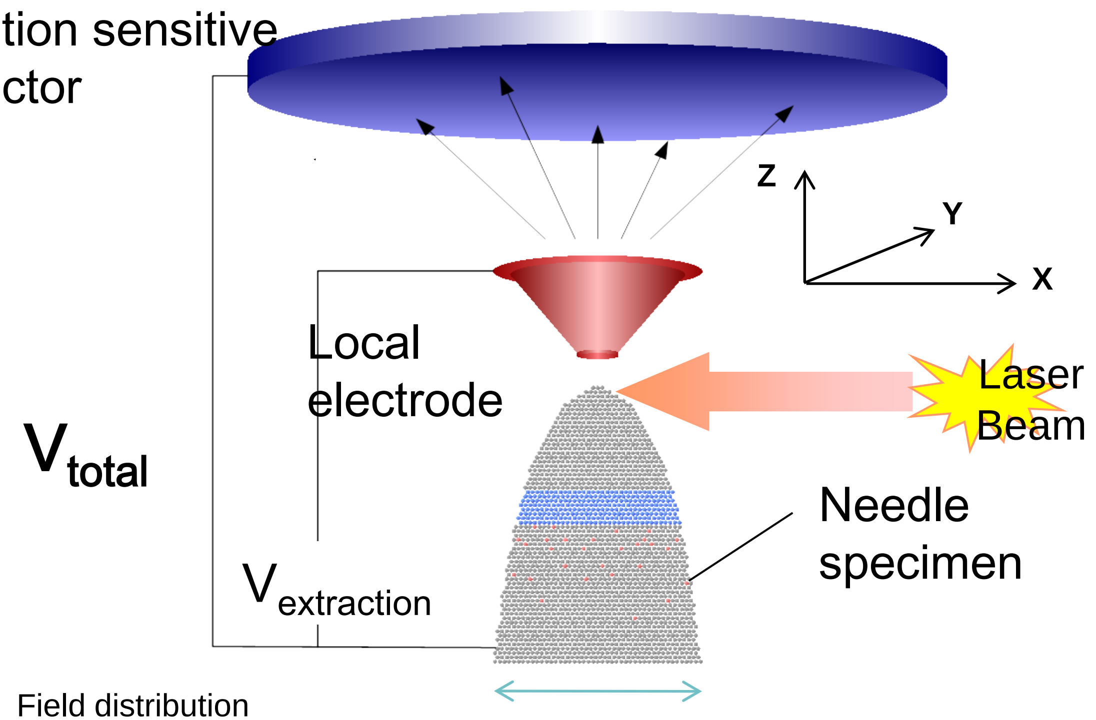

~ 100nm

Field distribution (simulation)

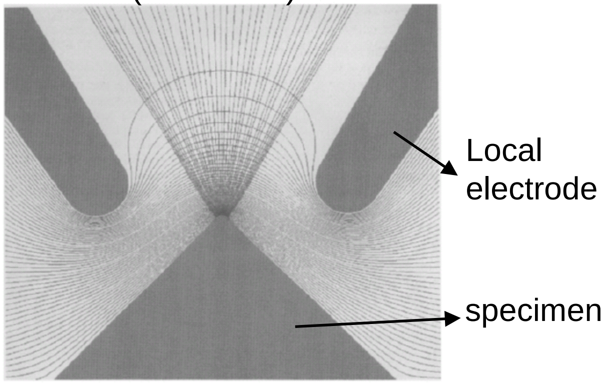

O. Nishikawa and M. Kimoto, Appl. Sur. Sci., 76/77(1994)424.

Atom information

Position : position sensitive detector X,Y

Layer-by-layer evaporation Z

Chemical identity : Time of Flight Mass

Laser - Local Electrode Atom Probe

1 . Count Rate: ×100 ~ 1000

- Detector: Closer to Sample
  observable area:
  <10nm → >50nm in width
- Pulse rate: ~×100
  Voltage pulse → Laser Pulse

Few Days → Few Hours
Huge Volume

Improvement of Statistics
Observation of Larger Structures
e.g. Grain boundary, Interface

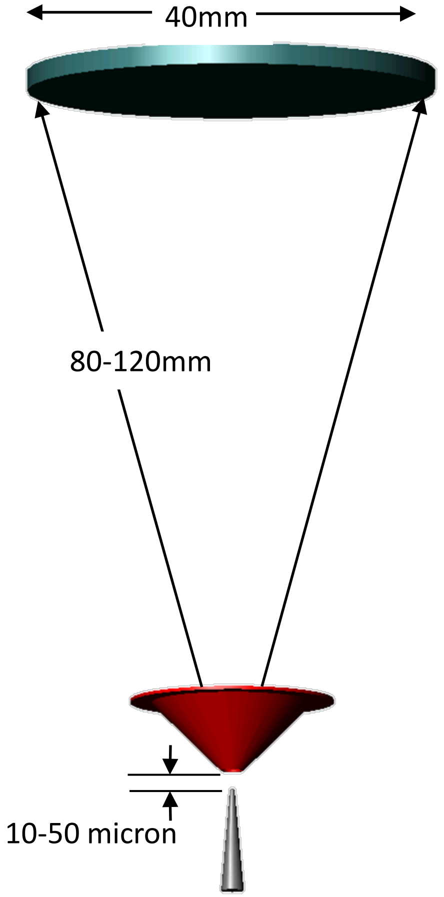

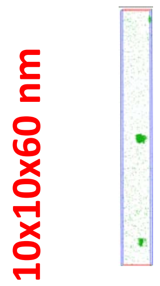

3x10^5 Atoms
6 hours

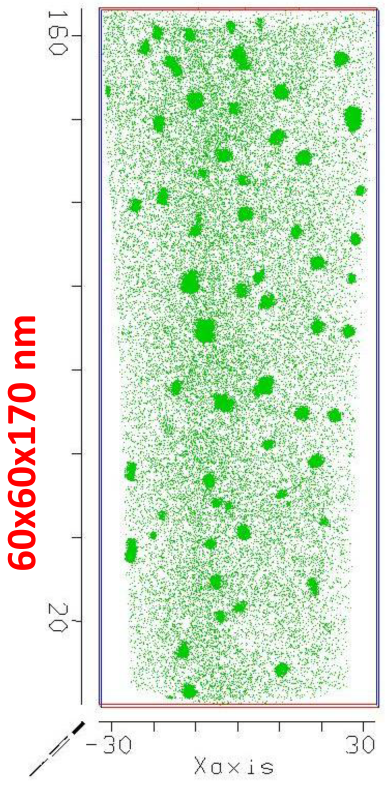

2x10^7 Atoms
1hour

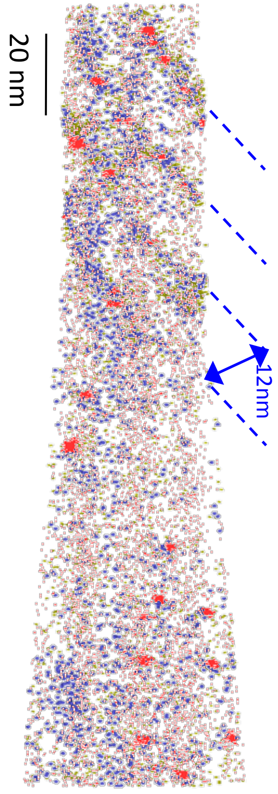

2 . Wide Application

- Array of needles, Semiconductors

3 . Reduction of Fracture Probability

- Brittle Materials

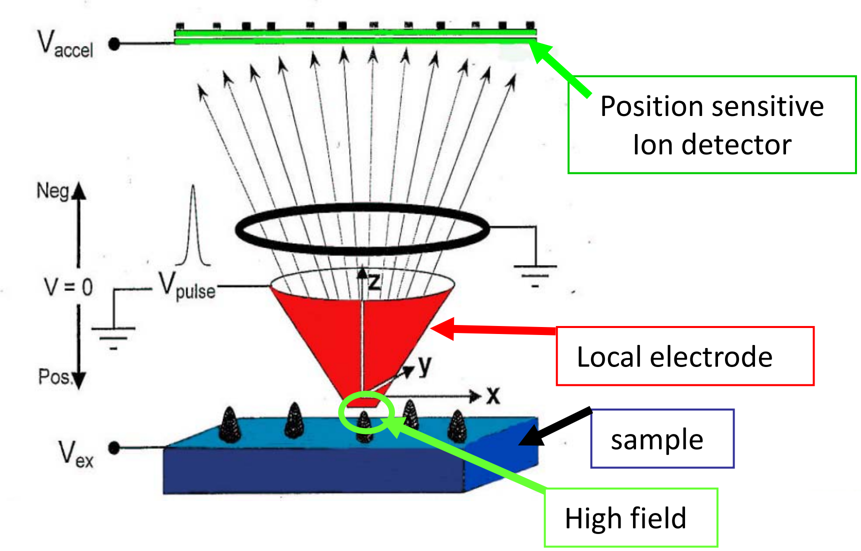

Position sensitive Ion detector

Local electrode

sample

High field

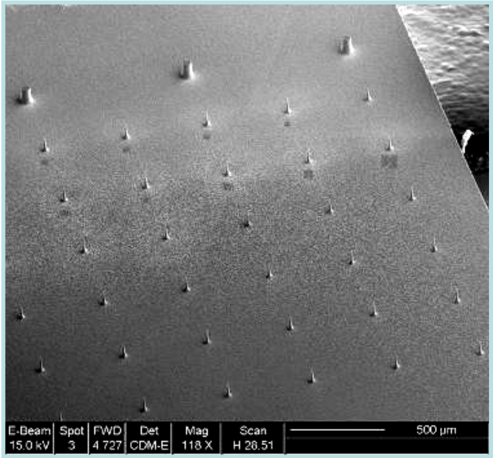

4 . Improvement of Mass Resolution

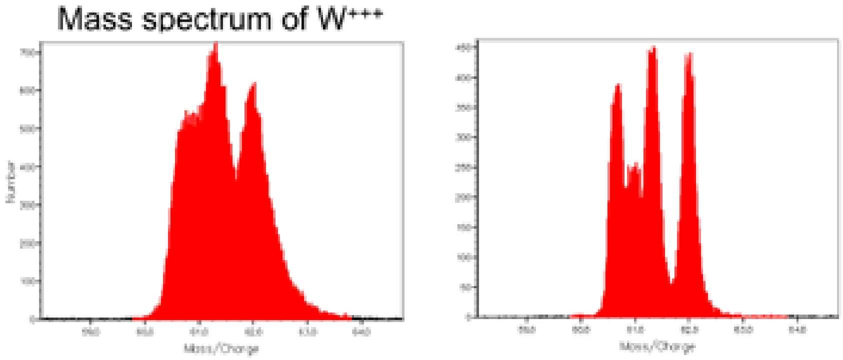

straight type 3DAP

laser 3DAP

Further improvements …

/ Reflectron lens

/ Ultraviolet Laser

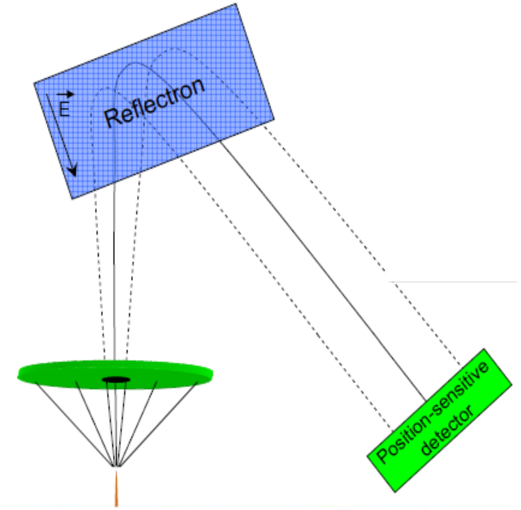

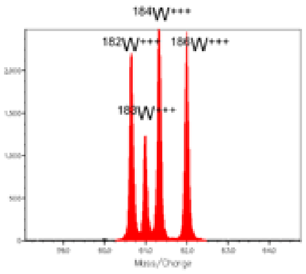

EC-3DAP

Laser-assisted LEAP equipped with a reflectron lens

LEAP 3000HR

(laser: 532nm)

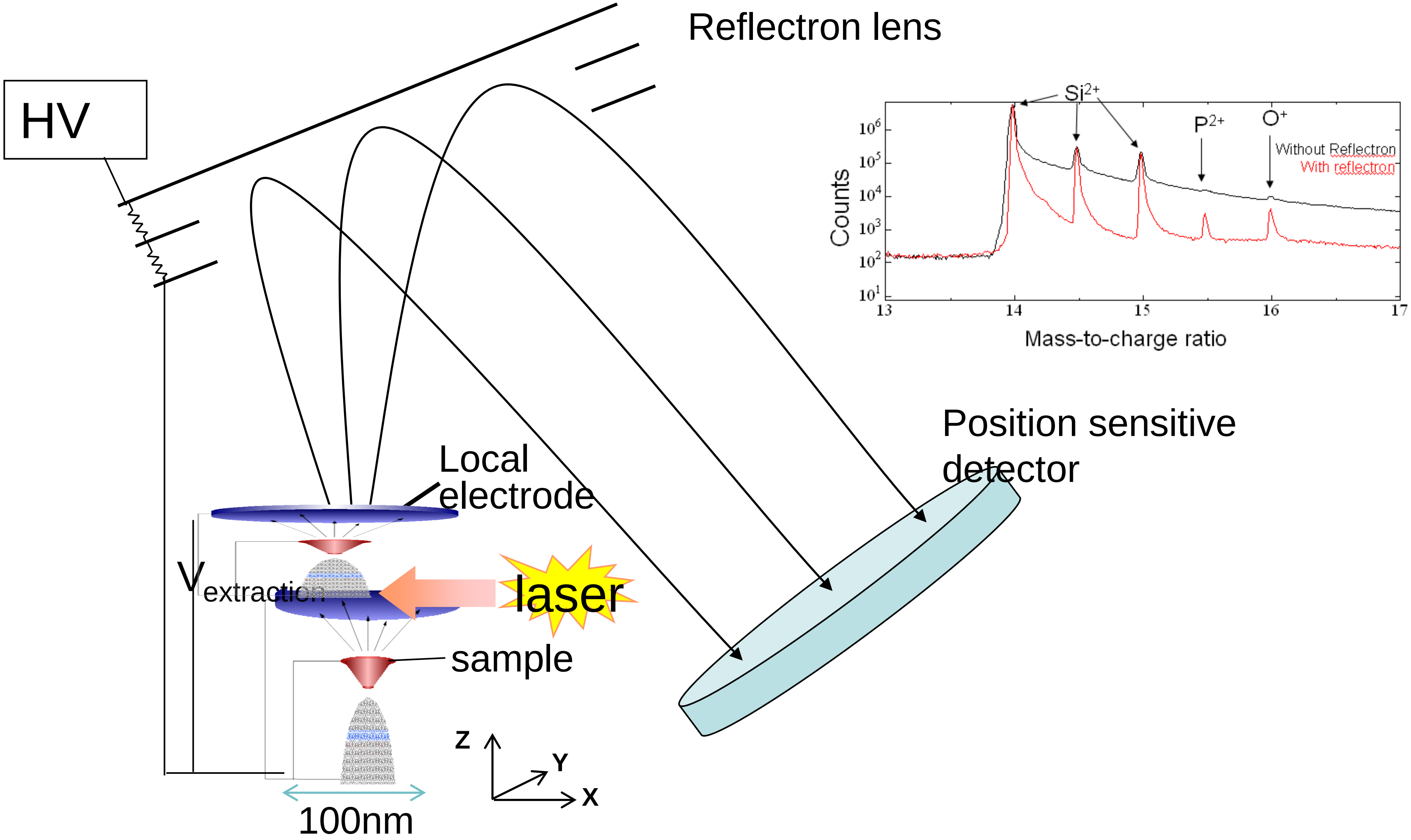

Reflectron lens

HV

Local electrode

$V_{extraction}$

laser

sample

100nm

Position sensitive detector

Specimen preparation for APT by Focused Ion Beam (FIB)

Cut and Lift-out

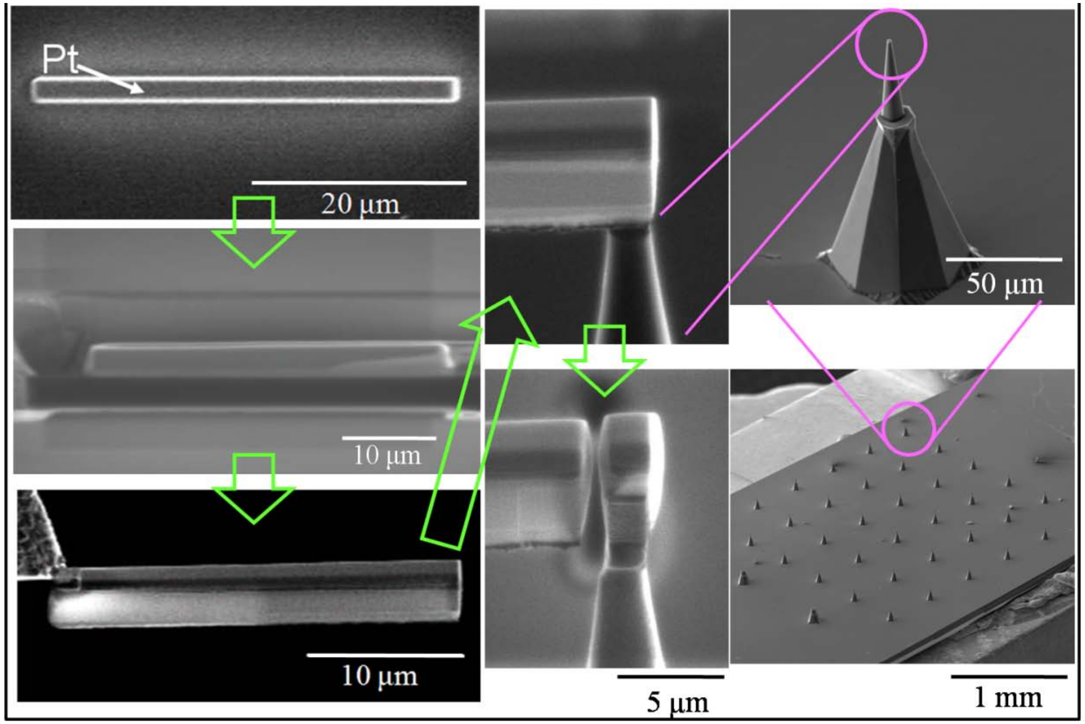

Milling by annular patten

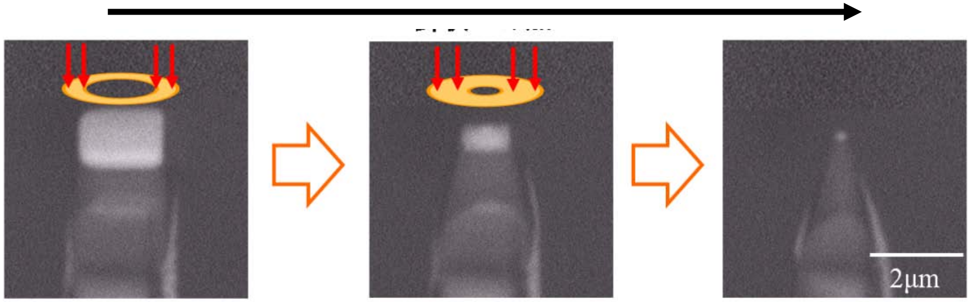

Example of dopant distributions by APT (our work)

motivation

V_{th} normal distribution and V_{th} histogram of the 1M DMATEG

(T. Tsunomura, et al., 2008 Symposium on VLSI Technology Digest of Technical Papers p156.)

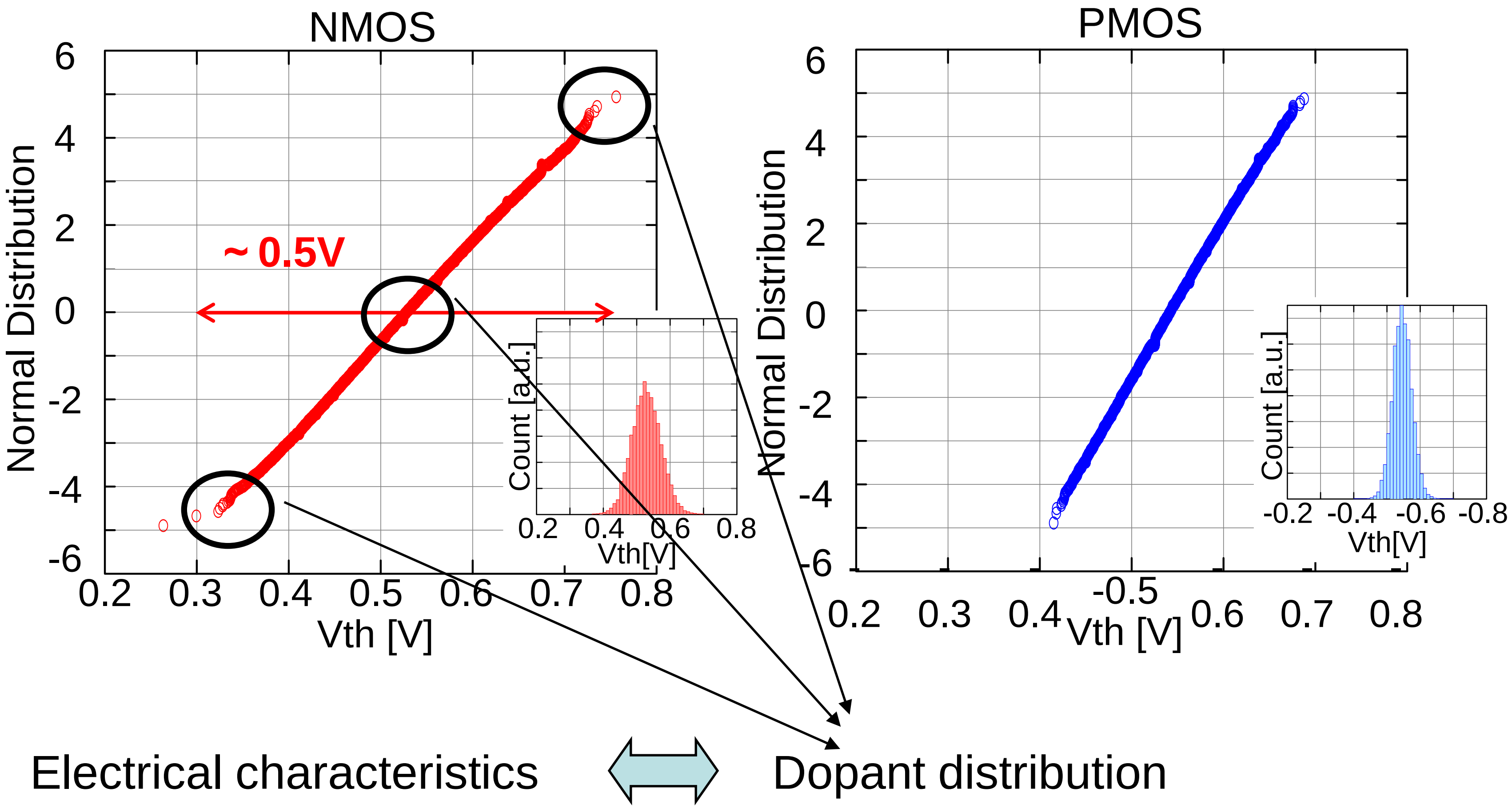

Electrical characteristics ⇔ Dopant distribution

Dopant in laterally uniform Sample

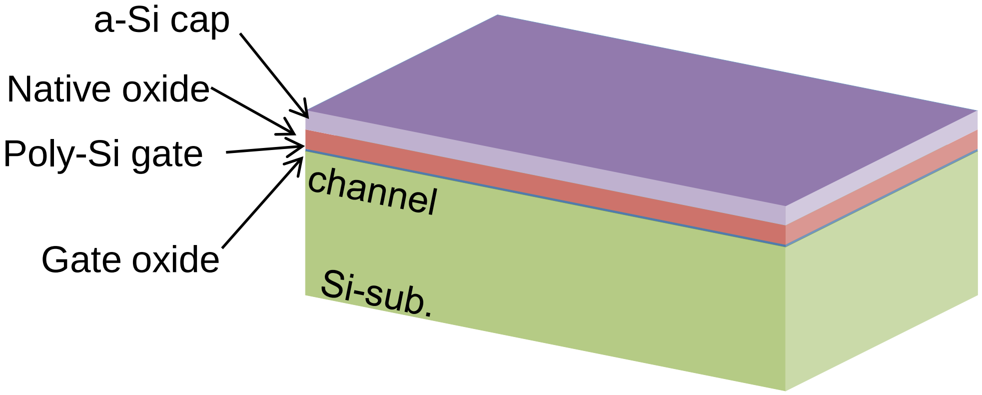

a-Si cap

Native oxide

Poly-Si gate

Gate oxide

channel

Si-sub.

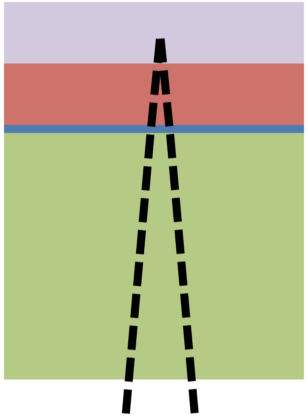

Needle sample were prepared by FIB

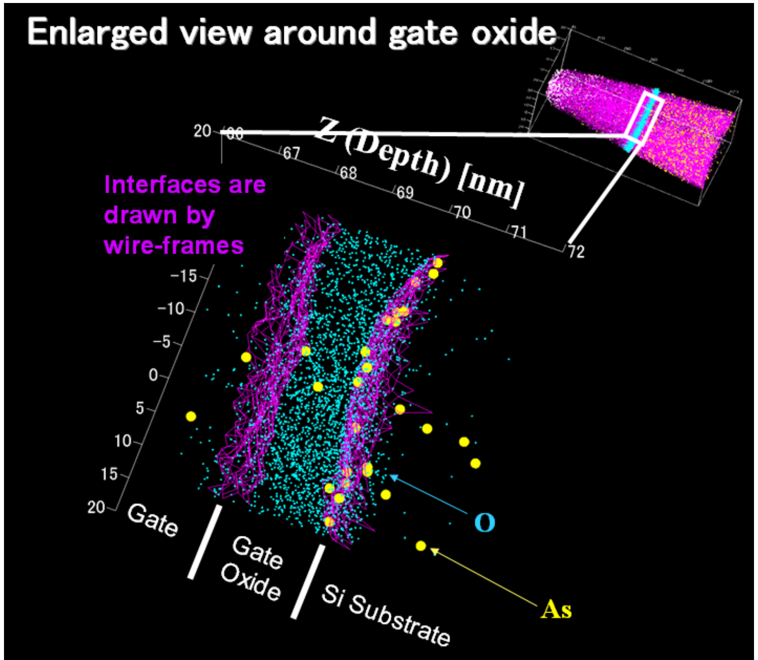

Comparison of dopant distribution in gate

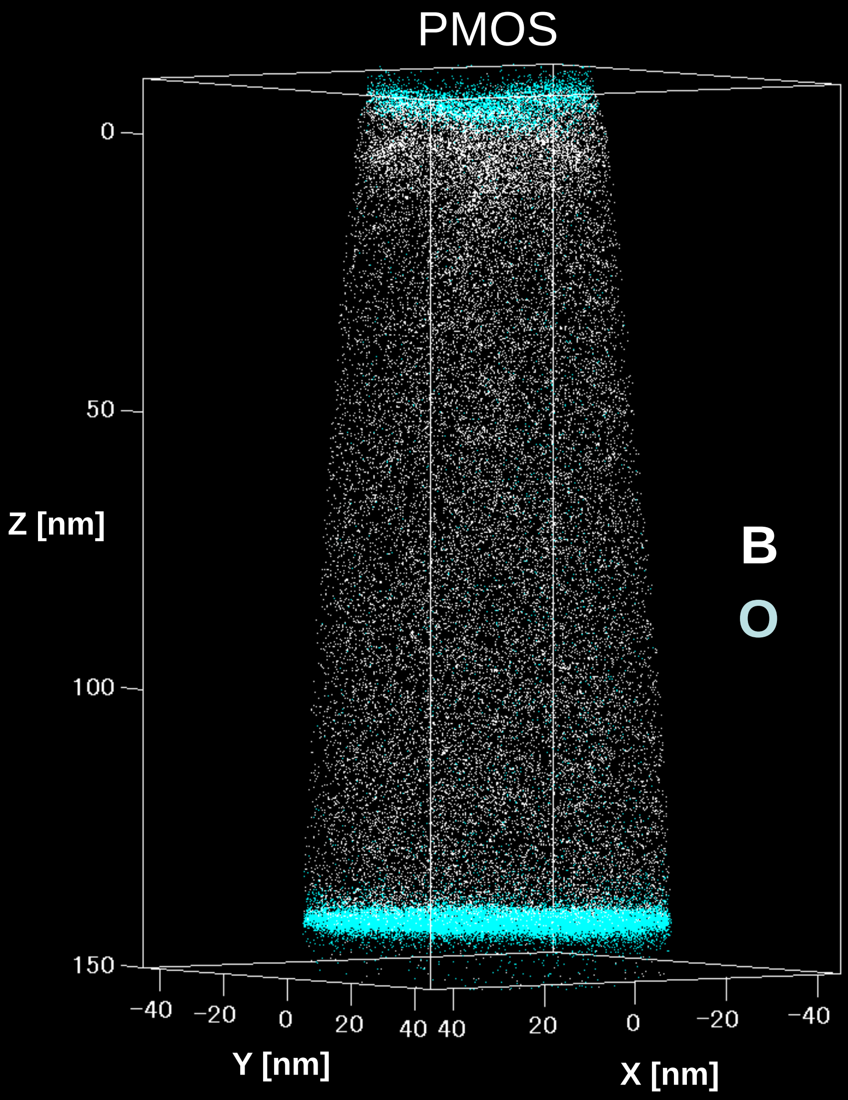

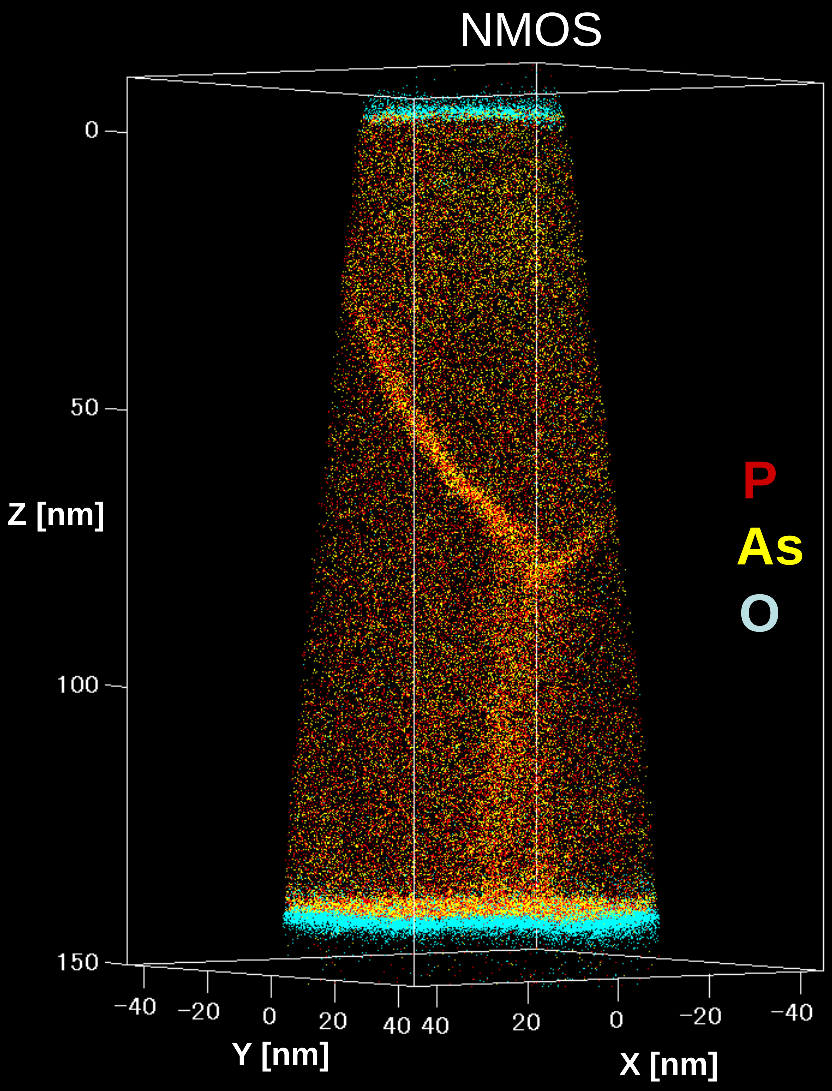

K. Inoue, F. Yano, A. Nishida et. al., Appl. Phys. Lett. 95 (2009) 043502.

Enlarged views around the gate oxides

PMOS

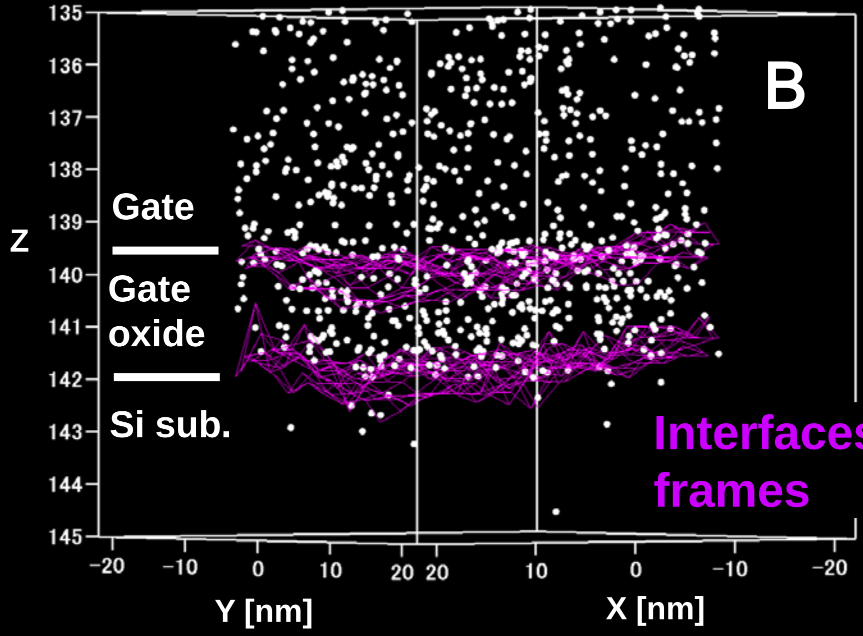

NMOS

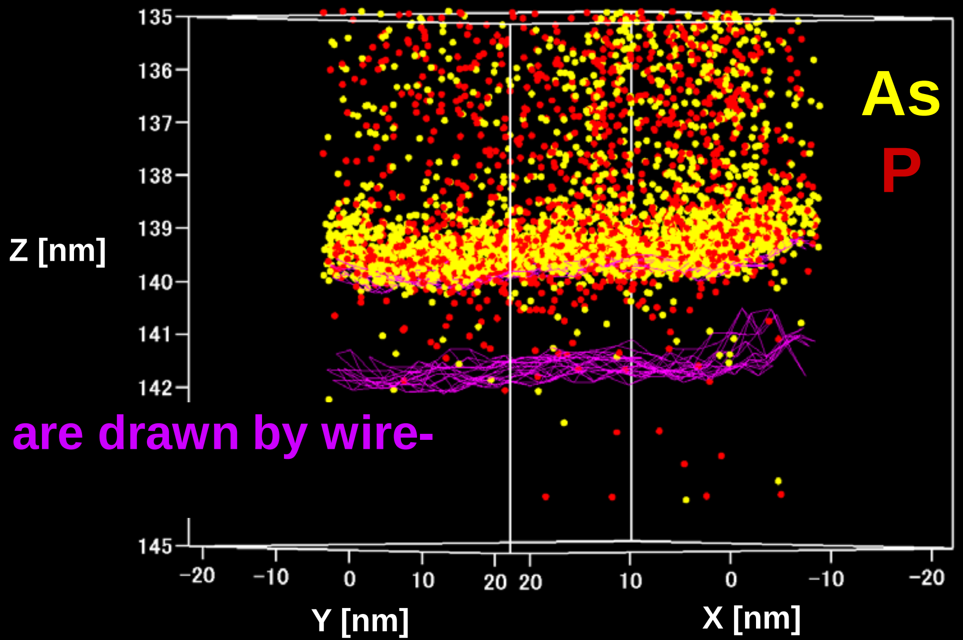

Interfaces are drawn by wire-frames

B

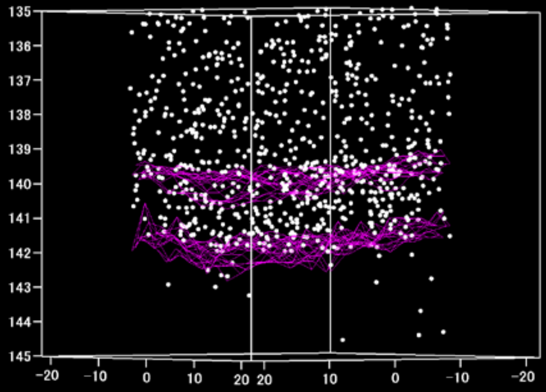

P

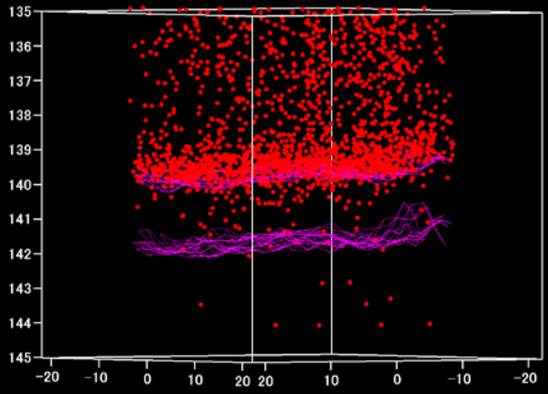

As

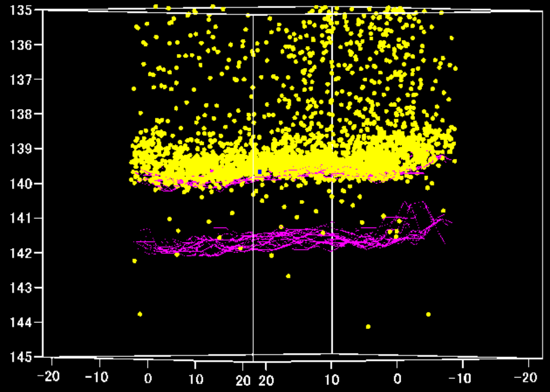

Recently dopant in sample with patten

3D maps of MOSFET

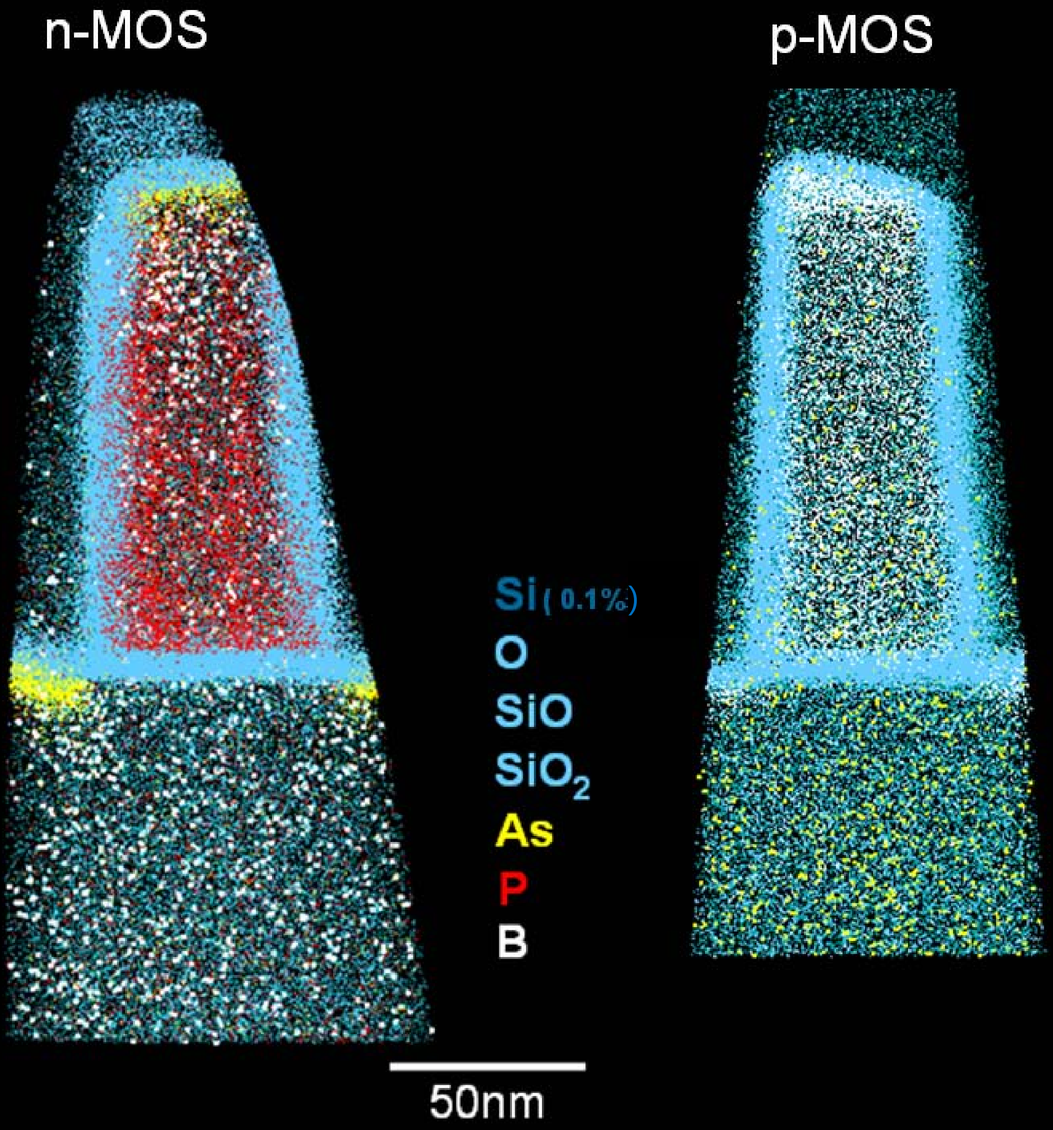

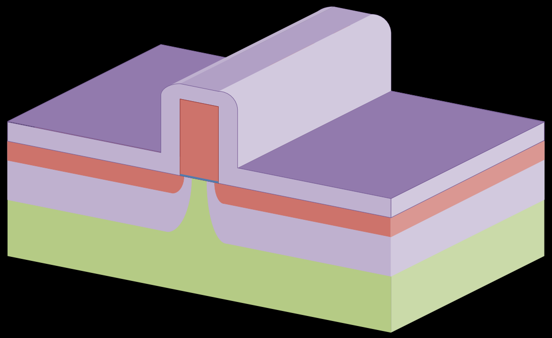

	N-MOS	P-MOS
Sub	B	As
Gate	P	B
Ext	As	B
Halo	B	P

Implantation, annealing: standard condition in 65nm process (not open)

Elemental maps in the slice 10nm thick (p-MOS)

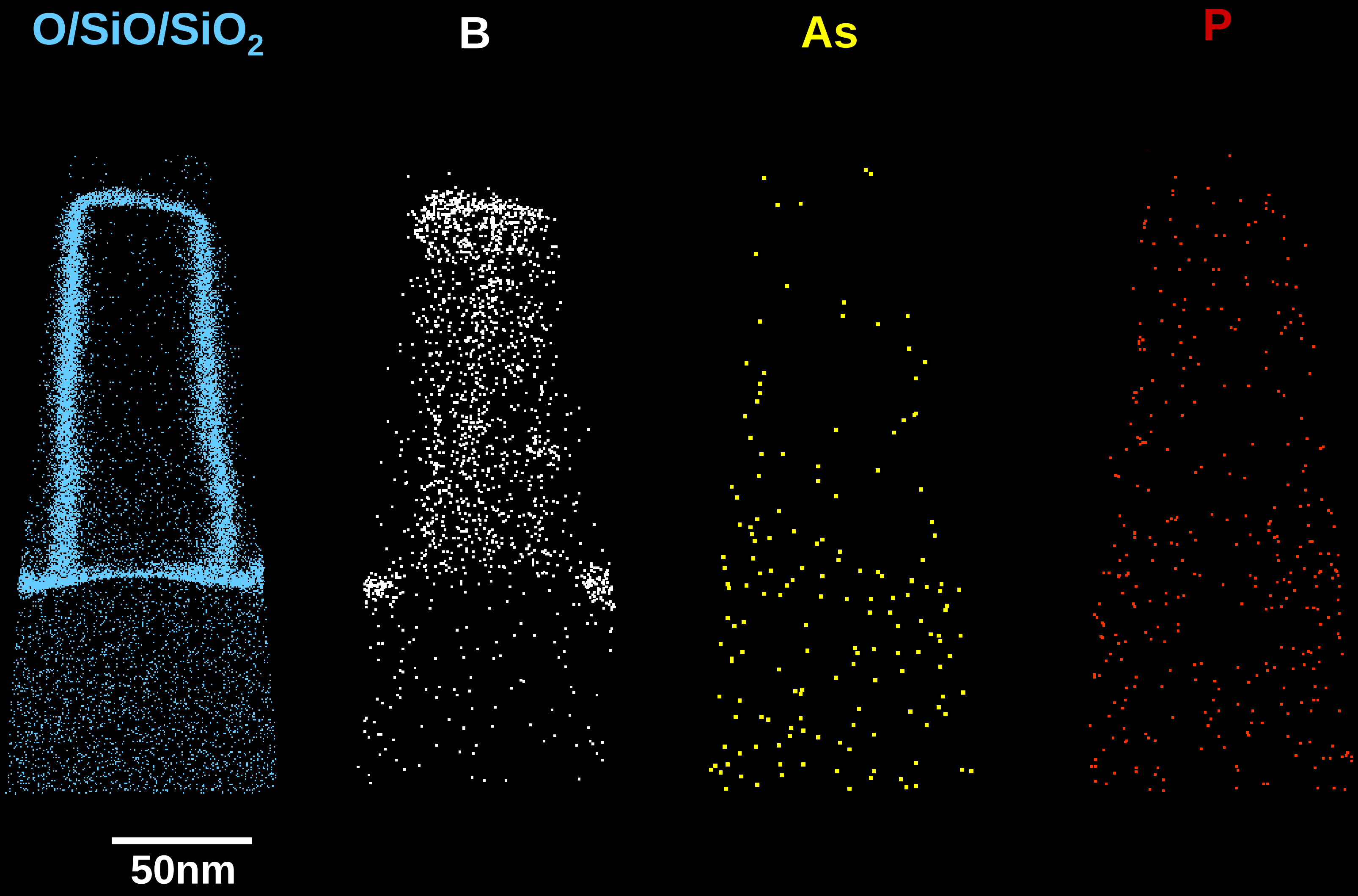

Elemental maps in the slice 10nm thick (n-MOS)

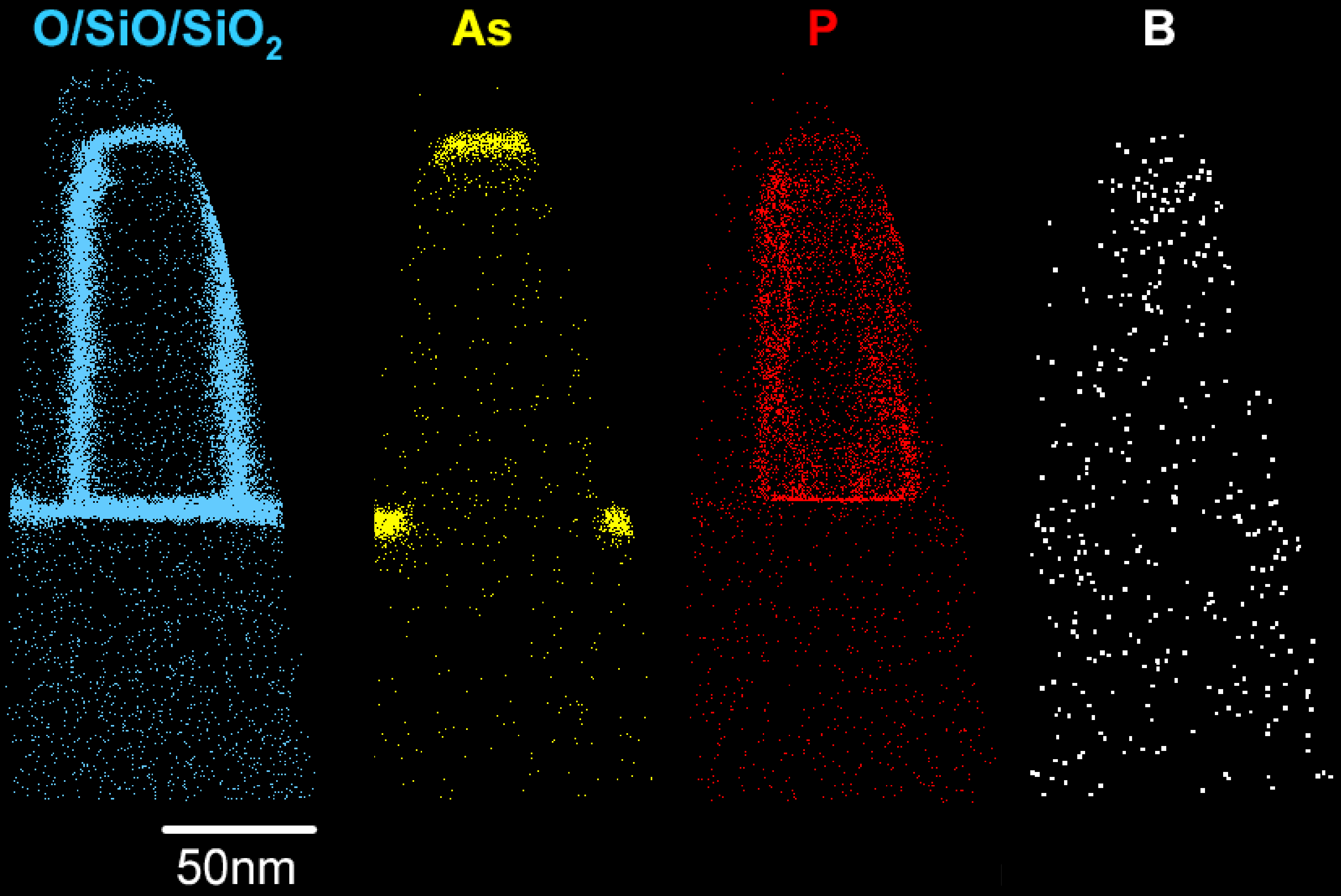

K. Inoue, F. Yano, A. Nishida et. al., Ultramicroscopy 109 (2009) 1479.

Enlarged view around the source/drain extension in n-MOS.

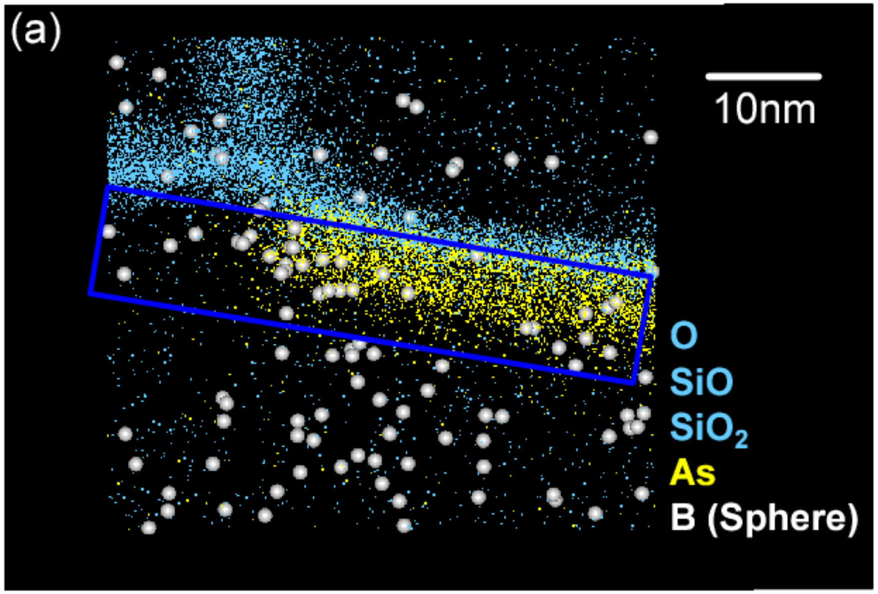

1D concentration profiles of B and As atoms

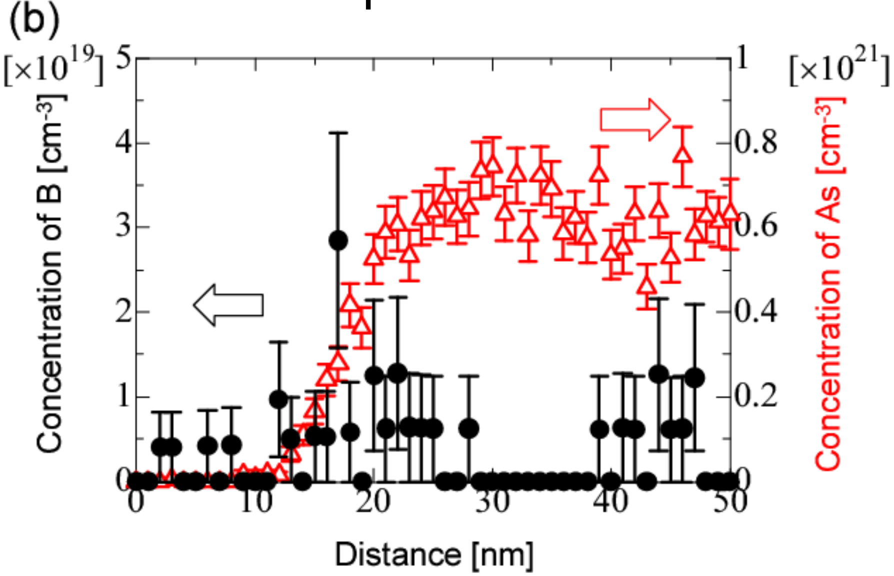

Dopant in commercial devices

- Joint research with Toray Research Center, Inc. -

B in center part of channel region

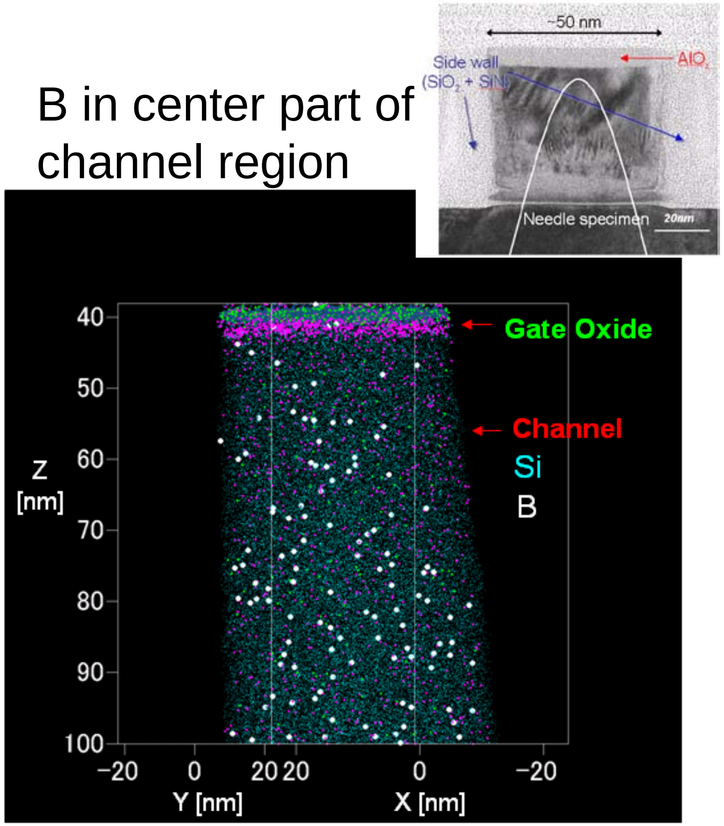

Dopant measurement in MOSFET Identified

Vth・・・now in progress

Problem to be solved for APT

- to observe dopant in further downsizing devices -

ex. 1×10^{18} dopant/cm^3 → 1 dopant in $10\times10\times10 nm^3$

- Detection efficiency

  Current detection efficiency ~ 50%

  :dominated by open area of MCP

  ⟶ Improving detector technology →100%

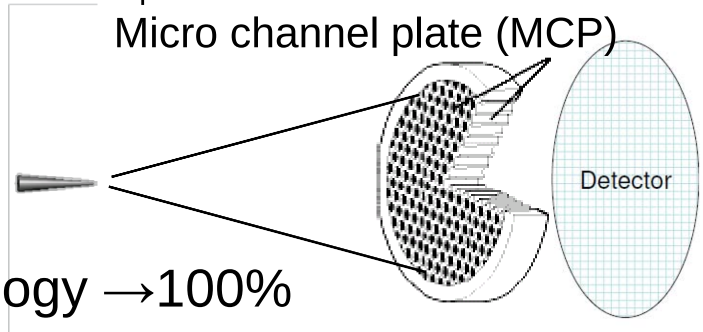

- S/N ratio

  ⟶ Increase of mass resolution

  Lower BG

  (Sensitivity: $>10^{17}$ - 10^{18} cm^{-3})

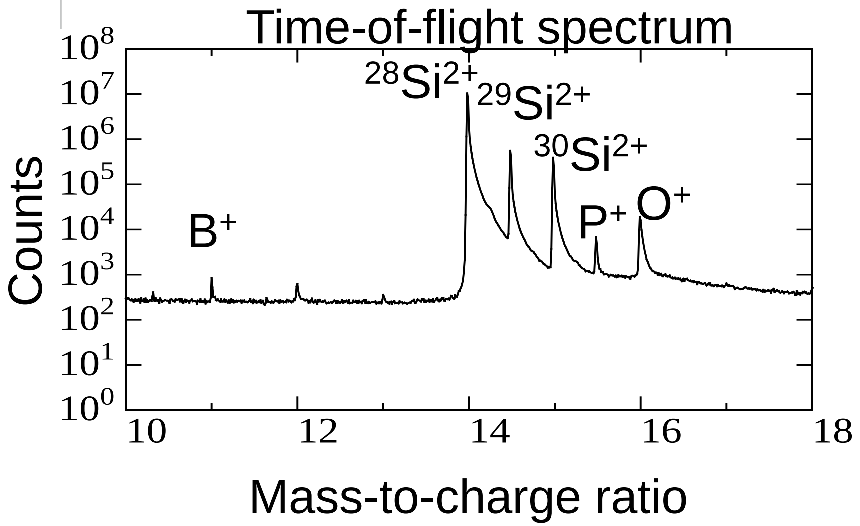

- Artifact of 3D reconstruction

  ⟶ Improvement of software analysis

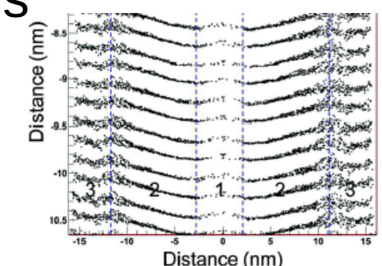

Atomic layers are not flat

IMC17

The Atomscope Concept – A New Branch of Microscopy

M.K. Miller[1]*and T.F. Kelly[2]

[1] Materials Science and Technology Division, Oak Ridge National Laboratory, Oak Ridge, TN 37831-6136, USA; millermk@ornl.gov
[2] Imago Scientific Instruments Corporation, Madison, WI 53711-4951, USA

Combination of STEM and APT into a single instrument

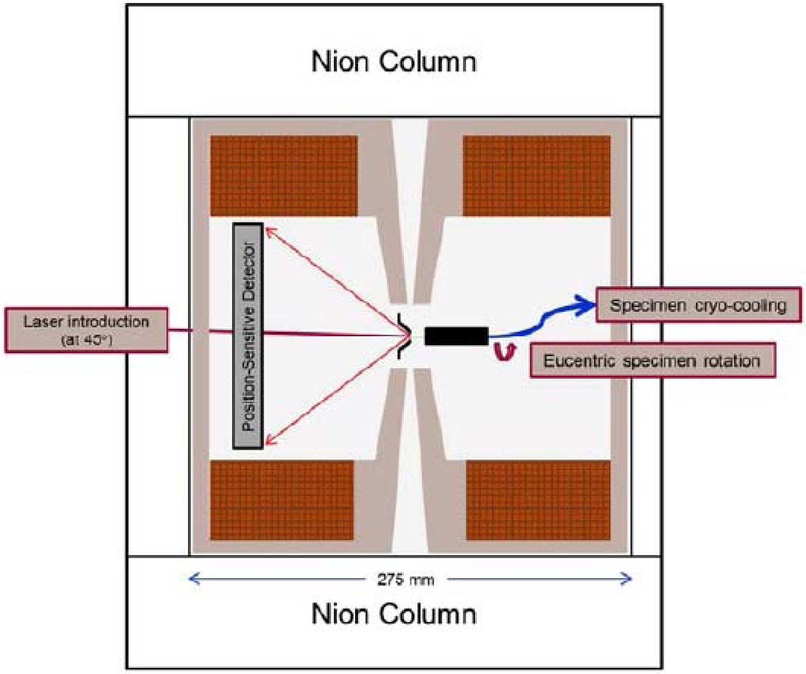

The ultimate aims of the ATOM project are to integrate a local electrode atom probe (LEAP) into an aberration-corrected, ultrahigh vacuum STEM to overcome these limitations to obtain accurate 3-D spatial information with quantitative elemental identification, Fig. 1. The resulting instrument is called an *atomscope*. In this combined instrument, individual atoms are field evaporated from the cryogenically-cooled specimen with a sub-picosecond duration laser pulse (which instantaneously increases the local temperature by less than 100 K) and their mass-to-charge-state ratios are determined in the LEAP's time-of-flight mass spectrometer. The spatial coordinates of each atom are derived by combining the data streams from the LEAP's single atom position-sensitive detector and the STEM detectors. All the normal functions and signals of the STEM, including high-angle annular dark field (HAADF) STEM imaging, electron diffraction, electron energy loss spectroscopy (EELS), and energy-dispersive spectroscopy (EDS), would be available. A new type of single-atom position-sensitive detector with a detection efficiency of 100% for all the isotopes of the elements will be integrated into the objective lens section for the APT functions. The detector will also be capable of simultaneous measurement of the kinetic energy of the field evaporated ions, which will enable the overlap of ions with different mass-to-charge states to be resolved for fully quantitative compositional measurements. A new multi-axis stage and cryogenic sample holder that are capable of all the sample movements required for electron tomography, including internal 360° rotation about the specimen axis, will be developed. The ability to perform 360° rotation will eliminate the so-called missing wedge problem in electron tomography. The stage and sample holder will also incorporate a high voltage connection to the specimen and a single-use local electrode for APT. An

APT apparatus

Local Electrode Atom Probe: LEAP

Large field of view ~150 nm in diameter

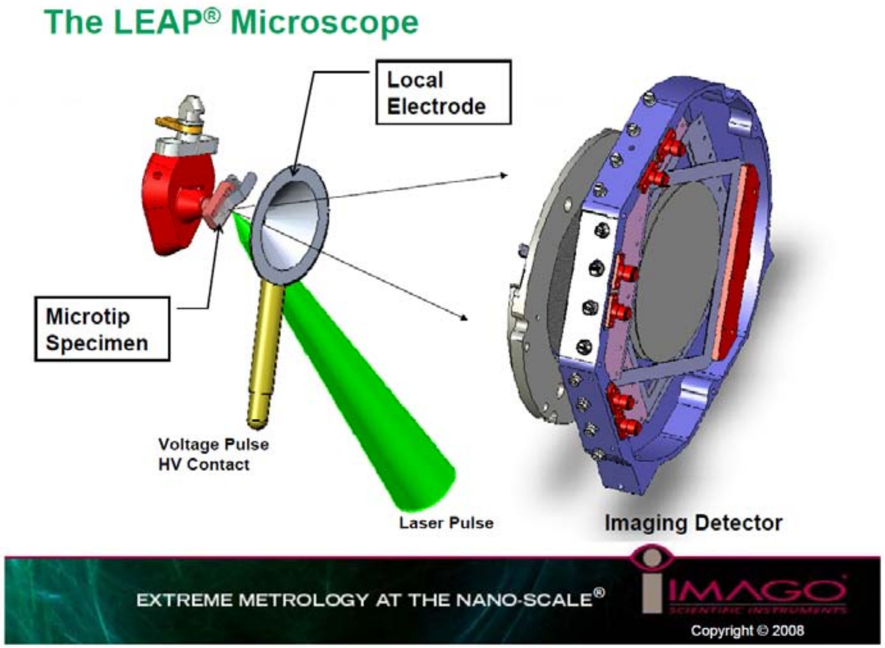

LEAP 3000 series (laser:visible)

LEAP 4000 series (laser: UV)

APT apparatus

Laser-Assisted Wide Angle Tomographic Atom Probe : LAWATAP

flexible (IR / visible / UV) ultrafast (400fs) laser setup

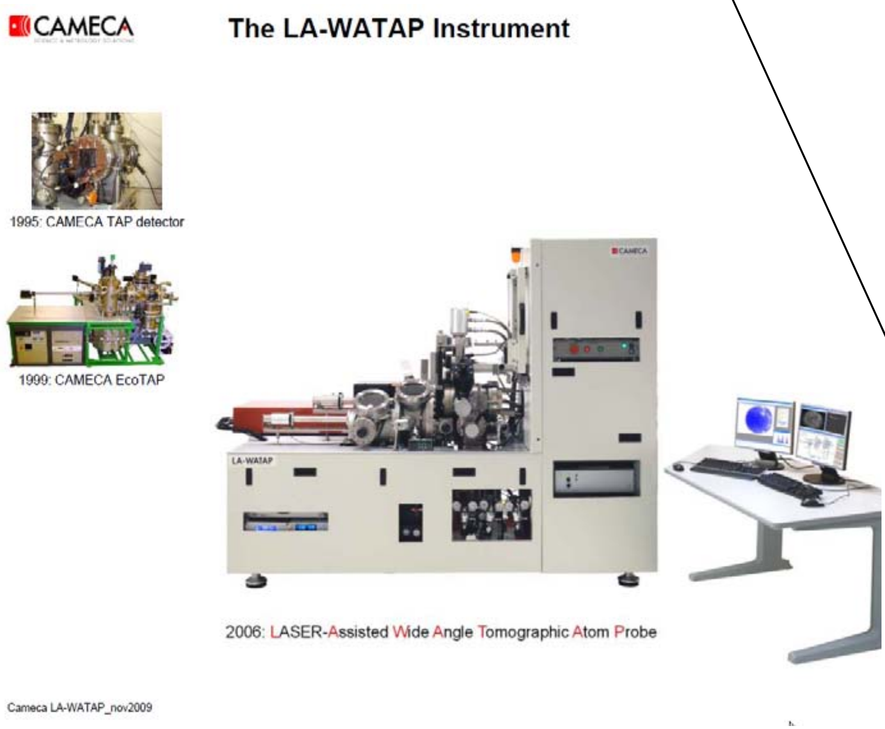

CAMECA

The LA-WATAP Instrument

1995: CAMECA TAP detector

1999: CAMECA EcoTAP

2006: LASER-Assisted Wide Angle Tomographic Atom Probe

Cameca LA-WATAP_nov2009

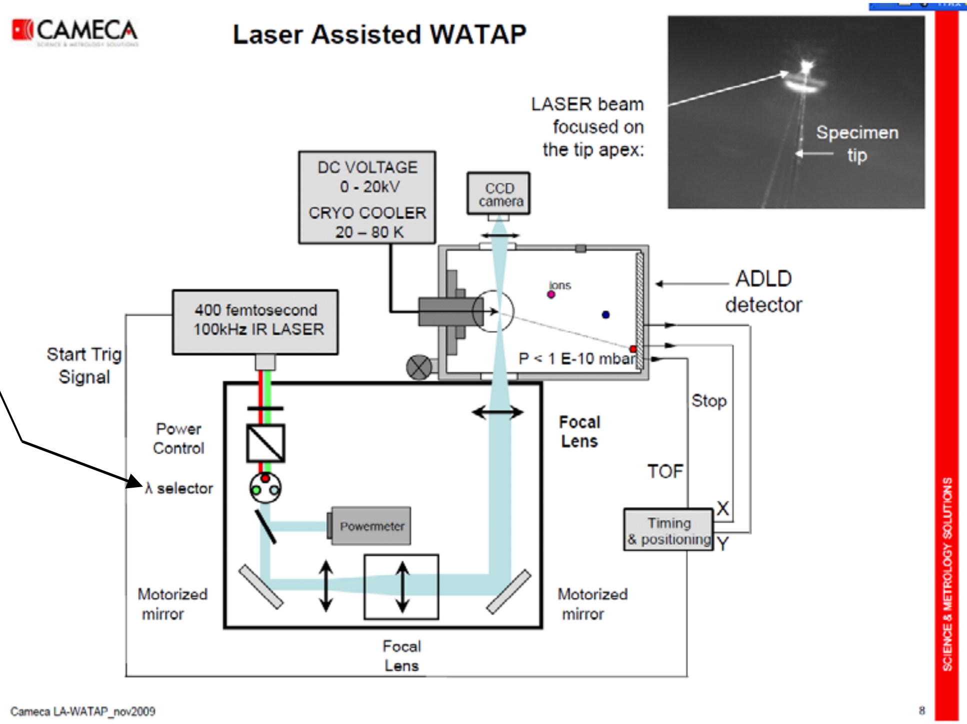

CAMECA

Laser Assisted WATAP

Cameca LA-WATAP_nov2009

8

Discontinued at this September

Installed Base (3DAP. LEAP & LA-WATAP)

Northwestern University Center for Atom Probe Tomography (NUCAPT)

Dopant distribution in Ge nanowire

4

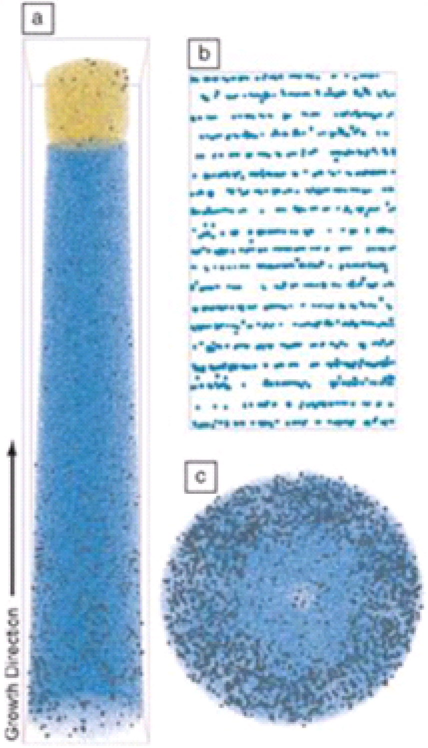

Three-dimensional reconstruction of doped Ge nanowire showing Au, Ge, and P atoms as gold, blue, and gray spheres respectively. (a) Side view of Au catalyst tipped nanowire. Arrow indicates growth direction. (b) Side view of a center portion of the same nanowire showing {111} planes perpendicular to the growth axis. (c) End-view showing a radially non-uniform doping profile due to surface growth.

D. E. Perea et al., Nature Nanotechnology 4, 315 - 319 (2009)

Blavette et al., Materials Science and Engineering 7(2010) 012004

R

- Ultraviolet pulse laser-assisted APT

Thick SiO_2 layer

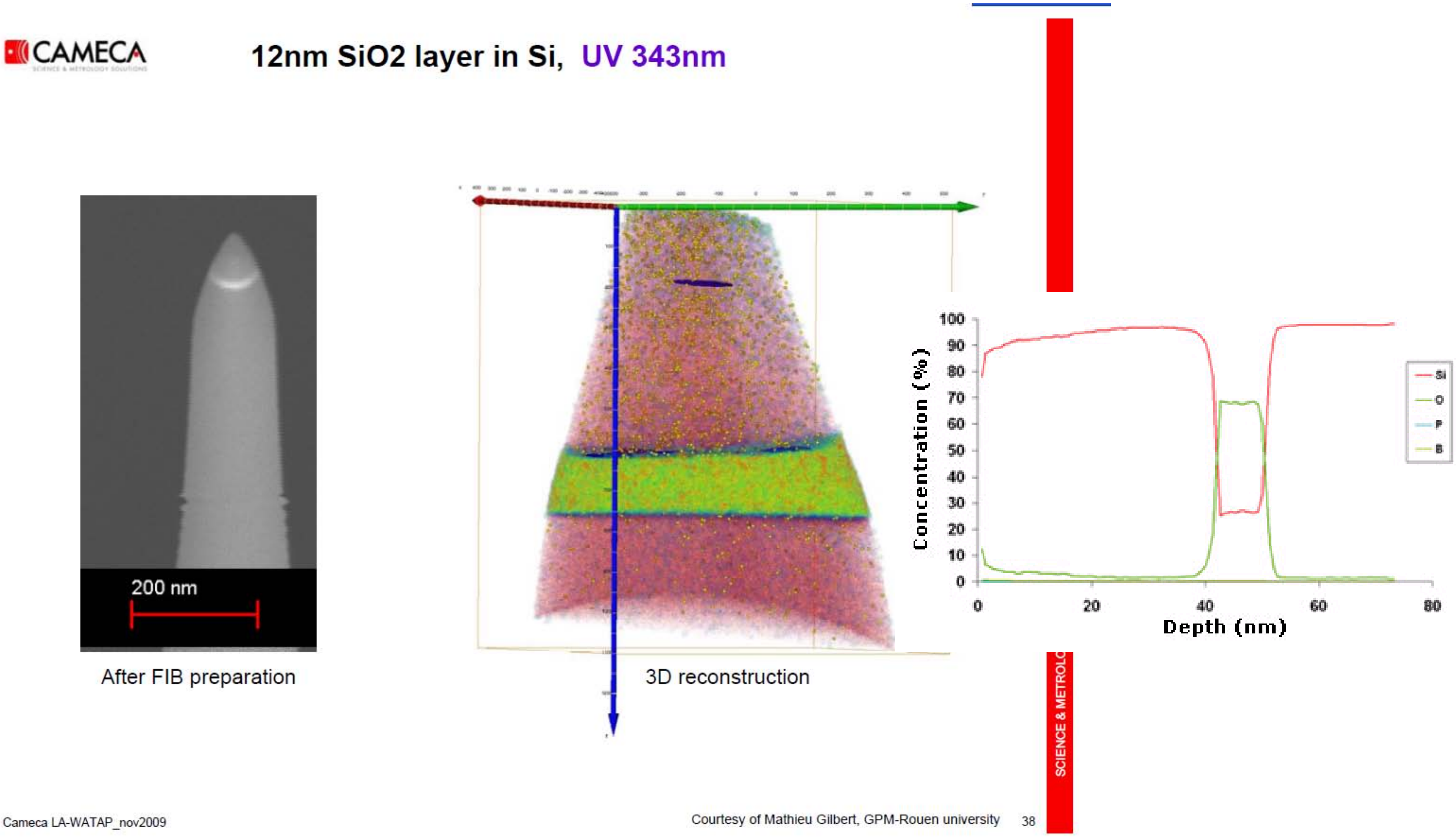

12nm SiO2 layer in Si, UV 343nm

After FIB preparation

3D reconstruction

Cameca LA-WATAP_nov2009

Courtesy of Mathieu Gilbert, GPM-Rouen university

38

Bulk insulating ceramics (ZrO$_2$-MgAl$_2$O$_4$)

$10^{9}\ \Omega\cdot$cm

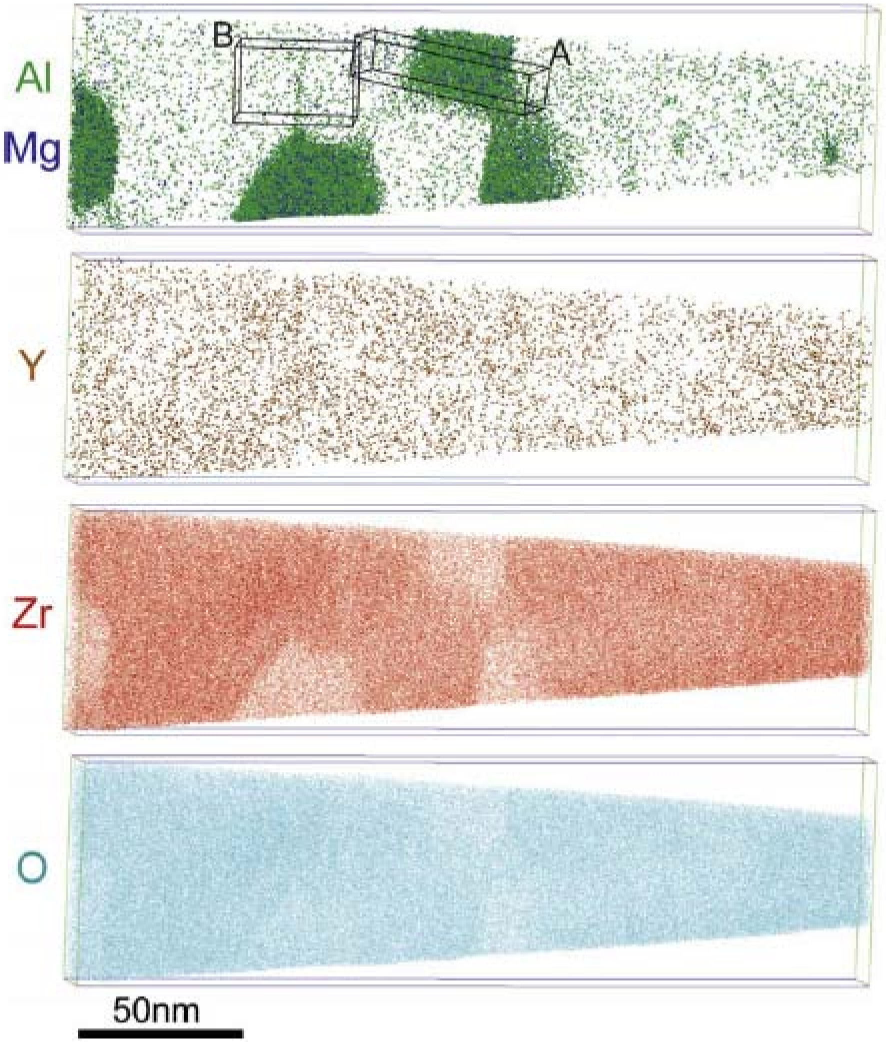

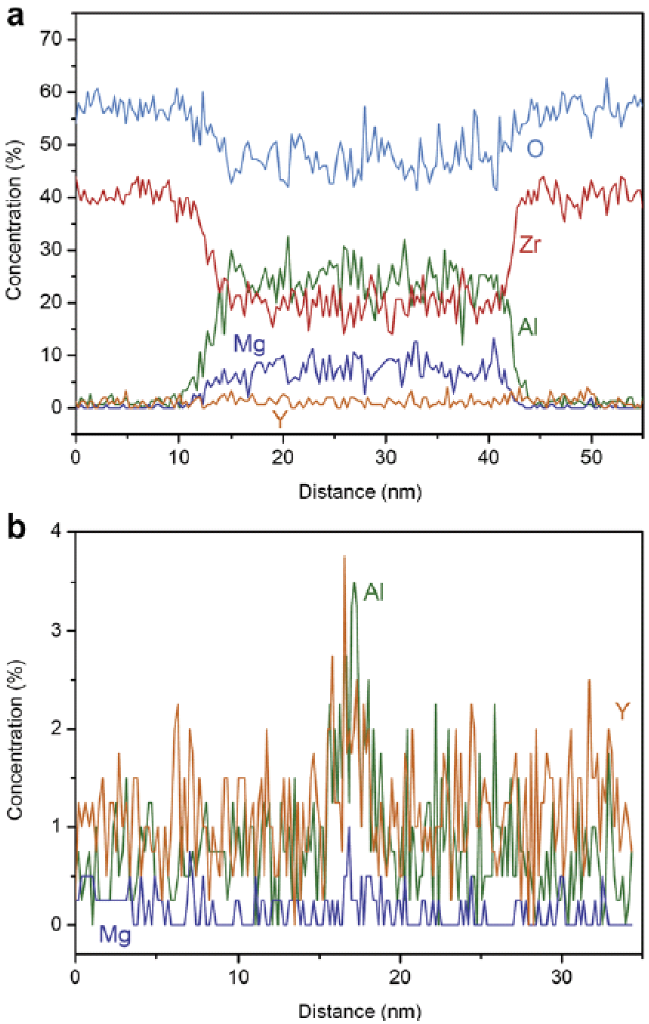

Y. M. Chen, T. Ohkubo, M. Kodzuka, K. Morita and K. Hono, Scripta Mater. 61 (2009) 693.

Field evaporation with LASER pulsing

- Rate of evaporation given by Arrhenius relation:

$$\exp\left(-\frac{Q_n}{kT}\right)$$

- Field required for constant evaporation rate depends on temperature
- Get ~10% enhancement per 200K temperature rise for tungsten
- Rate can be increased by raising T or **raising Field** (decreasing Q_n)

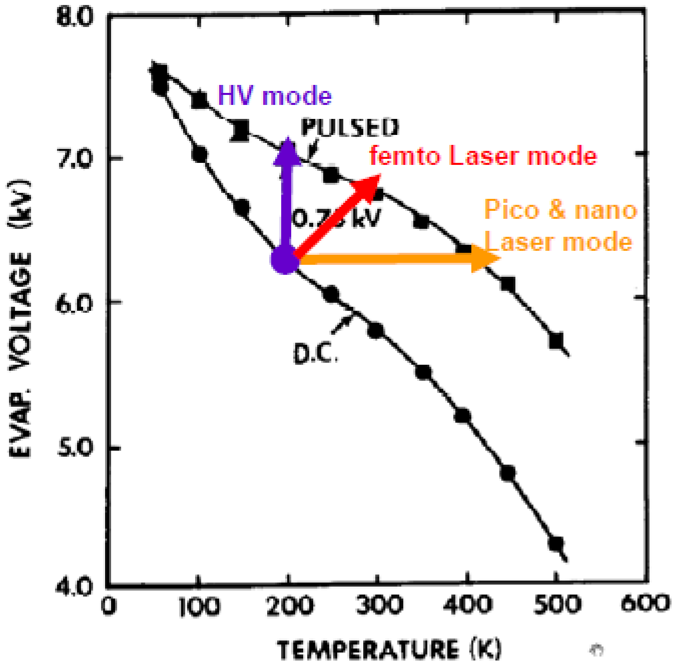

Copied from G.L. Kellogg, *J. Appl. Phys.* 82 (1981) 5320

Nanosecond laser (Tsong, 80s): raising T but prohibitive thermal effects,
Picosecond laser: raising T = Thermal evaporation mode (IMAGO mode),
Femtosecond laser: raising T + **raising Field** = reduced Heating with Optical Rectification (CAMECA mode)

The red arrow is an visual rendition: the electro-magnetic field induced by the fast light pulse does not increase the potential of the tip surface but decreases the evaporation barrier.

Major origin of the larger NMOS V_T variability

(T. Tsunomura, et al., 2009 Symposium on VLSI Technology Digest of Technical Papers p110.)

B in channel of NMOS → **re-distribution by interstitial Si introduced by Ext/Halo forming**

Transient Enhanced Diffusion (TED)

V_{th} variability **nonuniformity of channel dopant**

(concentration fluctuation increased by re-distribution)

NMOS

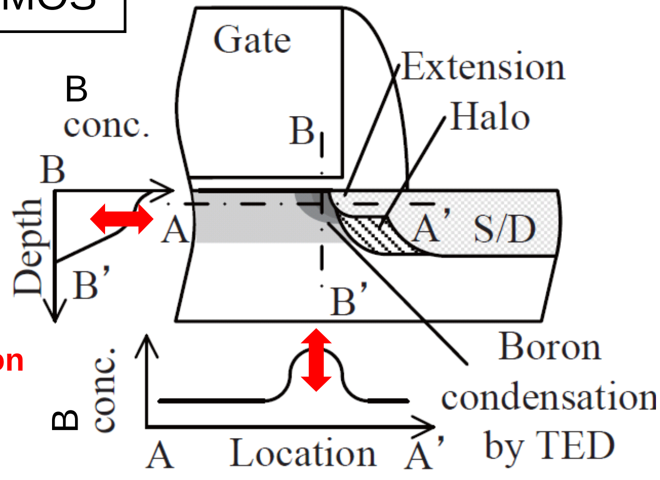

Concentration fluctuation

re-distribution

PMOS

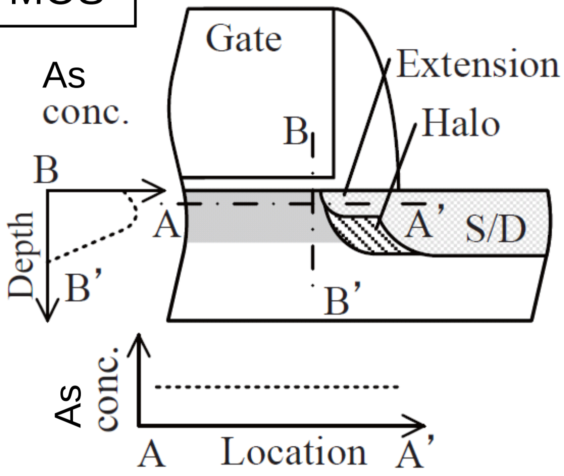

Distributin nochange

Needle specimen fabrication in real device - n-MOSFET (45nm node) -

which includes gate region and excludes thick dielectrics region such as side wall

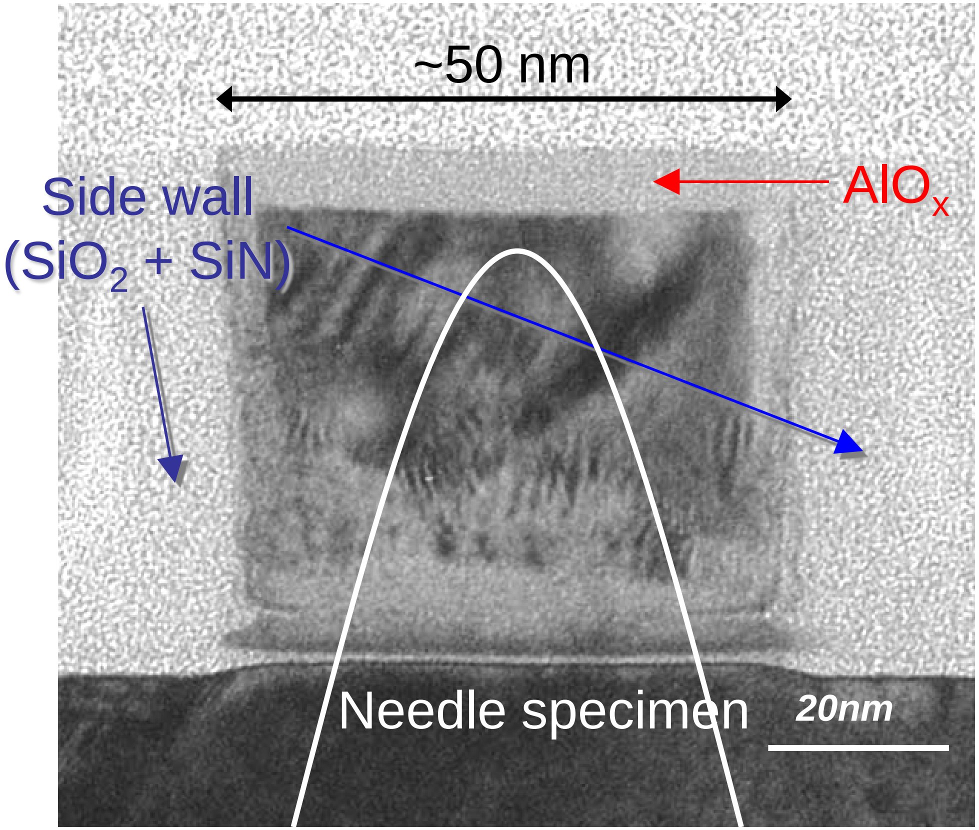

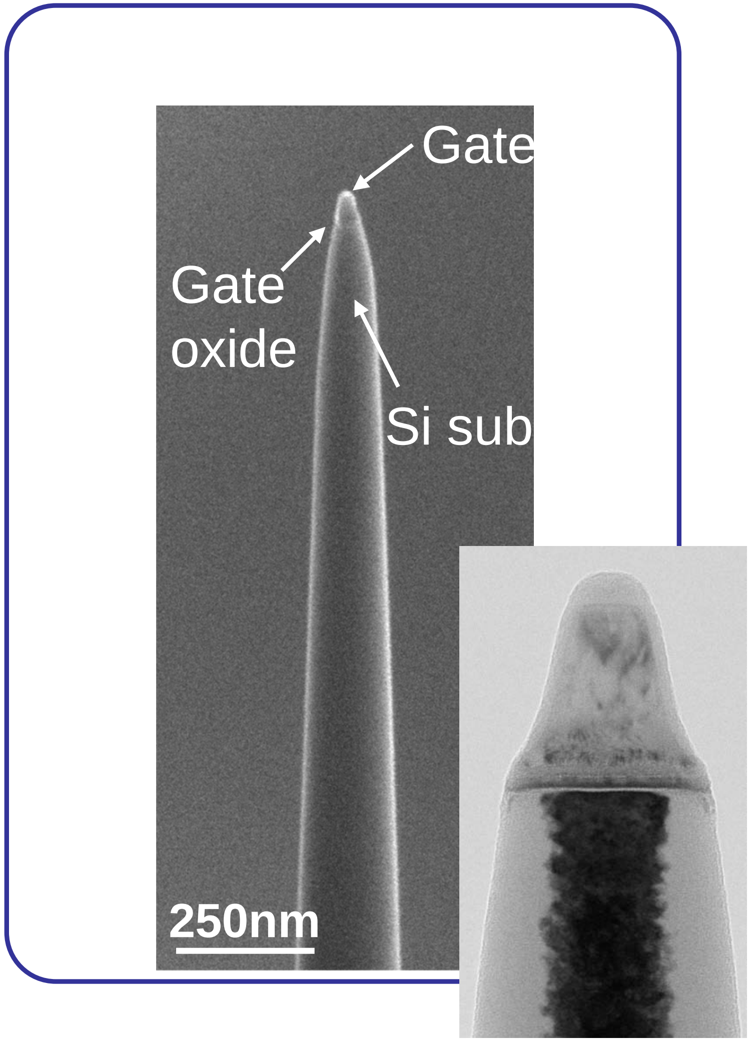

Joint research with Toray Research Center, Inc. / K. Kitamoto, J. Kato, T. Miyagi

Lateral dopant distribution in inversion layer

Verification of dopant distribution randomness in lateral directions

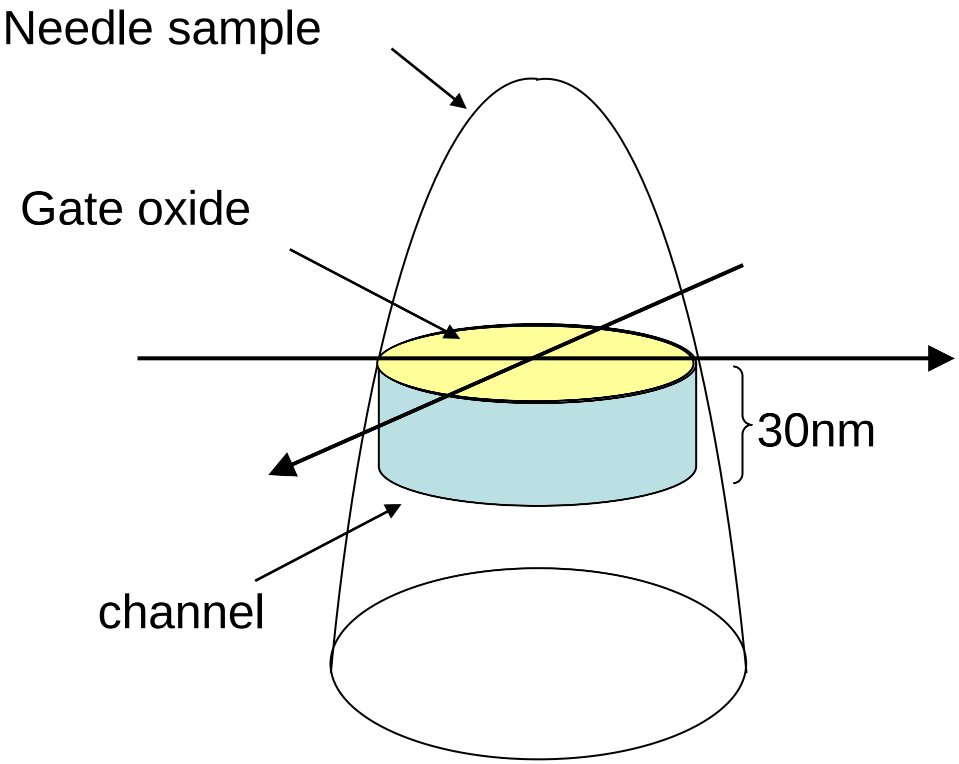

Randomness Verification

- large amount of data
  28 needle sample -NMOS
  38 needle sample -PMOS
- dividing into small ROI
- counting dopant number in the ROI
- Binominal distribution ?
  (Random distribution)?

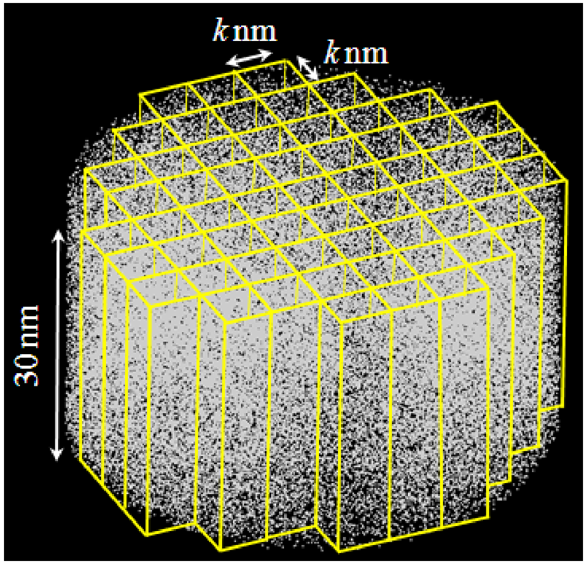

k=1nm

k=2nm

k=3nm

k=4nm

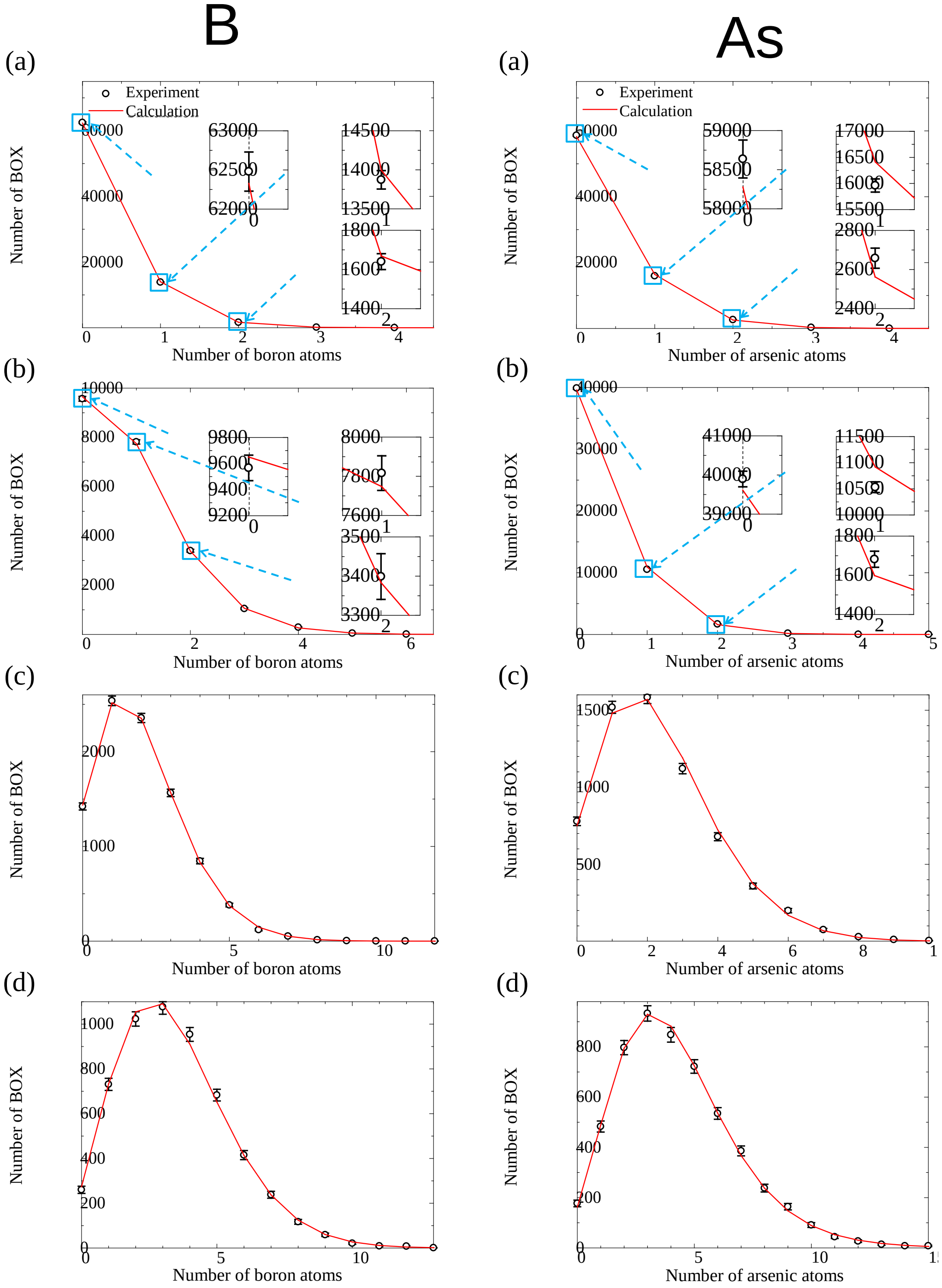

B distribute randomly in lateral directions

Following process (such as implantation for source/drain) may modulate B distribution?

Laser-assisted LEAP equipped with a reflectron lens

LEAP 3000HR

(laser: 532nm)

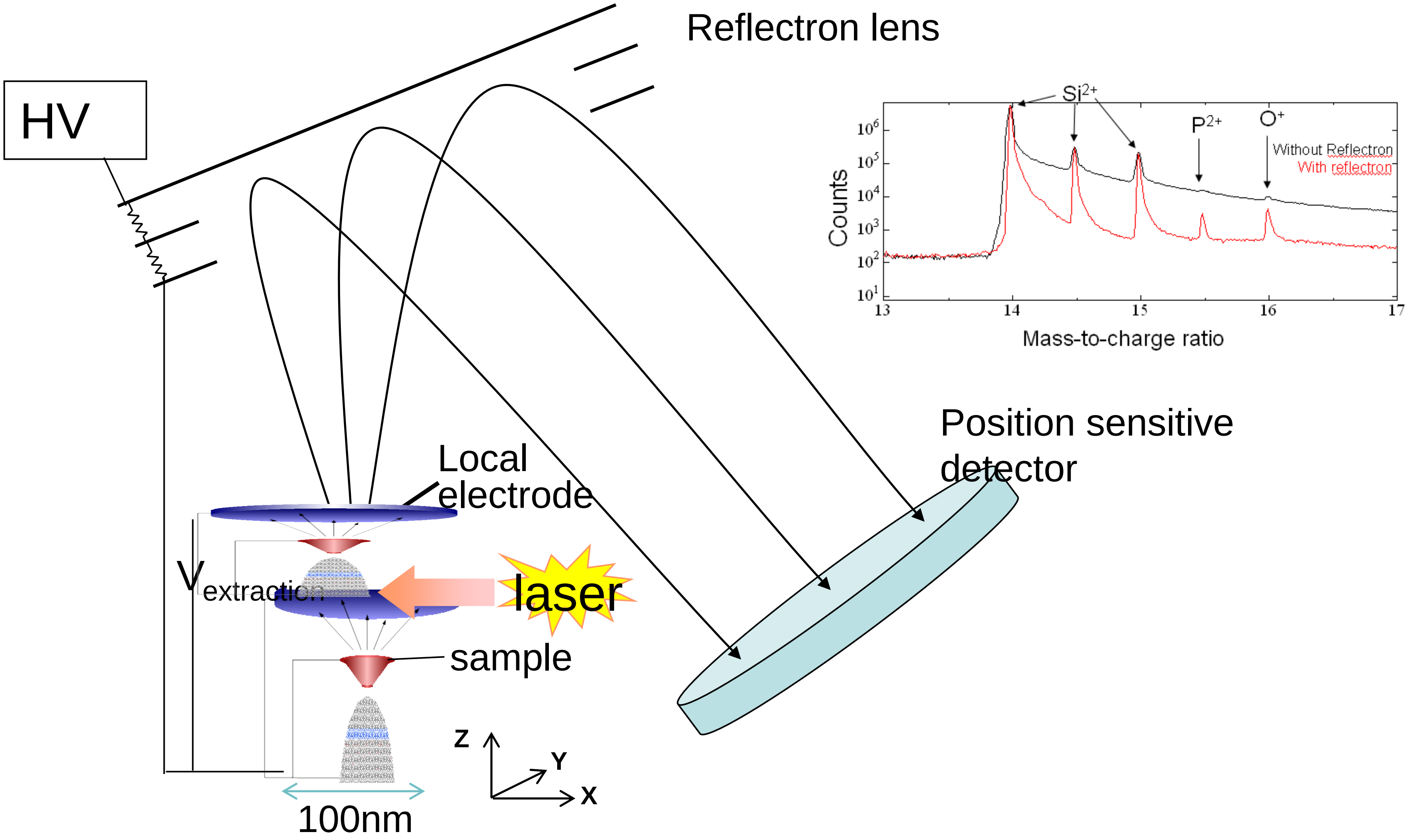

Reflectron lens

HV

Local electrode

$V_{extraction}$

laser

sample

100nm

Position sensitive detector

Sample

Laterally uniform dummy structure of MOSFET without pattern
(poly-Si gate, gate oxide, Si substrate in depth direction)

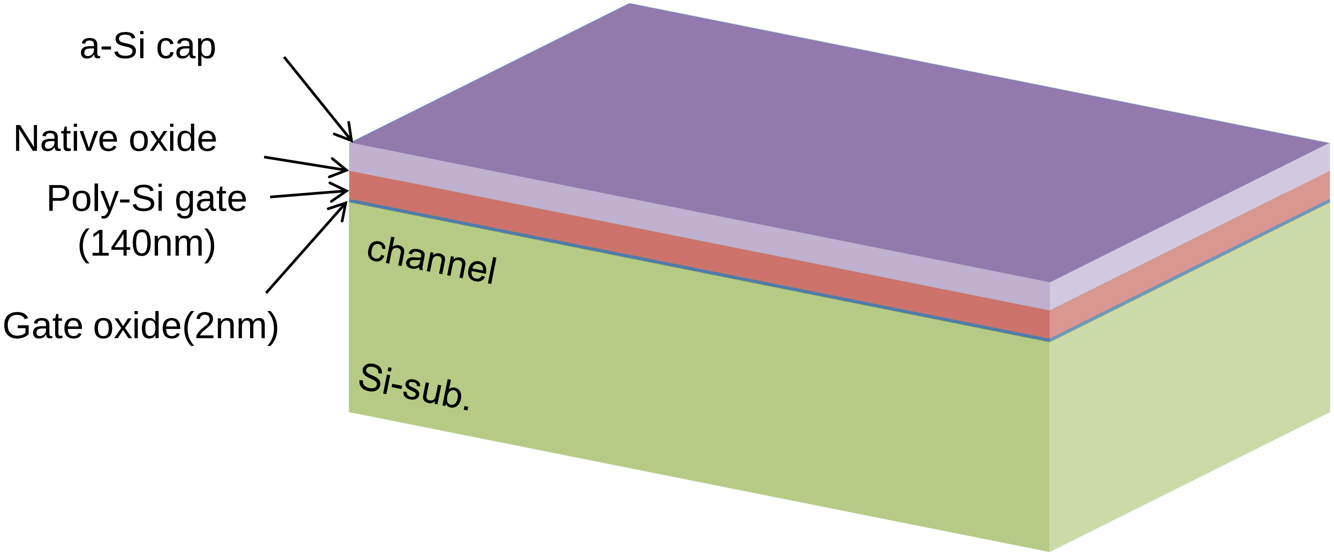

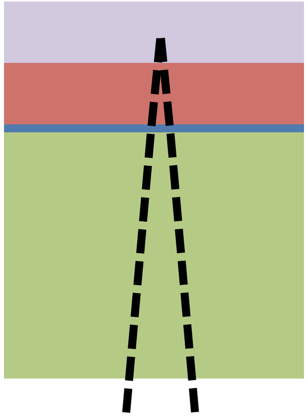

Needle sample were prepared by FIB

doping	n-POS	p-MOS
gate	P:10keV, 5.5×10^{15}cm^{-2} As: 20keV, 4×10^{15}cm^{-2}	B: 3keV, 2×10^{15}cm^{-2} B: 2keV, 4×10^{15}cm^{-2}
channel	B: 10keV, 2×10^{14}cm^{-2}	As: 70keV, 2×10^{14}cm^{-2}

+ annealing

One order higher dopant concentration in channel region

3D atom map

B atoms in the gate of this sample nonuniformity ← too short thermal aging time.

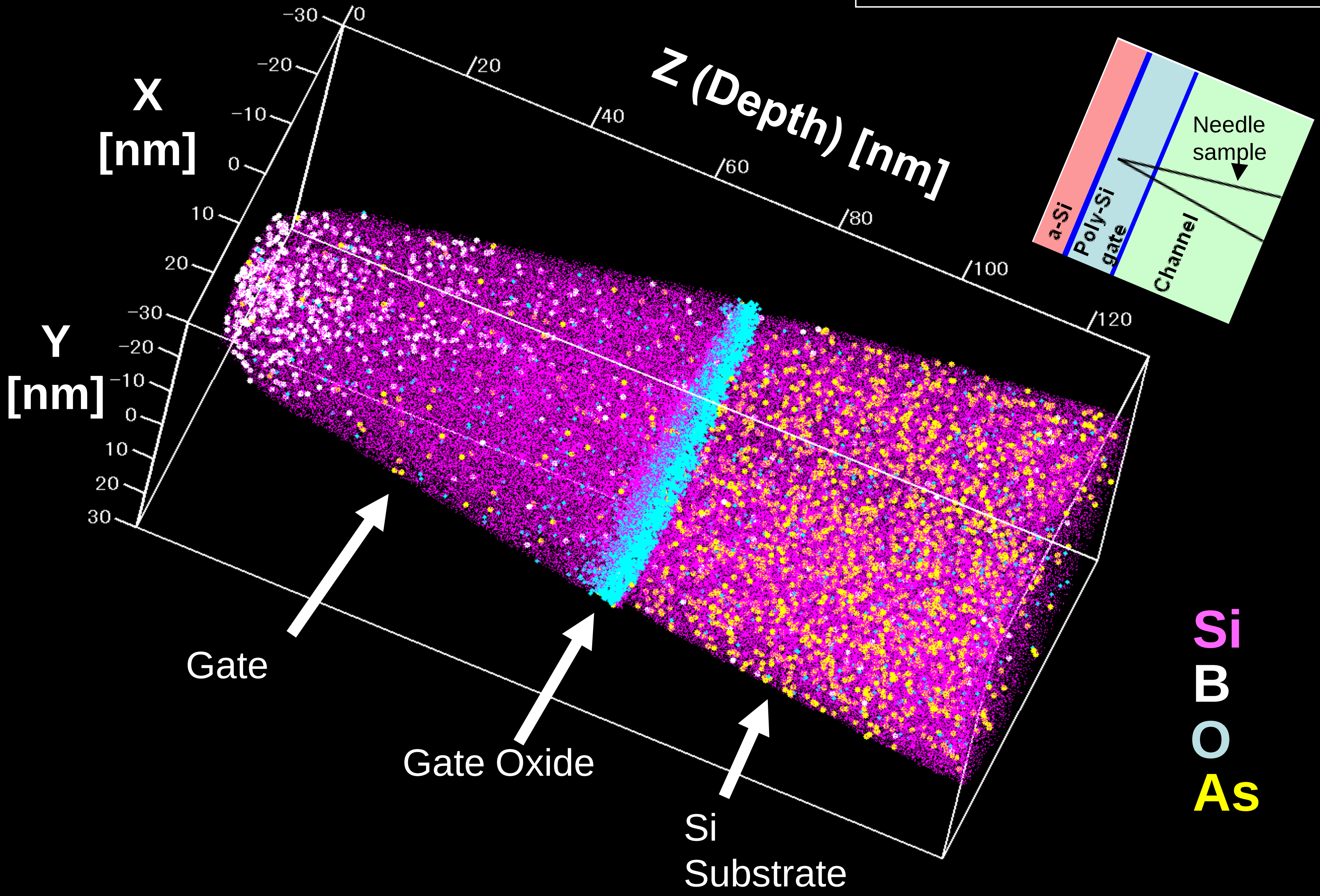

Enlarged view around gate oxide

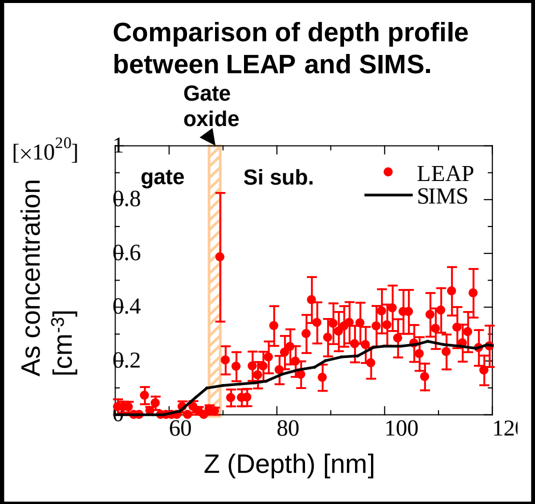

Comparison of depth profile between LEAP and SIMS.

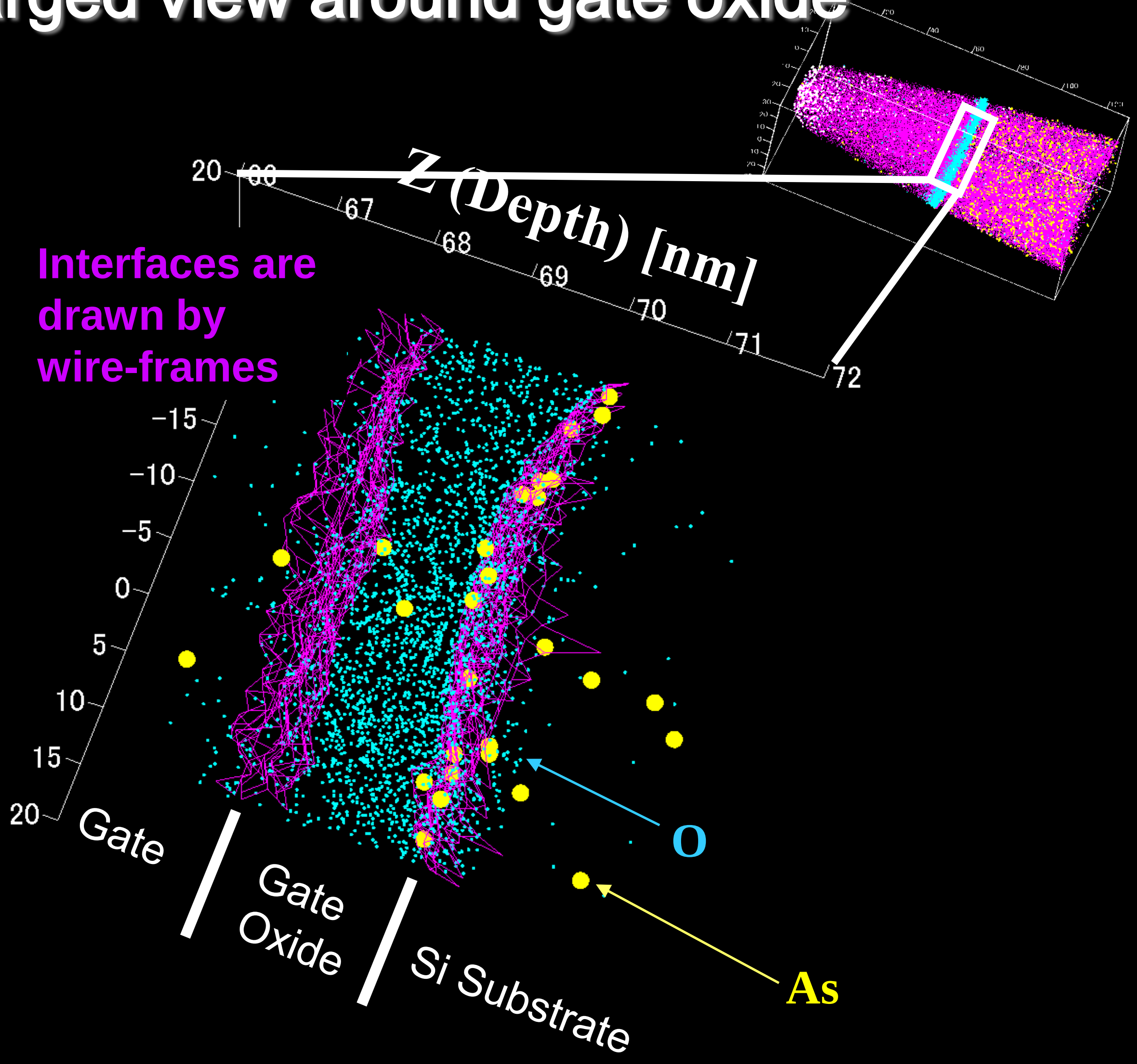

Interfaces are drawn by wire-frames

K. Inoue, F. Yano, A. Nishida et. al., Appl. Phys. Lett. 92 (2008) 103506.

Segregation on interfaces between gate oxide and Si substrate

- Dependence on dopant species -

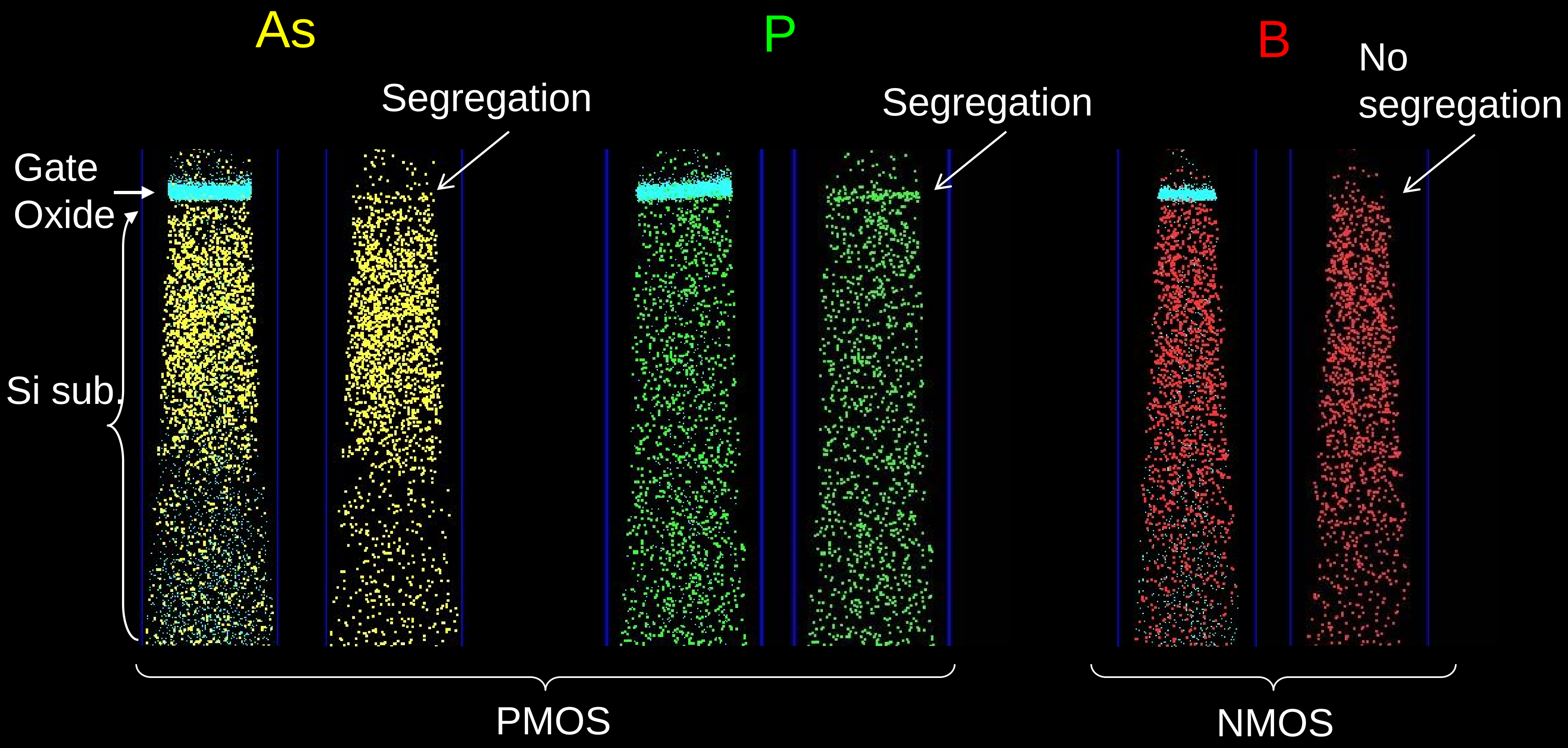

Comparison of depth profile between APT and SIMS

Observed region : SIMS~100μm in diameter
APT~100nm in diameter

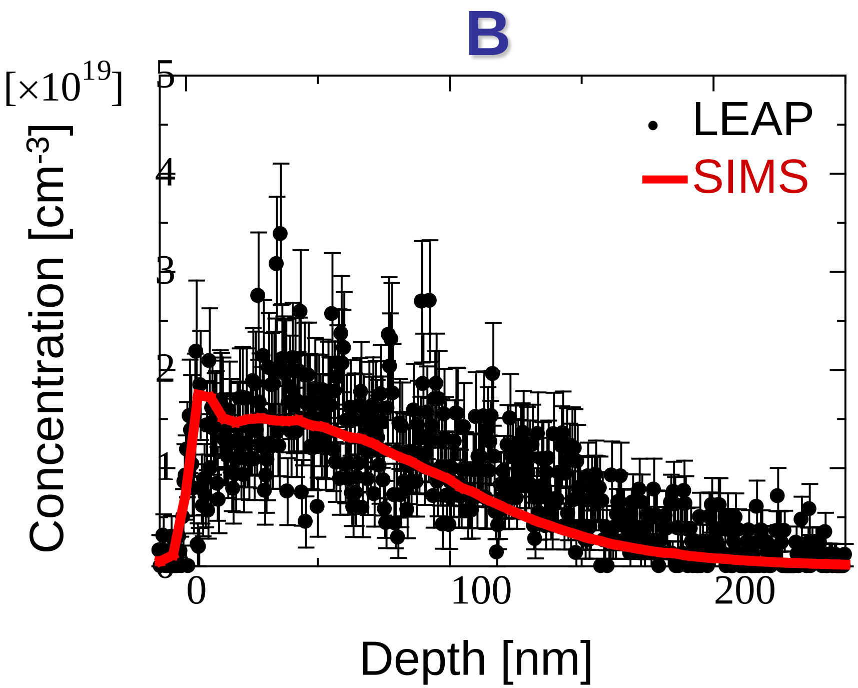
B

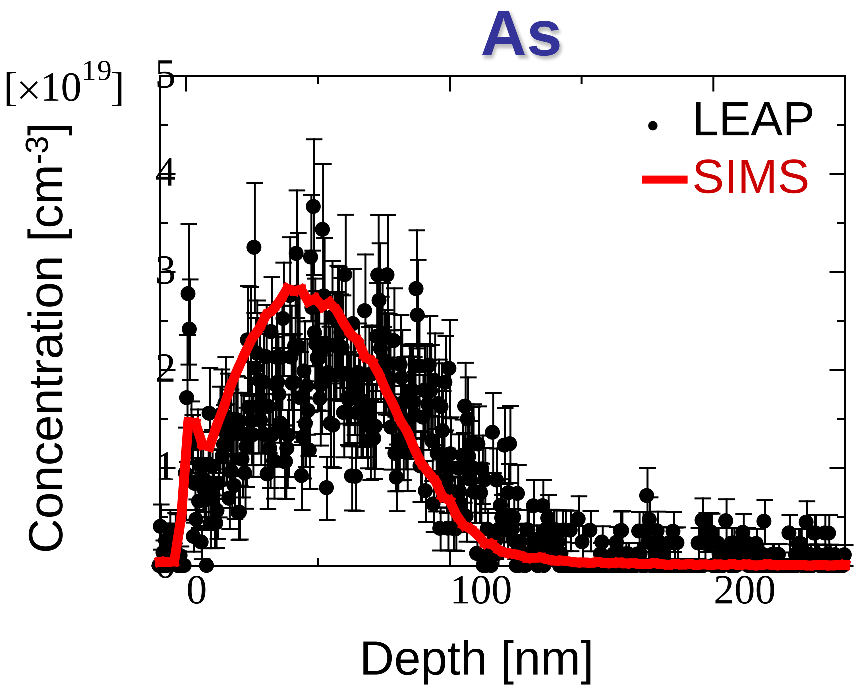
As

Dopant distribution in poly-Si gate (PMOS)

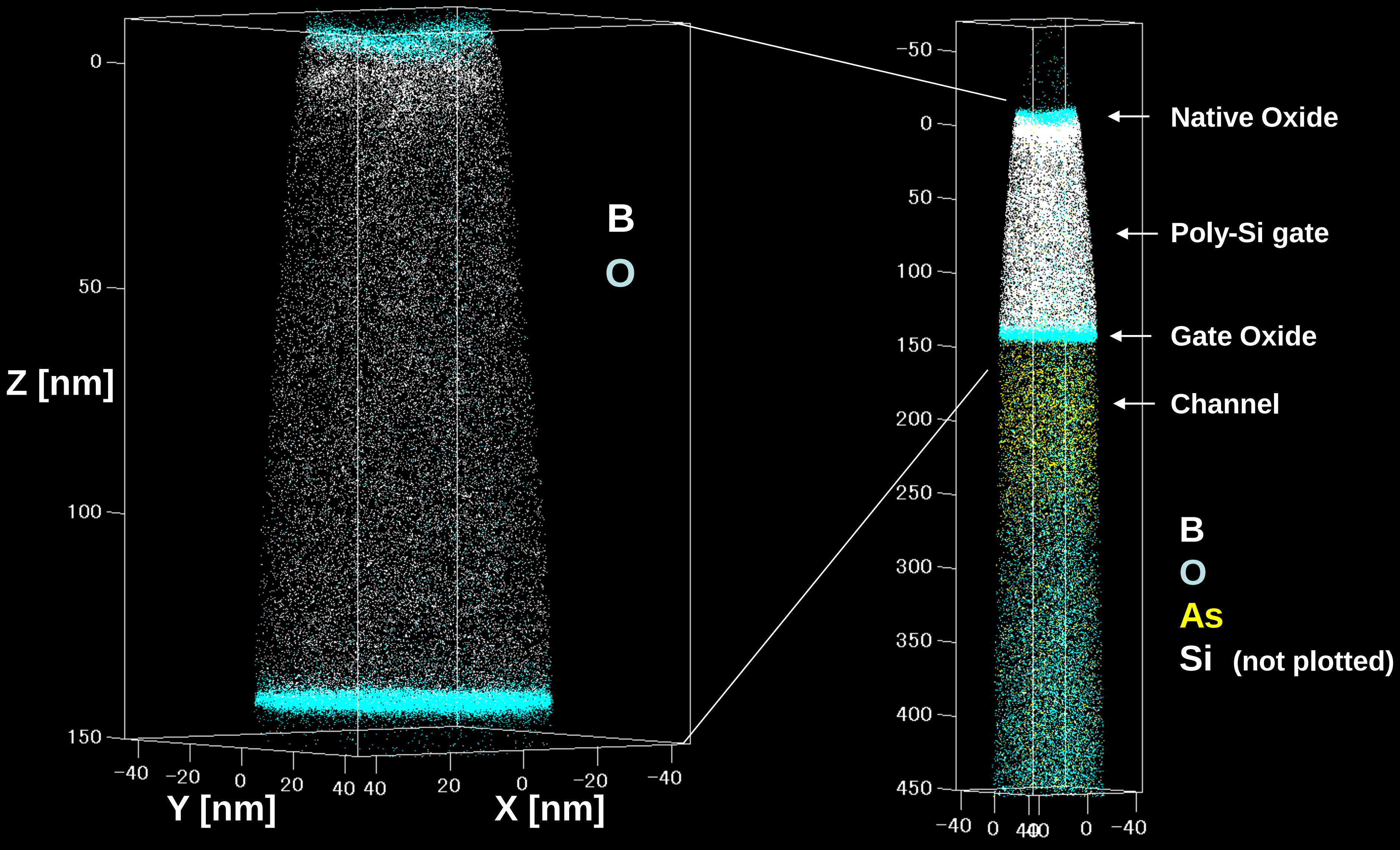

B
O

Native Oxide

Poly-Si gate

Gate Oxide

Channel

B
O
As
Si (not plotted)

Dopant distribution in poly-Si gate (NMOS)

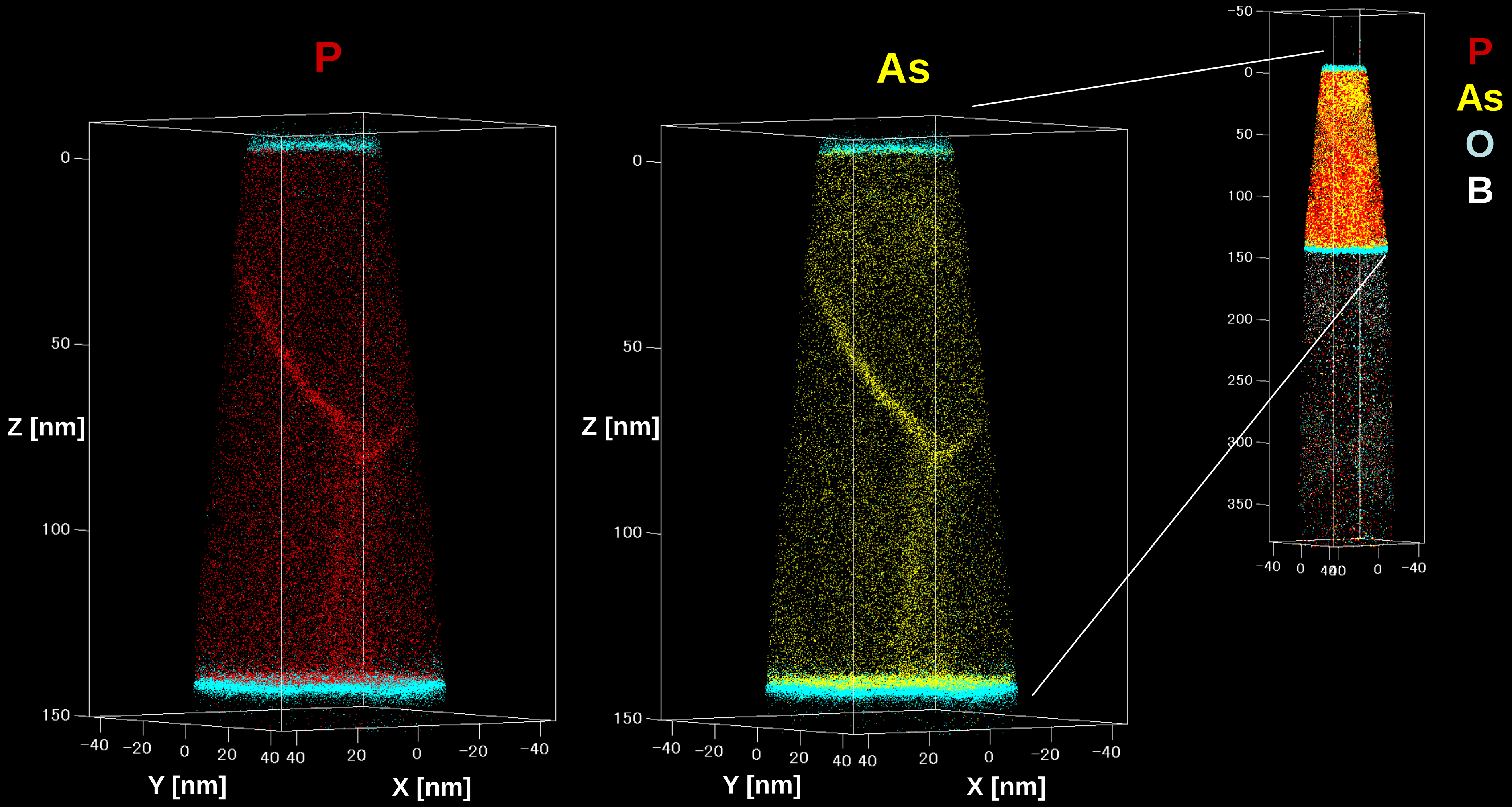

Concentration profile across grain boundary

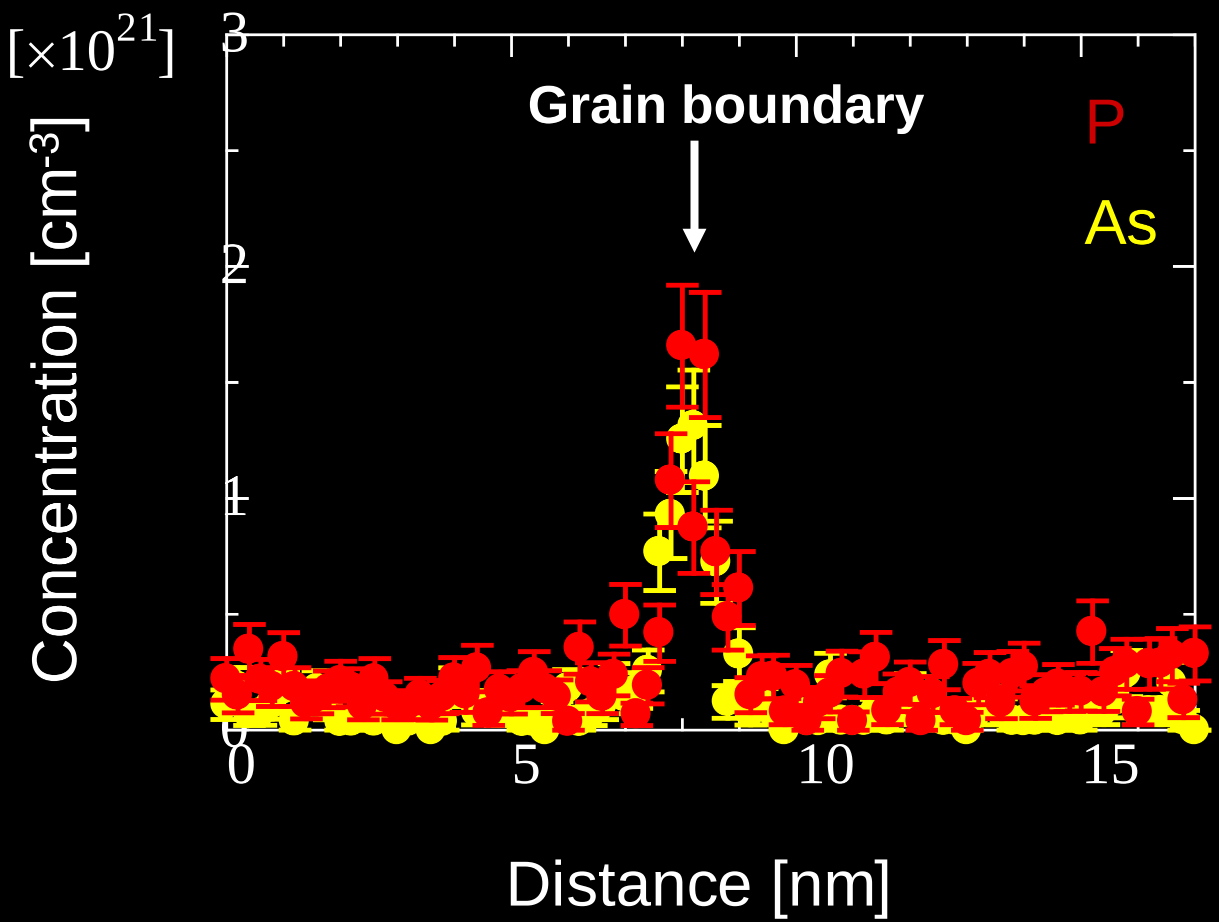

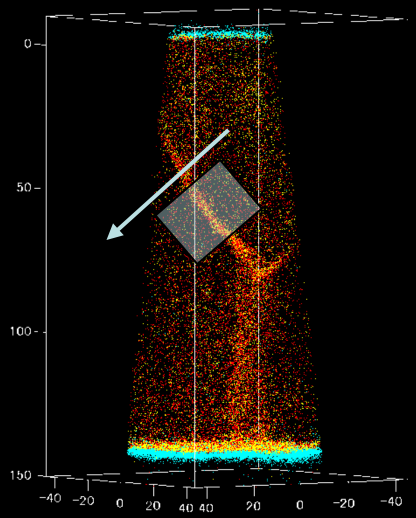

Comparison of dopant distribution in gate

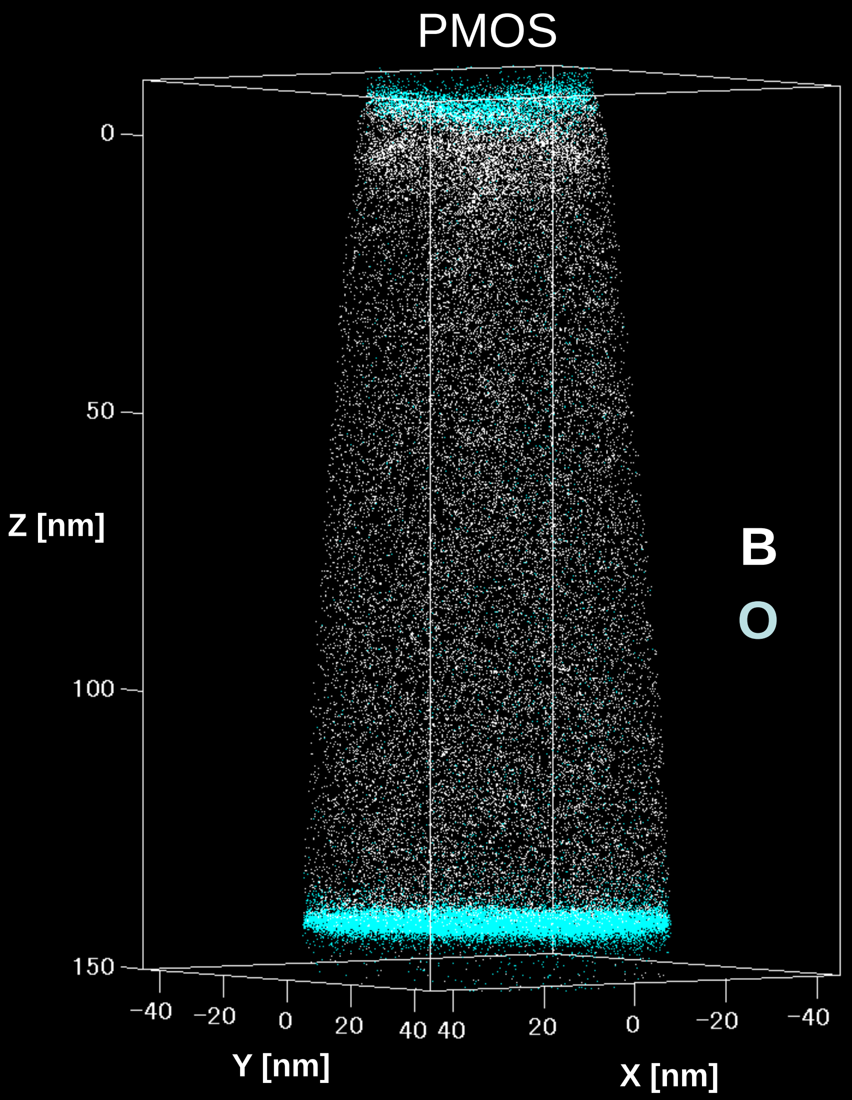

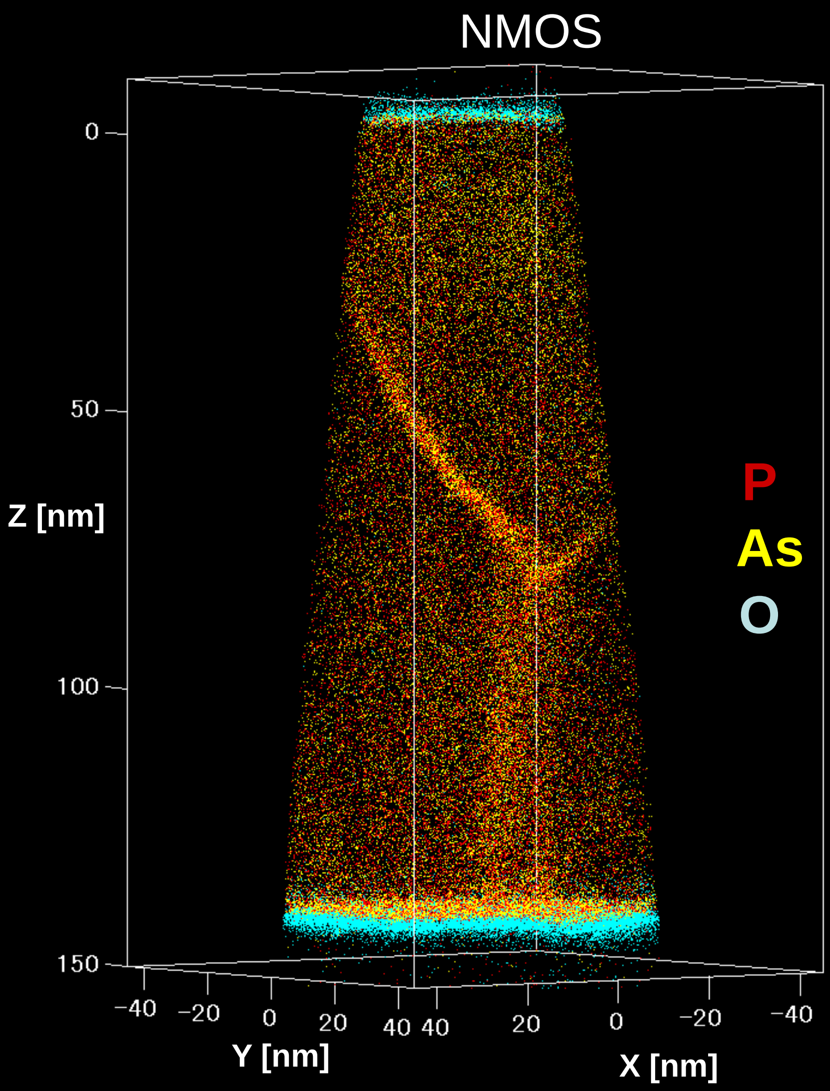

K. Inoue, F. Yano, A. Nishida et. al., Appl. Phys. Lett. 95 (2009) 043502.

Grain in the gate observed by TEM

- Dopant distribution in NMOS and PMOS gate is different.
  →TEM observation

TEM image

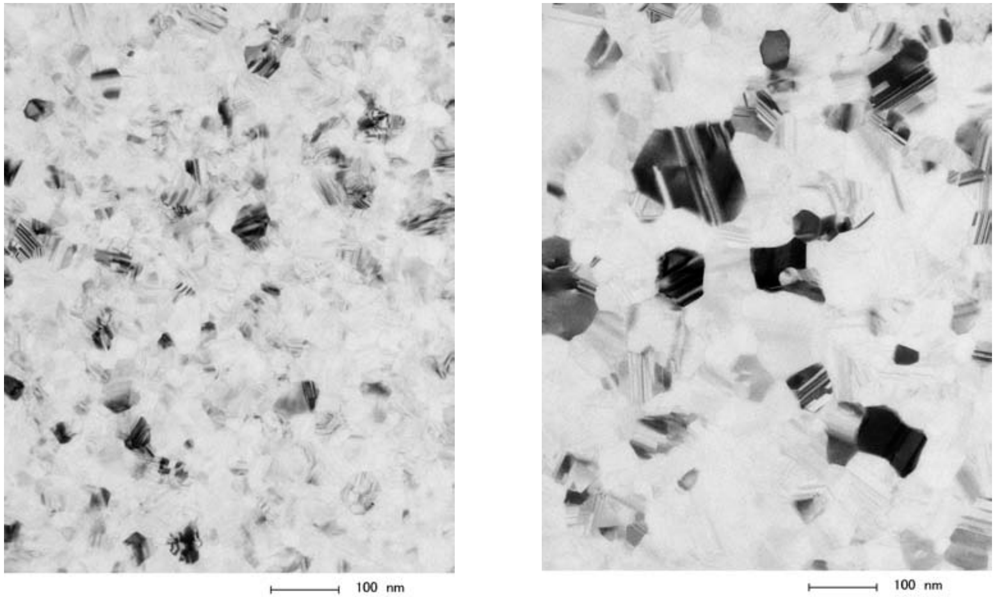

PMOS NMOS

Grain-size distribution

PMOS < NMOS

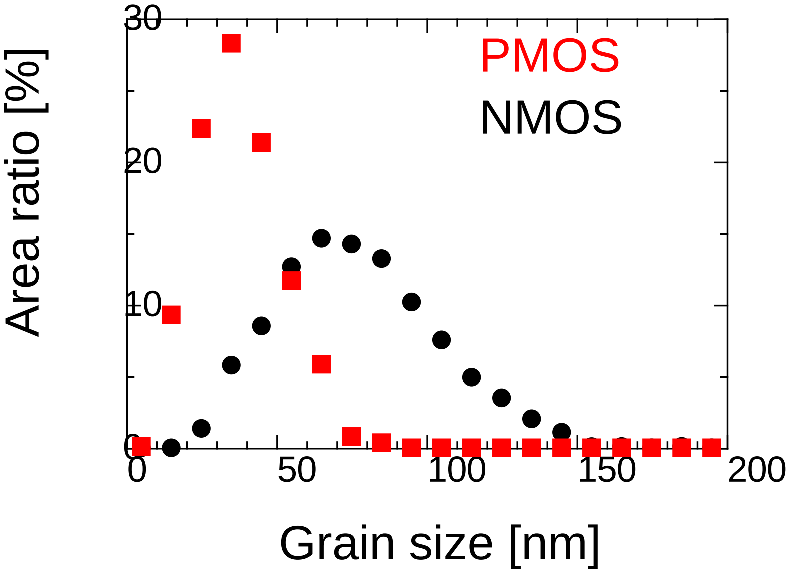

Comparison of dopant distribution in gate

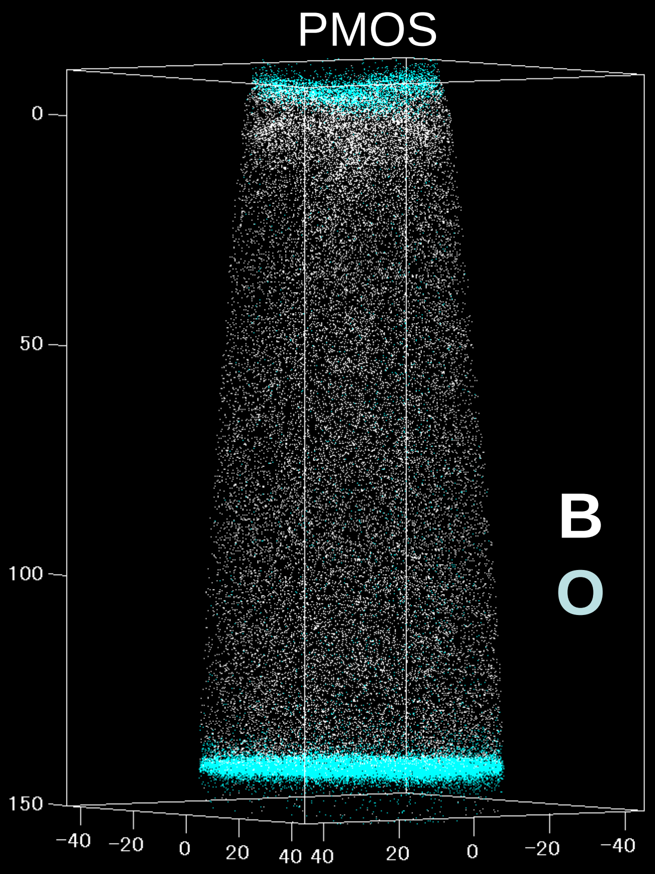
PMOS

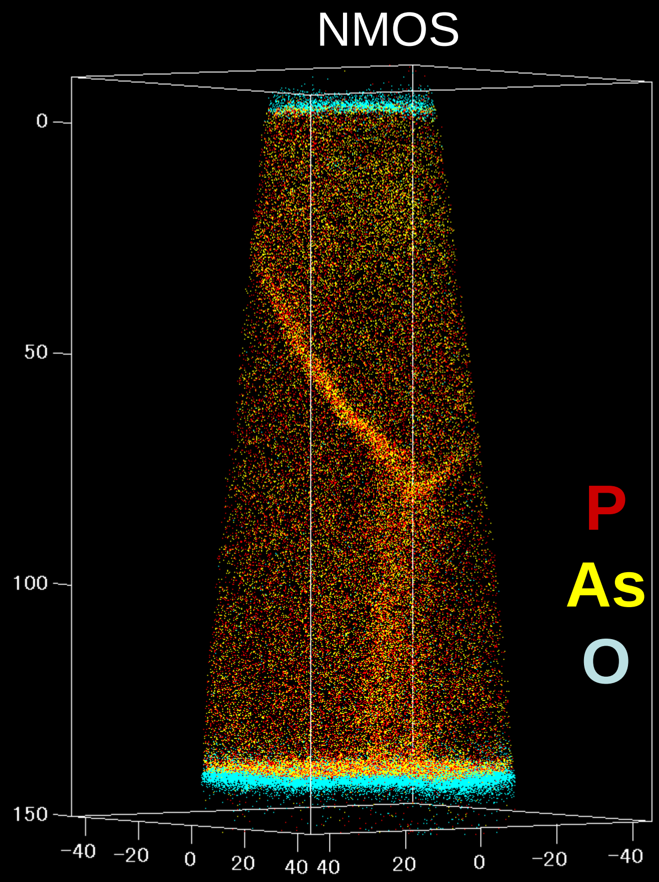
NMOS

- PMOS: clear segregations of B on the grain boundaries in the poly-Si gate are not observed. (B atoms hardly segregate at the grain boundaries)
- NMOS: Segregations of P and As on the grain boundaries in the poly-Si

Enlarged views around the gate oxides

PMOS

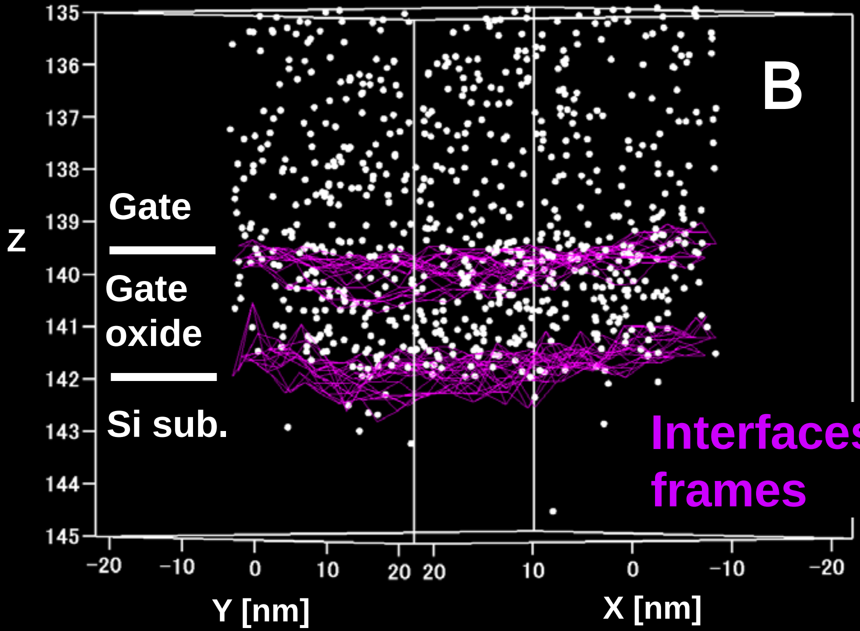

NMOS

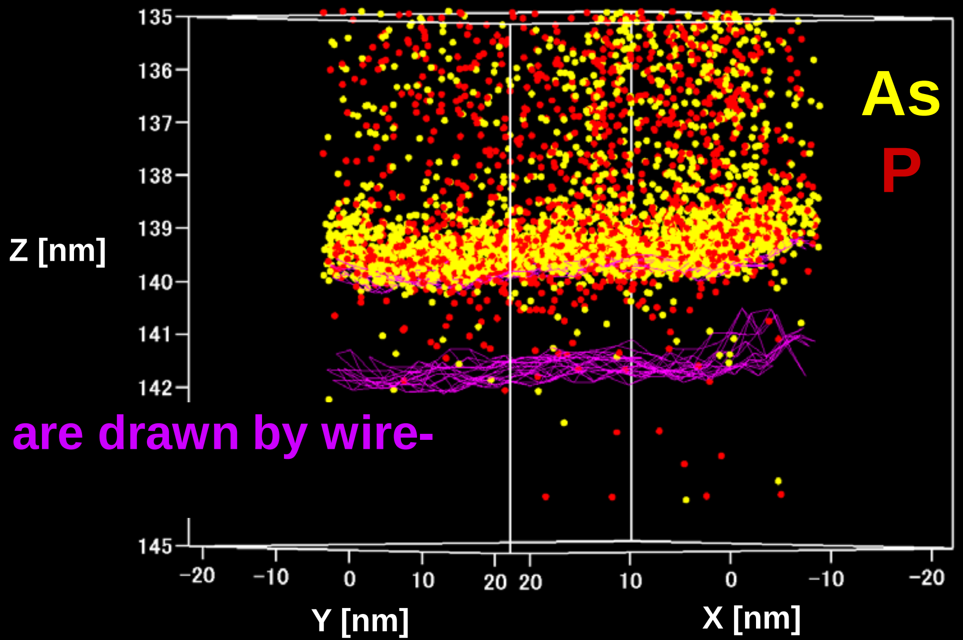

Interfaces are drawn by wire-frames

B

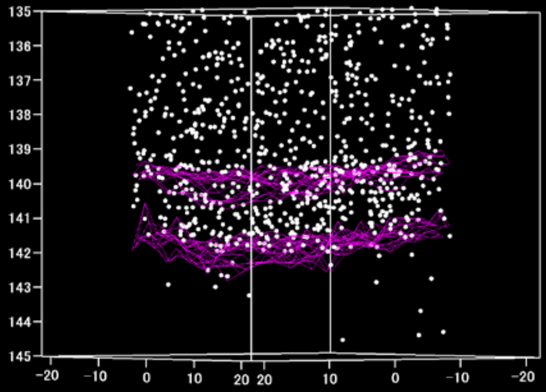

P

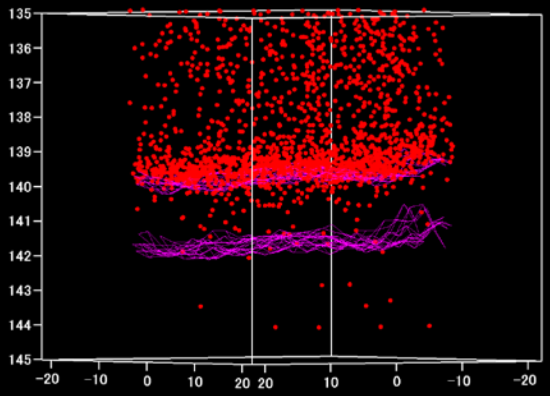

As

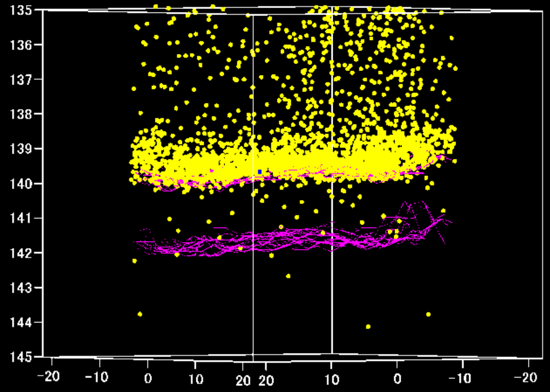

As Segregation on the dislocation? In Poly Si

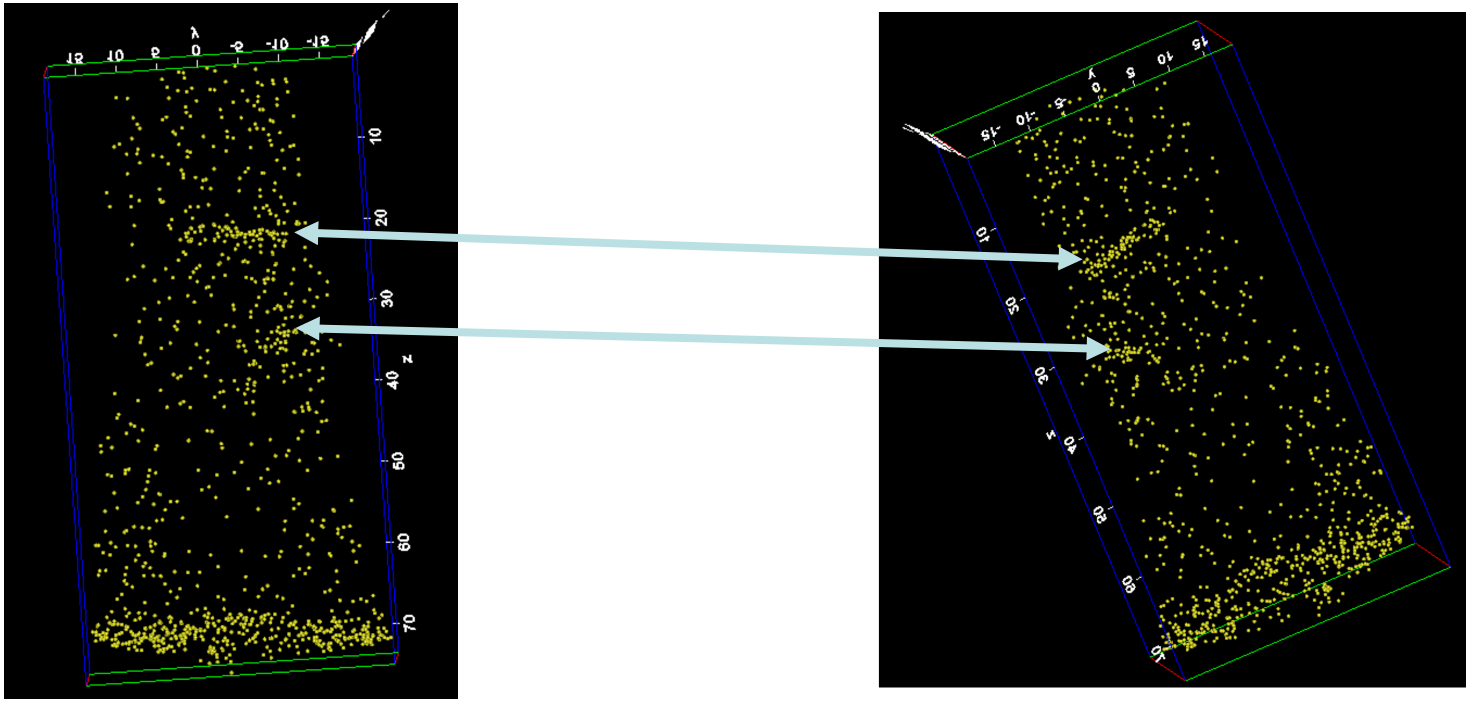

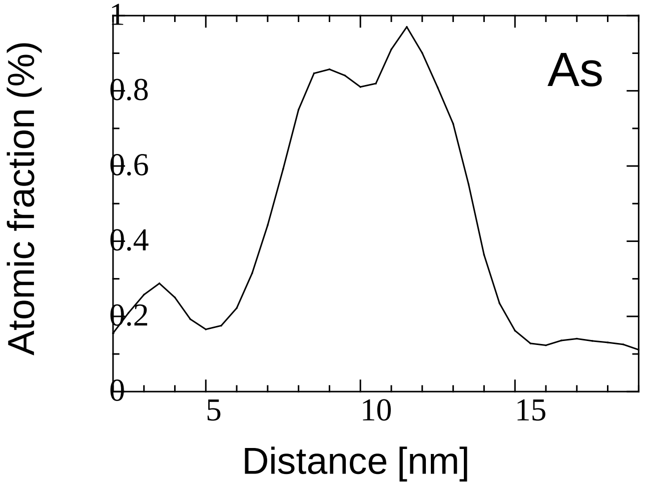

nonuniform dopant distribution in large grain

P

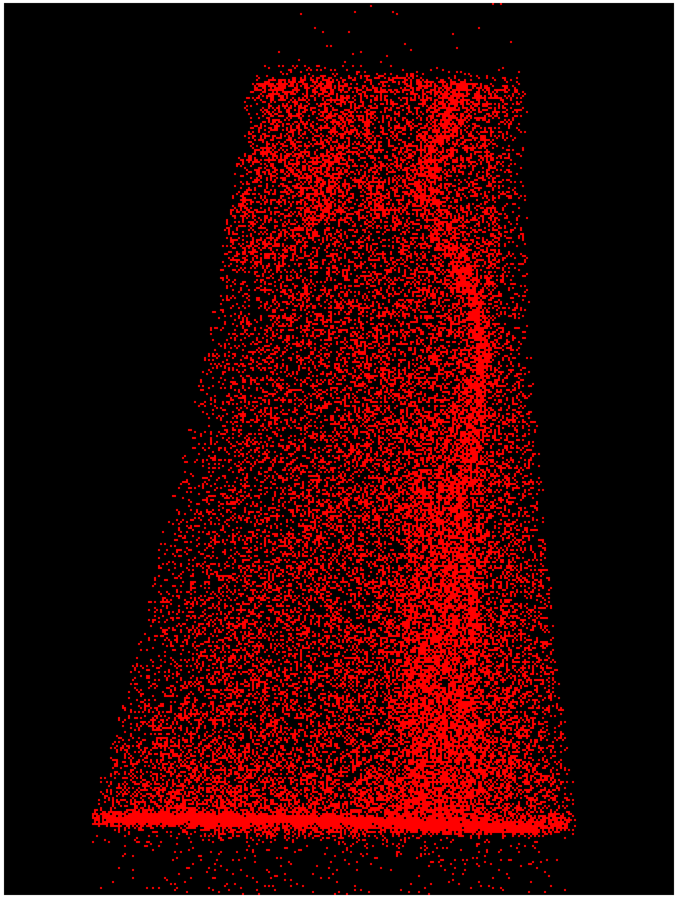

As

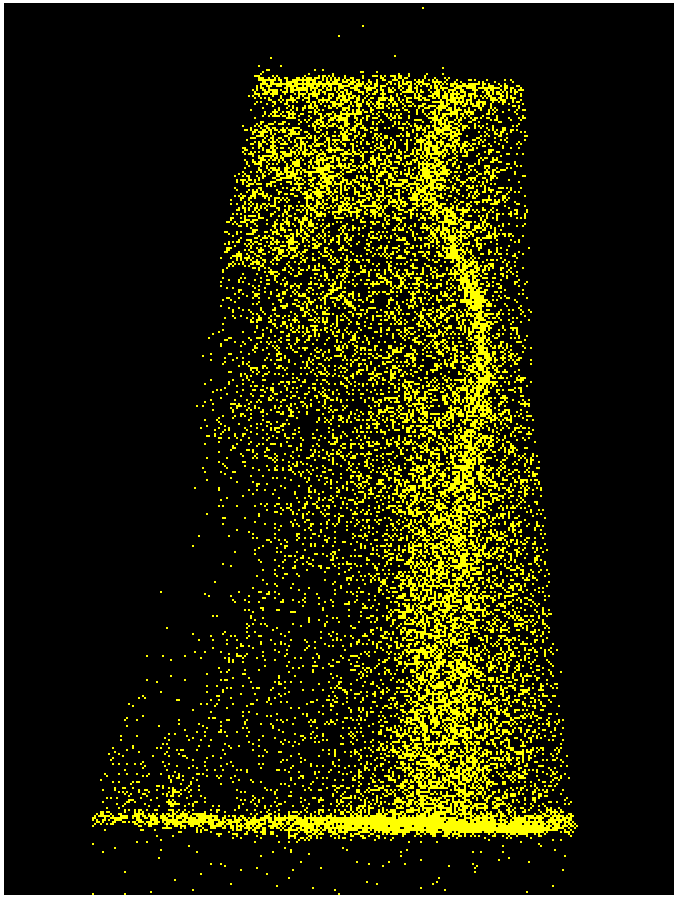

Installed Base (3DAP, LEAP & LA-WATAP)

NA: NWU (Chicago), **ORNL**, UNT (Denton), Sandia, UoA (Tuscaloosa), ISU (Ames), IBM (East Fishkill), PNNL (Richland), UCSB (Santa Barbara), INL (Idaho National Lab)

Europe: **Oxford**, QUB (Belfast), Chalmers, IM2NP (Marseille), **Leoben**, CNT (Dresden), MPI(Dusseldorf), Cameca (Paris), GPM

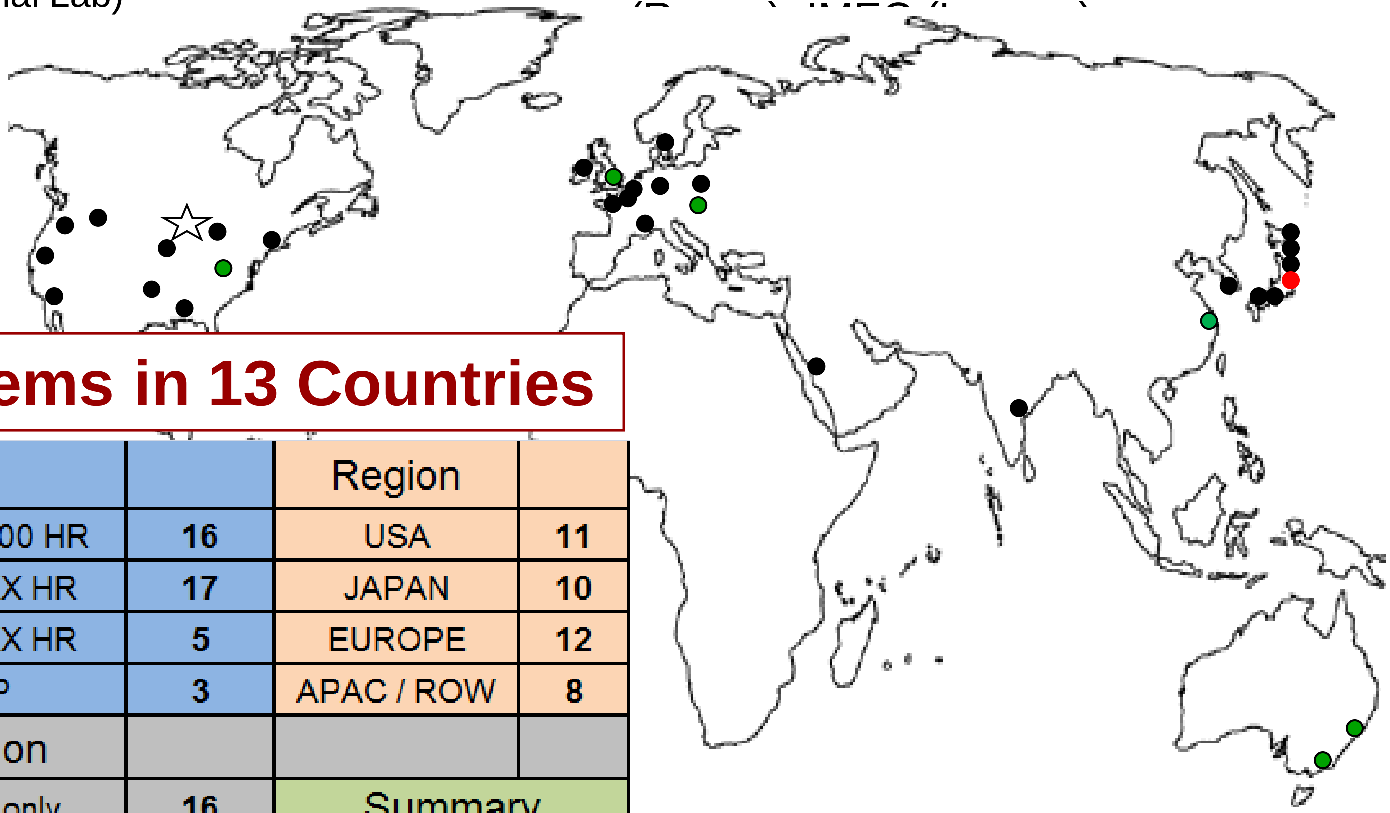

41 Systems in 13 Countries

Product		Region	
3DAP/ 3000/ 3000 HR	16	USA	11
3000X Si/ 3000X HR	17	JAPAN	10
4000X Si/ 4000X HR	5	EUROPE	12
LA-WATAP	3	APAC / ROW	8
Configuration			
Voltage-Mode only	16	Summary	
Laser & Voltage Mode	25	Total	41

Data Key:

Region: ● 1 system, ● **2 systems**, ● **3 systems**
☆ Cameca Instruments Inc. Factory, Madison

Japan: **CRIEPI**, NIMS, TNA, Tohoku (Oari), TITECH, KEPCO/ INSS

APAC/ ROW: **Sydney**, **SHU (Shanghai)**, DMRL (Hyderabad), **Monash,** KAUST (Saudi Arabia), NCNT (Korea)

3D atom map of another needle specimen which includes the edge of the source/drain extension nearly in the center of the needle specimen.

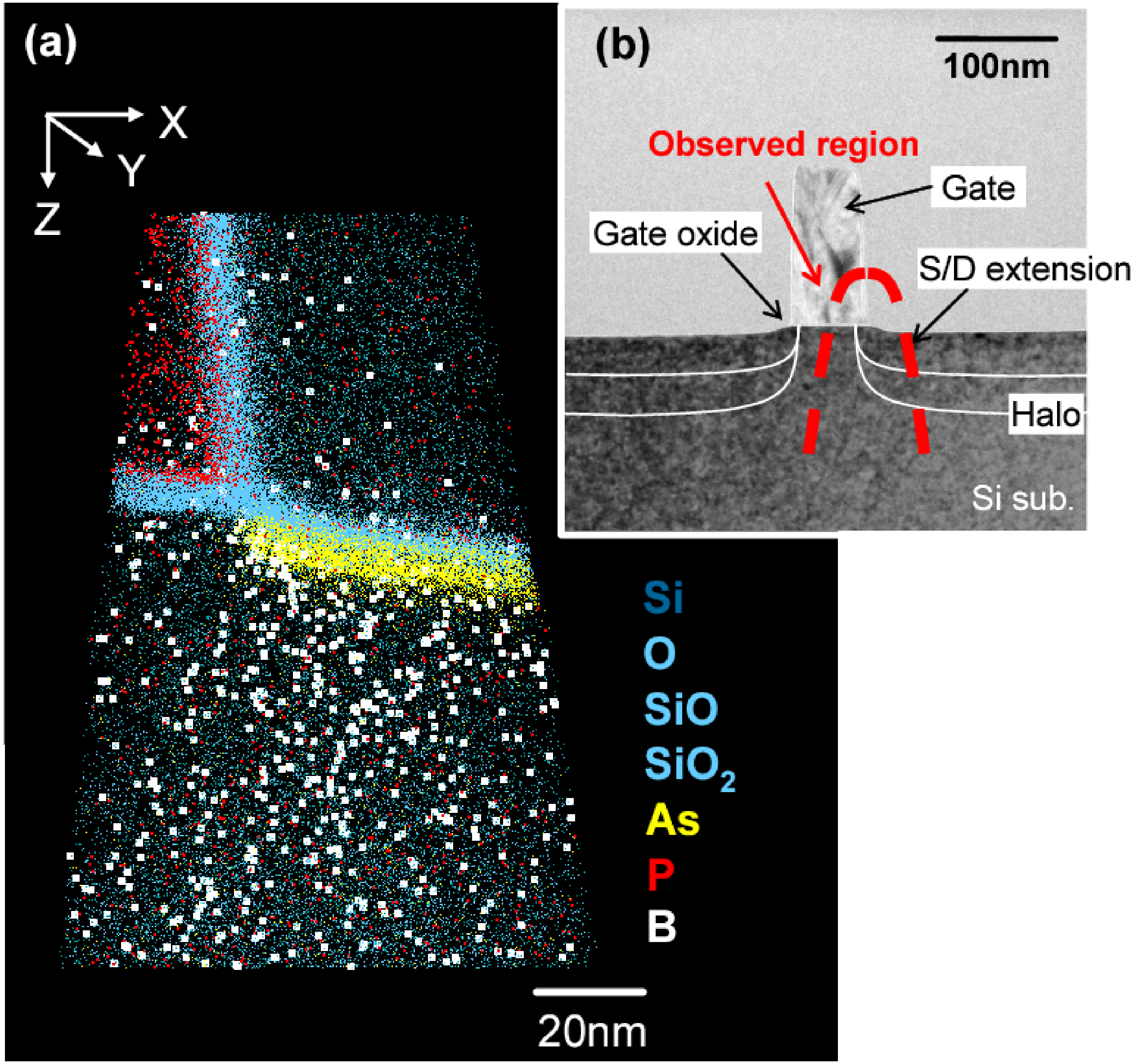

Atom map

gate structure (high-k) analysis

Region: Φ15nm×50nm

All elements

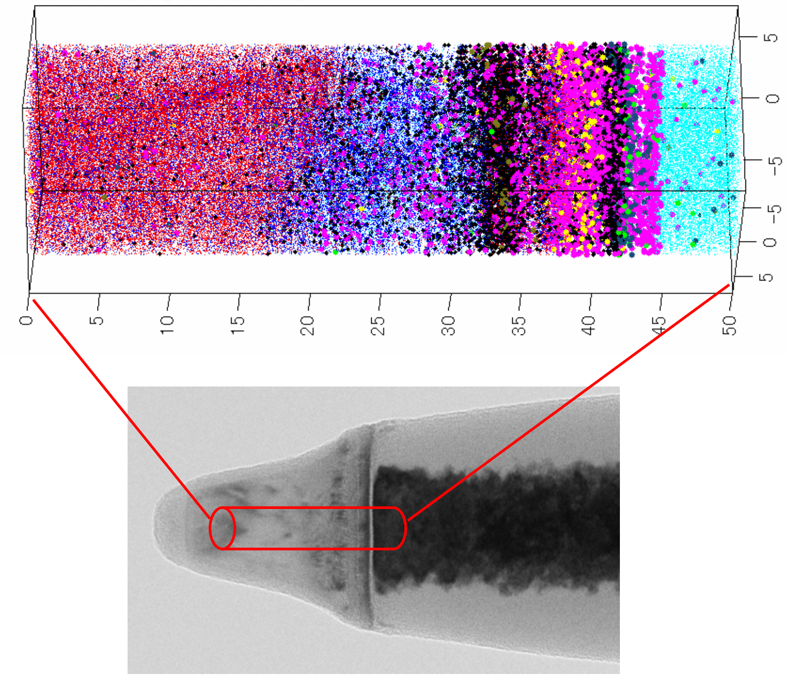

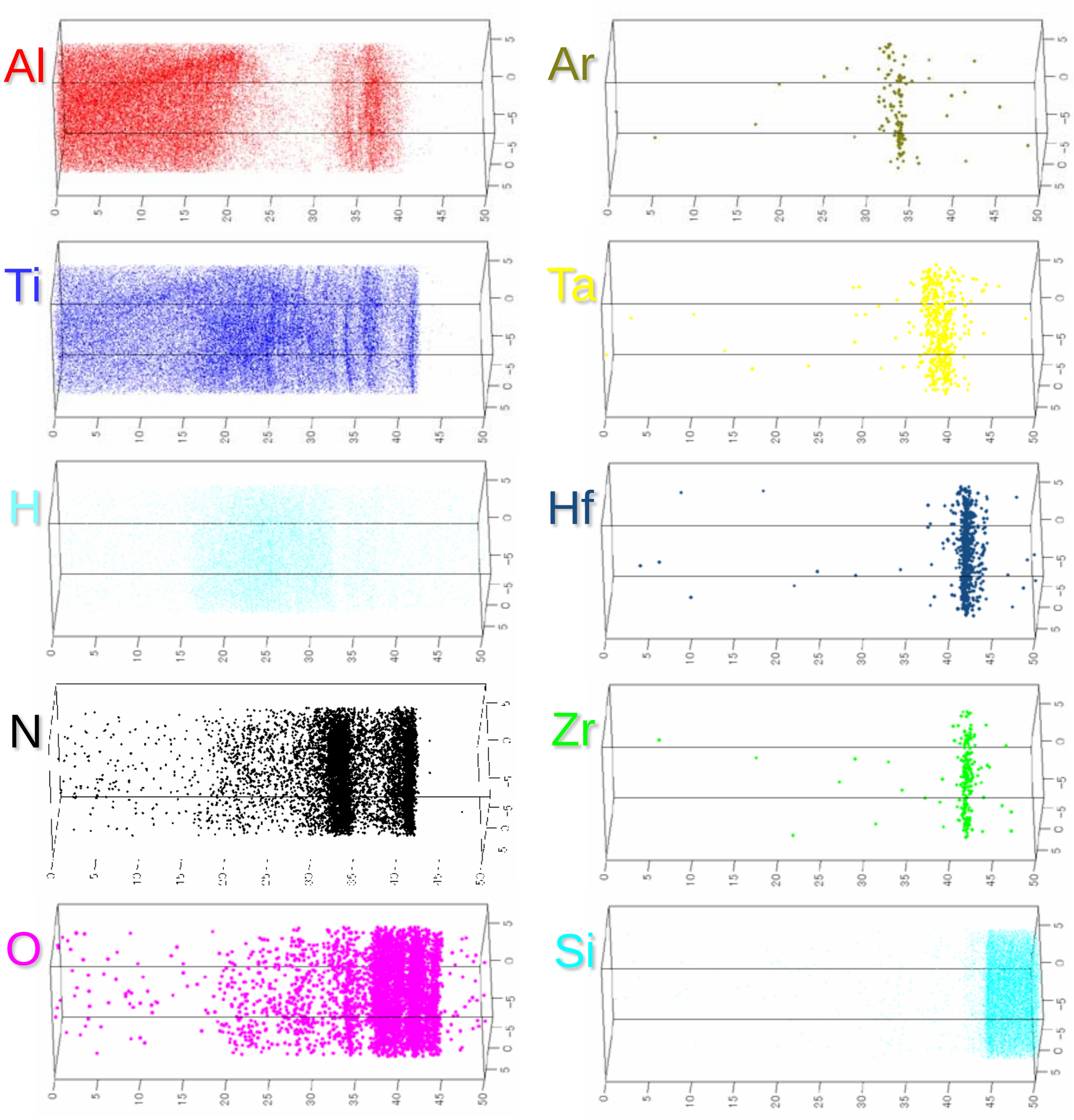

Scaling

2005年 ITRS(国際半導体技術ロードマップ)
2008年 ITRS(国際半導体技術ロードマップ)
2009年 ITRS(国際半導体技術ロードマップ)

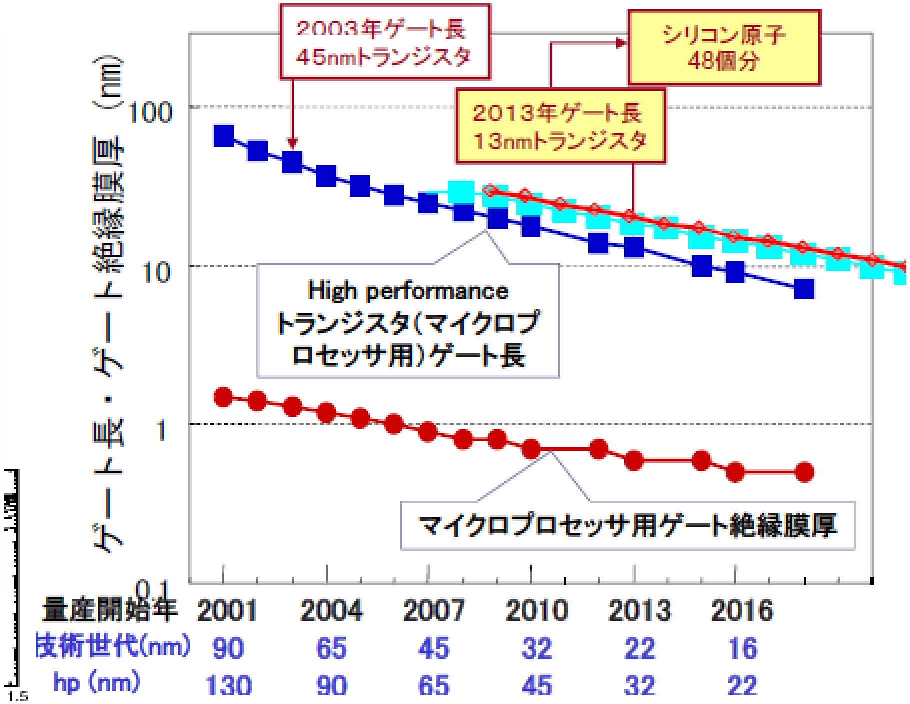

不純物分布の透過電子顕微鏡計測

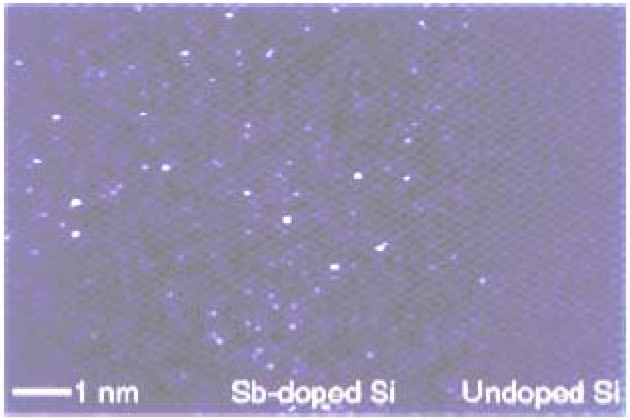

STEM: Sb原子のz contrast

Voyles et al., Nature **416**, 826, (2002)

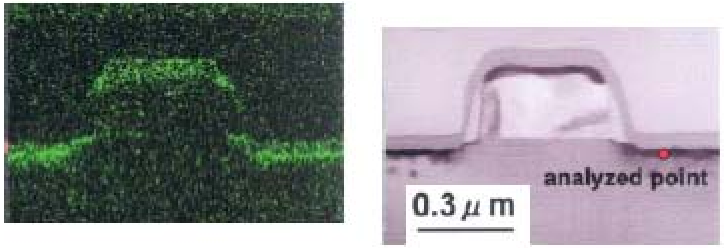

STEM EDX: As K X線

Tsuneta et a.l: J. Electron Microsc. 51 (2002) 167

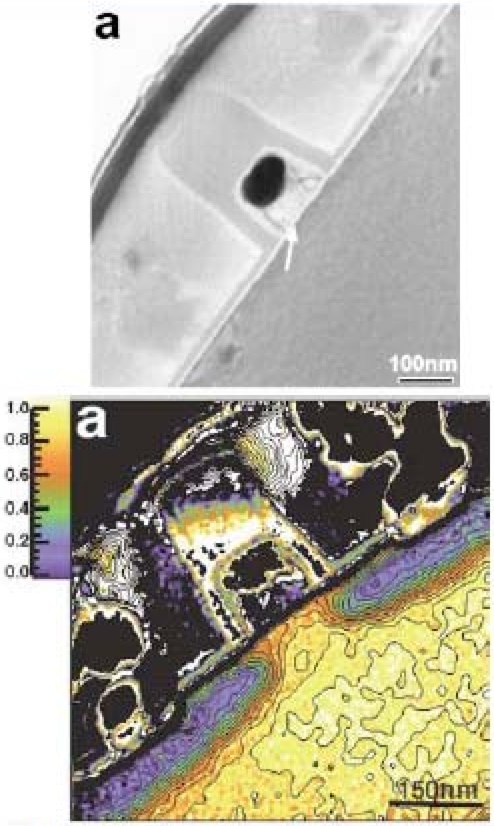

Electron Holography⇒ potential分布

Gribelyuk et al., Phys Rev Lett 89, 025502 (2002)

Laser Pulsing:

extending the capability to more materials

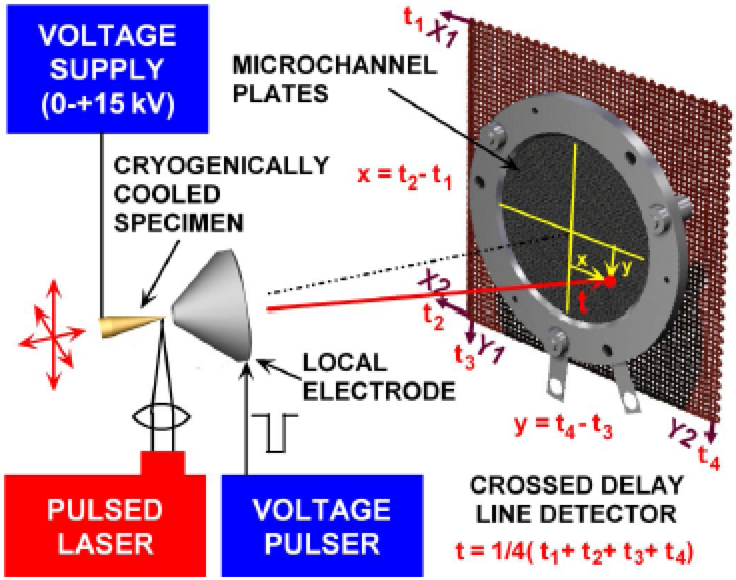

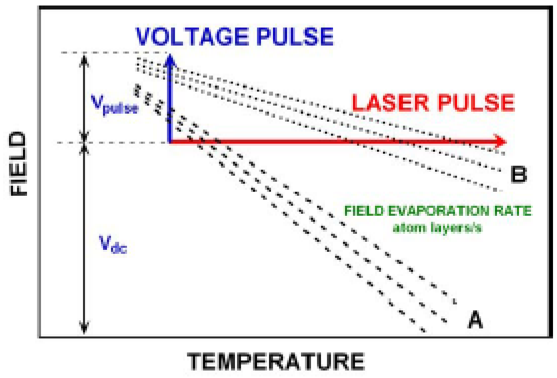

Instead of applying a voltage pulse to field evaporate atoms, a short duration laser pulse is used to momentarily heat the specimen so that field evaporation occurs on the standing voltage.

An additional advantage of laser pulsing is that under the correct experimental conditions, an improvement in the mass resolution may be obtained.

Slide text and figures courtesy of MK Miller, ORNL

Detectability Limits

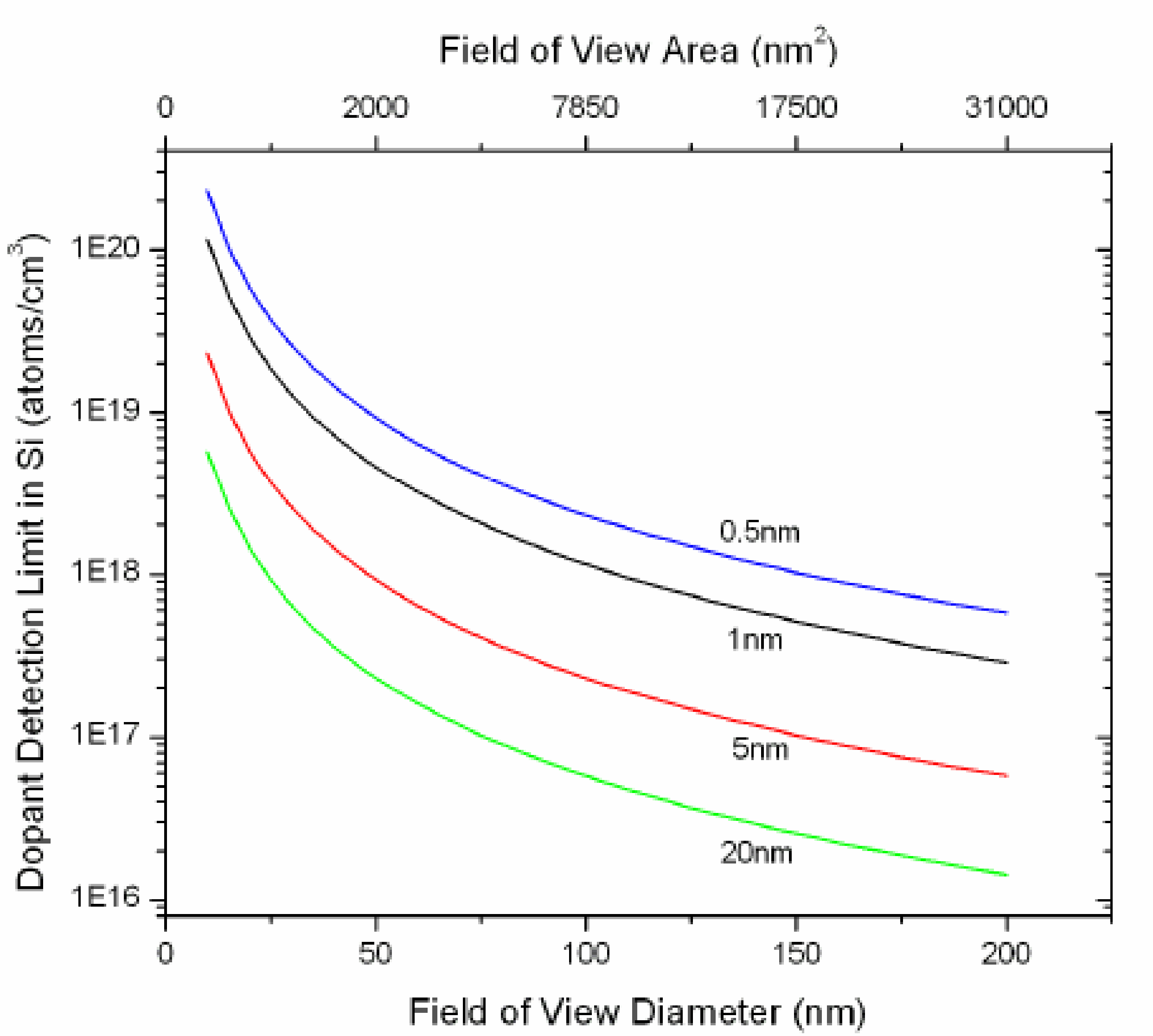

Field evaporation with LASER pulsing

- Rate of evaporation given by Arrhenius relation:

$$\exp\left(-\frac{Q_n}{kT}\right)$$

- Field required for constant evaporation rate depends on temperature
- Get ~10% enhancement per 200K temperature rise for tungsten
- Rate can be increased by raising T or raising Field (decreasing Q_n)

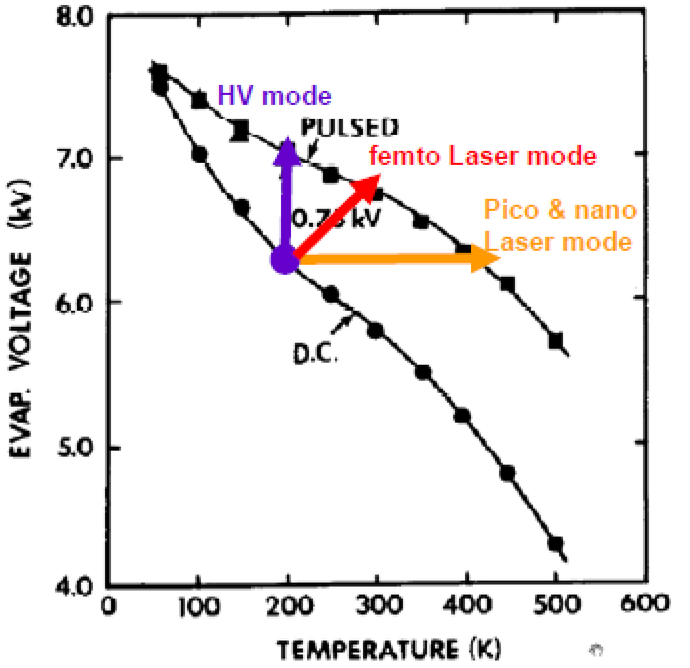

Copied from G.L. Kellogg, *J. Appl. Phys.* 82 (1981) 5320

Nanosecond laser (Tsong, 80s): raising T but prohibitive thermal effects,
Picosecond laser: raising T = Thermal evaporation mode (IMAGO mode),
Femtosecond laser: raising T + raising Field = reduced Heating with Optical Rectification (CAMECA mode)

The red arrow is an visual rendition: the electro-magnetic field induced by the fast light pulse does not increase the potential of the tip surface but decreases the evaporation barrier.

SCIENCE & METROLOGY SOLUTIONS

ゲート領域でＰの濃度分布

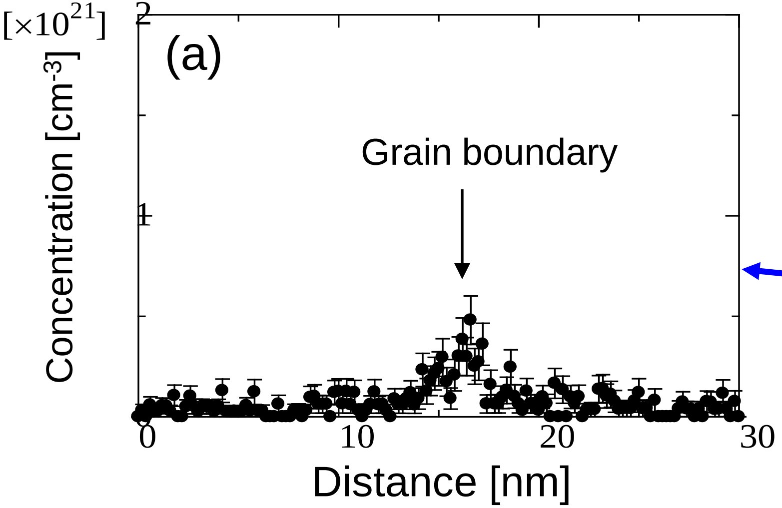

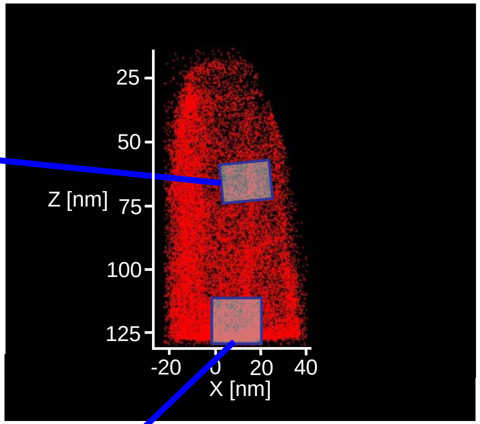

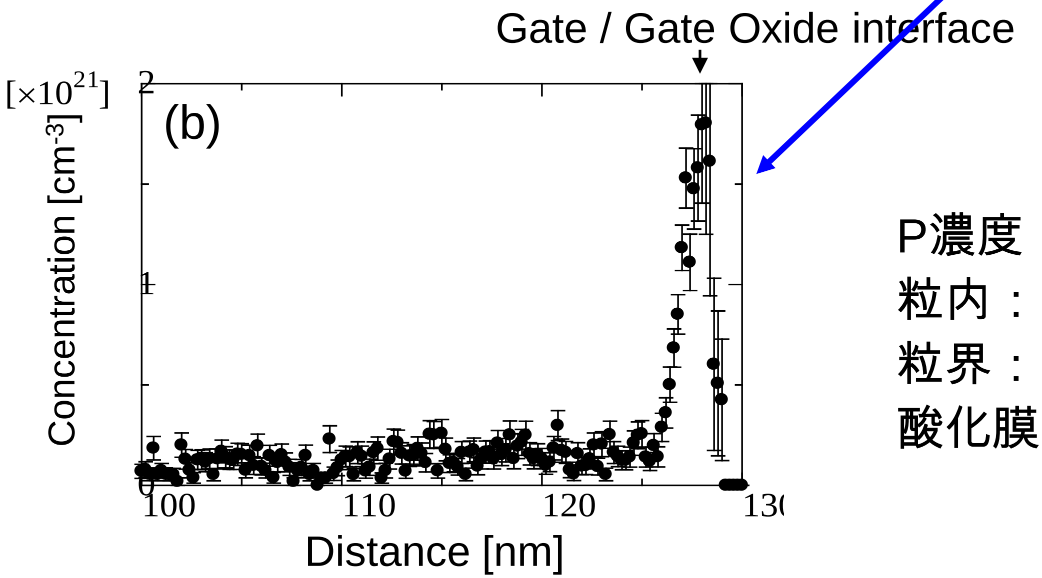

P濃度

粒内：5×10^{19} cm^{-3}

粒界： 5×10^{20} cm^{-3}

酸化膜界面：1.5×10^{21} cm^{-3}

PMOSゲートのBの濃度分布

SDE形成用打ち込み影響

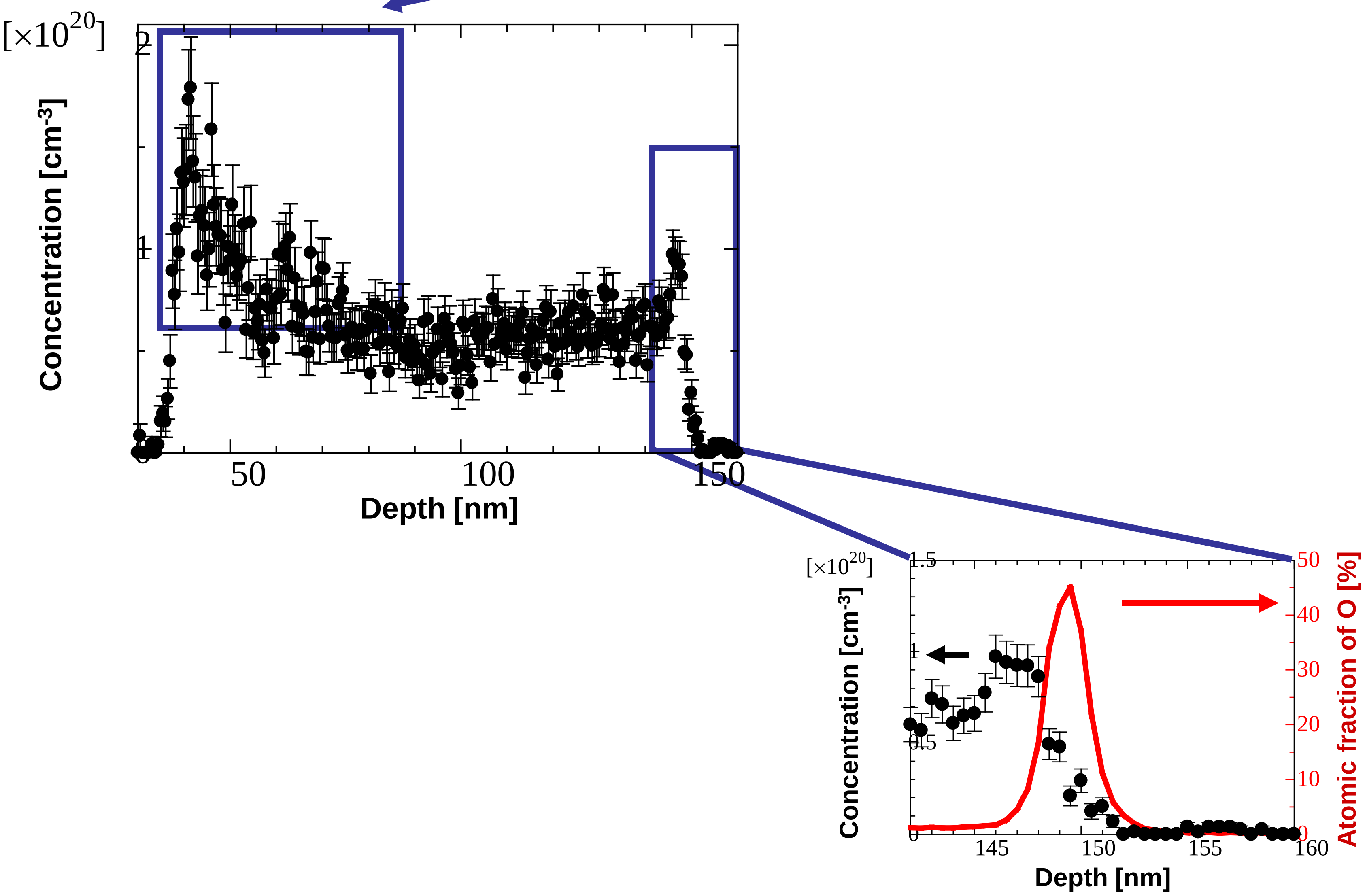

リフレクトロン効果(質量スペクトルの比較)

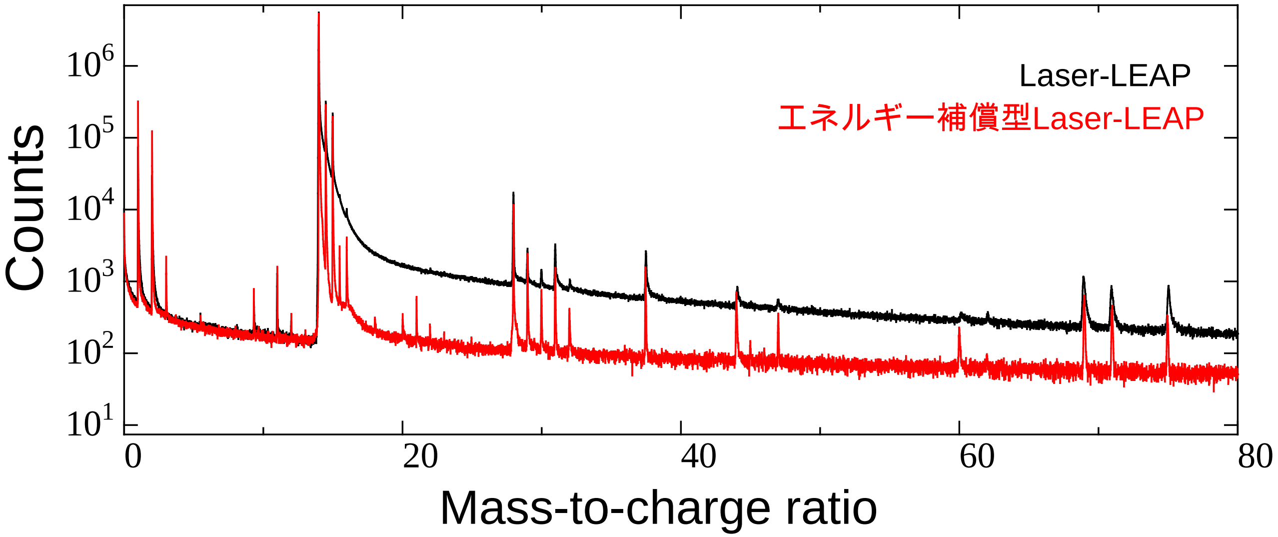

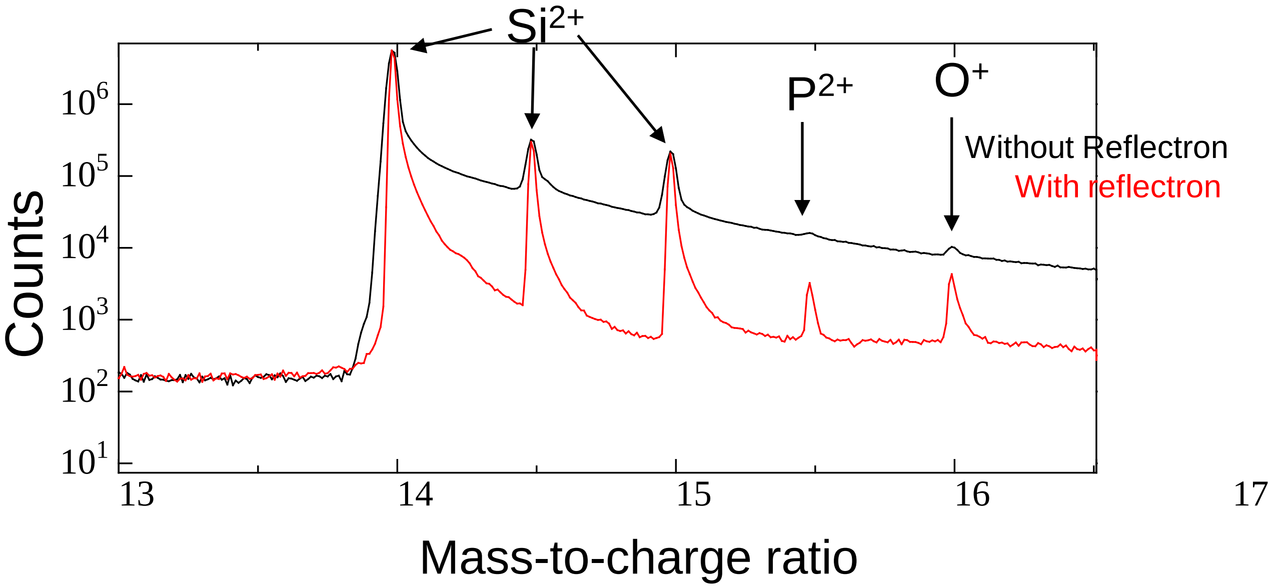

Ultrafast Manipulation of Single Spins in Diamond

G. D. Fuchs
Center for Spintronics and Quantum Computation
University of California, Santa Barbara

Outline:

1. Introduction to diamond NV centers
2. Gigahertz dynamics of a strongly-driven single spin
3. Nanofabrication of single spins in diamond

ITRS workshop: Deterministic Doping
November 12, 2010

Spin: a quantum degree of freedom

Stern-Gerlach experiment: 1922

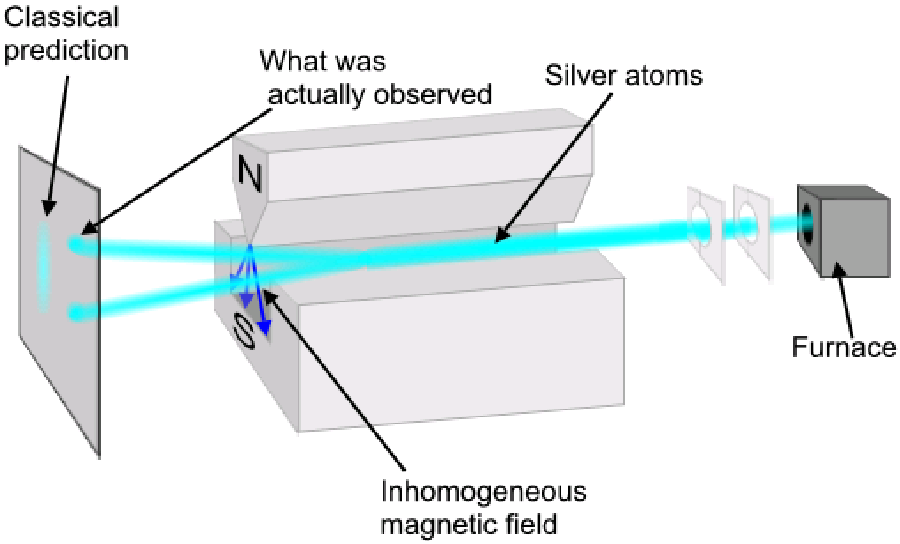

(spin-1/2)

Image credit: http://en.wikipedia.org/wiki/Stern–Gerlach_experiment

- Quantized states: when measured, can be only one or the other
- Coherent superposition is possible

$$|\Psi\rangle = (c_1|\uparrow\rangle + c_2|\downarrow\rangle)$$

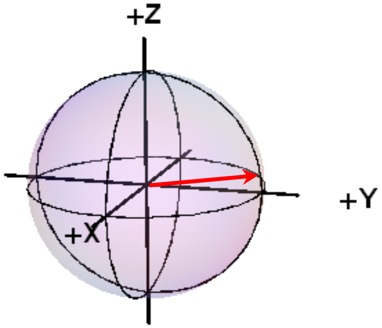

- Repeated preparation & measurement allows you to measure Ψ

Quantum vs. Classical

Quantum	**Classical**
A ‘coordinate’ on a surface	‘ON’ or ‘OFF’
Limited time (T_2)	Unlimited time
Probabilistic information	Definite information

What technology could come from quantum bits?

- Secure communication
- Rapid factoring
- Database searching
- Quantum simulation
- Quantum-limited sensing

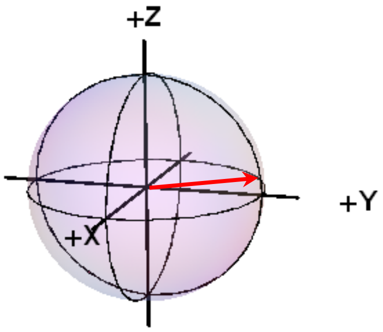

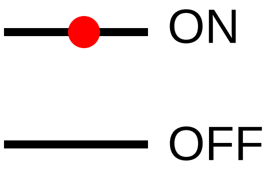

“Wish list” for (any) single quantum system

	Single NV spins in diamond:
• Coherent control, long coherence	Optical initialization and read out, long spin coherence (T_2 ~1 ms)
• Operate under ambient conditions	YES!
• Solid State	YES!
• Coupling to light	Optical transition in the visible
• Engineerable & scalable	High quality synthetic diamond Ion implanting technologies Optical cavities

Properties of the nitrogen-vacancy center

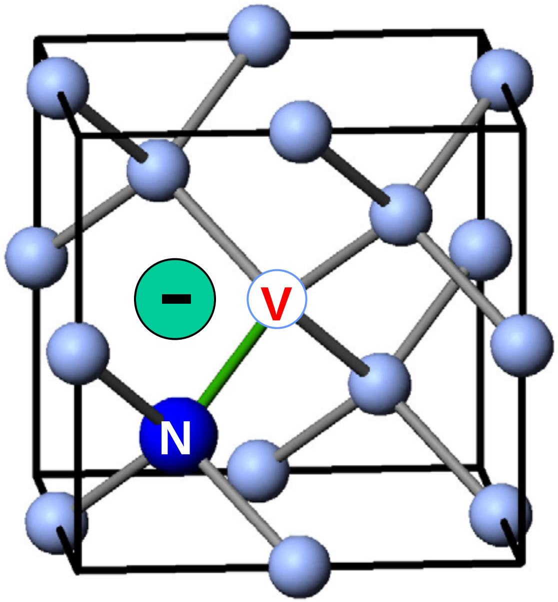

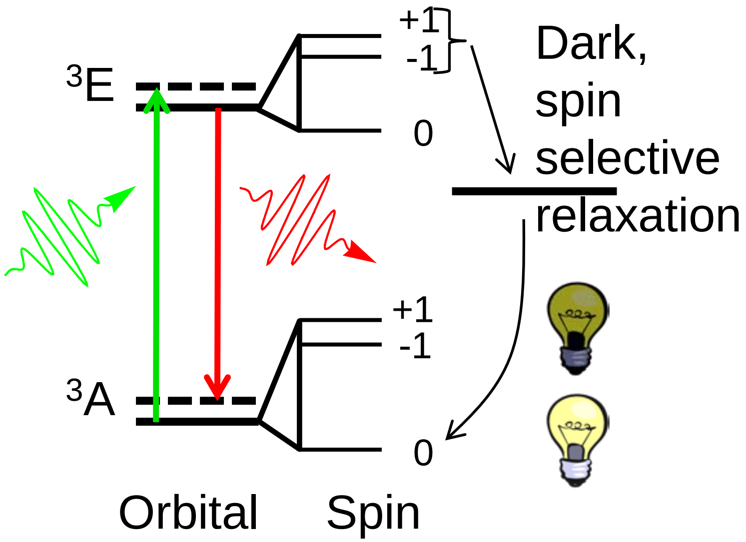

Negatively charged NV center: spin-1

Room temperature operation of a quantum 2-level system:
- Optical pumping into m_s=0 ground state (μK effective temperature)
- Optical spin read-out
- Millisecond duration spin coherence at room temperature is demonstrated

Spin levels of the nitrogen-vacancy center

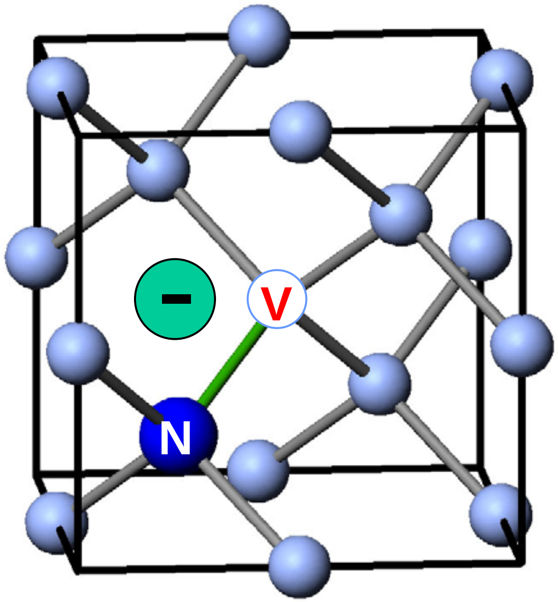

Electronic ground state is a spin triplet, with spin Hamiltonian (z-axis // [111]):

$$H_{NV} = D\, S_z^{\,2} + g\mu_B \mathbf{B}\,\mathbf{S} + \mathbf{S}\,A\,\mathbf{I}$$

Zero-field splitting along symmetry axis
D = 2.87 GHz (~12 μeV)

Hamiltonian is tunable with static magnetic field

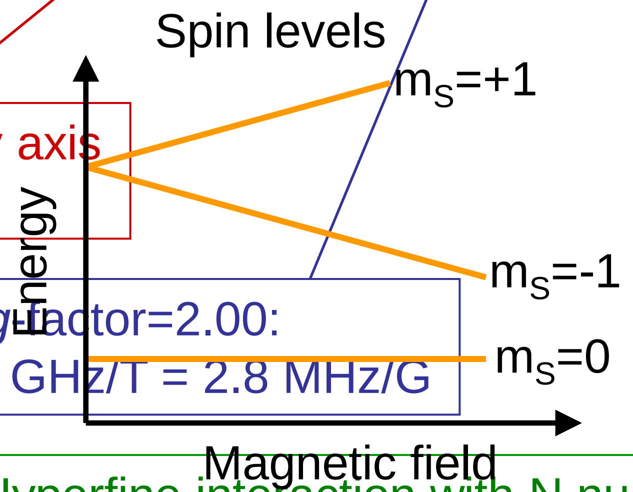

ergy, *g*-factor=2.00:
Zeeman shift ~28 GHz/T = 2.8 MHz/G

Hyperfine interaction with N nuclear spin;
2-3 MHz

G. D. Fuchs: ITRS deterministic doping 2010

Confocal microscopy to image single spins

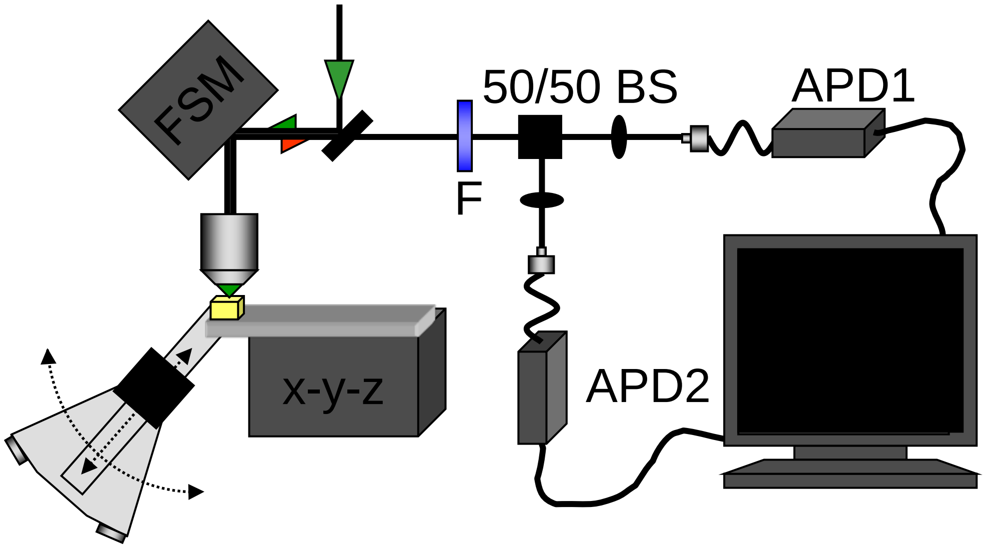

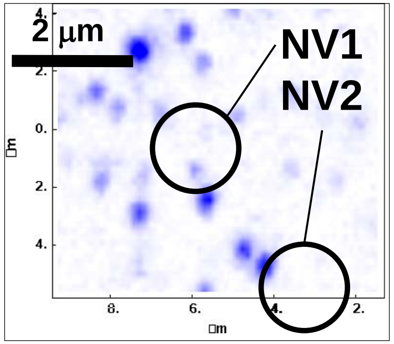

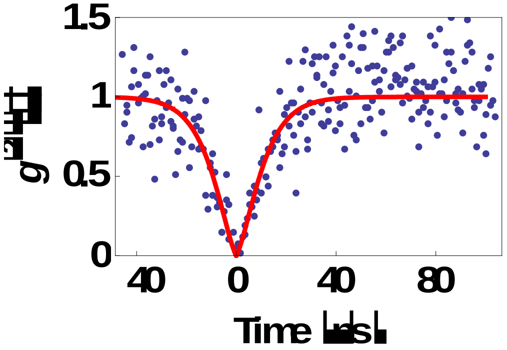

Confocal microscope
- Spatial imaging of single centers and thus *single* spins
- Precise control over angle and amplitude of magnetic field

Hanbury-Brown & Twiss detection of photon correlations
- Detection of single photon emission

Spin resonance: basic idea

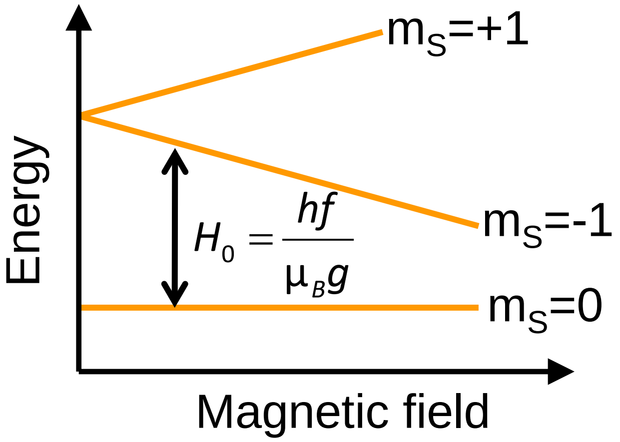

‘Rotating’ field

$$V_{0\to -1} = H_1 e^{i2\pi f t}$$

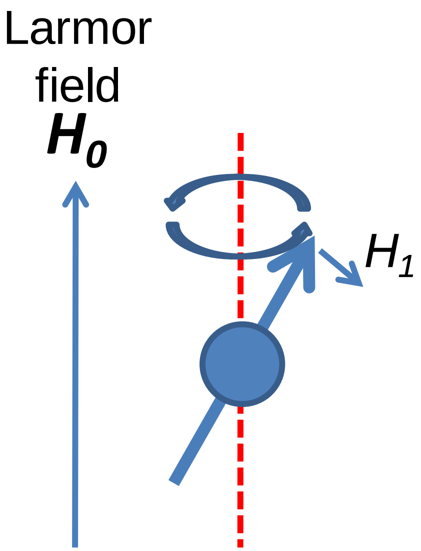

Rabi frequency

$$\Omega_{Rabi} = g\mu_B H_1$$

(on resonance)

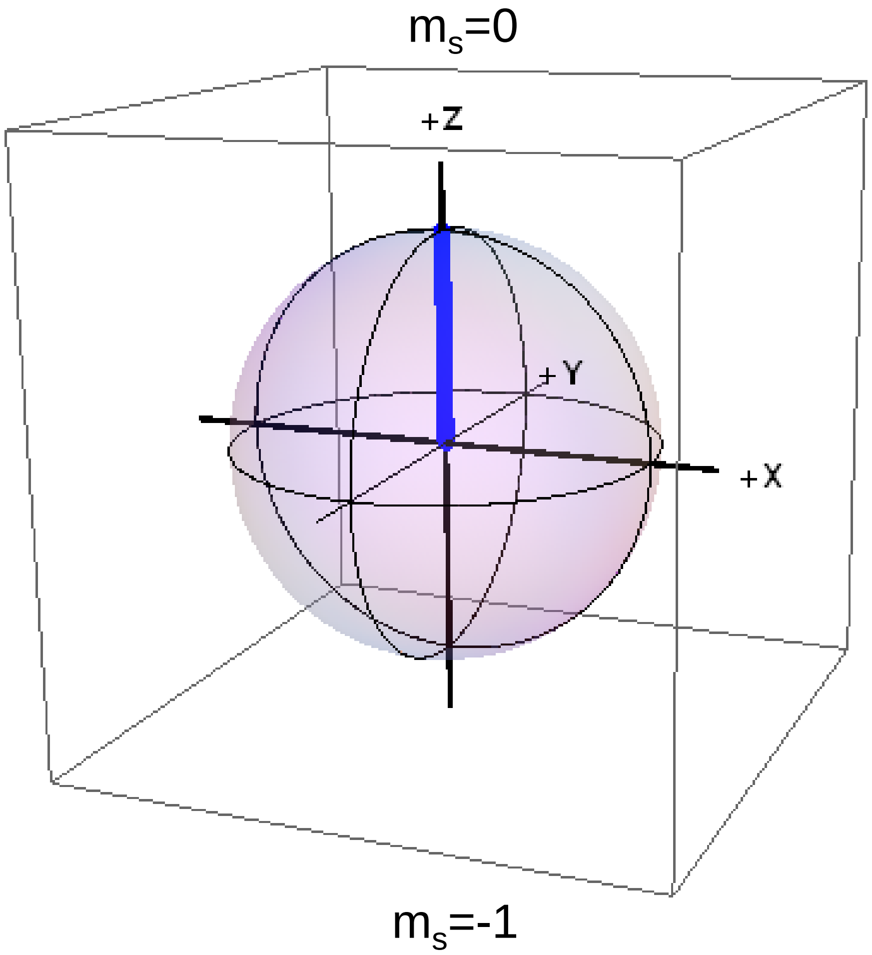

Coherent manipulation or spectroscopy

Measuring spin resonance in the time domain

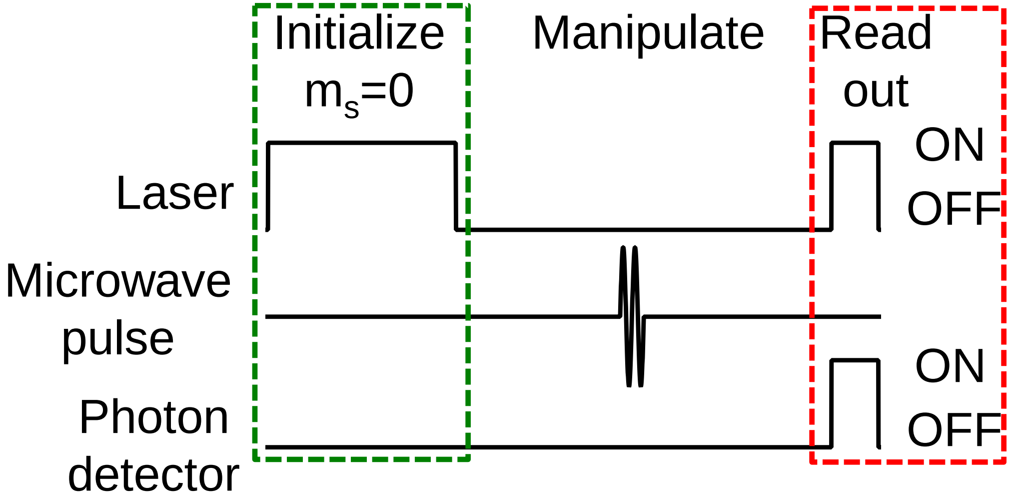

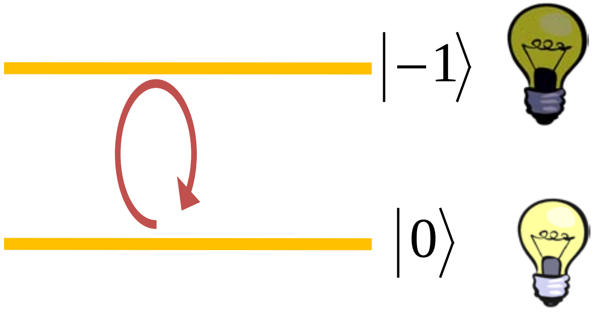

Can only measure final states

Calibration of I_{PL} using adiabatic passage

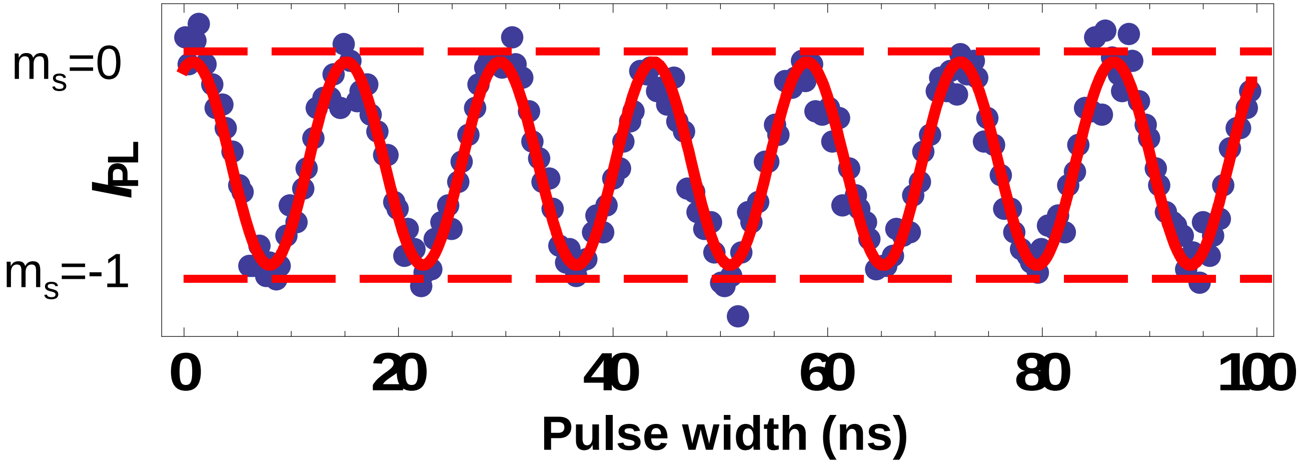

G. D. Fuchs: ITRS deterministic doping 2010

Dynamics of a “strongly-driven” single spin: motivation

Traditional spin resonance:
$H_0 >> H_1$

“Strong-driving” = large $H_1 \sim H_0$
- Fast (GHz) spin manipulations – what is the practical limit?

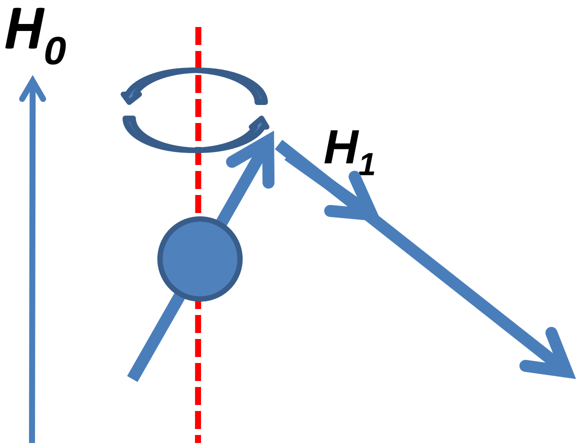

Fundamental physics:
- Different regime of two-level dynamics
- What new behavior can we observe?

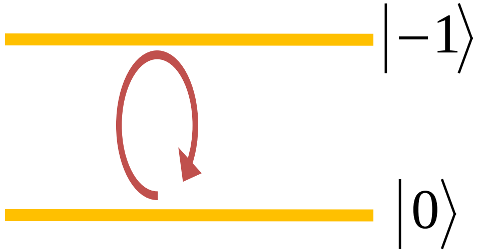

Quantum information: (T_2/t_{flip} is a figure of merit)
- How fast can you manipulate the spin? (time-optimal control theory)
- What is a problem and what can you live with? (this is an experiment)
- Quantum error correction

NV spins are a model 2-level system!

Coplanar waveguide: design and implementation

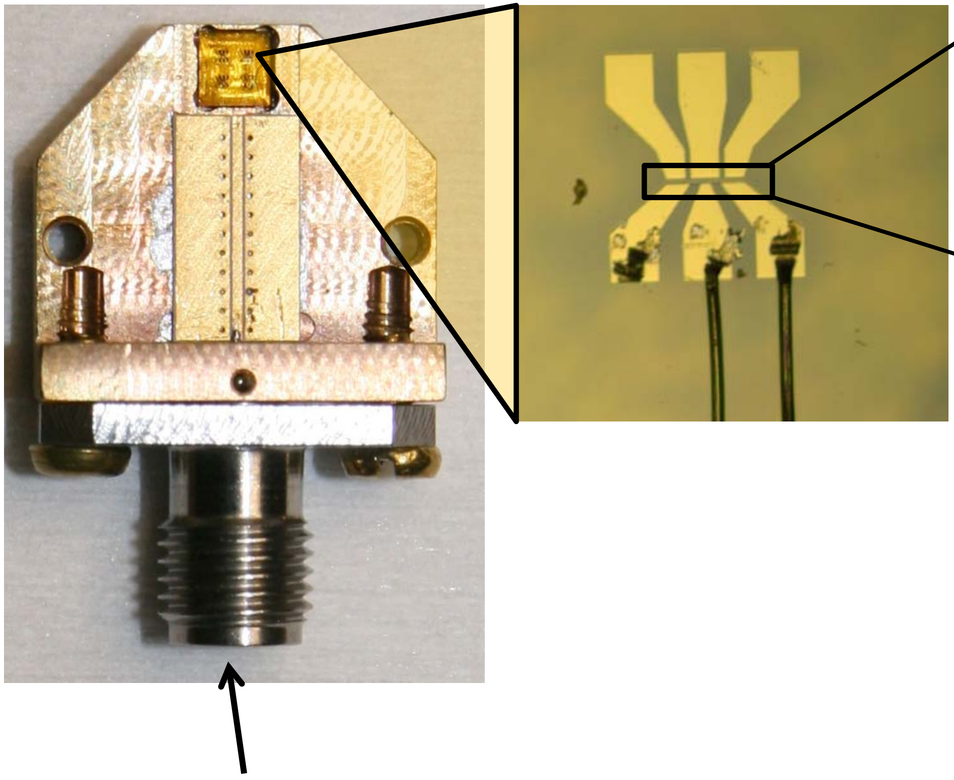

Fits SMA

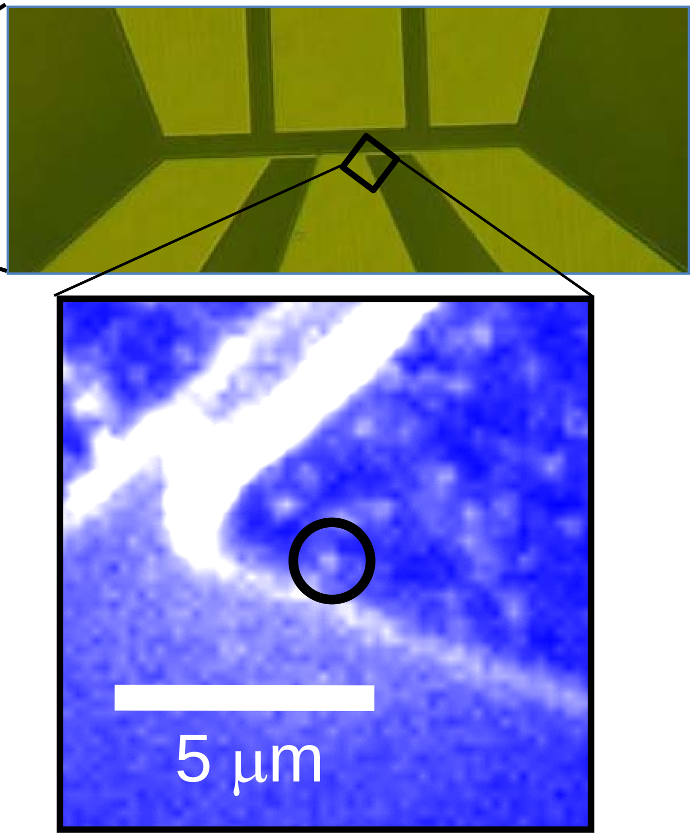

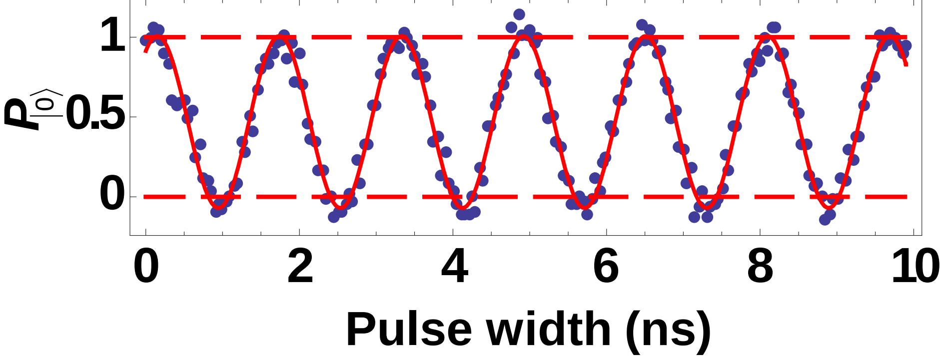

Example: 630 MHz Rabi oscillations
In conventional regime

cy magnetic fields B_{rf}~350 G

G. D. Fuchs *et al*., Science **326**, 1520 (2009)

Pushing the limits: strong-driving dynamics of a single spin

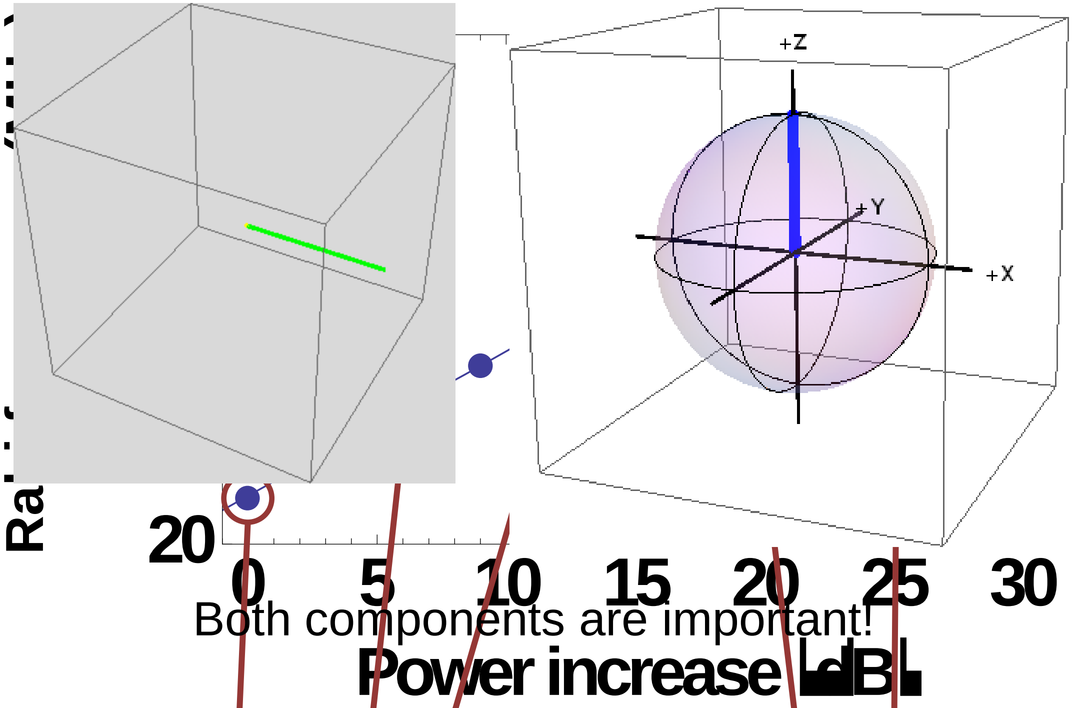

Both components are important!

H_0 is static splitting (0.49 GHz)
H_1 is microwave drive field

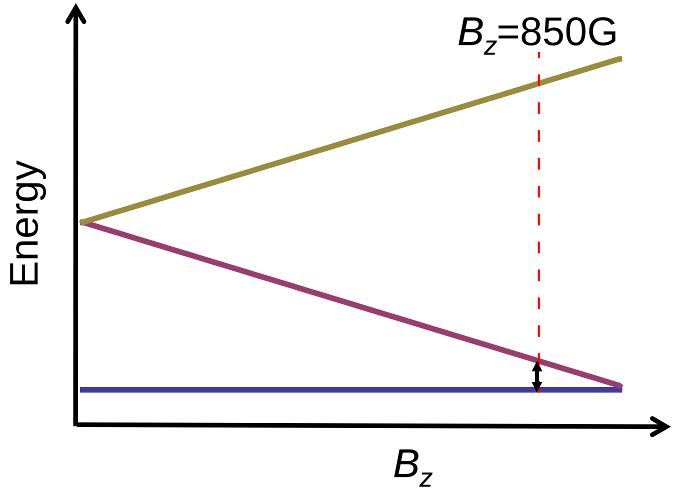

“fast” flips

“stalling”

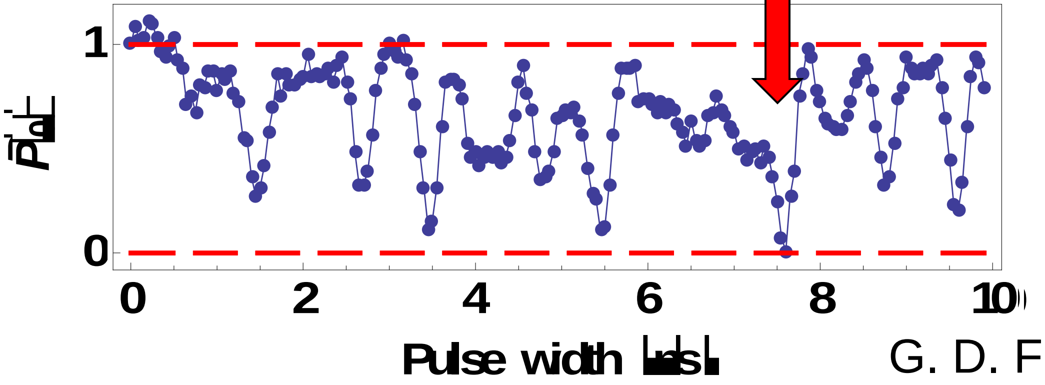

All data is reproducible
(average of ~10^5 measurements)

G. D. Fuchs *et al*., Science **326**, 1520 (2009)

Comparison with simulations

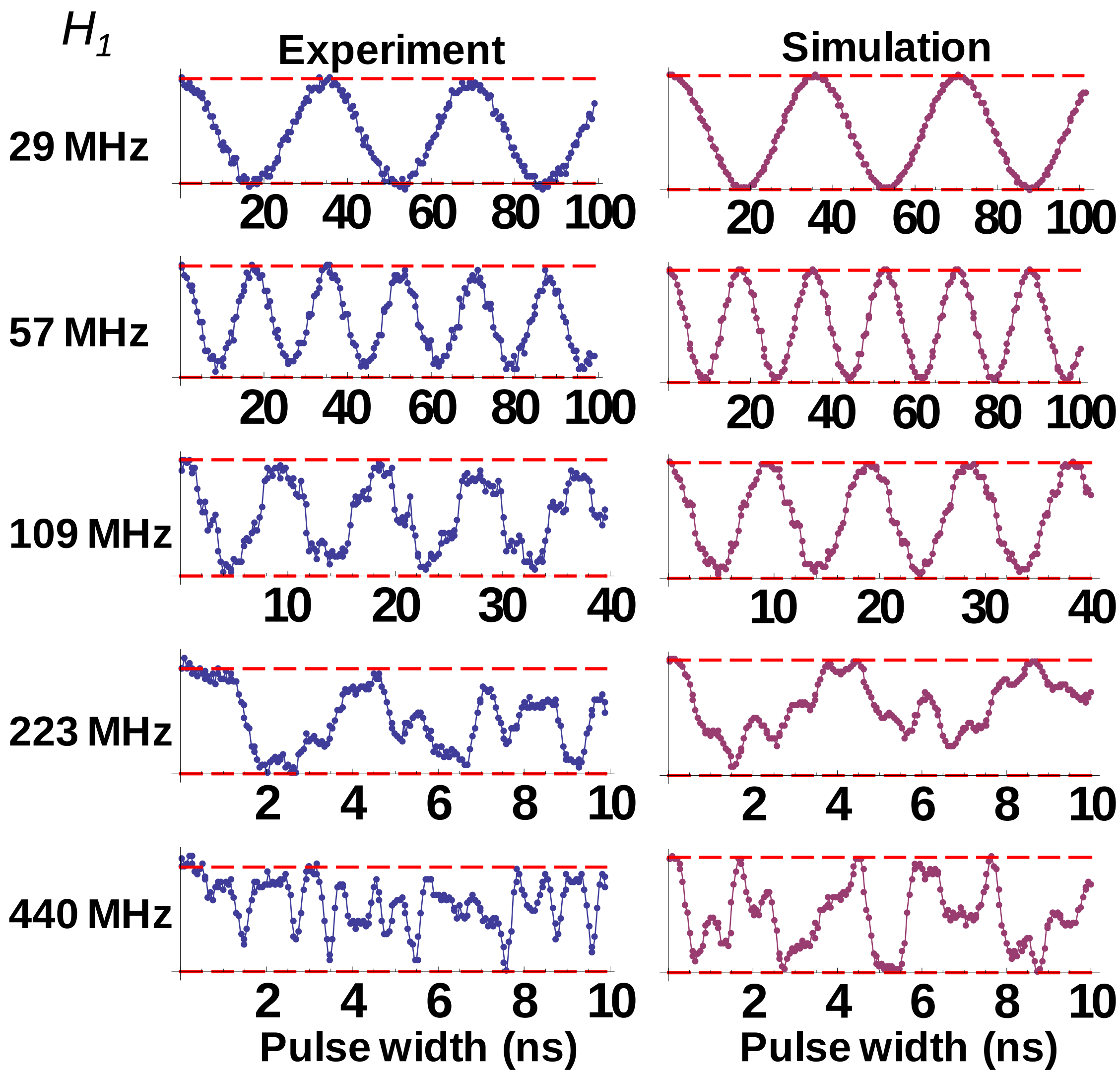

- We measured every pulse in the experiment for the simulation
- No free parameters
- Qualitative agreement
- Extremely sensitive to pulse shape at large H_1 (from theory & experiment)

Gaussian pulses - optimize fast manipulation

Long Gaussian pulses – smooth oscillations

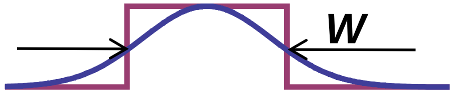

Short Gaussian pulses – fast spin-flips!

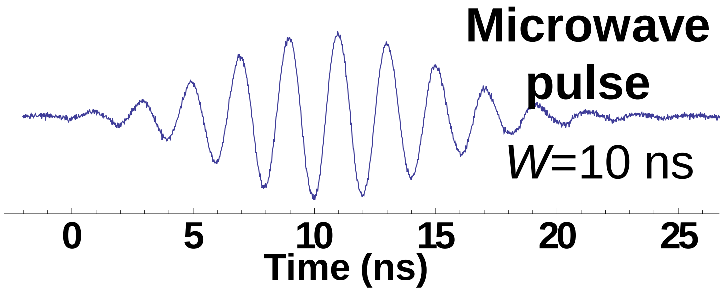

Why is this interesting?

T_{flip} ~ 1 ns

T_2 ~ 1 ms

Coherence/operation ~ 10^6

… > 1 million operations possible!

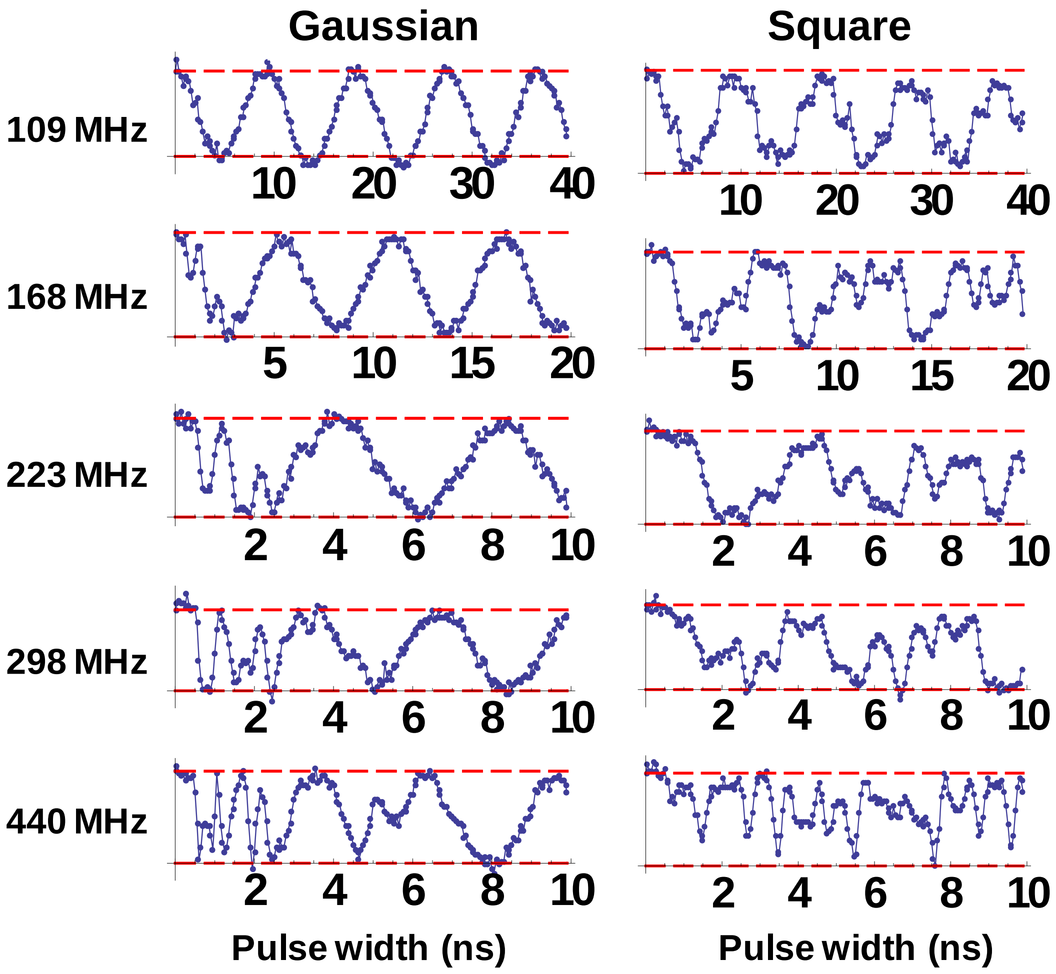

G. D. Fuchs: ITRS deterministic doping 2010

Spatially-controlled ion implantation

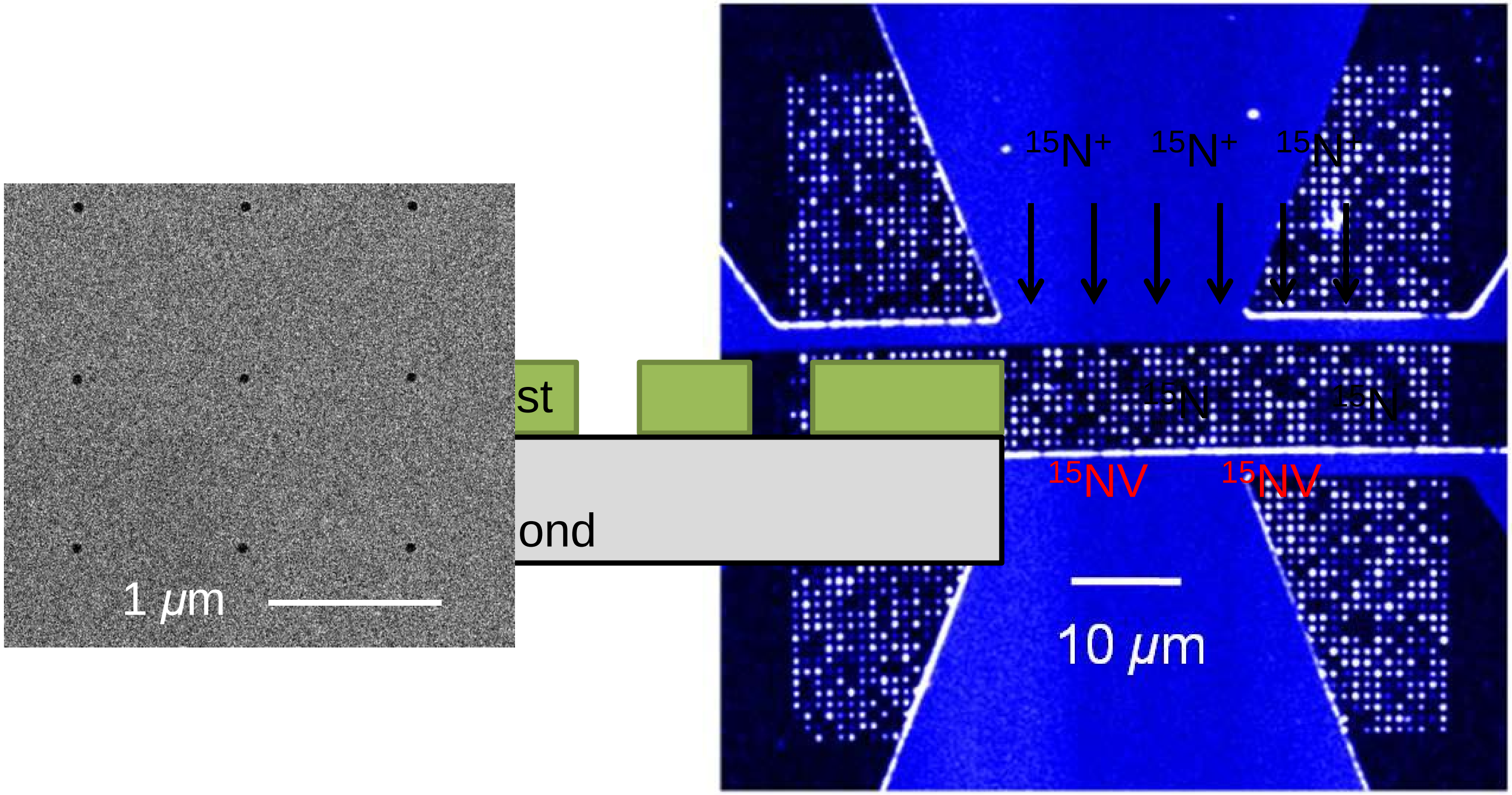

- Mask ion implantation with electron beam lithography resist
- Fabricate single NVs with high throughput
- Scalable to ~10 nm aperture diameters

D. M. Toyli *et al.*, Nano Lett. (2010)

Shallow implanted nitrogen: SIMS studies

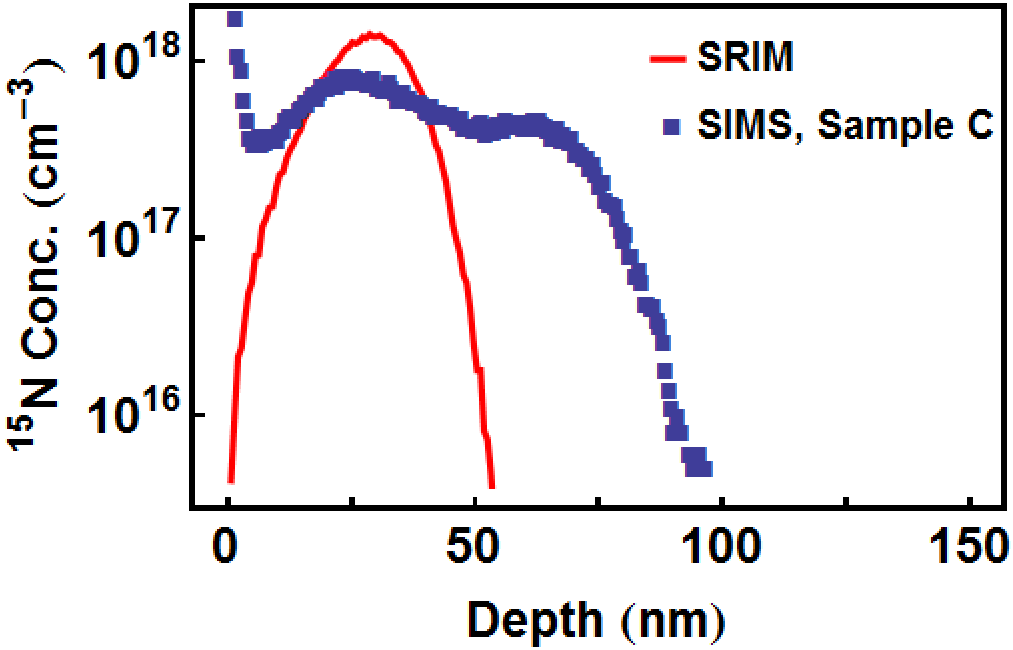

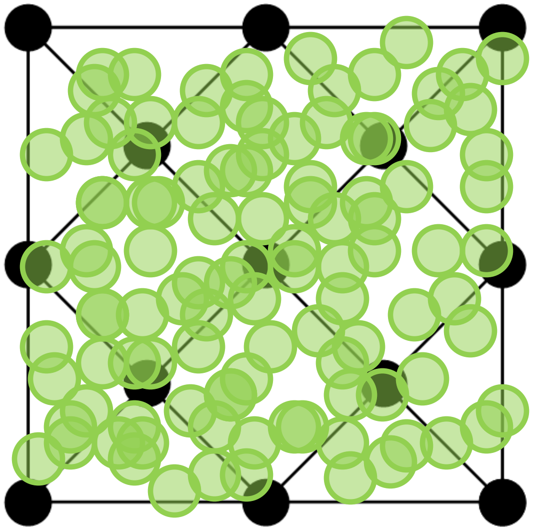

(100)

- SRIM accurate for primary ion peak
- Channeled ions penetrate deeper than expected
- Mitigate channeling with screening oxide

D. M. Toyli in collaboration with
T. Schenkel’s group (LBNL)

Summary and acknowledgements

High-speed coherent manipulation of a single spin

- Sub-nanosecond manipulation
- Faster than expected from conventional approach
- Perform *millions* of operations per coherence time!

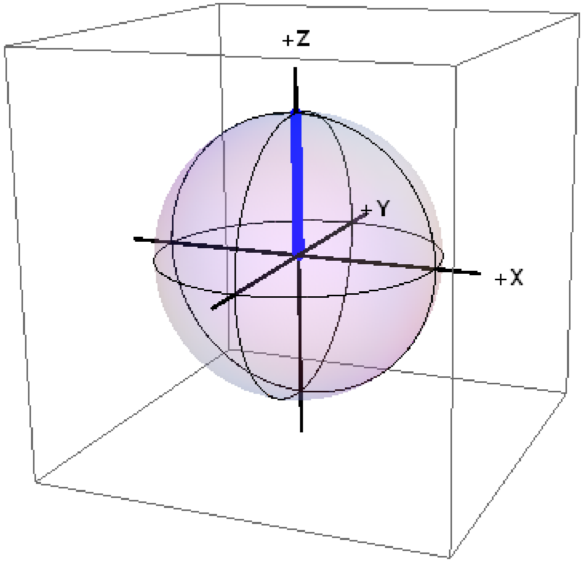

Nanofabrication of single spins

- Ion implantation to engineer NV centers
- Spatial control using resist apertures
- Depth profiling using SIMS studies

Collaborators:

UCSB
Prof. David Awschalom (PI)
D. M. Toyli
F. J. Heremans

Lawrence Berkeley National Lab
Thomas Schenkel
Christoph Weis

Ames Laboratory
V. V. Dobrovitski (theory)